

Sheffield Hallam University

Investigation of protein induction in vascular-targeted strategies.

COLE, Laura Margaret.

Available from the Sheffield Hallam University Research Archive (SHURA) at:

<http://shura.shu.ac.uk/19491/>

A Sheffield Hallam University thesis

This thesis is protected by copyright which belongs to the author.

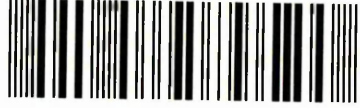
The content must not be changed in any way or sold commercially in any format or medium without the formal permission of the author.

When referring to this work, full bibliographic details including the author, title, awarding institution and date of the thesis must be given.

Please visit <http://shura.shu.ac.uk/19491/> and <http://shura.shu.ac.uk/information.html> for further details about copyright and re-use permissions.

Learning and Information Services
Assets Centre, City Campus
Sheffield S1 1WD

102 019 798 6



Sheffield Hallam University
Learning and Information Services
Assets Centre, City Campus
Sheffield S1 1WB

REFERENCE

ProQuest Number: 10694372

All rights reserved

INFORMATION TO ALL USERS

The quality of this reproduction is dependent upon the quality of the copy submitted.

In the unlikely event that the author did not send a complete manuscript and there are missing pages, these will be noted. Also, if material had to be removed, a note will indicate the deletion.



ProQuest 10694372

Published by ProQuest LLC (2017). Copyright of the Dissertation is held by the Author.

All rights reserved.

This work is protected against unauthorized copying under Title 17, United States Code
Microform Edition © ProQuest LLC.

ProQuest LLC.
789 East Eisenhower Parkway
P.O. Box 1346
Ann Arbor, MI 48106 – 1346

**Investigation of Protein Induction in Vascular-targeted
Strategies**

Laura Margaret Cole

**A thesis submitted in partial fulfilment of the requirements of
Sheffield Hallam University
for the degree of Doctor of Philosophy**

In collaboration with the University of Sheffield

February 2013

ACKNOWLEDGEMENTS

First and foremost, I would like to express my gratitude and appreciation of my principal supervisor Professor Malcolm R Clench, not only for his support and encouragement throughout my studies but for giving me many opportunities to extend my knowledge of analytical Mass Spectrometry through conferences and instilling faith in me during the presentation of my work. I am now a 'convert to Mass Spectrometry'!

I would also like to thank Dr Vikki A Carolan for her expertise and advice received during the writing of my thesis and comments on the structure of the many abstracts and posters I have emailed her over the last four years.

Special thanks and recognition is owed to the collaboration with the University of Sheffield. The guidance by Professor Gillian M Tozer has been invaluable. I would also like to express my gratitude to Professor Martyn N Paley and Professor Nicola J Brown for their input and support during the many Imaging update meetings.

I would like to say thank you to Dr Chris Sutton at the Institute of Cancer Therapeutics in Bradford for his patience and training during my time there.

For help with training and assistance on a variety of new techniques I am truly grateful to Dr Marie Claude Djidja, Emmanuelle Claude, Dr Adam Dowle, Dr Samira Kazan, Dr Florian Wulfert, Kevin Blake, Rachel Daniels, Jenny Globe and Matt Fisher.

I gratefully acknowledge Dr Simona Francese and Dr David Smith who not only have been helpful minds of information during my PhD but great conference travel cohorts too.

I would like to declare a special thank you to colleagues past and present for their friendship and support during my PhD who include Dr Paul J Trim, Leesa Ferguson, Dr Kate Phillips, Dr Louise Vickers, Eva Illes-Toth, Dr Philippa J Hart, Bryn Flinders, Robert Bradshaw, Chris Mitchell and Afnan Batubara, some of which are within the Mass Spectrometry group here at the BMRC.

A huge acknowledgement is extended to the 'coffee club ladies'; Dr Claire M Bradford, Dr Helenne Nyamwaro and Dr Rachel E Doherty who not only introduced me to cherry scones but also shared much laughter and discussion!

A very special thank you to my family and parents Tony and Laura who as always, support me in everything that I have ever set out to achieve.

Last, but certainly not the least, much love and endless thanks to my husband Wayne and daughter Alicia for support and encouragement words just cannot describe.

Abstract

The aims of the study reported in this thesis were to develop and utilise mass spectrometry imaging techniques (MALDI-MSI), in combination with conventional proteomic methodologies, to investigate protein induction in vascular-targeted strategies.

Proteins thought to be involved in tumourigenesis and drug treatment resistance were observed along with the responses from proteins identified via the techniques used, in this global analysis study. MALDI-MSI, LC-ESI-MS/MS, LC-MALDI-MS/MS with iTRAQ labelling and immunohistochemistry intended to provide cross validation of the effects post administration of vascular disrupting agent CA-4-P. Two mouse fibrosarcoma models (expressing VEGF120/VEGF188 isoforms only) following treatment with the tubulin-binding tumour vascular disrupting agent, combretastatin A-4-phosphate (CA-4-P) have been studied.

The gross haemorrhagic pharmacological response elicited by CA-4-P was visible by MALDI-MSI throughout the fibrosarcoma 120 time course. The latter encouraged the prospect that other proteins could potentially be observed induced via a dose response relationship. The haemoglobin time course using the resistant 188 tumour model gave quite different results to those previously seen in the MALDI-MSI of the fibrosarcoma 120 data set. The first indication of the '*switch back to tissue viability*' concept was revealed.

The experimental work using LC-ESI-MS/MS revealed many proteins connected with necrosis, apoptosis, cell structural reorganisation, polymerisation, tumour survival and stress induced molecular chaperones. The inverse correlation of structural proteins, haemoglobin and heat shock molecular chaperones gave the required validation and identification to relate these responses to those seen in MALDI-MSI. The relationship pathways generated by using STRING 9.0 proteomic network software gave an invaluable insight into the activity of the active tumour milieu and provided a means of linking the identified proteins to their functional partners. Protein-protein interactions could be observed to help interpretation of the MALDI-MSI, LC-ESI-MS/MS and iTRAQ LC-ESI-MS/MS response graphs.

Overall, the dose relationships observed in the iTRAQ data by the proteins involved in haemorrhaging, structural remodelling, were in good agreement with the other techniques employed here.

It could be said that MALDI-MSI could potentially forge a place in the workflow of clinical diagnostics. Targeted approaches for the observation of disease biomarkers could be visualised using MALDI-MSI and serve as a complimentary technique to standard clinical imaging. A novel method reported here using a multi-peptide recombinant standard could prove an important diagnostic tool for the analysis of patient biopsies and tissue micro-arrays. The exciting prospect is the diversity of a multi-peptide recombinant standard, an artificial construct that can be engineered to include any prospective biomarkers for both research and diagnostic screening applications.

Table of Contents

Table of Contents	1
List of Figures.....	6
Chapter 1	6
Chapter 2	7
Chapter 3	8
Chapter 4	10
Chapter 5	11
Abbreviations	13
Chapter 1.....	17
General Introduction.....	17
1.1 Cancer.....	18
1.1.1. Statistical information, incidence/ prevalence	18
1.1.2 Tumour types	22
1.1.3 Overview of current anti-cancer therapies	23
1.1.4 Vascular targeted strategies.....	30
1.1.5 Vascular disrupting agents	33
1.1.6 Biomarker Discovery	39
1.1.7 Considering Vascular disrupting agents for anti-cancer therapeutics	41
1.2 The Role of Mass Spectrometry in Biomarker Discovery.....	41
1.2.1. Overview of mass spectrometry as an analytical tool.....	41
1.2.2. Basic principles of mass spectrometry	42
1.2.3. Ionisation techniques and Mass analysers.....	46
1.3 Mass spectrometry instrumentation	49
1.3.1 LC-MS.....	49
1.3.2. Electrospray ionisation (ESI).....	51
1.3.3. Matrix assisted laser desorption ionisation (MALDI)	52
1.3.4. Quadrupole Time of flight mass spectrometry (QqToF)	54
1.3.5. Synapt HDMS – travelling wave ion mobility separation.	56
1.3.6. MALDI-mass spectrometry imaging	59
1.3.7. Quantitative Proteomics	60
1.3.8. Aims of the study.....	63
References.....	66

2.1 Introduction.....	75
2.2 Materials and Samples	76
2.2.1 Chemicals and Materials	76
2.2.2 Tissue samples.....	77
2.2.3. Experimental groups	77
2.2.4 Tissue preparation.....	77
2.2.5 <i>In situ</i> tissue digestion and trypsin deposition.....	77
2.3 Methods and instrumentation	78
2.3.1 Matrix deposition	78
2.3.2 Instrumentation	78
2.3.3 Haematoxylin and eosin staining	79
2.3.4 Data pre-processing using SpecAlign and Marker View software	79
2.3.5 Statistical analysis.....	79
2.3.6 Data pre-processing using Waters MassLynx™ Software and MATLAB®.....	79
2.4 Results and Discussion	80
2.4.1 Initial MALDI profiling and imaging of <i>in situ</i> tissue tryptic digests in mouse fibrosarcoma 120 models.....	80
2.4.2 Haematoxylin and Eosin staining of fibrosarcoma 120 tissue.....	83
2.4.3 Initial imaging of proteins according to theoretical digests using MALDI-MSI	86
2.4.4 Principle component analysis – discriminant analysis (PCA-DA)	88
2.4.5. Employment of Ion Mobility MALDI-Mass Spectrometry to study <i>in situ</i> tryptic digestion in fibrosarcoma 120 models	91
2.4.6 Rho GTPases: a target to help understand resistance to CA-4-P?	99
2.4.7. Statistical analysis of mouse fibrosarcoma 120 tumour tissue using MATLAB®	107
2.4.8 Region of interest (ROI) study for the analysis of tumour rim and necrotic regions within fibrosarcoma 120 tissue.....	112
2.4.9 Concluding Remarks.....	118
References.....	120
3.1 Introduction.....	124
3.2 Materials and Samples	126
3.2.1 Chemicals and Materials	126
3.2.2 Tissue samples.....	126
3.2.3. Experimental groups	126
3.2.4 Tissue preparation.....	126
3.2.5 <i>In situ</i> tissue digestion and trypsin deposition.....	127
3.3 Methods and instrumentation	127

3.3.1 Matrix deposition	127
3.3.2 Instrumentation	127
3.3.3 Haematoxylin and eosin staining	128
3.3.4 Statistical analysis.....	129
3.3.5 Data pre-processing using Waters MassLynx™ Software and MATLAB®	129
3.3.6 Protein network analysis.....	129
3.3.7 Immunohistochemical staining	129
3.3.8 Protein precipitation and digestion.....	130
3.3.9 Protein estimation – BCA assay.....	131
3.4 Results and Discussion	132
3.4.1 MALDI-MSI of fibrosarcoma 188 CA-4-P treated tumour tissue.....	132
3.4.2 Statistical analysis of mouse fibrosarcoma 188 tumour tissue using MATLAB®	150
3.4.3 Label free LC-ESI -MS/MS for the identification of proteins in a CA-4-P treated fibrosarcoma 188 mouse model	159
3.4.4 Protein relationship mapping of fibrosarcoma 188 LC-ESI-MS/MS data using String 9.0.....	182
3.4.5 Concluding remarks.....	186
References.....	188
4.1 Introduction.....	194
4.2 Materials and Samples	195
4.2.1 Chemicals and Materials	195
4.2.2 Tissue samples.....	195
4.2.3. Experimental groups	196
4.2.4 Tissue preparation.....	196
4.2.5 Tissue homogenisation and precipitation of protein	196
4.2.6 Protein Digestion.....	197
4.2.7 Preparation of samples for column loading.....	197
4.2.8 C18 bond-elute preparation.....	197
4.2.9 Sample re-suspension	198
4.2.10 iTRAQ labelling	198
4.2.11 SCX.....	199
4.3 Methods and instrumentation.....	199
4.3.1 Sample fractionation and matrix deposition.....	199
4.3.2 Instrumentation	199
4.3.3 Data pre-processing	200
4.3.4 Statistical analysis.....	201

4.3.5 Protein network analysis	201
4.4 Results and discussion - Fibrosarcoma 120.....	202
4.4.1. HPLC UV profiles of fibrosarcoma 120 tumour fractions.....	202
4.4.2 Frequency of unique peptides identified	203
4.4.3. Analysis using excel	203
4.4.4. Analysis with Scaffold Q+	207
4.4.5 Protein relationship mapping of fibrosarcoma 120 data using STRING 9.0.....	218
4.5 Results and discussion - Fibrosarcoma 188.....	224
4.5.1. HPLC UV profiles of fibrosarcoma 188 tumour fractions.....	224
4.5.2 Frequency of unique peptides identified	225
4.5.3. Analysis using excel	225
4.5.4. Analysis with Scaffold Q+	231
4.5.5 Protein relationship mapping of Fibrosarcoma 188 data using STRING 9.0.....	242
4.5.6 Protein dose response relationship analysis using String 9.0	247
4.5.7 Relation of MALDI-MSI to iTRAQ proteomic response	256
4.5.8 Concluding Remarks.....	259
References.....	260
5.1 Introduction.....	266
5.2 Materials and Methods.....	267
5.2.1 Peptide sequences chosen for a recombinant protein standard based on MALDI-MSI and conventional proteomic analysis of fibrosarcoma 120 and 188 tissue.....	267
5.2.2 Bacterial culture	268
5.2.3 Plasmid preparation	269
5.2.4 E. coli- transformation.....	269
5.2.5 Protein Purification	269
5.4.6 Digestion.....	270
5.4.7 MALDI-MSI - Chemicals and Materials.....	271
5.4.8 Methods and instrumentation	272
5.3 Results and Discussion	273
5.3.1 MALDI-IMS-MS Peptide mass fingerprint of the digested recombinant DNA construct	273
5.3.2 MALDI-IMS-MSI of fibrosarcoma 188 tumour tissue, Control and post CA-4-P treatment	275
5.3.3 Recombinant MALDI-IMS-MSI visualised through HDI 1.1 software	280
5.3.4 Cross validation of Plectin and HSP-90 response in fibrosarcoma 188 tissue employing a multimodal proteomic strategy.....	292

5.4 Concluding Remarks	295
References.....	297
Appendices	304
Appendix 1: Publications	305
Appendix 2: Oral presentations	306
Appendix 3: Poster presentations	307

List of Figures

Chapter 1

Figure 1. 1: Percentage of all deaths due to cancer in the different regions of the world (WHO) Regions of the World.....	19
Figure 1. 2: Cancer incidence worldwide map.....	20
Figure 1.3 : The 20 Most Common Causes of Cancer Death, UK.....	21
Figure 1.4 : Diagrammatical representation of the possible routes of cell division.....	22
Figure 1. 5 : Proposal of adding CSC specific predictive tests to therapy regimes for potential increase in tumour control probability.....	26
Figure 1. 6 : Images to illustrate the substandard tumour vasculature.....	33
Figure 1. 7 : Chemical structures of vascular disrupting agents.....	34
Figure 1. 8 : Proposed mechanism of action of Combretastatin A-4-3-O-phosphate.....	35
Figure 1. 9 : Fluorescent staining of Human umbilical vein endothelial cells, Control and post CA4P administration.....	36
Figure 1. 10 : CA-4-P and its effect on hypoxia induction and vascular shutdown.....	37
Figure 1. 11 : Exploitation of tumour vasculature by antiangiogenic treatment and vascular disrupting agents.....	37
Figure 1. 12 : Therapeutic targeting of the hallmarks of cancer.....	40
Figure 1. 13: The cells of the tumour microenvironment.....	40
Figure 1. 14 : Basic principles of a mass spectrometer.....	43
Figure 1. 15 : Basic ionisation techniques.....	46
Figure 1. 16 : Mass analysers used in mass spectrometers.....	47
Figure 1. 17 : Protein identification methods.....	48
Figure 1. 18 : Schematic representation of a liquid chromatography mass spectrometer.....	50
Figure 1. 19 : Schematic of Electrospray ionisation.....	51
Figure 1. 20 : Ionisation using MALDI.....	52
Figure 1. 21 : Diagrammatical representation of a tandem QqTOF mass spectrometer.....	55
Figure 1. 22 : Schematic representation of a ToF modulator.....	56
Figure 1. 23 : SYNAPT™ G2 HDMS system.....	57
Figure 1. 24 : Stacked ring ion guide.....	57
Figure 1. 25 : Travelling wave ion guide- schematic representation.....	58
Figure 1. 26 : MALDI-MSI workflow diagram.....	60
Figure 1. 27 : The concept of area peptide measurement coupled with a specific time domain, visualised through Progenesis LC- MS software.....	61
Figure 1. 28 : Simple workflow using Isobaric Tags for Relative and Absolute Quantitation (iTRAQ).....	62
Figure 1. 29 : VEGF isoform expression and exon structure.....	64

Chapter 2

Figure 2. 1: Representative peptide mass fingerprint (PMF) arising from an on-tissue digest of a VEGF120 tumour 24 h after dosing with 100 mg/kg i.p, CA-4-P.....	80
Figure 2. 2: Peptide mass fingerprints obtained from the fibrosarcom 120 tumour tissue sections treated with saline or 100 mg/kg i.p.....	81
Figure 2. 3: MALDI-MS images for the distribution of m/z 1274 throughout a fibrosarcoma 120 timecourse.....	82
Figure 2. 4 : Haematoxylin and eosin stained sections.	84
Figure 2. 5: Higher magnification images of the H&E staining of the tumour rim in the VEGF120 tumour sections.	85
Figure 2. 6: MALDI-MSI of peptides from tumour 5:1 (24hrs CA-4-P).	86
Figure 2. 7: PCA-DA of fibrosarcoma 120 tumour <i>in situ</i> tryptic digests.....	88
Figure 2. 8: Representative peptide mass fingerprint (PMF) arising from an on-tissue digest of a VEGF120 tumour 6 h after dosing with 100 mg/kg i.p, CA-4-P.....	92
Figure 2. 9: IMS-MS/MS data obtained from the peak observed in Figure 2.8 at m/z 1819.....	93
Figure 2. 10 a: A Drift scope plot of a tumour section 24 h post CA-4-P showing the ion mobility separation as a function of drift time.	94
Figure 2. 11: The distribution of two known peptides in tumour 5_6, i.e. a tumour 24 h after treatment with CA-4-P	97
Figure 2. 12: Overlaid MALDI MSI images showing differing spatial distribution and co-registration of peptides.....	98
Figure 2. 13: Major Functions of Rho GTPases <i>in vitro</i>	100
Figure 2. 14: Peptide mass fingerprints obtained from the fibrosarcom 120 tumour tissue 30min post CA-4-P(100 mg/kg i.p.) with peak of interest at m/z 844.	101
Figure 2. 15: IMS-MS/MS data obtained from the peak observed in Figure 2.14 at m/z 844.5.	102
Figure 2. 16: Mascot score histogram detailing the results in the identification of N-chimaerin.	102
Figure 2. 17: Zoomed in Driftscope plot showing ion of interest, arrow indicating the peak originally selected.....	103
Figure 2. 18: PMF's throughout a fibrosarcoma 120 time course with putative peptide of interest N-chimaerin visible in early time points .Control (saline), 0.5 h post CA-4-P, 6 h post CA-4-P and 24 h postCA-4-P.	104
Figure 2. 19: MALDI-MSI throughout a fibrosarcoma 120 time course of the putative peptide Rho GTPase activating protein 2 m/z 844 (183-189, RLTSLVR).....	105
Figure 2. 20 : PCA of fibrosarcoma 120 tumour tissue <i>in situ</i> tryptic digests.	108
Figure 2. 21: Partial least squares discriminant analysis (PLSDA) regression vector plot comparing MALDI "on-tissue" digest data from samples of fibrosarcoma 120 Control/Saline and 30 min post combretastatin-4-phosphate (CA-4-P) (a vascular disrupting agent), treatment tumour samples.	110
Figure 2. 22: HDI software displaying MALDI-MSI from a fibrosarcoma tumour section 24h post CA-4-P.....	113
Figure 2. 23: PLSDA regression vector plot showing fibrosarcoma 120 Control necrotic regions versus fibrosarcoma 120 necrotic regions post 24h CA-4-P.	114

Figure 2. 24: PLSDA regression vector plot showing fibrosarcoma 120 Control rim regions versus spectra from rim regions post 24h CA-4-P	115
Figure 2.25: VIP scores for the Control fibrosarcoma 120 tumour rim regions.....	116
Figure 2.26: VIP scores for the 24h post CA-4-P fibrosarcoma 120 tumour rim regions.....	117

Chapter 3

Figure 3. 1: Diagrammatical cross section of the region present at the end of growing long bones showing the areas involved in epiphysis and metaphysis.....	124
Figure 3. 2: Screen shot of protein delocalisation in MALDI-MSI, visualised using BioMap imaging software.....	133
Figure 3. 3: Screen shot of an on tissue tryptic digest using MALDI-MSI, visualised using BioMap imaging software.....	135
Figure 3. 4: PMF's of a fibrosarcoma 188 time course study. Spectra shown are Control, 0.5h, 6h, 24h and 72h post CA-4-P treatment.	137
Figure 3. 5: Zoomed in region of fibrosarcoma 188 PMF's. The blue arrows indicate the gross differences visible in the 24h and 72h time points, m/z 1416 being Hb and an unknown species at m/z 1577.	138
Figure 3.6: Comparison control tissue peptide mass fingerprints from fibrosarcoma 120 and 188 on tissue digests.	139
Figure 3. 7: MALDI-MSI multi image of a fibrosarcoma 188 time course.	141
Figure 3. 8: Fibrosarcoma 188 MALDI-MSI multi image showing spatial distribution of HSP-90. MALDI images showing spatial distribution of HSP-90 alpha at m/z 1168.	143
Figure 3. 9: Immunohistochemical staining of a fibrosarcoma 188 time course.....	144
Figure 3. 10: Immunohistochemical staining of HSP-90 in Fibrosarcoma 188 tissue.	145
Figure 3. 11: SYNAPT G2 MALDI imaging plate indicating tissue image regions.....	147
Figure 3. 12: 40µm MALDI-MSI of 24h post CA-4-P fibrosarcoma 188 tumour tissue.	148
Figure 3. 13: 40µm MALDI-MSI of m/z 944.5 in fibrosarcoma 188 tumour tissue	148
Figure 3. 14: 40µm MALDI-MSI of a on tissue tryptic digest and corresponding H and E histological section.....	149
Figure 3. 15: 30 µm MALDI-MSI of a Control fibrosarcoma 188 tumour on tissue tryptic digest	149
Figure 3. 16: PCA score plot of fibrosarcoma 188 tumour tissue in situ tryptic digests.	150
Figure 3. 17: PCA loadings plot fibrosarcoma 188 tumour tissue in situ tryptic digests.....	151
Figure 3. 18: Partial least squares discriminant analysis (PLSDA) regression vector plot comparing MALDI "on-tissue" digest data from samples of fibrosarcoma 188 Control and 0.5h post combretastatin-4-phosphate (CA-4-P), treatment tumour samples	152
Figure 3. 19: Partial least squares discriminant analysis (PLSDA) regression vector plot for the comparison of Control and 6h post CA-4-P fibrosarcoma 188 on tissue digests.....	153
Figure 3. 20: Partial least squares discriminant analysis (PLSDA) regression vector plot for the comparison of Control and 24h post CA-4-P fibrosarcoma 188 on tissue digests.....	154
Figure 3. 21: Partial least squares discriminant analysis (PLSDA) regression vector plot for the comparison of Control and 72h post CA-4-P fibrosarcoma 188 on tissue digests.....	155
Figure 3. 22: VIP scores for the 0.5h post CA-4-P fibrosarcoma 188 on tissue digest.	156

Figure 3. 23: VIP scores for the 6h post CA-4-P fibrosarcoma 188 on tissue digest.	156
Figure 3. 24: VIP scores for the 24h post CA-4-P fibrosarcoma 188 on tissue digest.	157
Figure 3. 25: VIP scores for the 72h post CA-4-P fibrosarcoma 188 on tissue digest.	157
Figure 3. 26: Scaffold proteomic tool software used for LC-ESI-MS/MS analysis.....	160
Figure 3. 27: Graph A - Fibrosarcoma 188 treatment time course results, exported from Scaffold 3.....	161
Figure 3. 28: Graph B - Fibrosarcoma 188 treatment time course results, exported from Scaffold 3.....	162
Figure 3. 29: Graph C - Fibrosarcoma 188 treatment time course results, exported from Scaffold 3.....	163
Figure 3. 30: Graph D - Fibrosarcoma 188 treatment time course results, exported from Scaffold 3.....	164
Figure 3. 31: Graph E - Fibrosarcoma 188 treatment time course results, exported from Scaffold 3.....	165
Figure 3. 32: Graph F - Fibrosarcoma 188 treatment time course results, exported from Scaffold 3.....	166
Figure 3. 33: Graph G - Fibrosarcoma 188 treatment time course results, exported from Scaffold 3.....	167
Figure 3. 34: Fibrosarcoma 188 time course results post CA-4-P treatment using LC-ESI-MS/MS.	168
Figure 3. 35: MS/MS spectrum and normalised intensity graph of Alpha-2-macroglobulin in fibrosarcoma 188 LC-ESI-MS/MS results.....	170
Figure 3. 36: Immunohistochemical staining of macrophage cell surface marker F4/80 using fibrosarcoma 188 tissue 10x.	172
Figure 3. 37: MS/MS spectrum and normalised intensity graph of Plectin in fibrosarcoma 188 LC-ESI-MS/MS results. Insert displays the normalised spectral counts for Plectin throughout the time course post CA-4-P.....	174
Figure 3. 38: Fibrosarcoma 188 MALDI-MSI multi image showing spatial distribution of Plectin. MALDI images showing spatial distribution of Plectin at m/z 977.	174
Figure 3. 39: Immunohistochemical staining of Plectin in Fibrosarcoma 188 tissue post CA-4-P treatment.	175
Figure 3. 40: Optical scans of anti-Plectin and HSP-90 Immunohistochemical staining in fibrosarcoma 188 serial sections, 72h post CA-4-P treatment	177
Figure 3. 41: Example MS/MS spectrum and normalised intensity graph of IQGAP1 in fibrosarcoma 188 LC-ESI-MS/MS results.....	178
Figure 3. 42: Example MS/MS spectrum and normalised intensity graph of Tenascin C in fibrosarcoma 188 LC-ESI-MS/MS results.....	179
Figure 3. 43: Example MS/MS spectrum and normalised intensity graph of Alpha-enolase in fibrosarcoma 188 LC-ESI-MS/MS results.....	180
Figure 3. 44: Example MS/MS spectrum and normalised intensity graph of Transforming growth factor-beta-induced protein ig-h3 (Tgfb1) in fibrosarcoma 188 LC-ESI-MS/MS results.	181
Figure 3. 45: LC-ESI-MS/MS proteins of interest from fibrosarcoma 188, visualised through proteomic pathway software STRING 9.0.....	182
Figure 3. 46: Proteomic network from LC-ESI-MS/MS fibrosarcoma 188 data.	184

Chapter 4

Figure 4. 1: The principles of multiplex tagging chemistry.	194
Figure 4.2: UV profiles from the fibrosarcoma 120 fractions after SCX.....	202
Figure 4. 3: Frequency of detection of unique peptides by LC-MALDI-MS/MS	203
Figure 4. 4: iTRAQ results from fibrosarcoma 120 fixed filtered search.....	204
Figure 4. 5: iTRAQ ratio response relative to the control (113), normalised to an average of 1.	205
Figure 4. 6: Scaffold proteomic software used for iTRAQ analysis.	208
Figure 4. 7: Scaffold proteomic software with the employment of 'Q+' function for iTRAQ ratio analysis	209
Figure 4. 8: iTRAQ fold change ratio using fibrosarcoma 120 tumour digest samples.....	210
Figure 4. 9: Vimentin peptides identified, response bar graph and related MS/MS spectrum from iTRAQ LC-MALDI-MS/MS Fibrosarcoma 120 tissue.....	212
Figure 4. 10: Haemoglobin subunit beta-1 peptides identified, response bar graph and related MS/MS spectrum from iTRAQ LC-MALDI-MS/MS Fibrosarcoma 120 tissue.....	213
Figure 4. 11: Peroxiredoxin-1 (Macrophage 23kDa stress protein) peptides identified, response bar graph and related MS/MS spectrum from iTRAQ LC-MALDI-MS/MS Fibrosarcoma 120 tissue.	214
Figure 4. 12: Tubulin beta-5 chain peptides identified, response bar graph and related MS/MS spectrum from iTRAQ LC-MALDI-MS/MS Fibrosarcoma 120 tissue.	215
Figure 4. 13: Annexin A5 peptides identified, response bar graph and related MS/MS spectrum from iTRAQ LC-MALDI-MS/MS Fibrosarcoma 120 tissue.....	216
Figure 4. 14: Keratin -1 (type II skeletal 1) peptides identified, response bar graph and related MS/MS spectrum from iTRAQ LC-MALDI-MS/MS Fibrosarcoma 120 tissue.....	217
Figure 4. 15: Fixed modification search showing proteins from iTRAQ using Fibrosarcoma 120 tumours, visualised by STRING 9.0 (Confidence view).....	219
Figure 4. 16: Fixed modification search of iTRAQ fibrosarcoma 120 proteomic data, compiled using STRING 9.0, evidence view.	220
Figure 4. 17: Zoomed in region of a fixed modification search, iTRAQ fibrosarcoma 120 samples.	221
Figure 4. 18: Zoomed in region of a fixed modification search, iTRAQ fibrosarcoma 120 samples.	222
Figure 4. 19: UV profiles from the fibrosarcoma 188 fractions after SCX.....	224
Figure 4. 20: Frequency of detection of unique peptides by LC-MALDI-MS/MS	225
Figure 4. 21: iTRAQ results from fibrosarcoma 188 fixed filtered search.....	226
Figure 4. 22: a iTRAQ ratio response relative to the control (113), normalised to an average of 1.	227
Figure 4. 23: Scaffold proteomic software used for iTRAQ analysis	232
Figure 4. 24: Scaffold proteomic software with the employment of 'Q+' function for iTRAQ ratio analysis.....	233
Figure 4. 25: iTRAQ fold change ratio using fibrosarcoma 188 tumour digest samples.....	234
Figure 4. 26: Vimentin peptides identified, response bar graph and related MS/MS spectrum from iTRAQ LC-MALDI-MS/MS Fibrosarcoma 188 tissue.....	237
Figure 4. 27: Haemoglobin subunit beta-1 peptides identified, response bar graph and related MS/MS spectrum from iTRAQ LC-MALDI-MS/MS Fibrosarcoma 188 tissue.....	238

Figure 4. 28: Pyruvate kinase isozymes M1/M2 peptides identified, response bar graph and related MS/MS spectrum from iTRAQ LC-MALDI-MS/MS Fibrosarcoma 188 tissue.....	239
Figure 4. 29: Tenascin peptides identified, response bar graph and related MS/MS spectrum from iTRAQ LC-MALDI-MS/MS Fibrosarcoma 188 tissue.....	240
Figure 4. 30: Fibronectin peptides identified, response bar graph and related MS/MS spectrum from iTRAQ LC-MALDI-MS/MS Fibrosarcoma 188 tissue.....	241
Figure 4. 31: iTRAQ Fixed modification search using Fibrosarcoma 188 tumours, visualised by STRING 9.0 (Confidence view).....	243
Figure 4. 32: iTRAQ Fixed modification search using Fibrosarcoma 188 tumours, visualised by STRING 9.0 (Evidence view).....	244
Figure 4. 33: Zoomed in region of a fixed modification search, iTRAQ fibrosarcoma 188 samples, visualised through STRING 9.0.	245
Figure 4. 34: iTRAQ fibrosarcoma 188 zoomed in region of a fixed modification search, visualised through STRING 9.0.	246
Figure 4. 35: iTRAQ fibrosarcoma 188 zoomed in region of a fixed modification search, visualised through STRING 9.0.	247
Figure 4. 36: iTRAQ proteomic response results using a Fibrosarcoma 120 treatment timecourse.....	248
Figure 4. 37: Fibrosarcoma 120 proteomic response using String 9.0.....	250
Figure 4. 38: iTRAQ combinations of fibrosarcoma 120 increased and decreased proteins....	251
Figure 4. 39: iTRAQ proteomic response results using a Fibrosarcoma 188 treatment time course.....	252
Figure 4. 40: iTRAQ proteomic response results using a 24h post CA-4-P Fibrosarcoma 188 treatment.	253
Figure 4. 41: iTRAQ proteomic response results using a 0.5h post CA-4-P Fibrosarcoma 188 treatment.	254
Figure 4. 42: iTRAQ combinations of fibrosarcoma 188 increased and decreased proteins....	255
Figure 4. 43: Bar graph showing protein response relative to the control (113) normalised to an average of 1, using fibrosarcoma 188 tissue.....	256
Figure 4. 44: MALDI-MSI multiple Fibrosarcoma 188 sample on tissue digest of Plectin at m/z 977.....	257
Figure 4. 45: MALDI-MSI multiple Fibrosarcoma 188 sample on tissue digest of Hb subunit alpha at m/z 1416.....	258

Chapter 5

Figure 5. 1: pETBlue-1 vector and sequence used for the synthesis of the recombinant protein standard.	268
Figure 5. 2: The final sequence of the recombinant standard.	268
Figure 5. 3: PMF of a novel recombinant standard for MALDI-IMS-MSI validation.....	274
Figure 5. 4: MALDI-MSI of on tissue tryptic digests and digested recombinant standard in 72h treated tissue.	275
Figure 5. 5: MALDI-MS images for the distribution peptides in fibrosarcoma 188 72h tissue, employing a DNA artificial construct for image validation.	276
Figure 5. 6: MALDI-MS images displaying peptides distribution in fibrosarcoma 188 6h treated tissue, employing a DNA artificial construct for image validation. The spatial distribution of peptides; Actin (m/z 1198) with arrow indicating position of the spotted recombinant standard,	

Histone H3 (m/z 1032) showing the absence of the standard and CHCA peak at 1066 to show inverse image correlation.....	277
Figure 5. 7: MALDI-MS images for the distribution peptides in fibrosarcoma 188 Control tissue, employing a DNA artificial construct for image validation.	278
Figure 5. 8: HDI visualisation of Actin at m/z 1198.7. Arrow indicates the ion of interest separated by drift time and yellow square denotes the ROI for exportation.....	281
Figure 5. 9: HDI visualisation of m/z 1198.6 to display the differentiation in tissue and standard image due to separation in drift time compared to m/z 1198.7.	283
Figure 5. 10: HDI visualisation of HSP-90 α at m/z 1168.5. Arrows indicates the ion of interest separated by drift time, and yellow ROI square is shown.....	284
Figure 5. 11: HSP-90 α at m/z 1168.5 after exportation to Mass Lynx software from the selected ROI in HDI 1.1.....	285
Figure 5. 12: HDI visualisation of Histone H3 at m/z 1032.7. The arrow indicates the ion of interest separated by drift time and no signal apparent in the standard.....	286
Figure 5. 13: HDI visualisation of Actin at m/z 1198.7. The arrow indicates the ion of interest separated by drift time.....	287
Figure 5. 14: HDI visualisation of Histone 2A at m/z 944.5. The arrow indicates the ion of interest separated by drift time.	288
Figure 5. 15: HDI software with image correlation filter for Plectin m/z 1032 displaying fellow Histones.....	290
Figure 5. 16: HDI software with image correlation filter for Plectin m/z 1350 showing no discrimination between other peaks.	291
Figure 5. 17: MALDI-MSI of fibrosarcoma 188 on tissue tryptic digests for the spatial distribution of Plectin at m/z 1385.....	292
Figure 5. 18: MALDI-MSI and conventional proteomic techniques to asses a dose relationship in Plectin.....	293
Figure 5. 19: MALDI-MSI and conventional proteomic techniques to asses a dose relationship in HSP-90.	294
Figure 5. 20: Issues and factors to consider when performing on tissue digestion for MALDI imaging experiments.....	296

List of Tables

Table 1 : Cancer incidence throughout the regions of the world	18
Table 2: Current anti-cancer treatments.....	29
Table 3: Categorisation of vascular targeted therapies	30
Table 4 : Example of drugs within each category.....	31
Table 5 : Inhibiting the process of angiogenesis	32
Table 6 : Mass spectrometers for proteomics	45
Table 7 : Common matrices used in UV- MALDI.	54
Table 8: Identities and Mascot scores from the IMS-MS/MS analyses of peptide signals.	91
Table 9: Twelve peptides from target proteins chosen for positive identification.....	267

Abbreviations

ACN: acetonitrile

Aldoart1: Fructose-bisphosphate aldolase A

ALO22784: alpha-enolase 1 (Eno1)

ANI: aniline

APCI: atmospheric pressure chemical ionisation

APPI: atmospheric pressure photoionisation

BCA: bicinchoninic acid assay

Calr: Calreticulin

CHCA: α -cyano-4-hydroxycinnamic acid

CHCl₃: chloroform

CID: collision-induced dissociation

CA-4-P: combretastatin A-4 -3-O phosphate

CSC: cancer stem cell

dH₂O: deionised water

DMXAA: 5,6-Di-methylxanthenone-4-acetic acid

Eef1a1: Elongation factor 1-alpha 1

ESI: electrospray ionisation

ESI-LC-MS: electrospray ionisation-liquid chromatography-mass spectrometry

ESI-LC-MS/MS: electrospray ionisation-liquid chromatography-tandem mass spectrometry

EtOH: ethanol

FFPE: formalin fixed paraffin embedded

GAPDH: Glyceraldehyde-3-phosphate dehydrogenase

Gpi1: Glucose-6-phosphate isomerase

GRP-78: glucose- regulated protein 78 (Hspa5)

HE: haematoxylin and eosin

HIF-1 α : hypoxia- inducible factor 1 alpha

HPLC: high performance liquid chromatography

HSP: heat shock protein

IHC: immunohistochemistry

IMS: ion mobility separation

IQGAP1: Ras GTPase-activating-like protein

iTRAQ: isobaric tag for relative absolute quantitation

KTR1: Keratin-1(type II skeletal-1)

LC: liquid chromatography

LC-MALDI: liquid chromatography-matrix assisted laser desorption ionisation

LC-MALDI-MS/MS: liquid chromatography-matrix assisted laser desorption ionisation-tandem mass spectrometry

LC-MS/MS: liquid chromatography -mass spectrometry tandem mass spectrometry

Lgals1: Galectin-1

MALDI: matrix assisted laser desorption ionisation

MALDI-MS: matrix assisted laser desorption ionisation-mass spectrometry

MALDI-IMS-MS: matrix assisted laser desorption ionisation-ion mobility separation-mass spectrometry

MALDI-IMS-MSI: matrix assisted laser desorption ionisation-ion mobility separation-mass spectrometry imaging

MALDI-MSI: matrix assisted laser desorption ionisation- mass spectrometry imaging

MALDi-ToF: matrix assisted laser desorption ionisation-time of flight

Mcm5: DNA replication licensing factor MCM5

MS: mass spectrometry

m/z: mass- to -charge ratio

MeOH: methanol

MudPIT: multidimensional protein identification technology

N₂ laser: nitrogen laser

Nd: YAG: neodymium-doped yttrium aluminium garnet

Nd:YVO₄: yttrium ortho-vanadate

NH₄HCO₃: ammonium bicarbonate

NHS: N-hydroxysuccinimide

OcGlc: Octyl- α/β -glucoside

PCA: principle component analysis

PCA-DA: principle component analysis-discriminant analysis

PLSDA: partial least squares discriminant analysis

PMF: peptide mass fingerprint

PRDX1: Peroxiredoxin-1

Q: quadrupole

QqTOF: quadrupole time of flight

ROI: region of interest

S100a6: Calcylin

SMA: smooth muscle actin

TAA: tumour associated antigen

TFA: trifluoroacetic acid

Tgfb β : Transforming growth factor-beta-induced protein ig-h3

Tnc: Tenascin C

TOF: time of flight

TOF MS: time of flight mass spectrometry

Tpi1: Triosephosphate isomerase

TSP: thermospray

TWIGS: travelling wave ion guides

VDA: vascular disrupting agent

VEGF: vascular endothelial growth factor

VEGFR: vascular endothelial growth factor receptor

VIP: variable importance in projection

VTs: vascular targeted strategy

VTT: vascular targeted therapy

Chapter 1

General Introduction

1.1 Cancer

1.1.1. Statistical information, incidence/ prevalence

At the time that this account was written the latest official current world population estimate was ~7,094,391,160. This approximation was made based on population figures on the 27th January 2013 (Worldometers 2013). Demographic predications state that by 2028 the number of our planet's inhabitants will exceed 8 billion (Cancer Research UK 2007).

The current population is described as 'aging', the relevance of this from a cancer perspective is that the disease has been known to predominantly affect the older generations (Cancer Research UK 2007). Worldwide life expectancy is increasing, people are living longer and the average lifetime expectancy at birth is said to be 65yrs possibly escalating to 76yrs by the year 2050. Throughout the world there are still ~12.7 million people who are annually diagnosed with cancer with estimations likely to increase to ~26 million by 2030 (World Cancer Research Fund 2010). The UK has the 22nd highest overall cancer rate in the world.

	New cases of cancer diagnosed	
	Number (2008 estimates)	5% of total
Africa	715,571	6
Asia	6,092,359	48
Europe	3,208,882	25
Latin America & Caribbean	906,008	7
North America	1,603,870	13
Oceania	135,864	1
Developed regions	5,555,281	44
Developing regions	7,107,273	56
World	12,662,554	100

Table 1 : Cancer incidence throughout the regions of the world (Adapted from Cancer Research UK 2011).

It is evident from Table 1 that Asia has the largest proportion of new cases diagnosed but this is understood to be a reflection of the magnitude of population size within that particular continent.

On a global scale the mortality rate is such that in 2008 there were an estimated 7.6 million deaths as a result of cancer, the bar graph below shows the proportion of deaths due to cancer in the regions of the world (World Health organisation 2012).

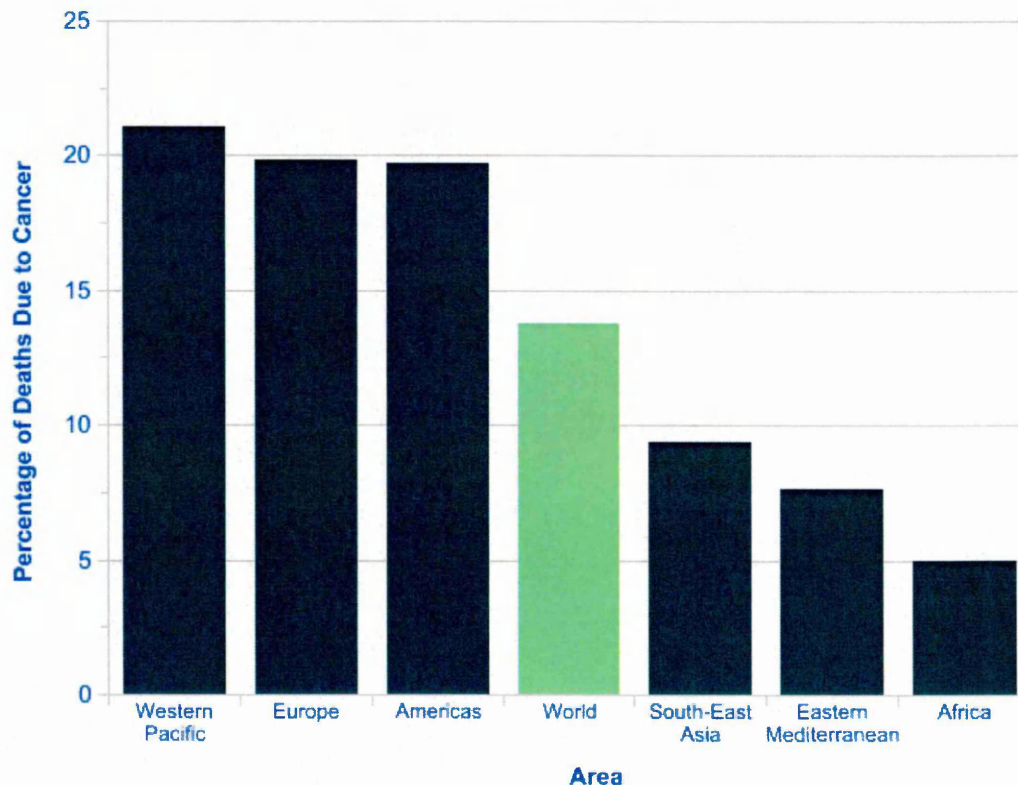


Figure 1. 1: Percentage of all deaths due to cancer in the different regions of the world (WHO) Regions of the World, 2008 Estimates (Cancer Research UK 2007).

The following map (Figure 1.2) entitled 'Cancer Incidence Worldwide' (Cancer Research UK 2011) represents the most frequently diagnosed cancers within the areas shown in 2008. The cancer types which account for the largest proportion of cases diagnosed are found to be; lung, breast, bowel, stomach and prostate.

It is stated that 47% of all cancer related death are from lung, bowel, breast and prostate cancers (Cancer Research UK 2011). Figure 1.3 displays the 20 most common causes of death from cancer in the UK.

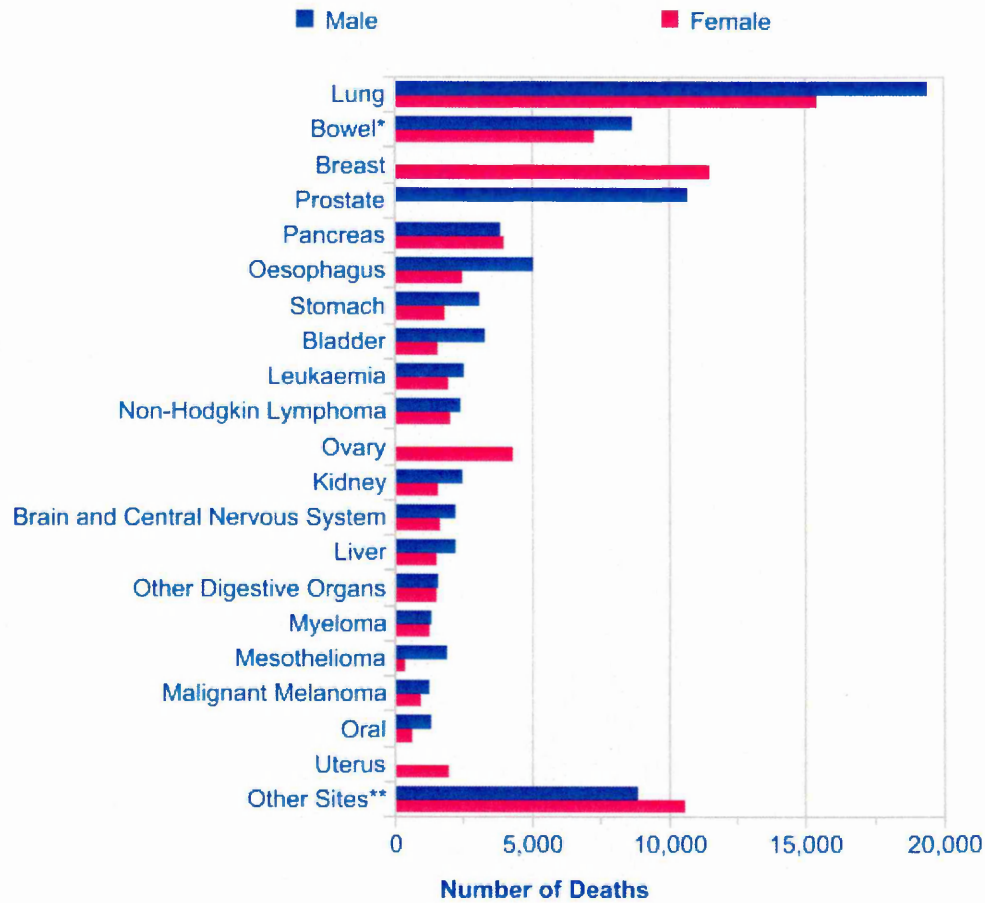


Figure 1.3 : The 20 Most Common Causes of Cancer Death, UK, 2010 (Cancer Research UK 2011).

1.1.2 Tumour types

There are over 200 different kinds of cancer which can be classified by cell of origin (Cancer Research UK 2009). Tumours are generally classified as benign or malignant to illustrate that not all are cancerous (Medline Plus 2010). Malignant is the term used to describe an abnormal neoplasm which is cancerous and benign is a non-cancerous growth. The cells which constitute the cancerous tumour types have metastatic capabilities and are able to reach other regions of the body to form secondary tumours whilst benign tumour types do not metastasize.

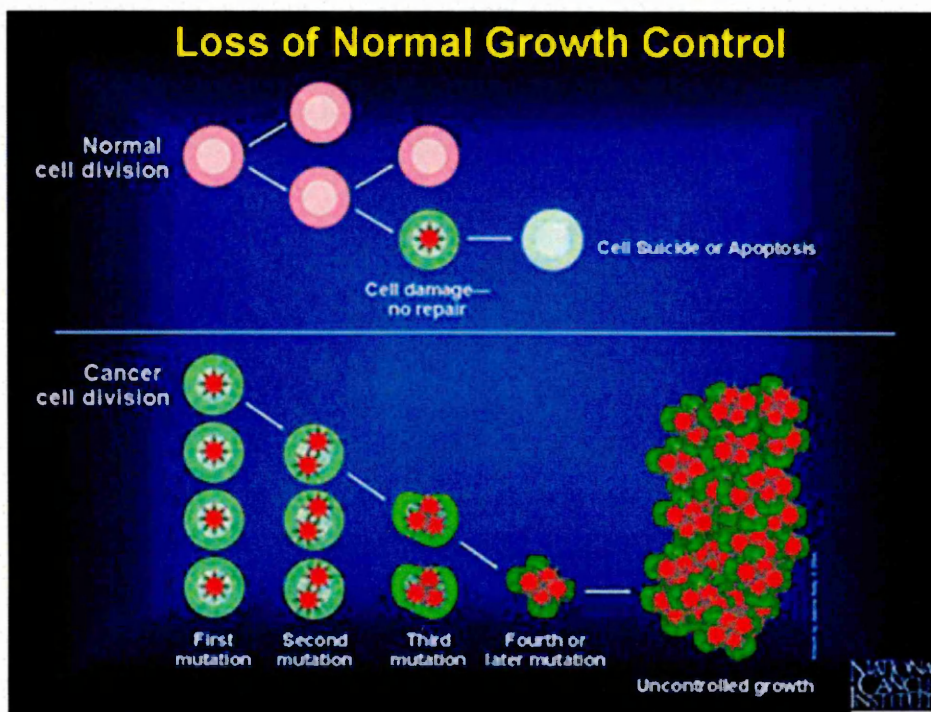


Figure 1.4 : Diagrammatical representation of the possible routes of cell division (National Cancer Institute 2009).

The cancer cell has the ability to elicit morphological changes as depicted in Figure 1.4., to ultimately disregard the usual signals for cell suicide or apoptosis.

It is possible to divide solid tumours into 3 broad categories these being; carcinomas which originate from altered epithelial cells which function as linings of a body surface region i.e. skin, gut, cervix, mouth, lung, sarcomas occur in connective tissue i.e. bone, muscle, cartilage and lymphomas/ leukaemia which describes cancers that arise from lymphoid organs (lymph nodes, spleen) and cells from bone marrow (<http://www.chemotherapy.com/> 2011).

1.1.3 Overview of current anti-cancer therapies

Pre-treatment clinical assessment of patient tumours is generally based on tumour size, through histological staining, tumour grade and is regularly coupled with the employment of various imaging techniques (Koch et al 2010). The tumour grading is a system that is used as a reference in order to classify cancer cells. Analysis of the abnormalities exhibited by cancer cells are visualised by microscopy, here the aggressiveness of the tumour can be determined. Although factors used for tumour grading vary in cancer type the cellular architecture and growth patterns are studied (National Cancer Institute 2009). The outcome of these evaluations will then determine the appropriate treatment route.

An example of a grading system commonly used by Doctors is the TNM system. This grading system is an accepted method by the International Union against Cancer (UICC) and the American Joint Committee on Cancer (AJCC) (National Cancer Institute 2009). In brief the rationale behind the TNM method is that the 'T' refers to the extent of the tumour, the 'N' amount of colonisation in the lymph nodes and 'M' the presence of metastasis. A number is assigned to the T/N/M indicative of size and metastatic status. The TNM system is further annotated, details are as follows:

Primary Tumours (T); TX - Primary tumour cannot be evaluated, T0 - no evidence of primary tumour, Tis - Carcinoma in situ and T1, T2, T3, T4 refer to the size/ severity of the primary tumour.

Regional Lymph Nodes (N); NX - regional lymph nodes cannot be evaluated, N0 - no regional lymph node involvement and N1, N2, N3 depicts the involvement of regional lymph nodes and to what extent.

Distant Metastasis (M) – MX distant metastasis cannot be evaluated, M0 - no distant metastasis and M1 distant metastasis is present.

Further categorisations of the above TNM combinations are then graded as follows;

Stage 0 - Carcinoma in situ, Stage I, Stage II, and Stage III Higher are indicative of the extent of cancer: Larger tumour size and/or spread of the cancer beyond the organ in which it first developed to nearby lymph nodes and/or organs adjacent to the location of the primary tumour. Stage IV - the cancer has metastasised to another organ(s).

The above information regarding the TNM system was taken from (National Cancer Institute 2009, <http://www.cancer.gov/cancertopics/factsheet/detection/staging>).

Currently the main course of action for the treatment of tumours is by surgical removal, chemotherapy, radiotherapy, systemic adjuvant treatments and in recent times some agents have been used to achieve a more targeted approach (Koch et al 2010).

A brief account follows which considers the history of how both chemotherapy and radiotherapy have been implemented as anticancer therapies within the clinical setting. Secondly, a compilation anticancer therapies in table format aims to summarise the range of treatments available with an overview of how they are administered, anti-cancer mechanisms and possible side effects.

It is documented that work by German scientist Paul Ehrlich lead to the adoption of the widely used term 'chemotherapy' (DeVita and Chu 2008). During turn of the 20th century, the focus of his work was the discovery and advancement of drugs to combat infectious disease. Amongst Ehrlich's achievement was the use of animal models to enable assessment of potential anticancer agents.

With reference to a cancer chemotherapy timeline by DeVita and Chu 2008, it took approximately 40 years to develop a suitable experiment model (DeVita and Chu 2008). Although this period included the revolutionary success of transplantable tumour rodent models by New Yorker George Clowes a surgeon/ researcher from the Roswell Park Memorial Institute.

With regard to early anticancer therapeutics, 1908 saw the use of arsenicals which had been originally used to eradicate Syphilis (DeVita and Chu 2008). 'Fowlers solution' (arsenicals) as it was known, was used to treat leukaemias and apparently a common practice well into the 1930's (Papac 2001).

Optimism arising from these early triumphs in cancer therapy was dampened following work investigating the use of nitrogen mustard (1943) to eradicate lymphomas. (DeVita and Chu 2008). Reports stated that patients suffering from lymphomas experienced only short-lived remission and thus began a decline of confidence in the concept of 'a drug to cure cancer'.

It was not until the opening of the Cancer Chemotherapy National Service Centre (CCNSC) in 1955 that a possible future for cancer drug development was confirmed (DeVita and Chu 2008). This change of heart was said to be encouraged by the positive response to the drug methotrexate in children with acute leukaemia. Since the 1960s, the development of anti-cancer drugs has been aided by many advances. Experimental models which employ xenografts and novel cell culture methods have been used. Adjuvant therapy (chemotherapy, radiation therapy, hormone therapy, targeted therapy, or biological therapy) given in addition

to the primary treatment was developed and investments into molecular biology have been made. From the beginning of the 21st century, there seems to have been a different approach in anticancer therapeutics emerging (DeVita and Chu 2008). Completion of sequencing of the genome appears to have led to a more targeted approach to cancer treatment. Through advancements in chemotherapy a major decrease in mortality is seen by 2007, the latter considering knowledge of prevention and improvements in diagnostics.

Radiotherapy/ Radiation Oncology are terms which are commonly associated with cancer treatment with an estimated 50% of patients receiving this form of anticancer therapy for both palliative and therapeutic means (Delaney et al 2005). In combination with other forms of management, radiation therapy features in approximately 40% of those patients who are cured of their disease (Shariq et al 2009).

After the German physicist Wilhelm Roentgen discovered x-rays in 1895, the concept of using x-rays as a therapeutic aid was not long to follow, assisted greatly through work on radioactive elements (radium, polonium) by Marie Curie and husband Pierre (Connell and Hellman 2009). There have been numerous clinical, technological and biological advances in radiotherapy since Roentgen's breakthrough over 115 years ago. Examples of key clinical advances are Henri Coutard using fractionated external beam radiotherapy (XRT) in 1928 to cure head/ neck malignancies, the use of the proton beam (1961) and the high precision accuracy of stereotactic body radiotherapy (1995) (Connell and Hellman 2009).

A large proportion of patients, however, still exhibit metastasising cancers even after treatments such as combination radiotherapy. (Koch et al 2010). One explanation could be the inadequate targeting of cancer stem cells (CSCs), i.e. CSCs could be sheltered by hypoxic tumour environments enabling them 'radio-resistant'. Therefore increased doses of radiation could be concentrated to these specific resistant areas. The following proposal (Figure 1.5) by Koch et al (2010) suggested how CSC-predictive test regime and radiotherapy could be implemented.

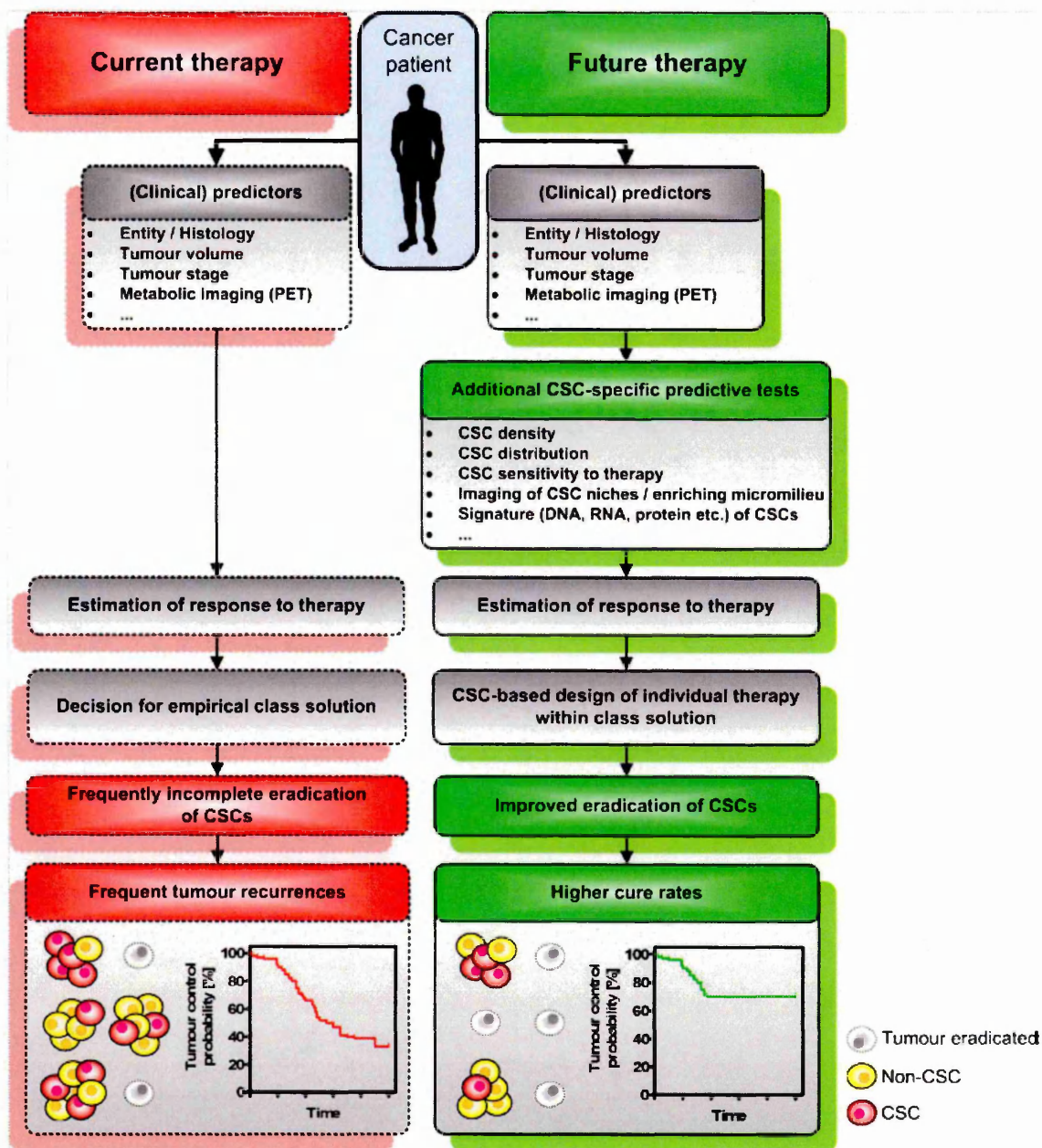


Figure 1. 5 : Proposal of adding CSC specific predictive tests to therapy regimes for potential increase in tumour control probability (Koch et al 2010).

Table 2 gives a list of current anti-cancer therapies, administration routes, mechanism and possible side effects related to the particular therapy.

Anti-cancer Therapy	Administration Route	Anti-cancer Action	Examples of Possible Side Effects
Biological therapy	Orally, injected, intravenous, intradermal/ intramuscular	Targets the immune system, retardation of cancer cells, e.g. IL-2, Interferon alpha,	Rashes, nausea, flu like symptoms, hypotension
Chemotherapy	Orally, injected, intravenous, intra-arterially, insufflation	Targets cells of high proliferative nature altering DNA synthesis/ function, interference with cell cycle e.g. alkylating agents(Cisplatin), antimetabolites (methotrexate), antitumor antibiotics (Bleomycin), anthracyclines (Idarubicin), plant alkaloids (Vinblastine), taxanes (Paclitaxel), monoclonal antibodies (Bevacizumab),	Hair loss, rashes. diarrhoea, nausea/ vomiting, digestion issues, fatigue
Radiation Therapy	Patient exposure to source of radiation, localised beam	Exploitation of rapid dividing cell types, exposure of radiation to tumour regions	Hair loss, rashes. diarrhoea, nausea/ vomiting, digestion issues, fatigue, neutropenia
Targeted Therapies	Orally (small molecule inhibitors), Intravenously (monoclonal antibodies),	Target high proliferative cells, Inhibitors of angiogenesis, tyrosine kinase receptor inhibitors, to impede tumour enlargement and survival	Nausea/ vomiting, rashes, diarrhoea, skin discoloration, dyspepsia, fluctuations in blood pressure

Proton Beam Therapy	Patient exposure to source of radiation, highly specific localised beam	Based on stability of protons enabling 3D manipulation of beam. Highly specific to tumour region with minimal exposure to normal tissue	Hair loss, rashes. diarrhoea, nausea/vomiting, digestion issues, fatigue, neutropenia
Surgical Oncology	Performed by Surgeon pre/post chemotherapy or radiotherapy if malignant	Surgical removal of tumour tissue plus some healthy tissue from periphery, transplantation of bone marrow	Risk of infection, hair loss, by 'preparative regimen' (bone marrow transplant surgery) diarrhoea, nausea/vomiting, fatigue
Gene Therapy	After transduction cells are reintroduced into patient by intravenous infusion, insufflation, directly into tumour if accessible	Cancer cells that have taken up transduced cells are said to have increased susceptibility to chemotherapy and other anticancer treatments	Long term side effects unknown, flu-like symptoms, hypotension, vomiting, nausea
Hormone Therapy	Orally, injection, surgical intervention	Interference with hormone cell surface receptors to block activation of a particular hormone thought to encourage tumour growth, e.g. Tamoxifen – anti-oestrogen, Fulvestrant – oestrogen receptor antagonist	Flu-like symptoms, weight gain, thrombosis in rare cases, alopecia, muscle/ joint pain
Vaccine Therapies	Presently trialled on patients with advanced illness, not yet amongst the mainstay of	Aim to induce tumour immunogenicity	Long term side effects unknown, flu-like symptoms, vomiting, nausea

	anticancer treatments, the search for novel tumour associated antigens is underway		
Complementary / Alternative Medicine	Various routes of administration	Numerous categories some which include; spiritual healers, dietary intervention, herbal medicines, psychological methods, cultural techniques based on tradition	Advice required for the patient to consider possibility of cross reactivity with convention means of treatment

Table 2: Current anti-cancer treatments (Oncolink 2010., National Cancer Institute 2009).

1.1.4 Vascular targeted strategies

Targeting the tumour vasculature is a promising anticancer strategy and drugs of this nature are in various stages of clinical trials. Here, the types of vascular -targeted therapies (VTTs) will be discussed looking at pitfalls, limitations and future aspirations regarding this kind of approach to anticancer medicine. Firstly a brief overview will describe the targets and mechanisms of VTTs focusing then on the vascular disrupting agent Combretastatin A-4-3-O-phosphate (CA-4-P/ ZybrestatTM/ Fosbretabulin).

The importance of angiogenesis in the development and rejuvenation of tumour tissue was initially suggested by Folkman in 1971 (Folkman 1971). *In vivo* experiments using rodent models carried out by Denekamp, showed that blocking and interference of the tumour blood supply resulted in deterioration of tumour tissue (Denekamp 1990). Denekamp then proposed the tumour endothelium as a therapy target by exploiting its high proliferative fragile nature to ultimately interfere and/or destroy the tumour vasculature.

Vascular targeted agents can be divided in to two main categories (Table 3) *i.e.* those which inhibit formation of new blood vessels (antiangiogenic) and the vascular disrupting agents which take advantage of the substandard micro-architecture of the tumour vasculature (Siemann et al 2005). Examples of VTTs and targets are shown in Table 4.

Vascular-targeted therapy	
Antiangiogenic agents	Vascular disrupting agents
Stop new vessel formation (neovascularisation)	Disrupt architecture of tumour blood vessels
Continual treatment	Acute treatment
Early stage – asymptomatic metastases	Established disease, effective against large tumour masses, cause central necrosis

Table 3: Categorisation of vascular targeted therapies (Siemann 2005).

Vascular-targeted strategies

Antiangiogenic		Vascular disrupting	
Target	Example	Target	Example
VEGF/VEGFR inhibition	1-3 Bevacizumab, Trap, ZD6474	VEGF- Tubulin	C-A-4-P, AVE8062A
Tie-2/angiopoietin	A422885.66	Cytokine induction	DMXAA
Avβ3 integrin	Vitaxin, cilengitide	Ab Toxin	VEGF-gelonin
Endogenous inhibitors	Angiostatin	Avβ3 integrin	Gene therapy, peptide targeting
VE-cadherin	E4G10	Unknown	PDT
Unknown	Thalidomide		

Table 4 : Example of drugs within each category (Siemann 2005).

The design hypothesis of antiangiogenic agents is to hamper the cascade of biochemical events that result in new vessel development (Siemann 2005). Amidst the complex array of signals and receptors which govern the latter process, vascular endothelial growth factor (VEGF) is thought to be an important target for impeding angiogenesis. An example of anti angiogenic therapy is Bevacizumab/ Avastin, this uses monoclonal antibodies to target VEGF or its' receptors, as does ZD6474 a tyrosine kinase inhibitor. (Wedge et al 2002). One treatment success story of Bevacizumab was when it was used in fluorouracil based combination chemotherapy to treat colorectal cancer. (Hurwitz et al 2004).

Table 5 illustrates the stages of angiogenesis and goals of the 'antiangiogenic' approach. (Siemann et al 2005).

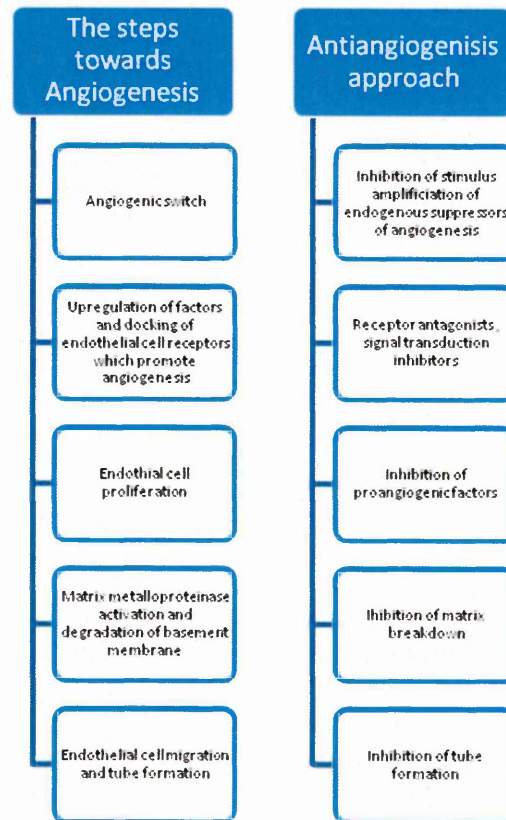


Table 5 : Inhibiting the process of angiogenesis (Siemann et al 2005).

1.1.5 Vascular disrupting agents

Vascular disrupting agents (VDAs) exploit the characteristic tumour vasculature (Figure 1.6) which is notoriously sinusoidal and leaky, and is hence susceptible to vascular disruption. (Tozer *et al* 2008). Shortly after administration of VDAs major shutdown occurs of the tumour vascular network.

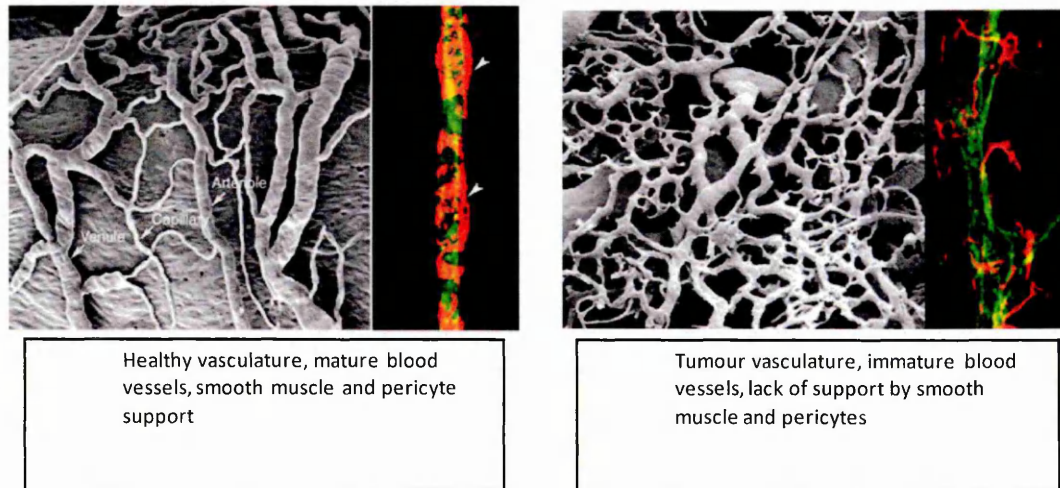
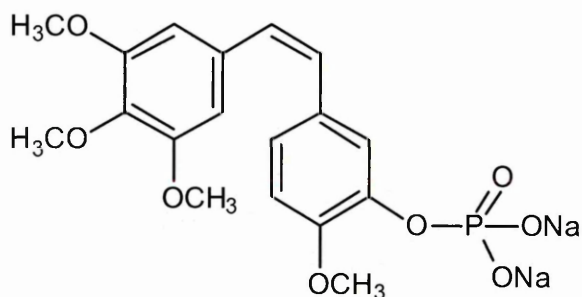


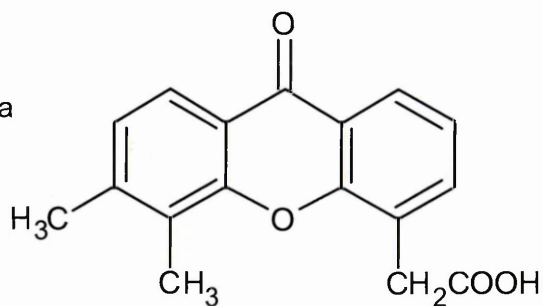
Figure 1. 6 : Images to illustrate the substandard tumour vasculature (Oxigene 2010).

Flavanoids (e.g. DMXAA) and tubulin-binding agents (e.g. CA-4-P) are VDAs, both are designed to disrupt tumour blood vessels but work in different ways as the chemical structures suggest in Figure 1.7.

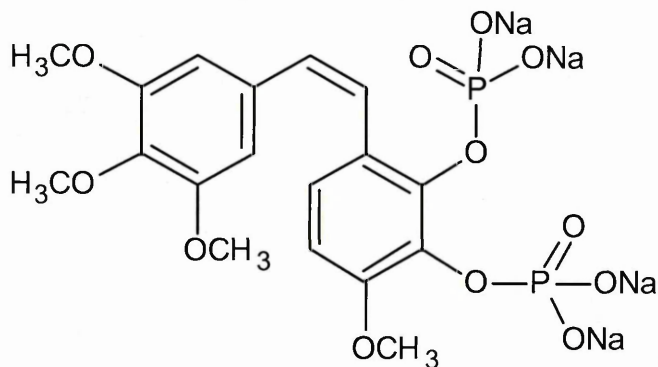
CA-4-P (Fosbretabulin)



DMXAA (Vadimezan)



CA-1-P (Oxi4503)



AVE8062 (Ombrabulin)

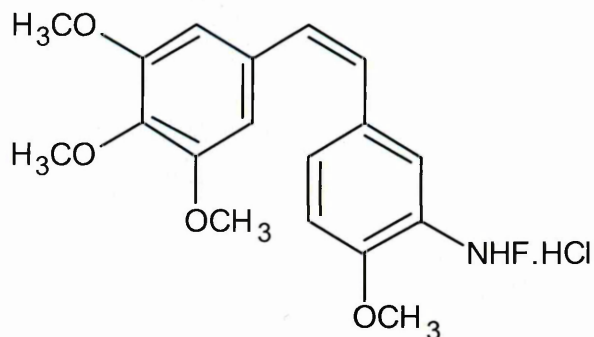


Figure 1. 7 : Chemical structures of vascular disrupting agents (Kanthou and Tozer 2007).

The mechanism of 5,6-dimethylxanthone-4-acetic acid (DMXAA/ ASA404) is still not yet fully understood but it is thought to operate via the induction of TNF- α . (Thorpe et al 2003). Through the action of DMXAA it is suggested that TNF- α is retained within the tumour microenvironment thus stimulating additional amounts of TNF- α amongst other cytokines. The tumour blood vessels are weakened with the subsequent changes in morphology leading to haemorrhagic necrosis (Kanthou and Tozer 2007). In Phase I clinical trials DMXAA showed the drug had a well tolerated anti-tumour action, Phase II involved combination with

conventional chemotherapy agents with positive outcomes when used in non-small cell lung cancer patients. DMXAA then moved into Phase III clinical trials which unfortunately did not produce the same effects as in its early trial success (Buchanan 2012).

Microtubule depolymerising agents have a destructive effect on the architectural integrity of 3D capillary composition (Bayless and Davies 2004). The following diagrammatical representation (Figure 1.8) from a paper by Kanthou and Tozer (2007) details the proposed mechanism of action of a microtubule depolymerising agent (e.g. Combretastatin A-4-3-O-phosphate).

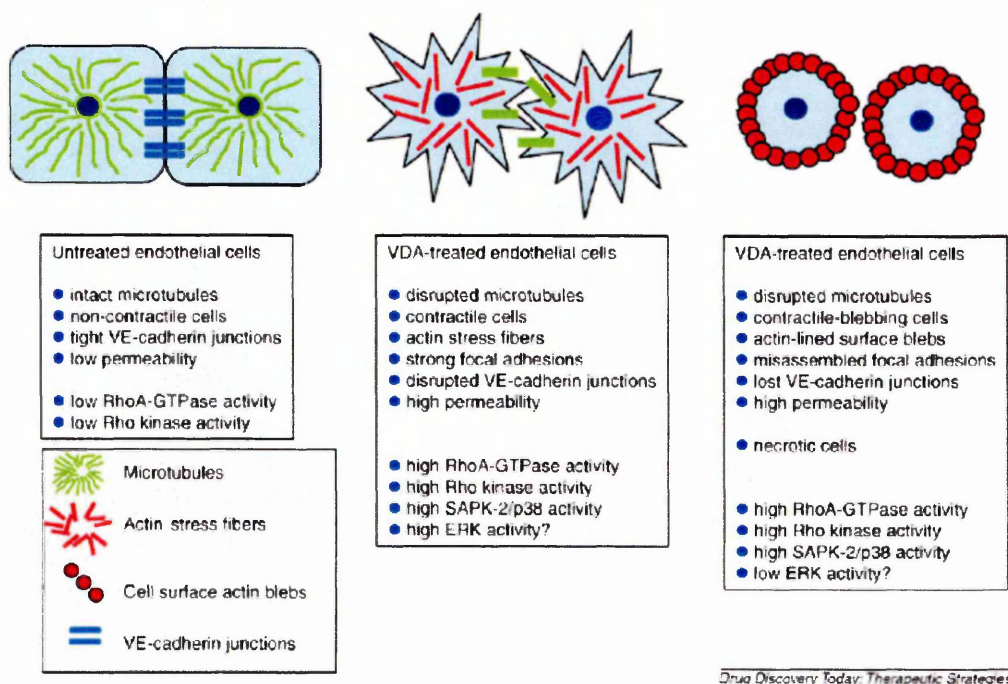


Figure 1. 8 : Proposed mechanism of action of Combretastatin A-4-3-O-phosphate (Kanthou and Tozer 2007).

It is suggested that increased permeability post CA-4-P administration is a major factor in the disruption of endothelial organisation; this is evident from Figure 1.8 (Kanthou and Tozer 2007). Interference in vascular integrity due to abnormality in the cytoskeleton, subsequently leads to stress fibre formation and endothelial cells as a result become more rounded ('blebbing'). Haemorrhagic necrosis follows exacerbating the already hypoxic regions within the tumour microenvironment.

The remodelling of the actin cytoskeleton and formation of actin stress fibres shown in Figure 1.8 is clearly demonstrated in the Figure 1.9 adapted from Kanthou and Tozer 2002 and has also been shown by Siemann (2010).

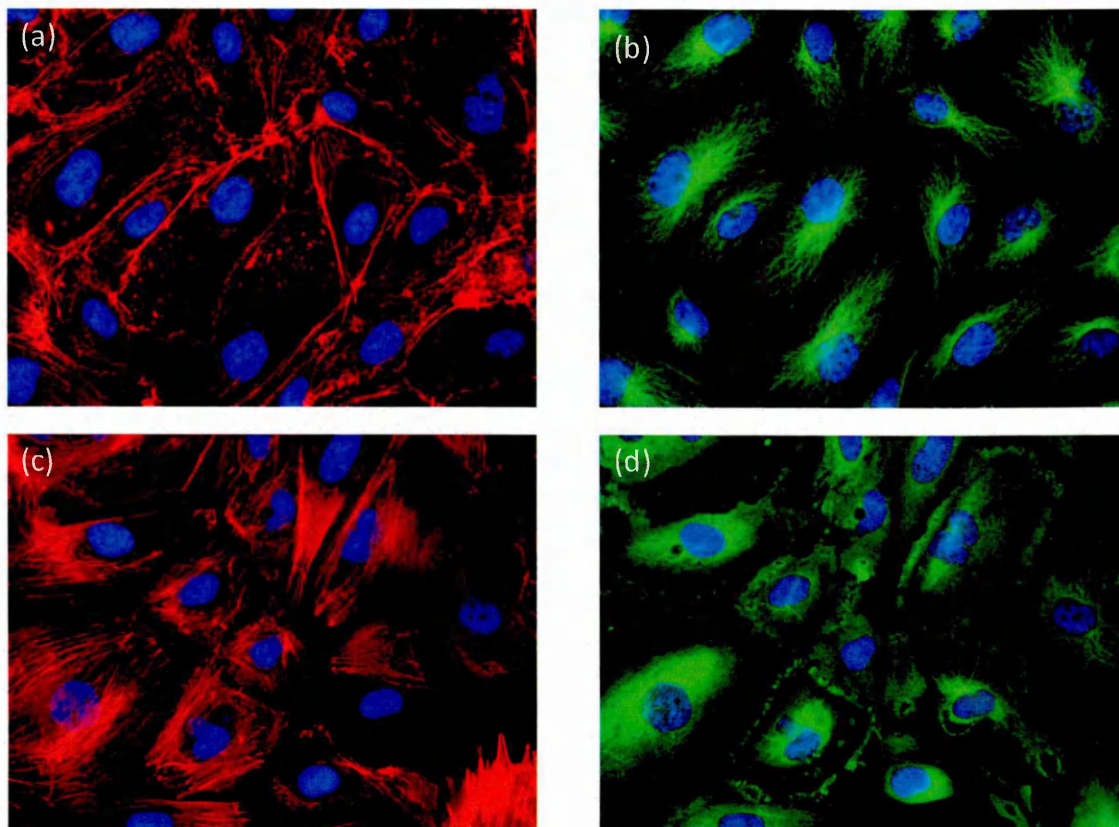


Figure 1. 9 : Fluorescent staining of Human umbilical vein endothelial cells, Control and post CA4P administration (Kanthou and Tozer 2002). Figure 1.9 shows dual staining for filamentous actin (Texas Red Phalloidin (red)) and beta tubulin (green): (a) control actin, (b) control tubulin, (c) CA4P (1 uM for 30 min) actin, (d) CA4P (1 uM for 30 min) tubulin.

In vivo studies using CA-4-P have clearly shown how the effects of the drug can induce vascular shutdown resulting in increased hypoxia. (Tozer et al 2008). Studies on mouse models (Figure 1.10) looking at hypoxic responses in mammary carcinomas after 50mg/kg CA-4-P, indicated increased pimonidazole staining compared to non treated. Similarly, dorsal skin flap experiments in mice (Figure 1.10) displayed the de-vascularising properties of CA-4-P 110mg/kg.

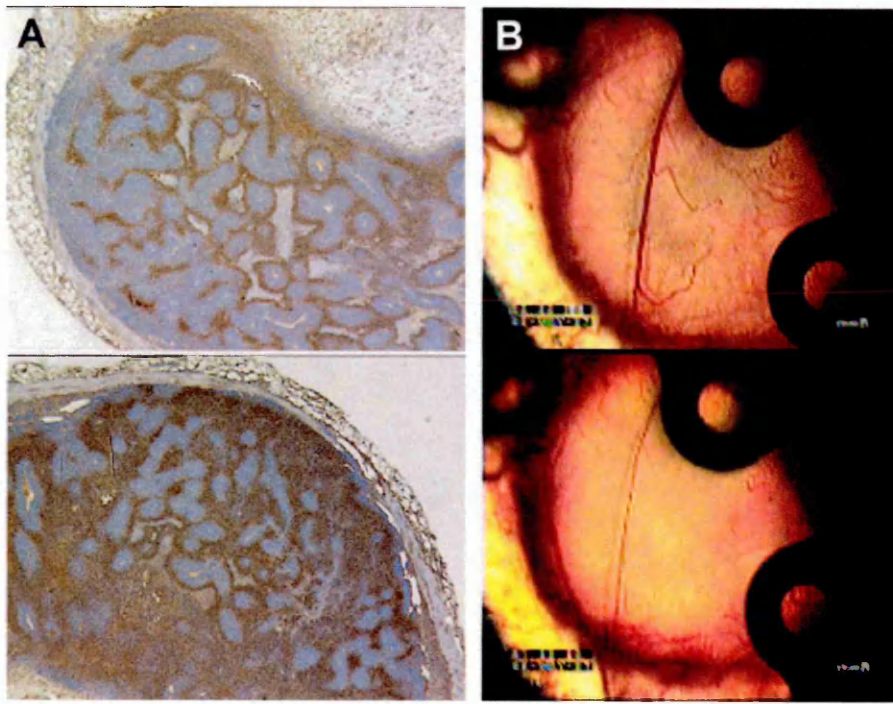


Figure 1. 10 : CA-4-P and its effect on hypoxia induction and vascular shutdown (Tozer et al 2008). Panel A shows pimonidazole staining of the control untreated tumour at the top with the bottom being 1 hour after CA-4-P, panel B is the untreated image of a rat bearing P22 sarcoma directly below is the tumour 1 hour 40 min post CA-4-P administration in vivo using a window chamber method for analysis of treatments effects.

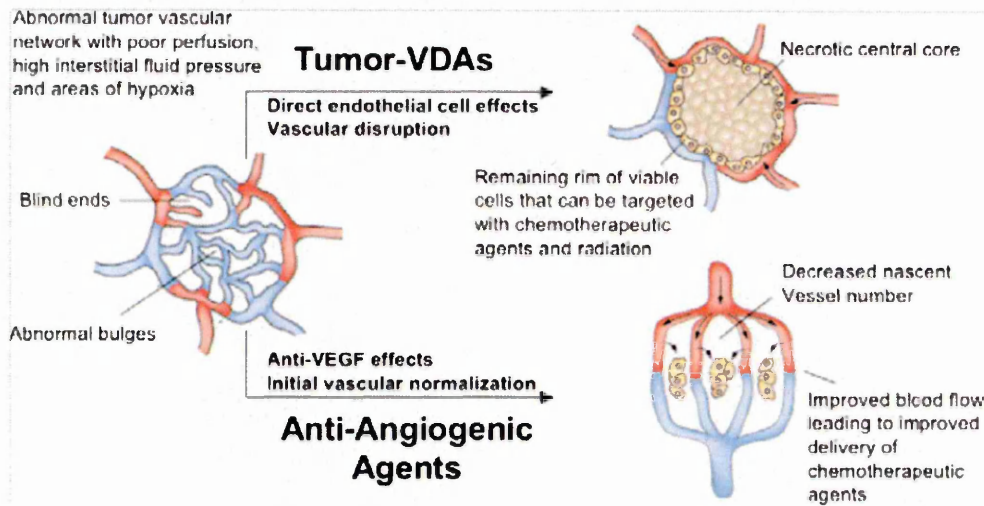


Figure 1. 11 : Exploitation of tumour vasculature by antiangiogenic treatment and vascular disrupting agents (Siemann 2010).

To summarise the different actions of both VDAs and antiangiogenic treatments a diagram (Figure 1.11) by Siemann (2010) highlights the preclinical effects of each type.

With all new drugs/ therapies in development there are numerous complications to overcome and consider i.e. the therapeutic window with the balance between safe dosage and the onset

of adverse effects. The phrase 'tumour evasion' frequents many article titles and appears to be a key issue in the advancement of this type of anti-tumour medicine.

Zhi-Chao and Jie (2008) present valid points within their review on tumour evasion in a section entitled "Hypoxia: Two sides of the coin". They state that disruption by vascular targeted treatment to increase hypoxia severing the lifeline of the tumour, can indeed have undesirable consequences. It is suggested that there is a requirement to unravel some 'cause-effect' connection. Hypoxia-inducible factors (HIF) have been known to correlate with the up-regulation of VEGF, involved in angiogenesis regulation. So could VTTs amplify the angiogenic process after the creation of an increased hypoxic tumour environment? Hypothetically speaking this could even help the metastatic process ensuing tumour invasion. (Abdollahi and Folkman 2010).

Evasion of the hosts' immune system is one feat that the tumour is capable of and there is a school of thought that claims there could be a similar evasion mechanism in place against VTTs. The heterogeneous nature of the tumour mass could well contain a cell population deemed oblivious to vascular targeted strategies. (Zhi-Chao and Jie 2008). The latter is supported by the hypothesis of four possible vascular phenotypes in existence; normal pre-existing, tumour phenotypic vessels, neo-vasculature which is normal and abnormal neo-vasculature. This could explain why some cells remain unaffected including the well documented viable tumour rim. (Hinnen and Eskens 2007).

The viable tumour rim being a speculative resistance factor is also thought to achieve evasion through its positioning, adjacent to the non-diseased tissue. (Tozer *et al* 2008). Consequently, seizing oxygen and essential nutrients as it resides in this prime location.

The explanations why resistance issues exist against VTTs appears to be complex and multi-factorial. That said progress is being made through various combination therapies. Xenograft experimental models displayed increased quantities of VEGF and basic fibroblast growth factor following doses of CA-4-P, with angiogenic circulating progenitor cells in murine studies. (Tozer *et al* 2008) Promising responses have been reported by using VDAs and anti-angiogenic VEGFR tyrosine kinase inhibitor treatments in combination therapy.

1.1.6 Biomarker Discovery

When considering biomarker discovery as it relates to oncology many complexities exist. There are countless biochemical pathways with numerous prospective targets, with more layers of complexity added by the multifaceted characteristics of the cancer cell. A cell unchallenged by host immunogenicity, that has mastered tissue invasion and anti-cancer drug evasion. Nevertheless a good place to start is given by the 'hallmarks' of cancer created by Hanahan and Weinberg (2000).

Whilst the 'hallmarks' of cancer reveal the attributes and capabilities of this lethal cell type, a further proposal by Lord and Ashworth (2010) relates the possible drug targets to each characteristic of the cancer cell to provide inspiration for biomarker exploration. (Lord and Ashworth 2010). A diagram in the article by Lord and Ashworth (2010) supplies a wealth of information on the latter subject however, one consideration to be made is the possible upshot from molecular interactions and when choosing one trait to target such as 'sustained angiogenesis' or 'proteotoxic stress'.

This concern is echoed by Lord and Ashworth (2010) as they discuss how in order to decipher cancer mechanistic, medicine should bear in mind how drugs disturb whole biochemical networks as opposed to solitary pathways. A concept which has been termed, "*drugging the undruggable*".

Over a decade after their original paper, Hanahan and Weinburg (2011) proposed an updated version of '*The Hallmarks of Cancer*' entitled '*Hallmarks of Cancer: The Next Generation*'. The idea of two additional hallmarks of cancer were put forward these being the "*reprogramming of energy metabolism*" and "*evading immune destruction*".

Figure 1.12 displays the original hallmarks with the addition of 'deregulating cellular energetics' this referring to reprogramming of cellular metabolism in favour of proliferation and 'avoiding immune destruction' which describes the ability to fend off advances from macrophages, natural killer cells and T/ B lymphocytes (Hanahan and Weinburg 2011). The article proposes two enabling characteristics, genome instability and mutation and tumour-promoting inflammation. Both of which are said to be key orchestrators in the original and emerging characteristics.

Hanahan and Weinburg also included therapeutic suggestions to hinder a particular cancer hallmark as shown in Figure 1.8.

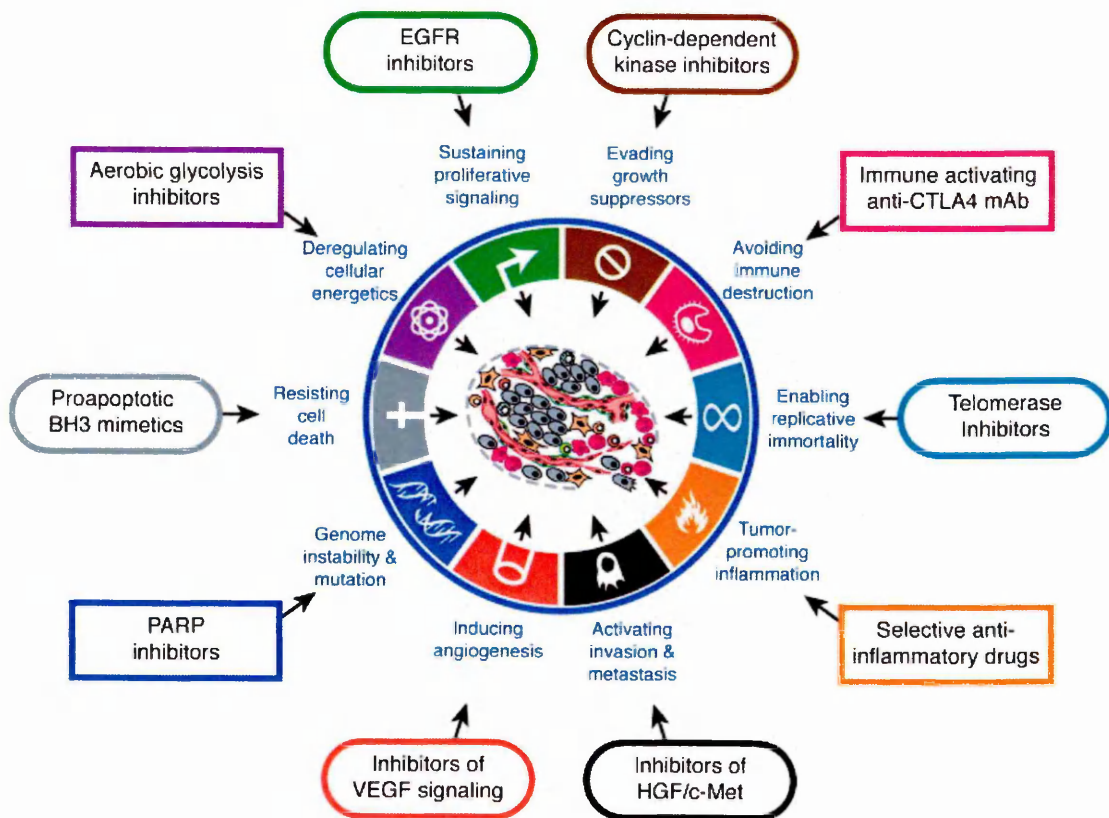


Figure 1. 12 : Therapeutic targeting of the hallmarks of cancer (Hanahan and Weinberg 2011).

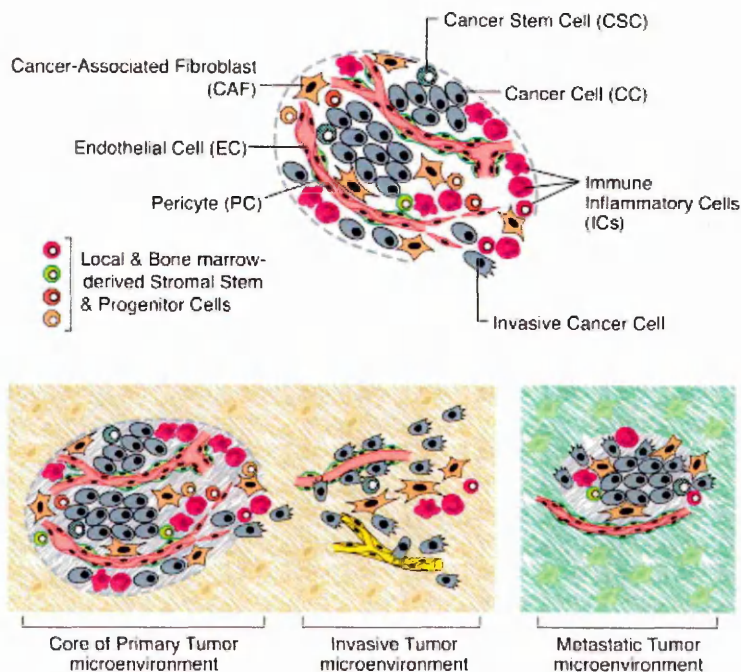


Figure 1. 13: The cells of the tumour microenvironment. (Hanahan and Weinberg 2011).

Advances in the knowledge of the individual cancer cells that make up the solid tumour have enabled appreciation of their influential drive on the tumour microenvironment. Figure 1.13

depicts the varied cell types and sub types. Each cell has a specialised role and collectively supports the plasticity required for tumourigenesis (Hanahan and Weinberg 2011). Interestingly it is known that the inflammatory immune cells present within this cellular assemblage, possess both pro-oncogenic and anti-tumour activity. The latter is thought to aid future tumour seeding during the metastatic process.

1.1.7 Considering Vascular disrupting agents for anti-cancer therapeutics

It is known that one vessel is primarily responsible for supplying the tumour cell population with oxygen and nutrients for growth, development and excretion of waste metabolites. (Thorpe et al 2003). Disruption of this vital sustenance by vascular disrupting agents causes rapid shutdown of blood flow to and from the tumour.

Unlike some conventional cancer therapies which focus on cell killing VDAs create damage via morphological changes to produce drastic effects on the tumour microenvironment. Drug deliverance is simple due to endothelial positioning near the bloodstream.

In addition to the above, another reason to support the use of vascular targeted therapy is that the diploid target cells are thought not to be as drug resistant due to low risk of mutations. The drug has good clinical measurability being blood flow, in most cases short-term exposure of a VDA creates sufficient hypoxic conditions. To conclude, intermittent dosage with regular treatments may be adequate to provide a synergistic effect, not true in the case of antiangiogenesis agents. (Thorpe et al 2003).

1.2 The Role of Mass Spectrometry in Biomarker Discovery

1.2.1. Overview of mass spectrometry as an analytical tool

Mass spectrometry can be applied to numerous analytical subject areas from the food industry to forensic applications to complement various diagnostic and prognostic techniques (Griffiths 2008). Techniques using mass spectrometry have supported the advancement of proteomics, metabolomics, lipidomics and atomic physics to forge a place within the clinical setting.

Proteomics is a platform for potential biomarker discovery and mass spectrometry is widely used as a discovery tool (Anderson 2005). Advances in mass spectrometry instrumentation have resulted in high mass accuracy and vast improvements in sensitivity and specificity (Al-Shahib 2012). The forward momentum of mass spectrometry has led to the analysis of diseased and non-diseased tissues supported by bioinformatics.

Recent experimental work by Röwer *et al* (2011) showed development in the early diagnosis of invasive ductal breast carcinoma through protein signatures and structural analysis. Such progress in the identification of disease biomarkers could not only benefit patients directly but support future drug design and development.

1.2.2. Basic principles of mass spectrometry

The mass spectrometer uses an ion source (liquid-phase/ solid-state) to transfer the analyte into gas phase ions which then travel to the mass analyser to be sorted according to mass-to-charge ratio (m/z), finally a detector accounts for the relative abundance of each ion at a particular m/z (Hoffmann and Stroobant 2007). Instrumental calibration and use of analytical standards is also vital to produce accurate mass measurements whilst using the many different mass spectrometric techniques. External calibration is performed before sample analysis where a known selected compound is used for spectral comparison against a reference list where assignment of exact masses can then be made. Internal calibration describes a calibration method where a reference compound is introduced into the mass spectrometer during sample analysis. This technique compensates for any possible changes in conditions in the analytical instrumentation (Hoffmann and Stroobant 2007).

Figure 1.14 is a representation of the basic principles of the mass spectrometer.

With regard to proteomics there are a variety of mass spectrometers available some of which are described in more detail in later.

The following table (Table 6) adapted from Han *et al* (2008) details commonly used instruments, applications and performance indicated by mass analyser type.

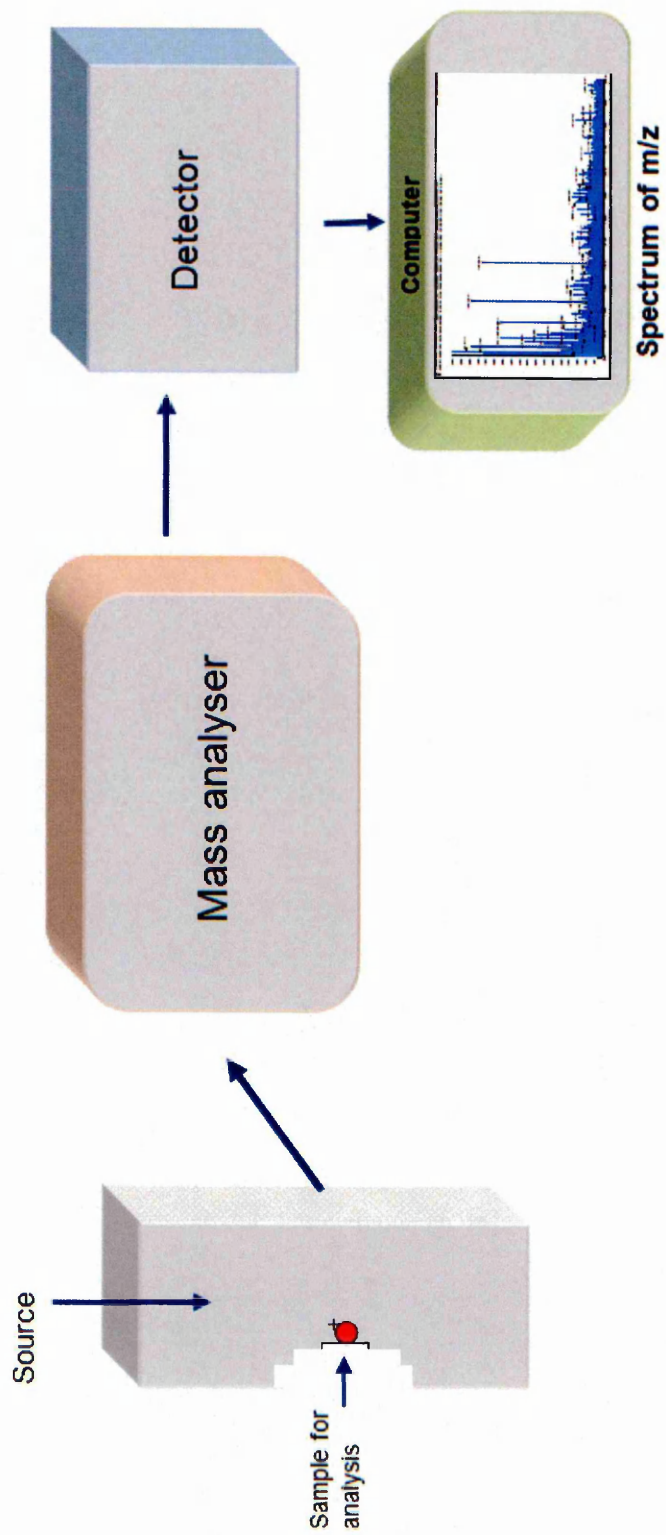


Figure 1. 14 : Basic principles of a mass spectrometer. The basic components comprise of an ion source, mass analyser, detector connected to a data output device allowing analysis of spectral acquisitions.

Instrument	Mass resolution	Mass Accuracy (ppm)	Sensitivity	m/z range	Scan rate	Dynamic rate	MS/MS capability	Ion source	Main applications
QIT	1000 a	100-1000	Picomole	50-2000, 200-4,000	Moderate	1E3	MS nd	ESI	Protein identification, PTM identification
LIT	2000 a	100-500	Femtomole	50-2000, 200-4,000	Fast	1E4	MS nd	ESI	High throughput protein identifications from complex samples, online identification assistance
Q-q-Q	1000	100-1000	Attomole-Femtomole	10-4,000	Moderate	6E6	MS/MS	ESI	Quantification in selective reaction monitoring mode (SRM), PTM detection
Q-q-LIT	2000 a	100-500	Femtomole	5-2,800	Fast	4E6	MS nd	ESI	Quantification in (SRM), PTM detection
TOF	10,000-20,000	10-20b, <5c	Femtomole	No upper limit	Fast	1E4	n/a e	MALDI	Protein identification from in-gel digestion PMF of gel protein band
TOF-TOF	10,000-20,000	10-20b, <5c	Femtomole	No upper limit	Fast	1E4	MS/MS	MALDI	Protein identification from in-gel digestion

	10,000-20,000	10-20b, <5c	Femtomole	No upper limit	Moderate to fast	1E4	MS/MS	MALDI;ESI	PMF of gel protein band, sequence tagging by CID MS/MS
Q-q-TOF									Protein identification from complex peptide mixtures, intact protein analysis, PTM
FTI-CR	50,000-750,000	<2	Femtomole	50-2000, 200-4,000	Slow	1E3	MS nd	ESI;MALDI	Top down proteomics, high mass accuracy, PTM
LITQ-Orbitrap	30,000-100,000	<5	Femtomole	50-2000, 200-4,000	Moderate to fast	4E3	MS nd	ESI;MALDI	Top down proteomics, high mass accuracy, PTM, Protein identification from complex peptide mixtures, quantification

Table 6 : Mass spectrometers for proteomics (Han et al 2008).a, mass resolution achieved at normal scan rate, higher resolution achievable at a lower scan rate, b, with external calibration, c, with internal calibration, d, n>2 up to 13, e, fragmentation available by post source delay.

1.2.3. Ionisation techniques and Mass analysers

In physical chemistry there are four main ways to produce gas phase ions from a molecule interest which are; spray ionisation, desorption ionisation, chemical ionisation and electron ionisation (Cooks 2010). Figure 1.15 shows these ionisation techniques schematically.

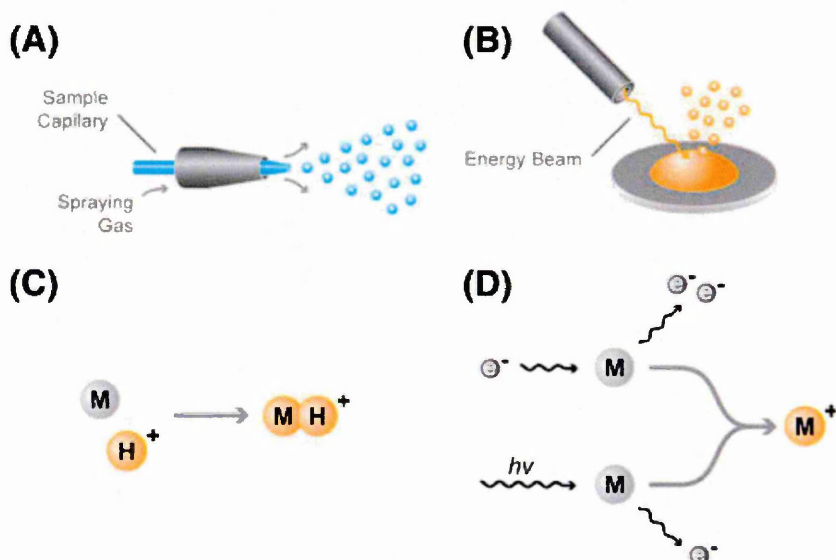


Figure 1. 15 : Basic ionisation techniques. (Pól et al 2010). (A) spray ionisation, (B) desorption ionisation, (C) chemical ionisation and (D) electron ionisation.

Examples of spray ionisation are electrospray and nanospray, these techniques require the sample to be in solution and regularly coupled to an LC system (Pól et al 2010). Secondary ion mass spectrometry (SIMS), desorption electrospray ionisation (DESI) and matrix assisted laser desorption ionisation (MALDI) are all methods using desorption ionisation from a solid surface (Pól et al 2010). The desorption methods previously mentioned are used for image acquisition. Chemical ionisation and electron ionisation use techniques involving gas-phase ion-molecule reactions at atmospheric pressure, atmospheric pressure chemical ionisation (APCI) and electron impact are such techniques. APCI can be applied to polar and relatively non-polar molecular analysis with electron ionisation is useful for organic compounds.

Figure 1.16 displays current mass analysers at use in the analytical laboratory.

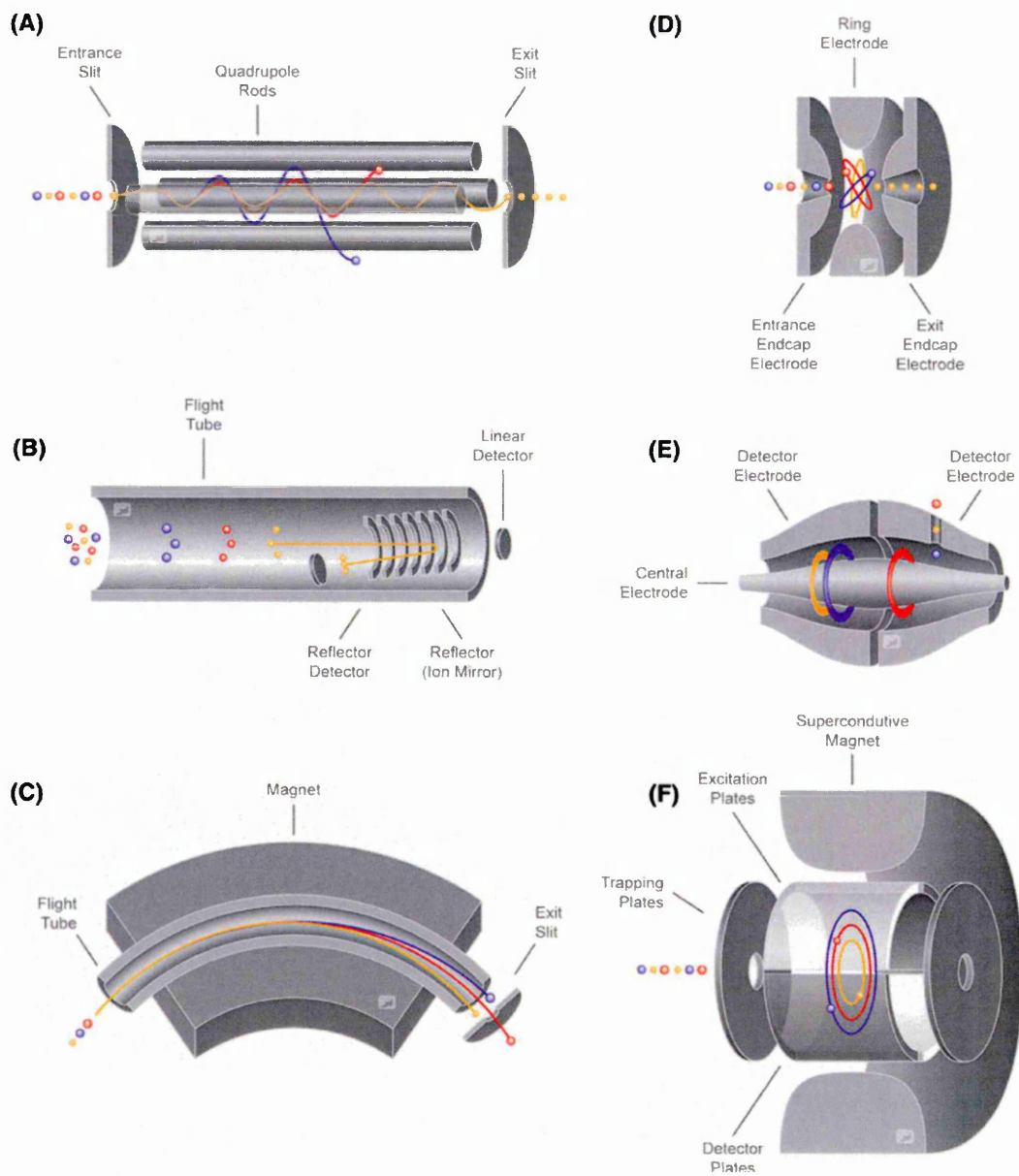


Figure 1. 16 : Mass analysers used in mass spectrometers. (a) Quadrupole, (b) Time-of-flight (TOF), (c) Magnetic sector, (d) Ion trap, (e) Orbitrap, (f) Ion cyclotron resonance. (Pól et al 2010,. Trim et al 2012).

1.2.4. Proteomics using mass spectrometry

Currently mass spectrometers allow interpretation of complex protein mixtures that contain post translational modifications (PTMs) through fragmentation techniques (Hoffmann and Stroobant 2007). Tandem mass spectrometry (MS/MS) describes the selection of a precursor ion which then undergoes collision induced dissociation (CID) by an inert gas to generate a product ion spectrum. b and y ions are generated due to shattering of the peptide C-N backbone (Hoffmann and Stroobant 2007). To illustrate the stages of protein identification in more detail the flowchart shown in Figure 1.17 adapted from Han *et al* (2008) segregates the various methods into either bottom-up or top-down proteomic methods (Han *et al* 2008).

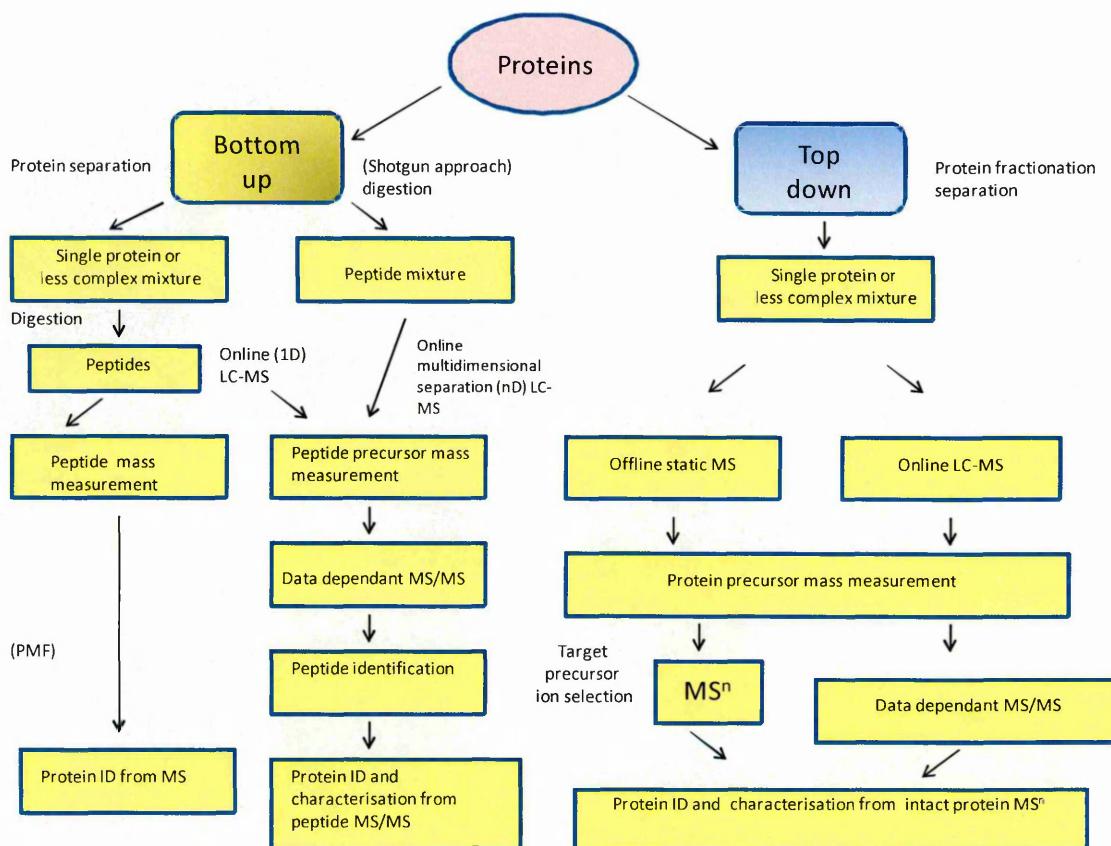


Figure 1. 17 : Protein identification methods (Han et al 2008).

An article by Djidja et al (2009) regarding the profiling and imaging of glucose-regulated protein 78 kDa (Grp78) contains an clear example of peptide identification from the peptide mass fingerprint (PMF) of a tryptic digest, a bottom-up method. Here in-situ tryptic digestion was performed directly onto tissue sections, the resulting PMF allowed selection of precursor

ion for MS/MS. Peptide sequences/ MS/MS spectra are then entered into algorithmic bioinformatics programmes i.e. MASCOT that can result in protein identification through searches performed against a protein database such as UniProt KB/ Swiss-Prot.

Interpretation of comparative proteomics data in itself presents a huge challenge and Hodgkinson *et al* (2011) published an antibody microarray proteomic study based on the theory proposed by Petrak *et al* (2008) that such experiments possibly result in '*repeatedly identified differentially expressed proteins*' (RIDEPs). Petrak *et al* (2008) devised a list of 15 'RIDEPs' that were commonly observable in human and rodent samples. Amongst the RIDEPs were heat-shock protein 27, peroxiredoxins, annexins and enolase 1 with proteins such as zyxin and smad4 found by Hodgkinson *et al* (2011). The latter could provide a good place to start in any shotgun proteomics experiment, especially assessment of a treatment response time course and how these proteins appear to be differentially expressed.

Frequently MS/MS alone is not sufficient enough to provide a good clear fragmentation spectrum from the parent ion. Especially when analysing the high abundance of ions generated from an *on tissue* digest. The novel concept of ion mobility-mass spectrometry which describes the further separation of isobaric ions indeed facilitates the task of precursor ion selection. (McLean *et al* 2005). Ion mobility separation (IMS) can be applied throughout MS acquisition and then again during MS/MS enabling a 'cleaner' peptide mass fingerprint with improved subsequent precursor fragmentation. IMS will be discussed further later on.

To conclude this section, the vast amount of data currently now attainable in proteomics experiments is remarkable. Dealing with the computational capacity required to process and analyse these data will remain a challenge. However this is imperative to contribute to and advance proteomic analysis.

1.3 Mass spectrometry instrumentation

1.3.1 LC-MS

The diagram in Figure 1.18 shows how the analytical technique of high performance liquid chromatography (HPLC) can be coupled to a mass spectrometer a combination generally referred to as LC-MS. The nature of this method requires the analyte to be in solution for injection onto a column packed with coated silica particles (stationary phase) (University of Bristol 2005). Varying the concentration of the mobile phase passing over the column will then determine what is eluted in to the mass spectrometer for analysis.

The sample can either be collected in fractions (Figure 1.18) or sent to the mass spectrometer via an interface: Electrospray ionisation (ESI), atmospheric pressure chemical ionisation (APCI), thermospray (TSP) and atmospheric pressure photoionisation (APPI) have been or are currently used (Hoffmann and Stroobant 2007).

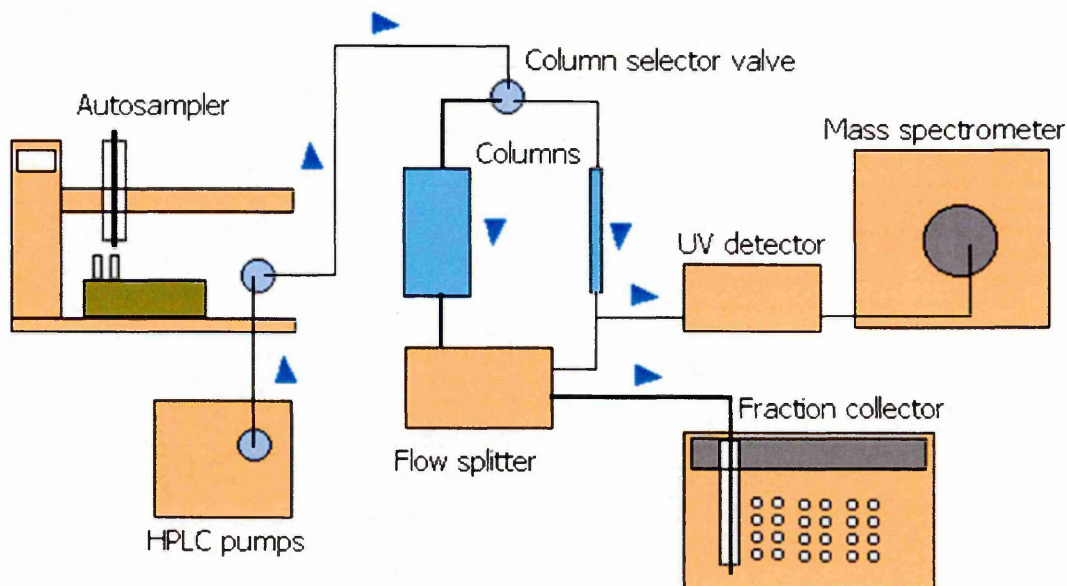


Figure 1. 18 : Schematic representation of a liquid chromatography mass spectrometer. (The LC/MS Unit 2009)

LC-MS/MS is regularly used in clinical chemistry for its universal capacity for the detection and quantification of small molecules (Jong et al 2011). The technique of LC-MS/MS has proven to be invaluable in the diagnosis of pheochromocytoma, a tumour that can develop in the centre of the adrenal gland (Lagerstedt et al 2004). Renowned for its specificity and sensitivity LC-MS has the ability to measure plasma free metabolites metanephrine and normetanephrine occurring in nmol/L, known markers for pheochromocytoma.

1.3.2. Electrospray ionisation (ESI)

Electrospray ionisation mass spectrometry (ESI-MS) is a highly sensitive soft ionisation technique capable of analysing low volume, non-volatile samples (Ho *et al* 2003).

During flow through the sample (in solution) is nebulised under atmospheric pressure via an electrical potential which has been applied to the needle (Gates 2004). Overtime as the multiply charged droplet travels towards the sample cone solvent evaporation occurs resulting in shrinkage. This is due to the 'Raleigh effect' which describes an event where the surface tension can no longer retain the charge (Figure 1.19). The droplet containing the analyte is then ripped apart by 'Coulombic explosion'.

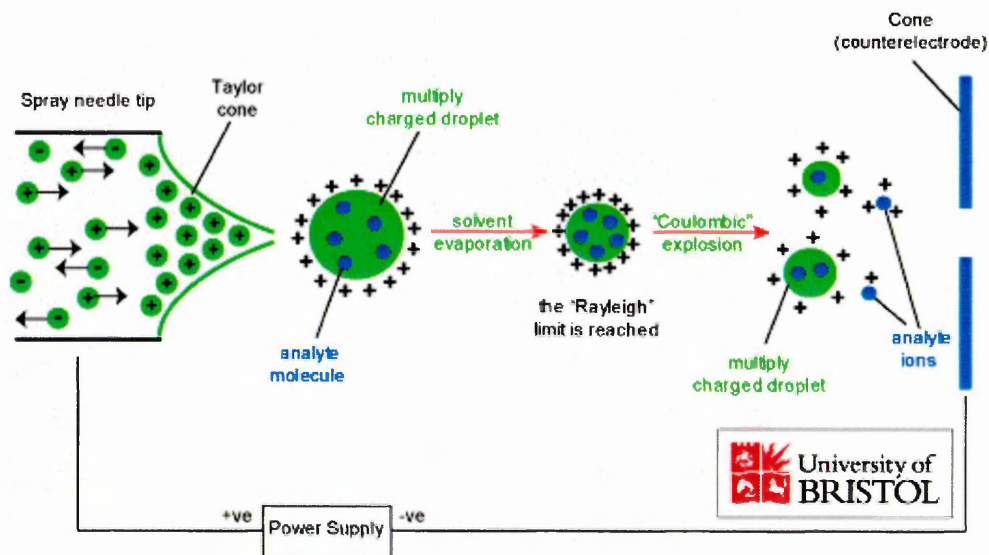


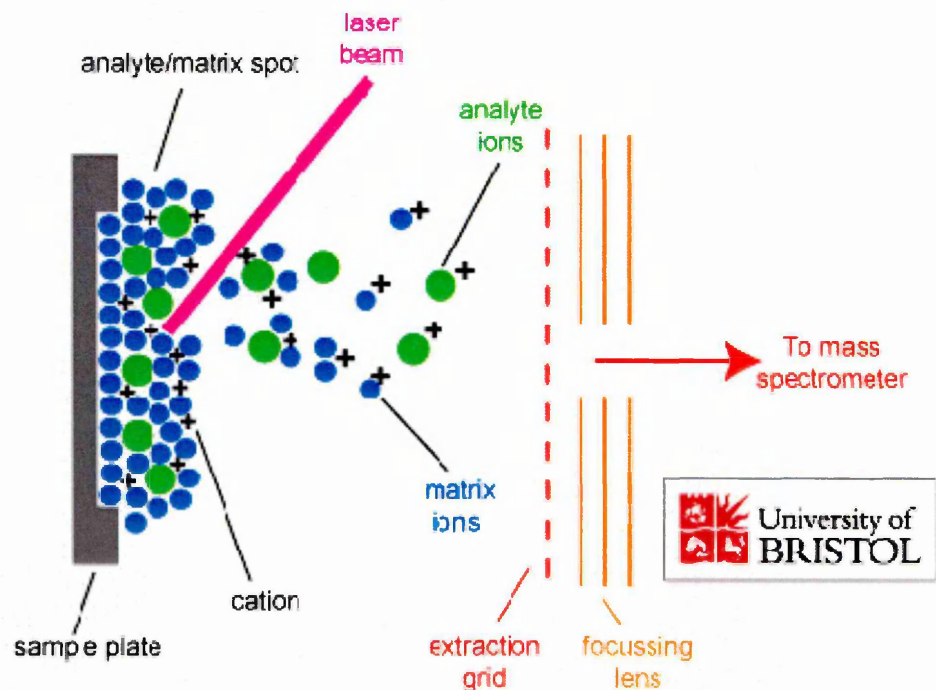
Figure 1. 19 : Schematic of Electrospray ionisation (Gates P 2004).

The multiply charged droplet is expelled from the needle, overtime solvent evaporation occurs resulting in shrinkage of the droplet leading to "Coulombic explosion". There are two models of ion generation in ESI, the ion evaporation model (IEM) and the charged residue model (CRM) (Wand and Cole 2000). The IEM was first introduced in 1976 by Iribarne and Thomson and due to an increasing electrical field present on the surface of the droplet, solvent-ion clusters are discharged (Wand and Cole 2000). In the case of the CRM, continuous droplet fission through continuous solvent evaporation results in the formation of gas-phase ions.

1.3.3. Matrix assisted laser desorption ionisation (MALDI)

Matrix assisted laser desorption ionisation (MALDI) is a soft ionisation technique which is widely used for analysis of non-volatile compounds in many applications including proteomics, lipidomics, synthetic polymers and the study of small molecules.

The matrix plays a key role in the successful ionisation of the analyte. After deposition of the matrix solution onto the sample, formation of matrix co-crystals occurs after drying/evaporation which form a protective coat from the ablation of the laser (Hoffmann and



Stroobant 2007). Under vacuum the laser is pulsed onto the matrix embedded sample and although not completely understood, it is thought that the energy is transferred from the surface of excitation of the matrix crystals to the analyte. The transfer of energy from the laser to the matrix then matrix to the analyte is a two step process resulting in the ionisation of both enabling the sample molecules to remain structurally intact. It is reported that gas phase ion proton transfer is the most accepted explanation for MALDI matrix ionisation (Breuher *et al*/1999). There are also other proposals for this mechanism these being; excited state proton transfer, gas phase photoionisation, ion-molecule reactions and desorption of preformed ions (Hoffmann and Stroobant 2007). Figure 1.20 aims to depict ionisation principles of MALDI.

Figure 1. 20 : Ionisation using MALDI. (Gates 2004). The protonated cloud of ions is shown above the analyte/matrix co-crystallisation.

The formation of Cations with the analyte takes place in the following way;



Selection of a MALDI matrix requires tailoring to the specific analyte chosen and wave length of the laser (Hoffmann and Stroobant 2007).

The matrix needs to exhibit stability under vacuum, be soluble in selected solvent, form adequate co-crystals with the analyte and absorb the laser wavelength (Sigma Aldrich 2001). Examples of common matrices used and the associated applications are listed in Table 7.

The MALDI source consists of a pulsed laser (varying pulse widths) to produce packets of ions to be introduced into the time of flight (ToF) analyser (Hoffmann and Stroobant 2007).

Nitrogen lasers were the initial choice for MALDI and are relatively inexpensive compared to other alternatives, although reports claim that irregularity of the beam can lead to ‘hot spots’ typically due to the heterogeneous nature of the N₂ laser. (Trim *et al* 2010). However the short lifespan of the N₂ laser is an issue when selecting this laser type for MALDI imaging. Therefore these have been largely superseded by the use of ND:YAG solid state lasers. These solid state lasers are a common choice for MALDI-MSI due to their high repetition rate and extended lifespan (Trim *et al* 2012). It is stated that up to 1 kHz having been employed using ND:YAG compared to 20 Hz on a standard N₂ laser and ~1×10⁹ shots compared to 2×10⁷–6×10⁷ shots respectively.

Trim *et al* (2010) proposed 2 other alternatives these being; Nd:YLF (yttrium lithium fluoride) and Nd:YVO₄ (yttrium ortho-vanadate). The latter paper continues to investigate the Nd:YVO₄ laser and details experiments to progress the appearance of the beam using mechanical oscillation to reduce laser ‘speckle’. Results with employment of beam enhancement displayed improved spectra with increased intensity.

Analyte	Matrix/ Abbreviation
Proteins/ peptides	α – Cyano-4-hydroxycinnamic acid (CHCA), 2,5-Dihydroxybenzoic acid (DHB), 3,5-Dimethoxy-4-hydroxycinnamic acid (sinapic) (SA_
Lipids	Dithranol (DIT)
Inorganic molecules	Trans-2-(3-(4-tert-Butylphenyl)-2methyl-2-propenyliedene)malononitrile (DCTB)
Organic molecules	2,5-Dihydroxybenzoic acid (DHB)

Carbohydrates	2,5-Dihydroxybenzoic acid (DHB), α - Cyano-4-hydroxycinnamic acid (CHCA), Trihydroxyacetophenone (THAP)
Oligonucleotides	Trihydroxyacetophenone (THAP), 3-Hydroxypicolinic acid (HPA)
Synthetic polymers	2,5-Dihydroxybenzoic acid (DHB), Dithranol (DIT), Trans-3-indoleacrylic acid (IAA)

Table 7 : Common matrices used in UV- MALDI. (Hoffmann and Stroobant 2007).

1.3.4. Quadrupole Time of flight mass spectrometry (QqToF)

The term QqToF refers to a hybrid mass spectrometer which employs a quadrupole, (an arrangement of four metal rods with applied potentials; $+(U+V\cos(\omega t))$ and $-(U+V\cos(\omega t))$) where fixed U and alternating $V\cos(\omega t)$ potentials can be applied to selected ions for MS/MS.

The quadrupole arrangement used in a typical QqTOF arrangement is shown in Figure 1.21, where Q refers to the mass resolving quad and q describes a hexapole collision cell which can further dissociate precursor ions which are then separated again by another quadrupole or time of flight mass analyser. (Chernushevich *et al* 2001). The diagram (Figure 1.21) shows Q0 which functions as a "collisional dampening" r.f. quad to focus ions prior entry into the Q1 mass filter and Q2 collision cell. In some cases instruments can feature Q0 (Figure 1.21) and Q2 both as hexapoles. The schematic diagram above also illustrates the location of the ToF mass analyser and other components within the Q-ToF instrumentation.

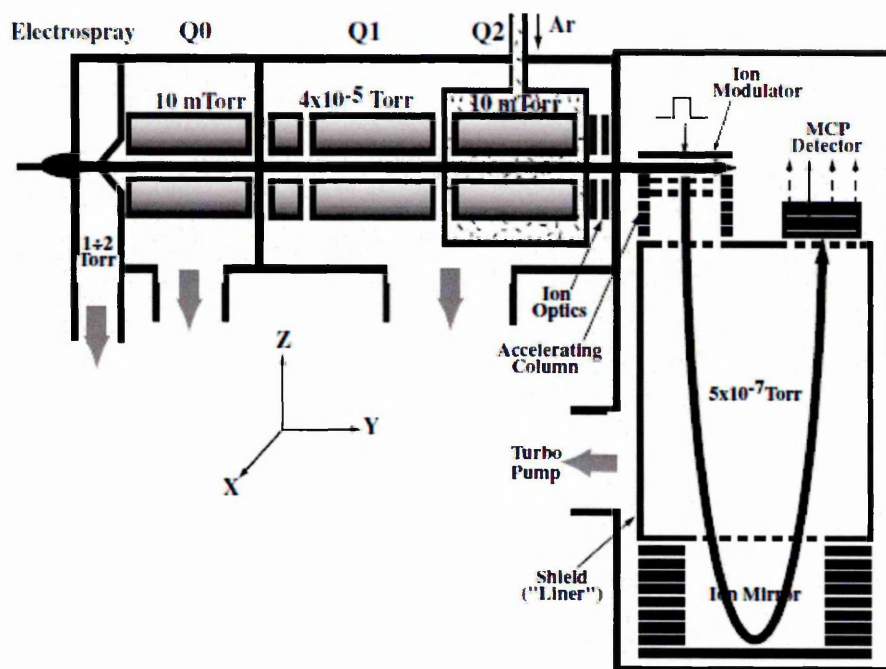


Figure 1. 21 : Diagrammatical representation of a tandem QqTOF mass spectrometer.(Chernushevich et al 2001).

If only mass spectra in ToF MS mode is required the Q1 quad operates in r.f. mode to simply provide a means of transmission for the ions generated which then continue to the ToF mass analyser. (Chernushevich et al 2001). Q2 parameters are maintained (<10 electron volts (eV)) as such to not induce fragmentation.

In MS/MS mode the precursor ion of interest is selected via the mass filtering Q1 which then reaches the Q2 and undergoes collision induced dissociation (CID) with an inert gas i.e. nitrogen/ argon. Subsequent acceleration then occurs of ion fragments and corresponding parent ions to the ion modulator (see Figure 1.21) in the formation of a continuous beam focused by ion optics. The pulsation of ions via an electric field at discreet bursts admits ions into the ToF mass analyser (Figure 1.22) in a way governed by the ion's characteristic trajectory.

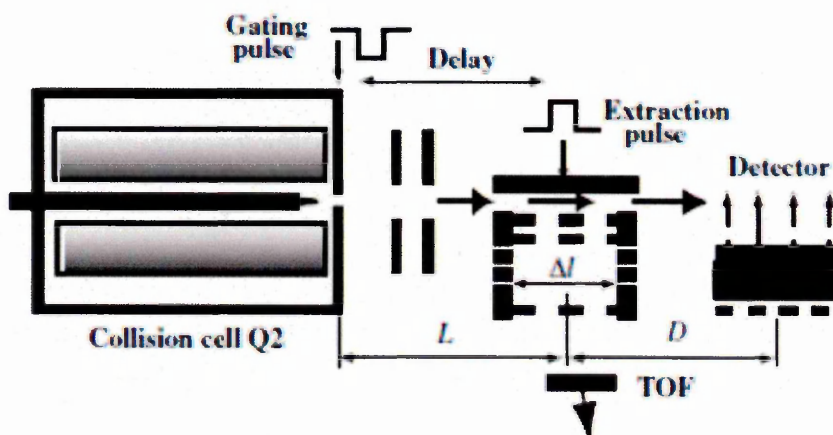


Figure 1. 22 : Schematic representation of a ToF modulator (Chernushevich et al 2001).

1.3.5. Synapt HDMS – travelling wave ion mobility separation.

Briefly mentioned earlier in section 1.2.4. (Proteomics using mass spectrometry), is the revolutionary concept of ion mobility separation (IMS) coupled with mass spectrometry. This novel concept allows visualisation into another dimension of spectral data. IMS has structural elucidation capabilities and the capacity to provide a further separation method of isobaric ions. (Pringle et al 2007).

The theory of ion mobility describes the separation of bundles of ions under a static electric field with the use of a 'background' gas (Pringle et al 2007, Clemmer and Jarrold 1997, Valentine et al 1997). A novel idea which uses molecular separation by mass, shape (cross sectional area) and chiral spin. Work reported in this thesis was performed using SYNAPT™ G1/G2 HDMS systems (Waters Corp., Milford, MA) (Figure 1.23). A series of 3 travelling wave stacked ring ion guides (Figure 1.24) constitute the ion mobility segment of the Synapt series instruments where packets of ions are allowed to accumulate from previous IMS then released to the ion guide for further mobility separation.

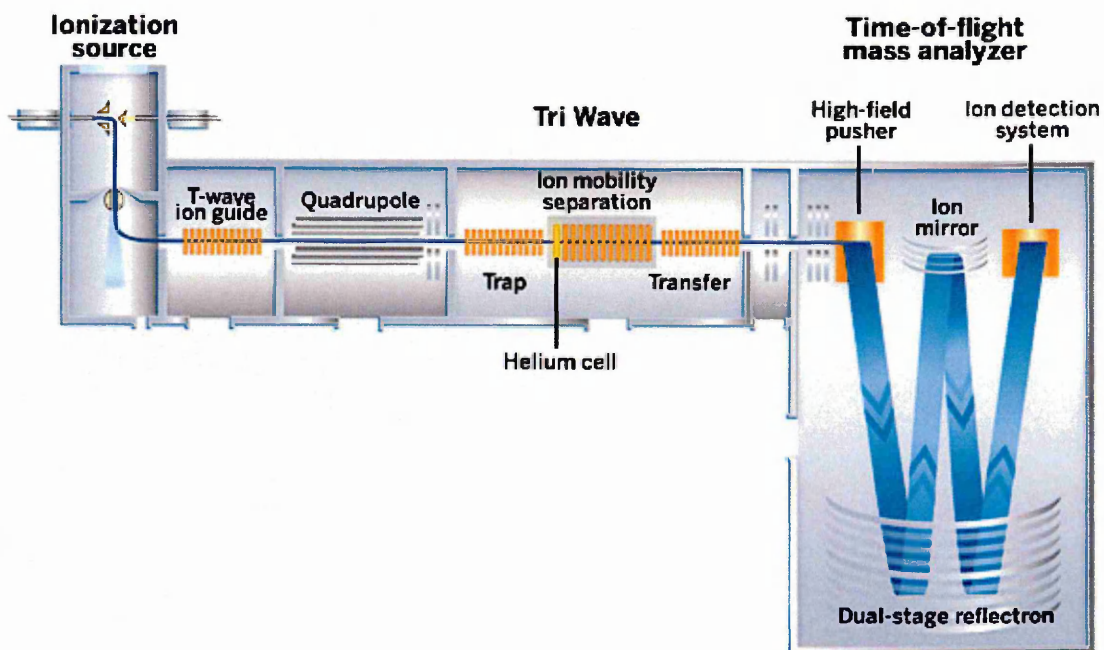


Figure 1. 23 : SYNAPT™ G2 HDMS system (Waters Corp., Milford, MA). (Waters 2012). The Tri Wave ion mobility cell is shown where selected ions of interest are separated dependant on size, cross sectional area and chiral spin. The mass analyser is set to dual reflectron mode to aid the focusing of high energy ions to achieve high mass resolution.

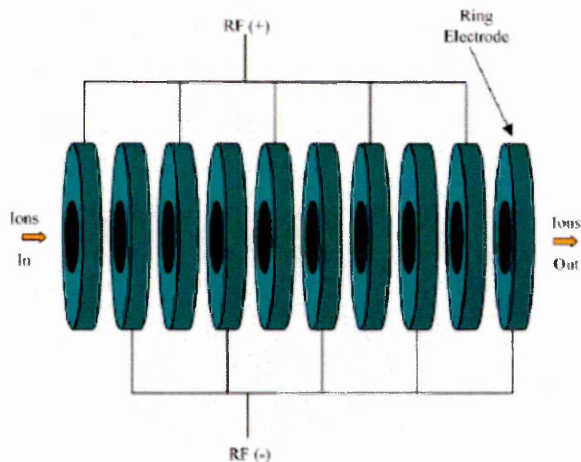


Figure 1. 24 : Stacked ring ion guide (Pringle et al 2007).

Travelling wave ion guides (TWIGs) which carry the ions through are the result of a temporary dc voltage applied to the RF of opposite electrodes in constant succession throughout the instrument. (Pringle et al 2007). The motion of the ions is likened to the “surfing of ions on the wave”. (Giles et al 2004). Figure 1.25 illustrates the travelling wave ion guide, the driving force for the movement of ions.

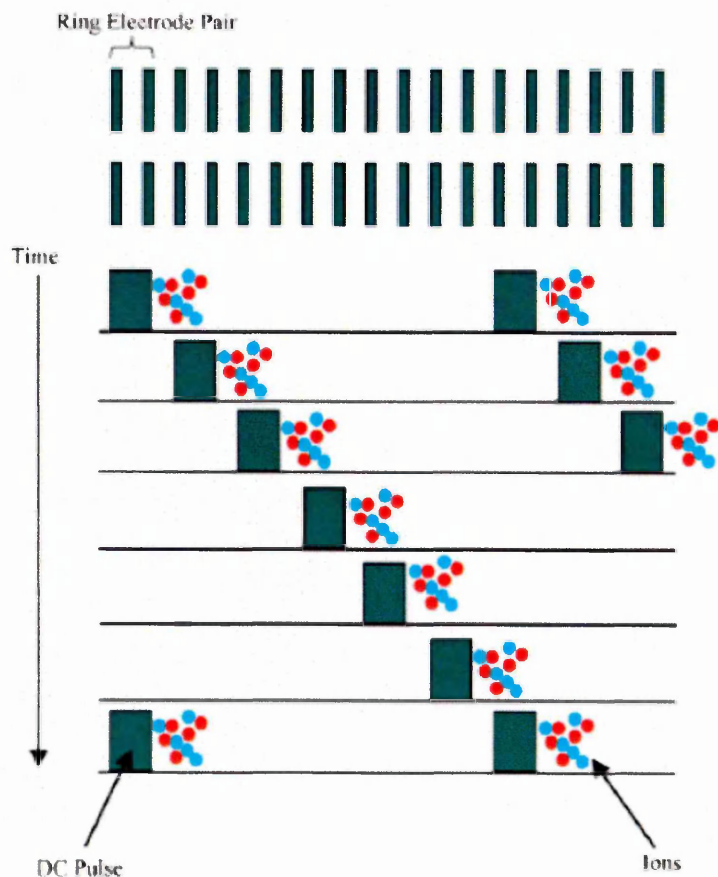


Figure 1. 25 : Travelling wave ion guide- schematic representation. (Pringle et al 2007).

The principle of ion mobility separation is based on the collision cross-section (Ω) as the ions traverse through a field of inert gas, this can be expressed in the following equation. The values relate to gas-phase collision cross-section (Clemmer and Jarrold 1997):

$$\Omega = \frac{3ze}{16N} \left[\frac{2\pi}{\mu k_b T} \right]^{0.5} \frac{1}{K_0}$$

Where N is the background gas number density, ze is the ionic charge, μ the reduced mass of the ion and the drift gas molecules, k_b Boltzmann’s constant, T gas temperature, K_0 is the mobility to 273.2 K and 760 Torr.

1.3.6. MALDI-mass spectrometry imaging

Matrix assisted laser desorption ionisation – mass spectrometry imaging (MALDI-MSI) is an advanced analytical tool that allows molecular profiling and imaging of many classes of compounds including; proteins, peptides, lipids, drugs and many other molecules directly from tissue sections. The use of this technique for the study of biological tissue was first described by Caprioli *et al.* in 1997 and it has been improved and adapted for use in many other studies (Caprioli *et al* 1997., Chaurand *et al* 2006., Chaurand *et al* 2003., Stoeckli *et al* 2007., Burrell *et al* 2007., Djidja *et al* 2008., Trim *et al* 2008., Fournier *et al* 2008).

MALDI-MSI allows the acquisition of multiple single mass spectra across the tissue section at a spatial resolution predefined by the operator (typically 20–200 μm) (Figure 1.27). These mass spectra are then combined together in order to generate molecular maps or images which represent the distribution and the relative abundance and/or intensity of a specific ion signal detected within the tissue section. MALDI-MSI has been shown to be a powerful technique for direct protein analysis within tissue sections and in tumour tissue samples, it has been used for discrimination between tumour and non tumour regions with no requirement for predefined targets (Schwartz *et al* 2004., Chaurand *et al* 2001., Lemaire *et al* 2007., Schwamborn *et al* 2007., Lemaire *et al* 2007). A recent and exciting development in the technique is the use of “on-tissue” tryptic digestion in order to achieve direct identification of proteins within a tissue section (Lemaire *et al* 2007., Shimma *et al* 2006., Groseclose *et al* 2007).

Such molecular profiling and imaging could be described as a bottom-up shotgun approach to protein identification, performed directly on cryo-sectioned tissue samples, rather than through protein extraction methods. The chance to visualise the position of peptides within an image generated by MALDI-MSI could indeed advance our knowledge in cancer research studies. Also being able to observe co-localisation of peptides and possibly relate them to disease states can provide complementary information regarding cancerous tissues.

A 2009 article by Djidja *et al* mentioned earlier, described the profiling and imaging of glucose-regulated protein 78 kDa (BiP/Grp78) in pancreatic tumour sections. As described within the article, the MALDI images were the first of their kind, with the discussion emphasising the low abundance of this particular heat shock protein. However its importance is not to be underestimated in the aggressiveness, progression and drug resistant nature of tumours. The paper then goes on to describe how the combination of ion mobility and MALDI helped to selectively target specific proteins for imaging. This technique has been called Matrix-Assisted Laser Desorption-Ionisation-Ion Mobility Separation-Mass Spectrometry Imaging (MALDI IMS-

MSI) and its advantages for imaging of specific proteins has also been described by others (McDonnell *et al* 2010).

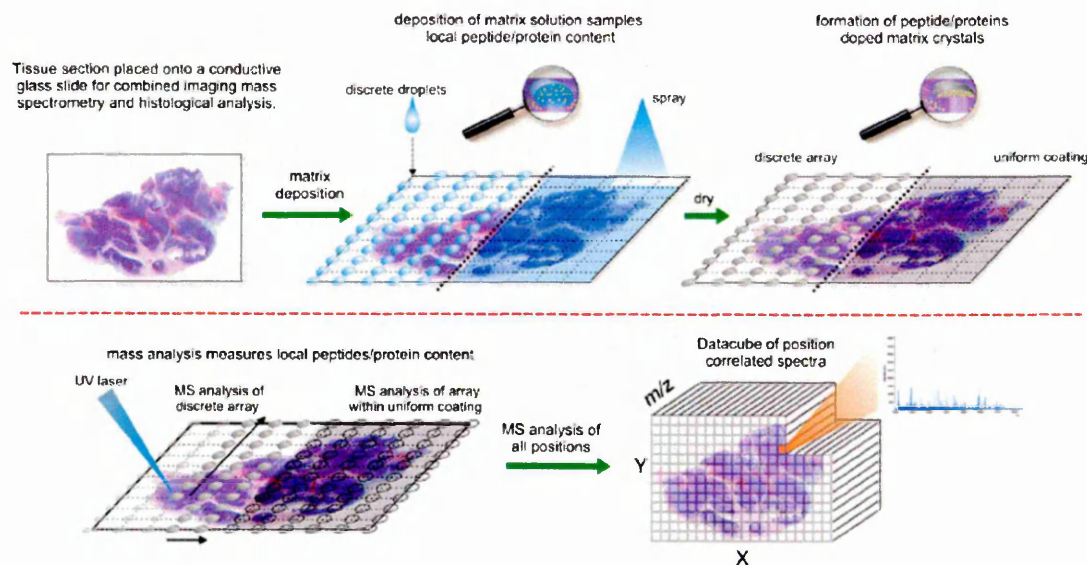


Figure 1. 26 : MALDI-MSI workflow diagram (McDonnell *et al* 2010).

In addition to the matrix deposition shown above in Figure 1.26 displaying a discrete arrangement of matrix/ reagent droplets, other methods include manual or automated spraying to achieve a finer more homogenous coating for co-crystallisation.

Examples of commercially available sample preparation for enzyme and/or matrix deposition are; Chemical Inkjet Printer by Shimadzu a sprayer using vibration vaporisation, Suncollect by SunChrom an automated spraying system, Portrait™ 630 Multispotter by Labcyte which works using high precision acoustic ejection from a reservoir source. (McDonnell *et al* 2010).

1.3.7. Quantitative Proteomics

A number of methods have been proposed for quantitative proteomics which include both label and label free quantitation.

1.3.7.1 Label free quantitation

Immunoassays and immunoblots are methods which are widely used, however development and optimisation of protein specific antibodies can be considered both time expensive and time consuming (Tate *et al* 2012). Cross reactivity can also be one of the main pitfalls of immune targeted approaches. It can be said that the latter includes some of the reasoning behind a shift towards mass spectrometry.

One of the most basic label free methods of quantitation in proteomics is spectral counting. Shotgun proteomics (as shown in Figure 1.17) describes an experiment where MS/MS results are summed for each peptide and comparison of summed events for each peptide can then be analysed throughout a time course of results (Tate *et al* 2012). More detailed analysis of spectral counting can involve i.e. counting of unique peptides before and after normalisation.

Measurement of the area generated from peptide signal intensity in the MS1 scan is another quantitative label free approach (Tate *et al* 2012). Quantitative information is acquired via an extracted ion chromatogram. This value from the ion of interest is taken at a specific region in time. This information is then used to associate the LC elution peak with the selected mass of interest. Processing of these data involves the alignment of MS1 chromatographic peaks throughout the samples/ time course samples analysed, the areas are then profiled.

Figure 1.27 shows an example using Progenesis, one of the proteomic software packages that can be used to analyse area measurements as previously described.

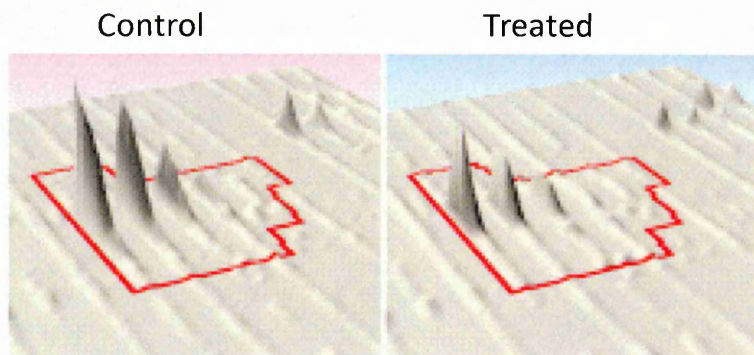


**Figure 1. 27 :The concept of area peptide measurement coupled with a specific time domain, visualised through Progenesis LC -MS software.
(<http://www.nonlinear.com/products/progenesis/lc-ms/overview/>)**

1.3.7.2 Labelling for proteomic quantitation

Isobaric Tags for Relative and Absolute Quantitation (iTRAQ) have been applied to numerous mass spectrometry studies (Song *et al* 2008,. Ross *et al* 2004,. Gygi *et al* 1999). iTRAQ enables samples to be labelled and then combined to perform 4 plex / 8 plex experiments to analyse tryptic digests from cells/ tissue (Shilov *et al* 2007). Each isobaric tag is comprised of a reporter group, balance group and a peptide reactive group. This proteomic bottom up approach requires tandem MS to give relative absolute quantitation information using reporter groups from 113 – 121. A control is included as a reference in the combined labelled samples and quantitation ratios are then relative to the control. MS/MS spectra can then be submitted to protein search software which can result in identification of the labelled peptides.

An example of an iTRAQ workflow is shown in Figure 1.28.

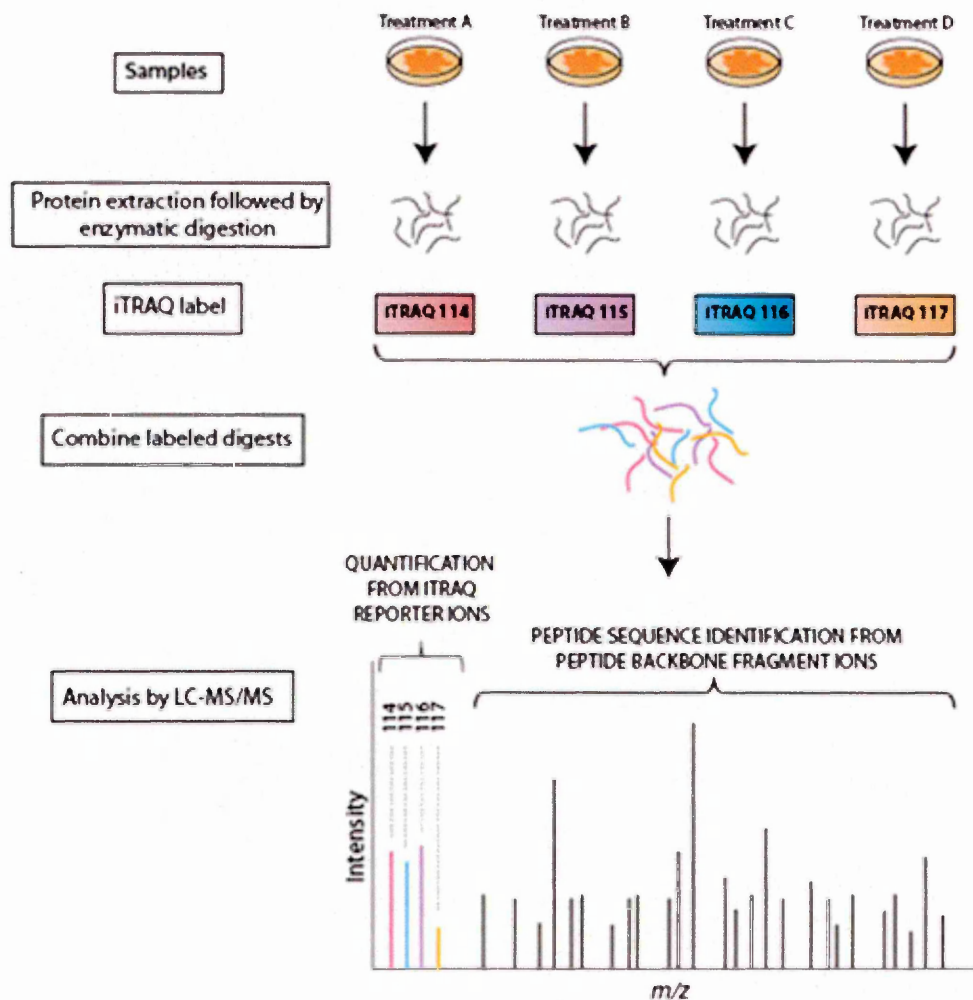


Figure 1. 28 : Simple workflow using Isobaric Tags for Relative and Absolute Quantitation (iTRAQ). (Broad Institute 2013).Relative quantitation can be measured by observation of the isobaric MS/MS fragments in the region of the spectra that correspond to a particular labelled specimen.

1.3.8. Aims of the study

The aims of the study reported in this thesis are to develop and utilise mass spectrometry imaging techniques (MALDI-MSI), in combination with conventional proteomic methodologies, to investigate protein induction in vascular-targeted strategies.

Here MALDI-MSI intended to compliment conventional proteomics to provide information relating the spatial distribution of protein/ peptides throughout time course experiments. Both CA-4-P susceptible (fibrosarcoma 120) and resistant (fibrosarcoma 188) tumour models were used to perform profiling and imaging experiments.

The tumour models used within this study originate from a mouse embryonic fibrosarcoma cell line and had been genetically engineered to either express solely the vascular endothelial growth factor (VEGF) 120 or 188 isoforms. Vasculature derived from the VEGF 120 growth factor characteristically favours cell proliferation but produces an erratic disorganised network of blood vessels with 'blind ends' lending itself to haemorrhagic disruption by CA-4-P. Tumour blood capillaries in the fibrosarcoma 188 model are less substandard and as a consequence mimic a more normal vascular arrangement (Tozer *et al* 2008). Tozer *et al* (2008) found that VEGF 188 tumour vasculature had increased pericyte support hence adding to CA-4-P resistance.

Nine different VEGF isoforms have currently been discovered in humans, with VEGF189, VEGF165 and VEGF121 isoforms being the most documented and VEGF120, VEGF164 and VEGF188 in mice (Tozer *et al* 2008,. Harris *et al* 2012). VEGF mRNA is transcribed from eight exons and splice variants result in the various isoforms mentioned previously. Each isoform is known to have its own distinctive vascular modelling and angiogenic configuring capability.

Each VEGF isoform is thought to govern angiogenesis in relation to whether it is matrix bound or not and yet little is known with regards to VEGF biological / mechanistic function (Harris *et al* 2012). VEGF120 does not possess a heparin-binding site and is described as being 'readily diffusible'. VEGF188 on the other hand is bound to proteoglycans, components of the extracellular matrix or at the cell surface (Figure 1.29) (Tozer *et al* 2008).

In tumours VEGF is associated with tumour growth and metastasis, increased levels of VEGF is said to correlate with poor patient survival.

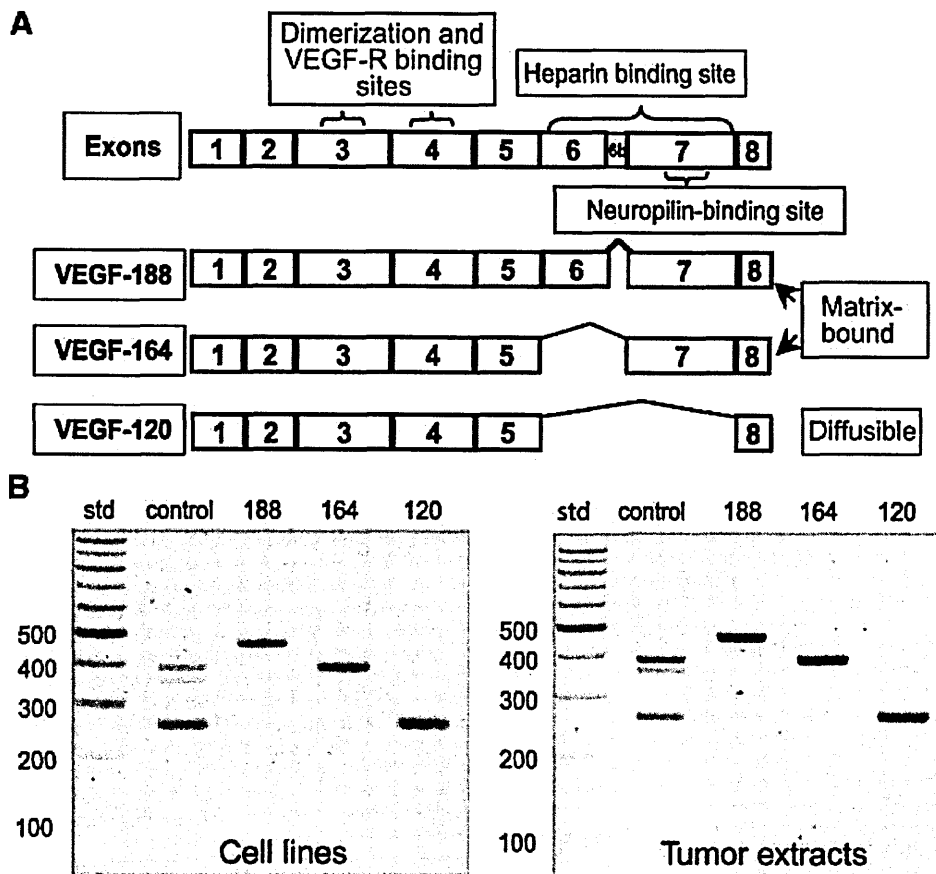


Figure 1.29: (A) The exon structure of the mouse VEGF isoforms showing the differences /similarities between exons and nature of each isoform whether diffusible or matrix bound. (B) The reverse transcription-PCR of cDNA showing the bands representative of each VEGF isoform. Traces of bands relating to other isoforms are present in the control but still align with the specific isoform bands (Tozer et al 2008).

PMFs were acquired from *in-situ* tissue tryptic digestion and proteins thought to be involved in tumourigenesis and drug treatment resistance were observed and targets which could be linked with hypoxic conditions of the tumour microenvironment.

Multivariate Statistical analysis aimed to observe grouping and classification within data time courses post CA-4-P administration.

The techniques used; MALDI-MSI, ESI-LC-MS/MS, LC-MALDI-MS/MS with iTRAQ labelling intended to provide cross validation of the effects post administration of vascular disrupting agent CA-4-P.

MALDI imaging of proteins related to tumour biology and the stress response could forge a place in the clinical setting providing alternative tool in the field of cancer research.

References

Abdollahi A, Folkman J (2010) *Evading tumour evasion: Current concepts and perspectives of anti-angiogenic cancer therapy*. Drug Resistance Updates. **13**. 16-28

Al-Shahib A, Misra R, Ahmod N, Fang M, Shah H, Gharbia S (2010) *Coherent pipeline for Biomarker discovery using mass spectrometry and bioinformatics*. BMC Bioinformatics. **11**. (437) 1-9

Anderson NL (2005) *The Roles of Multiple Proteomic Platforms in a Pipeline for New Diagnostics*. Molecular and Cellular Proteomics. **4**. 1441-1444

Bayless K and Davies GE (2004) *Microtubule depolymerisation rapidly collapses capillary tube networks in Vitro and angiogenic vessels in Vivo through small GTPase Rho*. The Journal of Biological Chemistry. **279**. (12) 11686-11695

Breuer K, Knochenmuss R, Zenobi R (1999) *Proton transfer reactions of matrix assisted laser desorption/ionisation matrix monomers and dimmers*. Journal of American Society of Mass Spectrometry. **10**. 1111-1123

Broad institute (2013) *iTRAQ*. Available at URL: <http://www.broadinstitute.org/>. Last accessed 29/07/13.

Buchanan CM, Shih JH, Astin JW, Rewcastle GW, Flanagan JU, Crosier PS, Shepherd PR (2012) *DMXAA (Vadimezan, ASA404) is a multi-kinase inhibitor targeting VEGFR2 in particular*. **122**.(10):449-57.

Burrell MM, Earnshaw CJ, M. Clench MR (2007) *Imaging Matrix Assisted Laser Desorption Ionization Mass Spectrometry: a technique to map plant metabolites within tissues at high spatial resolution* Journal of Experimental Botany **58**. (4) 757–763.

Cancer Research UK (2007) *Demographic facts for the world population*. Cancer Stats Worldwide. Available at URL: <http://info.cancerresearchuk.org/>. Last accessed 05/07/10

Cancer Research UK (2009) *How many types of cancer are there?* Available at URL: <http://info.cancerresearchuk.org/>. Last accessed 05/07/10

Caprioli RM, Farmer TB, Gile J (1997) *Molecular Imaging of Biological Samples: Localization of Peptides and Proteins Using MALDI-TOF MS*. Analytical Chemistry. **69**. (23) 4751–4760.

Chaurand P, DaGue BB, Pearsall RS, Threadgill DW, Caprioli RM (2001) *Profiling proteins from azoxymethane-induced colon tumors at the molecular level by matrix-assisted laser desorption/ionization mass spectrometry*. *Proteomics*. **1**. (10) 1320–1326.

Chaurand P, Cornett DS, Caprioli RM (2006) *Molecular imaging of thin mammalian tissue sections by mass spectrometry*. *Current Opinion in Biotechnology*. **17**. (4) 431–436.

Chaurand P, Fouchécourt S, DaGue BB, Xu BJ, Reyzer ML, Orgebin-Crist M, Caprioli RM (2003) *Profiling and imaging proteins in the mouse epididymis by imaging mass spectrometry*. *Proteomics* **3**.(11)2221–2239.

Chemotherapy (2011) *Types of cancer*. Available at URL: <http://www.chemotherapy.com/>. Last accessed 21/11/12

Chernushevich IV, Loboda AV, Thomson BA (2001) *An introduction to quadrupole-time-of-flight mass spectrometry*. *Journal of Mass Spectrometry*. **36**. 849-865

Clemmer DE and Jarrold MF (1997) *Ion mobility measurements and their applications to clusters and biomolecules*. *Journal of Mass Spectrometry*. **32**. 577-592

Connell PP, Hellman S (2009) *Advances in radiotherapy and implications for the next century: A historical perspective*. *Cancer Research*. **69**. (2) 383-392

Cooks RG (2010) *Foreward: desorption ionization and spray ionization: connections and progress*. In Cole RB (ed) *Electrospray and MALDI mass spectrometry: fundamentals, instrumentation, practicalities, and biological applications*. Wiley. Hoboken.

Delaney G, Jacob S, Featherstone C, Barton M (2005) *The role of radiotherapy in cancer treatment*. *Cancer*. **104**. (6) 1129-1137

Denekamp J (1990) *Vascular attack as a therapeutic strategy for cancer*. *Cancer Metastasis Rev*. **9**. (3) 267-282

DeVita VT and Chu E (2008) *A history of cancer chemotherapy*. *Cancer Research*. **68** (21) 8643-8653

Djidja M, Carolan V, Loadman PM, Clench MR (2008). *Method development for protein profiling in biological tissues by matrix-assisted laser desorption/ionisation mass spectrometry imaging*. *Rapid communications in mass spectrometry*, **22**. (10) 1615-1618.

Djidja M-C, Claude E, Snel MF, Scriven P, Francese S, Carolan V, Clench MR (2009) *Maldi-ion mobility separation-mass spectrometry imaging of glucose-regulated protein 78 kDa (Grp78) in*

human formalin fixed paraffin-embedded pancreatic adenocarcinoma tissue sections. Journal of Proteome Research. **8.** (10) 4876-4884

Folkman J (1971) *Tumor Angiogenesis: Therapeutic Implications.* The New England Journal of Medicine. **285.** 1182-1186

Fournier I, Wisztorski M, Salzet M (2008) *Tissue imaging using MALDI-MS: a new frontier of histopathology proteomics.* Expert Review of Proteomics. **5.** (3) 413–424.

Gates P (2004) *Mass spectrometry resource: Electrospray ionisation (ESI).* University of Bristol. Available at URL: <http://www.chm.bris.ac.uk/>. Last accessed 28/11/12

Giles K, Pringle SD, Worthington KR, Little D, Wildgoose JL, Bateman RH (2004) *Applications of travelling wave-based radio-frequency-only stacked ring ion guide.* Rapid Communications in Mass Spectrometry. **18.** 2401-2414

Griffiths J (2008) *A brief history of mass spectrometry.* Analytical Chemistry. **80.** 5678-5683

Groseclose MR, Andersson M, Hardesty WM, Caprioli RM (2007) *Identification of proteins directly from tissue: in situ tryptic digestions coupled with imaging mass spectrometry.* Journal of Mass Spectrometry. **42.** (2) 254–262.

Gygi PS, Rist B, Gerber SA, Turecek F, Gelb MH, Aebersold R (1999) *Quantitative analysis of complex protein mixtures using isotope-coded affinity tags.* Nature Biotechnology. **17.** (10) 994–999

Han X, Aslanian A, Yates JR (2008) *Mass spectrometry for proteomics.* Current Opinion in Chemical Biology. **12.** 483-490

Hanahan D and Weinberg RA (2000) *The hallmarks of cancer.* Cell. **100.** 57-70

Hanahan D and Weinberg RA (2011) *Hallmarks of Cancer: The Next Generation.* Cell. **144.** 646-674

Harris S, Craze M, Newton J, Fisher M, Shima DT, Tozer GM, Kanthou C (2012) *Do Anti-Angiogenic VEGF (VEGFxxx) Isoforms Exist? A Cautionary Tale.* PLoS ONE **7.** (5) 1-14

Hinnen P, Eskens FALM (2007) *Vascular disrupting agents in clinical development.* British Journal of Cancer. **96.** 1159-1165

Ho CS, Lam CWK, Chan MHM, Cheung RCK, Law LK, Lit LCW, Ng KF, Suen MWM, Tai HL (2003) *Electrospray Ionisation Mass Spectrometry: Principles and Clinical Applications*. The Clinical Biochemist Reviews. **24**.(1) 3-12

Hodgkinson VC, ELFadl D, Drew PJ, Lind MJ, Cawkwell L (2011) Repeatedly identified differentially expressed proteins (RIDEPs) from antibody microarray proteomic analysis. *Journal of Proteomics*. **74**. 698-703

Hoffmann E de and Stroobant (2007) *Mass spectrometry principles and applications*. 3rd Edition. Chichester: John Wiley & Sons Ltd

Hurwitz H, Fehrenbacher L, Novotny W, Cartwright T, Hainsworth J, Heim W, Berlin J, Baron A, Griffing S, Holmgren E, Ferrara N, Fyfe G, Rogers B, Ross R, F Kabbinavar (2004) *Bevacizumab plus irinotecan, fluorouracil and leucovorin for metastatic colorectal cancer*. *New England Journal of Medicine*. **350**.(23) 2335-2342

Jong W HA de, Vries E, Kema IP (2011) *Current status and future developments of LC-MS/MS in clinical chemistry for the quantification of biogenic amines*. *Clinical Biochemistry*. **44**. (1) 95–103

Kanthou and Tozer (2007) *Selective destruction of the tumour vasculature by targeting the endothelial cytoskeleton*. *Drug discovery today: Therapeutic strategies*. **4**. (4) 237-243

Kanthou C, Tozer GM (2002) *The tumor vascular targeting agent combretastatin A-4-phosphate induces reorganization of the actin cytoskeleton and early membrane blebbing in human endothelial cells*. *BLOOD*. **99**. (6) 2060-2069

Koch U, Krause M, Baumann M (2010) *Cancer stem cells at the crossroads of current cancer therapy failures - Radiation oncology perspective*. *Seminars In Cancer Biology*. **20**. (2) 116-124

Lagerstedt SA, O’Kane DJ, Singh RJ (2004) *Measurement of plasma free metanephrine and normetanephrine by liquid chromatography-tandem mass spectrometry for diagnosis of pheochromocytoma*. *Clinical Chemistry*. **50**. 603-611

Lemaire R, Desmons A, Tabet JC, Day R, Salzet M, Fournier I (2007) *Direct analysis and MALDI imaging of formalin-fixed, paraffin-embedded tissue sections*. *Journal of Proteome Research* **6**. (4) 1295–1305.

Lemaire R, Menguellet SA, Stauber J, Marchaudon V, Lucot J, Collinet P, Farine M, Vinatier D, Day R, Ducoroy P, Salzet M, Fournier I (2007) *Specific MALDI Imaging and Profiling for*

- Biomarker Hunting and Validation: Fragment of the 11S Proteasome Activator Complex, Reg Alpha Fragment, Is a New Potential Ovary Cancer Biomarker.* Journal of Proteome Research. **6.** (11) 4127–4134.
- Lord CJ and Ashworth A (2010) *Biology-driven cancer drug development: back to the future.* BMC Biology. **8.** (38) 1-12
- Medline Plus (2010) *Tumour.* Available at URL: <http://www.nlm.nih.gov/medlineplus/> . Last accessed 21/11/12
- McLean JA, Ruotolo BT, Gilling KJ, Russell DH (2005) *Ion mobility-mass spectrometry: a new paradigm for proteomics.* International Journal of mass Spectrometry. **240.** 301-315
- McDonnell LA, Corthals GL, Willems SM, Remoortere van A, Zeijl van RJM, Deelder AM (2010) *Peptide and protein imaging mass spectrometry in cancer research.* Journal of Proteomics. **73.** (10) 1921–1944.
- National Cancer Institute (2009) *Understanding Cancer series - Loss of Normal Growth Control.* Available at URL: <http://www.cancer.gov/>. Last accessed on 21/11/12
- Oncolink (2010) *Cancer treatment information.* Available at URL: <http://www.oncolink.org/>. Last accessed 21/11/12
- Oxigene (2010) *Abnormal vasculature.* Available at URL: [URL http://www.oxigene.com/](http://www.oxigene.com/) Last accessed 21/09/10
- Papac RJ (2001) *Origins of cancer therapy.* Yale Journal of Biology and Medicine. **74.** (6): 391–398.
- Petrk J, Ivanek R, Toman O, Cmejla R, Cmejlova J, Vyoral D, Zivny J, Vulpe CD (2008) *Déjà vu in proteomics. A hit parade of repeatedly identified differentially expressed proteins.* Proteomics. **8.** 1744-1749
- Pringle SD, Giles K, Wildgoose JL, Williams JP, Slade SE, Thalassinou K, Bateman RH, Bowers MT, Scrivens JH (2007) *An investigation of the mobility separation of some peptide and protein ions using a new hybrid quadrupole/travelling wave IMS/oa-ToF instrument.* International Journal of Mass Spectrometry. **261.** 1-12
- Ross PL, Huang YN, Marchese JN, Williamson B, Parker K, Hattan S, Khainovski N, Pillai S, Dey S, Daniels S, Purkayastha S, Juhasz P, Martin S, Bartlett-Jones M, He F, Jacobson A, Pappin

D J (2004) *Multiplexed protein quantitation in Saccharomyces cerevisiae using amine-reactive isobaric tagging reagents*. *Molecular and Cellular Proteomics*.**3**. (12) 1154–1169

Röwer C, Koy C, Hecker M, Reimer T, Gerber B, Thiesen H-J, Glocker MO (2011) *Mass Spectrometric Characterization of Protein Structure Details Refines the Proteome Signature for Invasive Ductal Breast Carcinoma*. *Journal of American Society for Mass Spectrometry*.**22**. 440 - 456

Saharinen P, Eklund L, Pulkki K, Bono P, Alitalo K (2011) *VEGF and angiopoietin signaling in tumor angiogenesis and metastasis*. *Trends in Molecular Medicine*.**17**. (7) 347-362

Schwamborn K, Krieg RC, Reska M, Jakse G, Knuechel R, Wellmann A (2007) *Identifying prostate carcinoma by MALDI-Imaging*. *International Journal of Molecular Medicine*. 20. (2) 155–159.

Schwartz SA, Weil RJ, Johnson MD, Toms SA, Caprioli RM (2004) *Protein profiling in brain tumors using mass spectrometry: feasibility of a new technique for the analysis of protein expression*. *Clinical Cancer Research: an official journal of the American Association for Cancer Research*.**10**. (3) 981–987.

Shariq J, Barton M, Noble D, Lemer C, Donaldson LJ (2009) *An international review of patient safety measures in radiotherapy practice*. *Radiotherapy and Oncology*.**92**. 15-21

Shilov IV, Seymour SL, Patel AA, Loboda A, Tang WH, Keating SP, Hunter CL, Nuwaysir LM, Schaeffer DA (2007) *The Paragon Algorithm: A next generation search engine that uses sequence temperature values and feature probabilities to identify peptides from tandem mass spectra*. *Molecular and Cellular Proteomics*.**6**. (9) 1638–1655.

Shimma S, Furuta M, Ichimura K, Yoshida Y, Setou M, (2006) *A Novel Approach to in situ Proteome Analysis Using Chemical Inkjet Printing Technology and MALDI-QIT-TOF Tandem Mass Spectrometer*. *Journal of Mass Spectrometry Society Japan*. 54. (4) 133–140.

Siemann DW, Bibby MC, Dark GG, Dicker AP, Eskens F A.L.M, Horsman MR, Marme D, LoRusso PM (2005) *Differentiation and definition of vascular-targeted therapies*. *Clinical Cancer Research*.**416**. (11) 416-420

Siemann DW (2010) *The unique characteristics of tumour vasculature and preclinical evidence for its selective disruption by tumour-vascular disrupting agents*. *Cancer Treatment Reviews*.**37**. (1) 63-74

Sigma Aldrich (2001) *MALDI mass-spectrometry*. Available at URL: <http://sigmaaldrich.com/>
Last accessed 27/09/10

Song X, Bandow J, Sherman J, Baker JD, Brown PW, McDowell MT, Molloy MP (2008) *iTRAQ Experimental Design for Plasma Biomarker Discovery*. *Journal of Proteome Research*. **7**. 2952–2958

Stoeckli M, Staab D, Schweitzer A, Gardiner J, Seebach D (2007) *Imaging of a β -Peptide Distribution in Whole-Body Mice Sections by MALDI Mass Spectrometry*. *Journal of American Society of Mass Spectrometry* **18**. (11) 1921–1924.

Tate S, Larsen B, Bonner R, Gingras A-C (2012) *Label-free quantitative proteomics trends for protein–protein interactions*. *Journal of Proteomics*. ARTICLE IN PRESS

The LC/MS Unit (2009) *The LC instrument details*. Available at URL: <http://home.iprimus.com.au/> Last accessed 24/09/10

Thorpe PE, Chaplin DJ, Blakely DC (2003) *The first international conference on vascular targeting: Meeting overview*. *Cancer Research*. **63**. 1144-1147

Tozer GM, Akerman S, Cross NA, Barber PR, Björndahl MA, Greco O, Harris S, Hill SA, Honess DJ, Ireson CR, Pettyjohn KL, Prise VE, Reyes-Aldasoro CC, Ruhrberg C, Shima DT, Kanthou C (2008) *Blood Vessel Maturation and Response to Vascular-Disrupting Therapy in Single Vascular Endothelial Growth Factor-A Isoform–Producing Tumors*. *Cancer Research*. **68**. (7) 2301-2311

Tozer GM, Kanthou C, Lewis G, Prise VE, Vojnovic B, Hill A (2008) *Tumour vascular disrupting agents: combating treatment resistance*. *The British Journal of Radiology*. **81**. S12-S20

Trim P J, Atkinson S J, Princivalle AP, Marshall PS, West A and Clench MR (2008) *Matrix-assisted laser desorption/ionisation mass spectrometry imaging of lipids in rat brain tissue with integrated unsupervised and supervised multivariate statistical analysis*. *Rapid Communications in Mass Spectrometry*. **22**. (10), 1503-1509.

Trim PJ, Djidja M-C, Atkinson SJ, Oakes K, Cole LM, Anderson DMG, Hart PJ, Francese S, Clench MR (2010) *Introduction of a 20kHz Nd:YVO4 laser into a hybrid quadrupole time-of-flight mass spectrometer for MALDI-MS imaging*. *Analytical and Bioanalytical Chemistry*. **397**. (8) 3409-3419

Trim PJ, Djidja M-C, Muharib T, Cole LM, Bryn Flinders, Carolan VA, Francese S, Clench MR (2012) *Instrumentation and software for mass spectrometry imaging—Making the most of what you've got*. *Journal of Proteomics*. **75**. (16) 4931–4940

- University of Bristol (2005) High performance liquid chromatography mass spectrometry. URL <http://www.bris.ac.uk/> Last accessed 24/09/10
- Valentine SJ, Counterman AE, Clemmer DE (1997) *Conformer-dependant proton-transfer reactions of ubiquitin ions*. *Journal of the American Society for Mass Spectrometry*.**8**. 954-961
- Wang G and RB Cole (2000) *Charged residue versus ion evaporation for formation of alkali metalhalide cluster ions in ESI*. *Analytica Chimica Acta*.**406**. 53–65
- Waters (2012) *SYNAPT G2-S HDMS*. Available at URL: <http://www.waters.com/>Last accessed on 29/11/12
- Wedge SR, Ogilvie DJ, Dukes M, Kendrew J, Chester R, Jackson JA, Boffey SJ, Valentine PJ, Curwen JO, Musgrove HL, Graham GA, Hughes GD, Thomas AP, Stokes ESE, Curry B, Richmond GHP, Wadsworth PF, Bigley AL, Hennequin LF (2002) *ZD6474 inhibits vascular endothelial growth factor signalling, angiogenesis, and tumour growth following oral administration*. *Cancer Research*.**62**. 4645-55
- Worldometers (2013) *Worldometers – realtime world statistics*. Available at URL: <http://www.worldometers.info/>. Last accessed on 27/01/13
- World cancer Research Fund (2010) *World cancer statistics*. Available at URL: <http://www.wcrf-uk.org/>. Last accessed on 21/11/12
- World Health organisation (2012) *Cancer* . Available at URL: <http://www.who.int/>. Last accessed on 21/11/12
- Zhi-chao SI, Jie L (2008) *What ‘helps’ tumours evade vascular targeting treatment?* *Chinese Medical Journal*.**121**. (9) 844-849

Chapter 2

Protein induction in a CA-4-P
susceptible tumour model using
MALDI-MSI

2.1 Introduction

The discovery of biomarkers that can be used to determine success of cancer therapy or resistance to it, at an early stage, presents a very complex problem. There are countless biochemical pathways to be considered and the multifaceted characteristics of the cancer cell have also to be taken into account; a cell that can largely evade the host's immune responses, has mastered tissue invasion and anti-cancer drug resistance.

One promising class of anti-cancer drug currently under development is the vascular disrupting agents (VDAs) (Kanthou and Tozer 2007). VDAs cause rapid, selective and sustained shutdown of tumour blood flow. This produces drastic effects on the tumour microenvironment. Certain aspects of blood flow modification are due to the direct effects of the drug on the endothelial cells that line the luminal surface of blood vessels. The article by Kanthou and Tozer describes a proposed mechanism of action for CA-4-P (Kanthou and Tozer 2007). It is suggested that increased permeability after the administration of CA-4-P is one major factor in the disruption of endothelial organisation. Interference in vascular integrity due to abnormality in the cytoskeleton, subsequently leads to stress fibre formation and endothelial cells become more rounded ('blebbing'). Haemorrhagic necrosis follows exacerbating the already hypoxic regions within the tumour microenvironment.

As mentioned in the introductory chapter, the remodelling and formation of actin stress fibres is clearly demonstrated using immunofluorescence by Siemann (Siemann 2010). The images contained in this article are good examples of the "rounding" of endothelial cells and "condensation" of the microtubules post CA-4-P treatment.

Drug delivery of VDAs is relatively simple due to endothelial positioning near the bloodstream. The diploid target cells are thought not to be directly drug-resistant due to low risk of mutations (Thorpe *et al* 2003).

VDAs have relatively good clinical measurability, i.e. bloodflow and in most cases short-term exposure to a VDA creates sufficient hypoxic conditions to induce necrosis. However, the use of VDAs to increase hypoxia can also have undesirable consequences (Zhi-chao and Jie 2008), (Tozer *et al* (2008) . Hypoxia-inducible factors (HIF), which are prevalent under hypoxic conditions, cause up-regulation of pro-angiogenic factors such as VEGF. VDA might amplify the angiogenic process after the creation of an increased hypoxic tumour environment. Hypothetically speaking this could even help the metastatic process ensuring tumour invasion (Zhi-chao and Jie 2008).

In addition to acquired resistance to treatment, the heterogeneous tumour mass could well contain a cell population oblivious to vascular targeted strategies, i.e. innate resistance (Thorpe *et al* 2003). Support for this comes from the hypothesis that there are four possible micro-vascular phenotypes in existence i.e. normal pre-existing, tumourphenotypic vessels, normal neo-vasculature and abnormal (pathological) neo-vasculature. It may explain why some tumour regions remain unaffected by VDA treatment, including the well documented viable tumour rim (Abdollahi and Folkman 2010). The viable tumour rim is also thought to achieve evasion through its positioning, adjacent to the non-diseased tissue, which is well supplied with oxygen and essential nutrients (Kanthou and Tozer 2009). Resistance mechanisms to VDAs are clearly complex and multifactorial but increased knowledge in this area could provide strategies for future combination therapies.

The largest group of VDAs are tubulin binding, microtubule-depolymerising drugs such as combretastatin A-4-3-O-phosphate (CA-4-P/Fosbretabulin/ZybrestatTM), which is currently in late stage clinical trials. Combination of CA-4-P or a related compound, Oxi4503 (CA-1-P), with anti-angiogenic therapies such as VEGF receptor tyrosine kinase inhibitors has already shown promise and novel concepts aimed at targeting circulating angiogenic endothelial progenitor cells have also been proposed. This area has been recently reviewed by Siemann (Siemann and Horsman 2009).

The experimental work reported here, describes a study, by MALDI MSI and MALDI IMS-MSI, of the proteins induced in a mouse transplanted fibrosarcoma model (VEGF120 tumours), at a number of time points, following treatment with CA-4-P. Imaging of peptide signals after *in situ* tissue tryptic digestion was carried out using MALDI-MS and MALDI IMS-MSI to observe their spatial distribution. MALDI-IMS-MS/MS of the peptide signals was performed to identify proteins involved in the pharmacodynamic responses to treatment.

2.2 Materials and Samples

2.2.1 Chemicals and Materials

α -Cyano-4-hydroxycinnamic acid (CHCA), aniline (ANI), ethanol (EtOH), chloroform (CHCl₃), acetonitrile (ACN), octyl-a/b-glucoside (OcGlc), tri-fluoroacetic acid (TFA), ammonium bicarbonate, haematoxylin, eosin, xylene and DPX mountant were from Sigma–Aldrich (Dorset,

UK). Modified sequence grade trypsin (20 µg lyophilised) was obtained from Promega (Southampton, UK).

2.2.2 Tissue samples

Severe combined immunodeficiency (SCID) mice were injected sub-cutaneously in the flank with a 50 µl tumour cell suspension containing 1×10^6 cells in serum-free medium. The cells employed in this study were from the mouse fibrosarcoma cell line, VEGF120. This has been engineered to express only the VEGF 120 isoform. Tumours were allowed to grow to approximately 500 mm³, before CA-4-P treatment (a single dose of 100 mg/kg i.p). The dosage for CA-4-P are consistent with animal studies performed at clinically relevant doses (Galbraith 2003., Prise 2002). Treatment was either Saline/ Control, Mice were killed and tumours excised at various times after treatment. In the case of 0h CA-4-P, the tumour was excised immediately (within 2mins) after dispatchment. All animal work carried out documented herein was performed by Dr. J. E. Bluff, Tumour Microcirculation Group, University of Sheffield, UK. Samples were provided as frozen excised tumours and stored at -80°C.

2.2.3. Experimental groups

Controls (no treatment, saline i.p), n = 6 (labelled tumour1_1 – tumour 1_6), C-A4-P (0 h after treatment), n = 6, (labelled tumour2_1 – tumour 2_6), C-A4-P (0.5 h after treatment), n = 6, (labelled tumour 3_1 – tumour 3_6), C-A4-P (6 h after treatment), n = 6, (labelled tumour 4_1 – tumour 4_6), C-A4-P (24 h after treatment) n = 6, (labelled tumour 5_1 – tumour 5_6).

2.2.4 Tissue preparation

Frozen tissue sections were cut to give approximately 10µm sections, using a Leica CM3050 cryostat (Leica Microsystems, MiltonKeynes, UK) (Djidja *et al* 2009). The sections were then freeze thaw mounted on poly-lysine glass slides. Mounted slides were either used immediately or stored in an airtight tube at -80 °C for subsequent use.

2.2.5 *In situ* tissue digestion and trypsin deposition

The triplicate tissue samples to undergo MALDI-MS/MSI were washed initially with 70% and then 90% ethanol for 1 min then left to dry, subsequently slides were immersed in chloroform for 10 s. Prior to matrix application,

in situ tissue digestion was performed with trypsin solution prepared (from lyophilised trypsin) at 20 µg/ml by addition of 50 mM ammonium bicarbonate (NH₄HCO₃) pH 8, containing 0.5% octyl-a/b-glucoside (OcGlc) based on a protocol by Djidja *et al* (2009).

Two automated systems were used for trypsin application. The “Suncollect” (SunChrom, Friedrichsdorf, Germany) automatic pneumatic sprayer was used to spray trypsin in a series of layers. The Portrait™ 630 Multispotter (Labcyte, Sunnyville CA) was used to apply trypsin in a 200–300 μm array of spots. The sections for MALDI-MS and MALDIMS were incubated overnight in a humidity chamber containing H₂O 50%: methanol 50% overnight at 37 °C and 5% CO₂.

2.3 Methods and instrumentation

2.3.1 Matrix deposition

The matrix, α -cyano-4-hydroxycinnamic acid (CHCA) and aniline in acetonitrile:water:TFA (1:1:0.1 by volume), was applied using either the Suncollect (at 5 mg/ml) or the Portrait™ 630 Multispotter (at 10 mg/ml), as described above. Identical coordinate settings were used as with the trypsin deposition, to ensure sample uniformity. Equimolar amounts of aniline were added to the CHCA solution, i.e. 1 ml of 5 mg/ml CHCA solution contained 2.4 μl of aniline. These matrix deposition parameters were based on methods from Djidja *et al* (2009).

2.3.2 Instrumentation

Peptide mass fingerprints and images were acquired by MALDI-MS/MSI using a Q-Star Pulsar i hybrid quadrupole time-of-flight mass spectrometer (Applied Biosystems/MDS Sciex, Concord, Ontario, Canada) fitted with a variable repetition rate Nd:YV04 laser set at 5 kHz. Image acquisition was performed using raster imaging mode at 150 μm spatial resolution, Biomap 3.7.5.5 software (<http://www.maldi-msi.org/>) was used for image generation. Instrument calibration was performed using standards consisting of a mixture of 217 polyethylene glycol (Sigma-Aldrich, Gillingham, UK) ranging between m/z 100 to 218 3000 Da prior to MALDI-MS/MSI analysis. To enable simple visual comparison between images all data were normalised to m/z 877 (a peak arising from the α CHCA matrix) and intensity scales in the BioMap software were all set to the same value. MALDI-MS/MS, MALDI-MS/MSI and MALDI-MS/MS/MS were performed using a HDMS SYNAPT™ G1/G2 system (Waters Corporation, Manchester, UK) and Drift scope 2.1 software (Waters Corporation, UK). In order to achieve good quality MS/MS spectra, they were acquired manually moving the laser position and adjusting the collision energy to achieve good signal to noise for product ions across the full m/z range of the spectrum. Collision energies were adjusted from 70 to 100 eV during acquisition and acquisition times were generally of the order of 5–10 s per spectrum. MS/MS spectra were uploaded to perform a Mascot (Matrix Science, London, UK) search which used the UniProt database in order to generate a sequence match (see Table 1 for results).

2.3.3 Haematoxylin and eosin staining

Slides were immersed in haematoxylin for 1 min, rinsed in tap water until the water ran clear, immersed in 1% eosin for 30 s and rinsed in tap water until the water ran clear. They were then dehydrated as follows: 50% ethanol for 2 min, 70% ethanol for 2 min, 80% ethanol for 2 min, 95% ethanol for 2 min and 4 changes of xylene applied to each slide for 1 min at a time. Finally, they were mounted with DPX mountant and left to dry in the fumehood overnight.

2.3.4 Data pre-processing using SpecAlign and Marker View software

Data lists were exported from Analyst QS software (Applied Biosystems/MDS Sciex, Concorde, Ontario, Canada) as text files, then imported into SpecAlign (Oxford, UK) to undergo the following data processing; baseline subtraction, smooth, denoise, normalise TIC, remove negative, generate average spectrum, processing spectral alignment, PAAFT correlation method max shift 20. Files were then exported as text files for import into Marker View software 1.2 (Applied Biosystems/MDS Sciex, Concorde, Ontario, Canada).

2.3.5 Statistical analysis

PCA-DA was performed using Marker View software 1.2 (Applied Biosystems/MDS Sciex, Concorde, Ontario, Canada). Post SpecAlign text files were imported and data was transposed into table format. A minimum intensity of 0.1 was selected, with a maximum number of peaks of 20,000. Monoisotopic peaks selected by Marker View were used in the supervised PCA-DA. PCA and PLSDA was performed using MATLAB® (Matrix Laboratory) (MathWorks, Inc., Natick, MA 486USA). The PCA-DA/ PCA/ PLSDA data that follows is representative of the fibrosarcoma 120 data where 6 biological replicates per time point with 6 technical replicates for each. (control – 24 hours). PLSDA Data for ROI study using HDI software (Waters Corporation, Manchester, UK) was analysed using one tumour per time point with 9 technical replicates per ROI. Variable Importance in Projection (VIP) scores were used from PLSDA regression modelling to determine the importance of variables within the data time course.

2.3.6 Data pre-processing using Waters MassLynx™ Software and MATLAB®

MS results are imported into MATLAB® in .txt or .csv format either post “SpecAlign” or after application of “automatic peak detection” if using the instrument data processing software (Waters MassLynx™ Software). Normalisation (2-Norm) and mean centre were selected, “contiguous blocks” was used for cross validation.

2.4 Results and Discussion

2.4.1 Initial MALDI profiling and imaging of *in situ* tissue tryptic digests in mouse fibrosarcoma 120 models

Initial profiling and imaging experimental work was performed using an Applied Biosystems Q-Star Pulsar i Quadrupole ToF Mass Spectrometer. Preliminary peptide mass fingerprints (PMF's) (Figure 2.1) were acquired to provide insights into typical high abundant potential peptides in order to observe any gross pharmacological responses post CA-4-P administration.

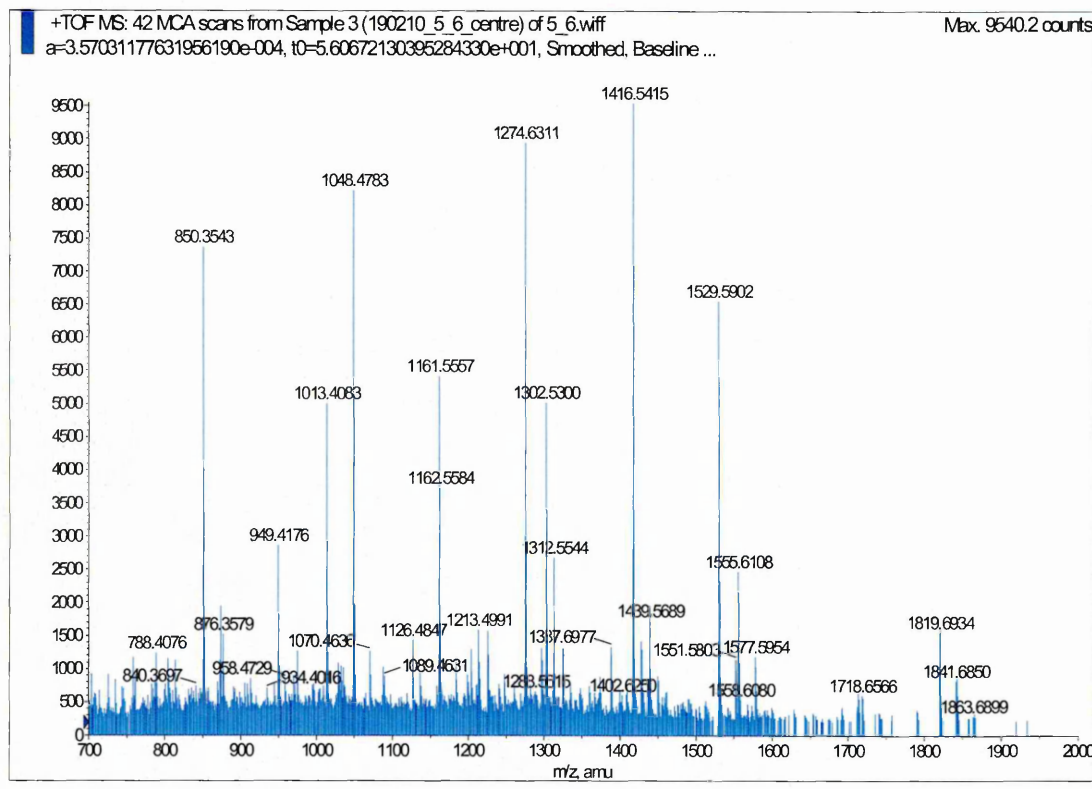


Figure 2. 1: Representative peptide mass fingerprint (PMF) arising from an on-tissue digest of a VEGF120 tumour 24 h after dosing with 100 mg/kg *i.p.* CA-4-P. Prior to matrix application *in situ* tissue digestion was performed with trypsin solution prepared (from lyophilised trypsin) at 20 $\mu\text{g/ml}$ by addition of 50 mM ammonium bicarbonate (NH_4HCO_3) pH 8.12, containing 0.5% octyl- α / β -glucoside (OcGlc). The matrix employed was α -cyano-4-hydroxycinnamic acid (CHCA, 5 mg/ml) and aniline in acetonitrile:water:TFA (1:1:0.1 by volume).

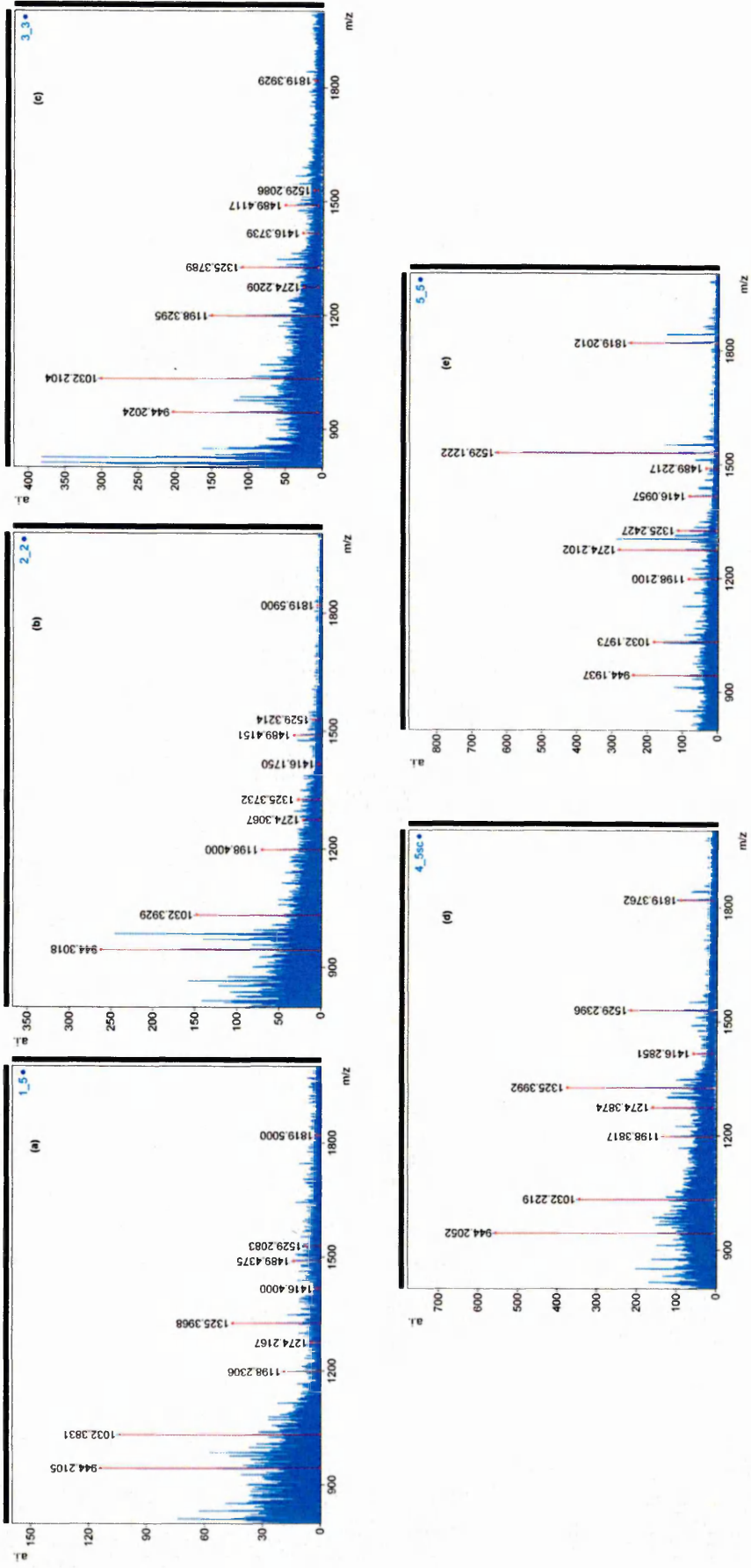


Figure 2. 2: Peptide mass fingerprints obtained from the fibrosarcoma 120 tumour tissue sections treated with saline or 100 mg/kg i.p. CA-4-P in the time course experiments; (a) (Control/saline), (b) 0 h post CA-4-P, (c) 0.5 h post CA-4-P, (d) 6 h post CA-4-P and (e) 24 h post CA-4-P. In the case of 0h CA-4-P, the tumour was excised immediately (within 2mins) after dispatchment

The spectra shown in Figure 2.2 are from the following samples: (a) control/saline, (b) 0 h post CA-4-P, (c) 0.5 h post CA-4-P, (d) 6 h post CA-4-P and (e) 24 h post CA-4-P. The increase in the relative intensity of m/z 1819.3 along with other readily identifiable haemoglobin peptides (e.g. m/z 1529.7 HbAa 18-32 (IGGHGAEYGAELER), m/z 1274.3 HbAb 52-41 (LLVVPWTQR)) can be seen. This increase in tissue haemoglobin is as would be expected considering the vascular damaging properties of CA-4-P. Due to disruption of the 3D capillary architecture, endothelial cell necrosis, apoptosis and leakage of blood cells into tumour tissues is inevitable. This is clearly illustrated by Figure 2.3, where MALDI-MS images for the distribution of m/z 1274 (HbAb 52-41) at each time point are shown along with photographs of the corresponding haematoxylin and eosin stained sections. It is debatable in the 0h treatment how much of the drug reaches the tumour, however there is an apparent signal in Figure 2.3 corresponding to m/z 1274. Further drug distribution studies would clarify presence of CA-4-P and its metabolites.

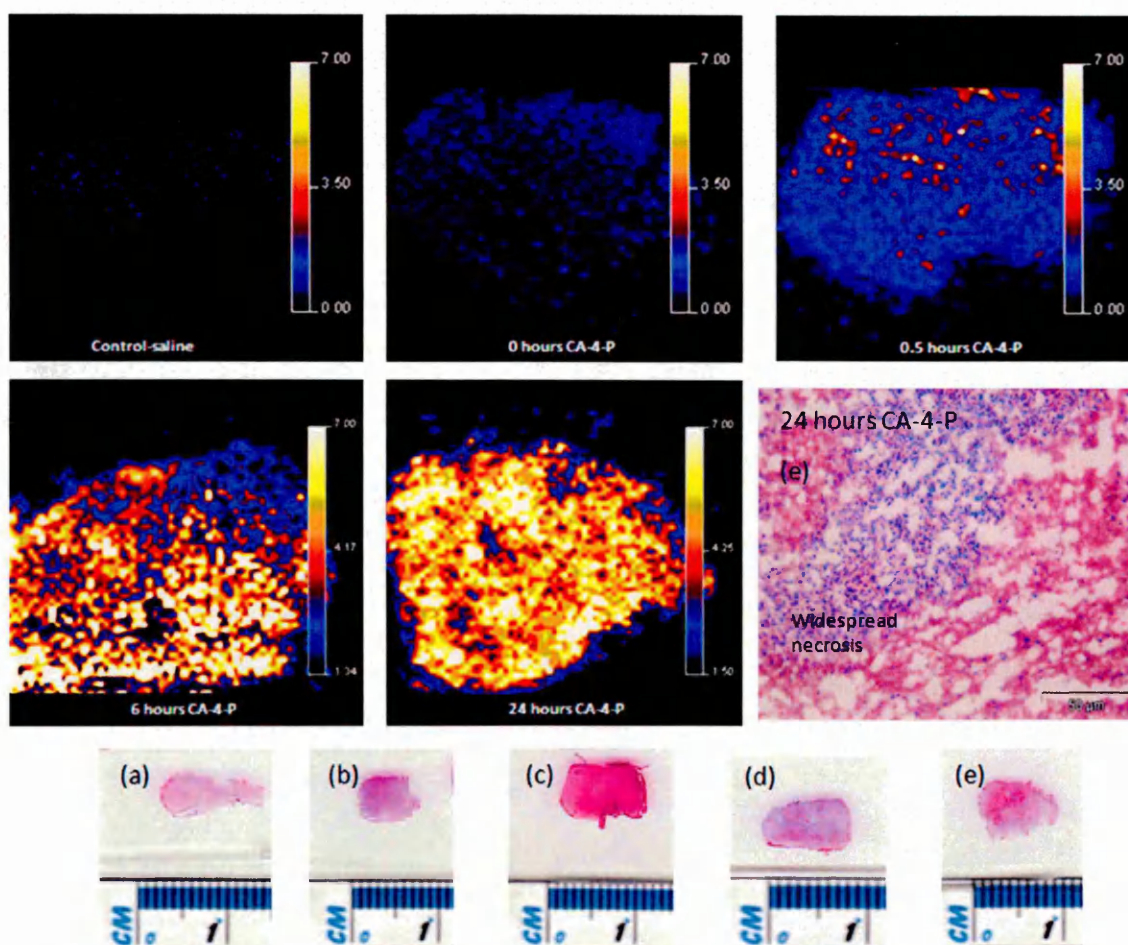


Figure 2. 3: MALDI-MS images for the distribution of m/z 1274 throughout a fibrosarcoma 120 timecourse. (HbAb 52-41) in (a) control (saline), (b) 0 h post CA-4-P (c) 0.5 h post CA-4-P, (d) 6 h post CA-4-P and (e) 24 h post CA-4-P, along with photographs of the corresponding haematoxylin and eosin stained sections.

2.4.2 Haematoxylin and Eosin staining of fibrosarcoma 120 tissue

Haematoxylin and eosin (H&E) staining of each fibrosarcoma 120 serial section was performed after imaging for identification of viable and necrotic tissue and to make observations of the tumour rim.

Examples of viable and necrotic tissue are shown in Figure 2.4: (a) control saline-treated tumour which is essentially viable, (b) control tumour with a small necrotic region, (c) 0 h CA-4-P showing viable tissue, (d) 0 h CA-4-P showing viable and necrotic regions, (e) 0.5 h after CA-4-P showing viable tissue, (f) 0.5 h after CA-4-P showing viable and increasing necrotic regions, (g) 6 h after CA-4-P showing partially viable regions, (h) 6 h after CA-4-P with haemorrhage and necrosis and (i) 24 h after CA-4-P treatment showing total necrosis.

Higher magnification images of the H&E staining of the tumour rim in the VEGF120 tumour sections are shown in Figure 2.5: (a) control/ saline, (b) 0 h CA-4-P, (c) 0.5 h after CA-4-P, (d) 6 h after CA-4-P and (e) 24 h after CA-4-P. The H&E tissue sections indeed reflect the heterogeneous nature of the tumour especially considering the control with no CA-4-P (Figure 2.5 a), however the effect of the vascular disrupting agent is still apparent and the 0.5 h image (Figure 2.5 c) suggests a good example of the viable tumour resistant rim.

In all images, viable tumour cells have densely packed nuclei which appear as regions of “organised cells” which stain blue in H&E staining whereas regions of necrosis, due to cell lysis tend to show as a disorganised region with less blue staining. In these data, haemorrhaging also gives a pink colour to the tissue e.g. Figure 2.4h.

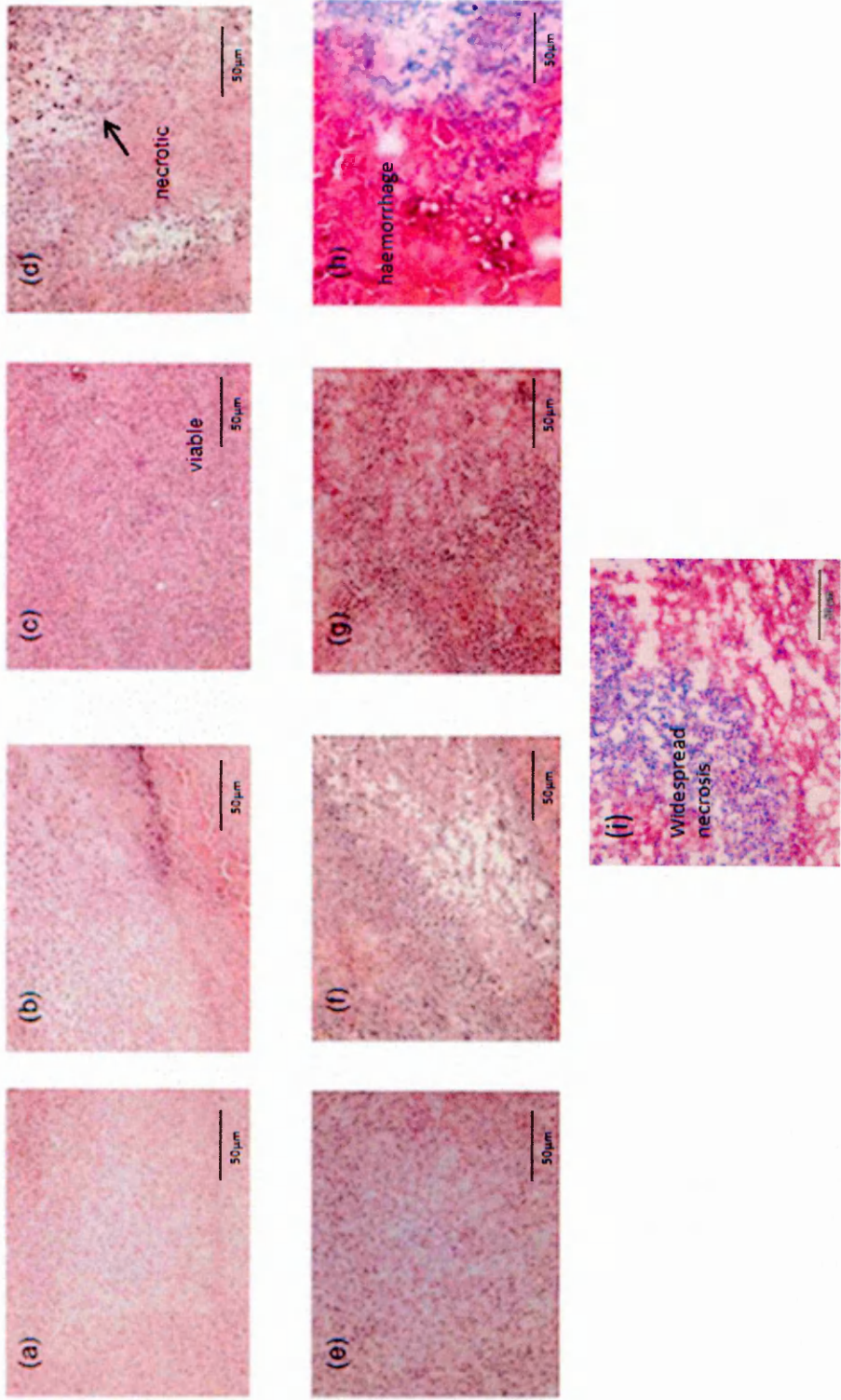


Figure 2. 4 : Haematoxylin and eosin stained sections. (a) Control (saline) showing viable tissue, (b) control showing a small necrotic region, (c) 0 h CA-4-P showing viable tissue, (d) 0 h CA-4-P showing viable and necrotic regions, (e) 0.5 h post CA-4-P showing viable tissue, (f) 0.5 h post CA-4-P showing viable and increasing necrotic regions, (g) 6 h CA-4-P showing partially viable regions, (h) 6 h CA-4-P with haemorrhaging and necrosis, (i) 24 h after CA-4-P treatment showing total necrosis.

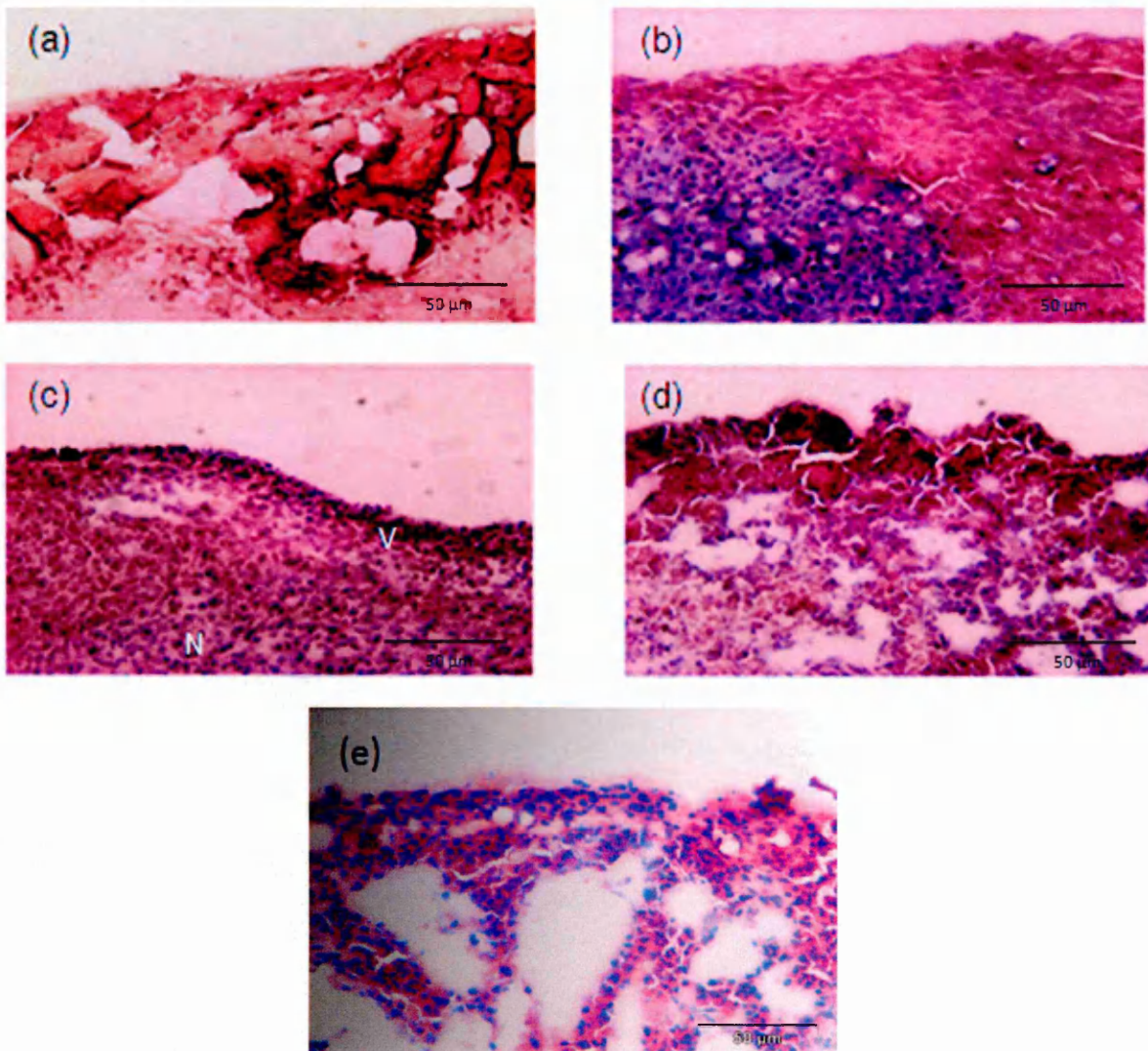


Figure 2. 5: Higher magnification images of the H&E staining of the tumour rim in the VEGF120 tumour sections. Control (saline), (b) 0 h post CA-4-P, (c) 0.5 h post CA-4-P, (d) 6 h post CA-4-P and (e) 24 h post CA-4-P. The 0.5 h image displays a good example of the viable tumour resistant rim.

2.4.3 Initial imaging of proteins according to theoretical digests using MALDI-MSI

Proteins which could be of relevance to tumour biology and the stress response were tentatively identified according to theoretical digests (Li *et al* 2011). The following preliminary MALDI images were observed to aid focus on potential future protein targets to consider in this dose response relationship study.

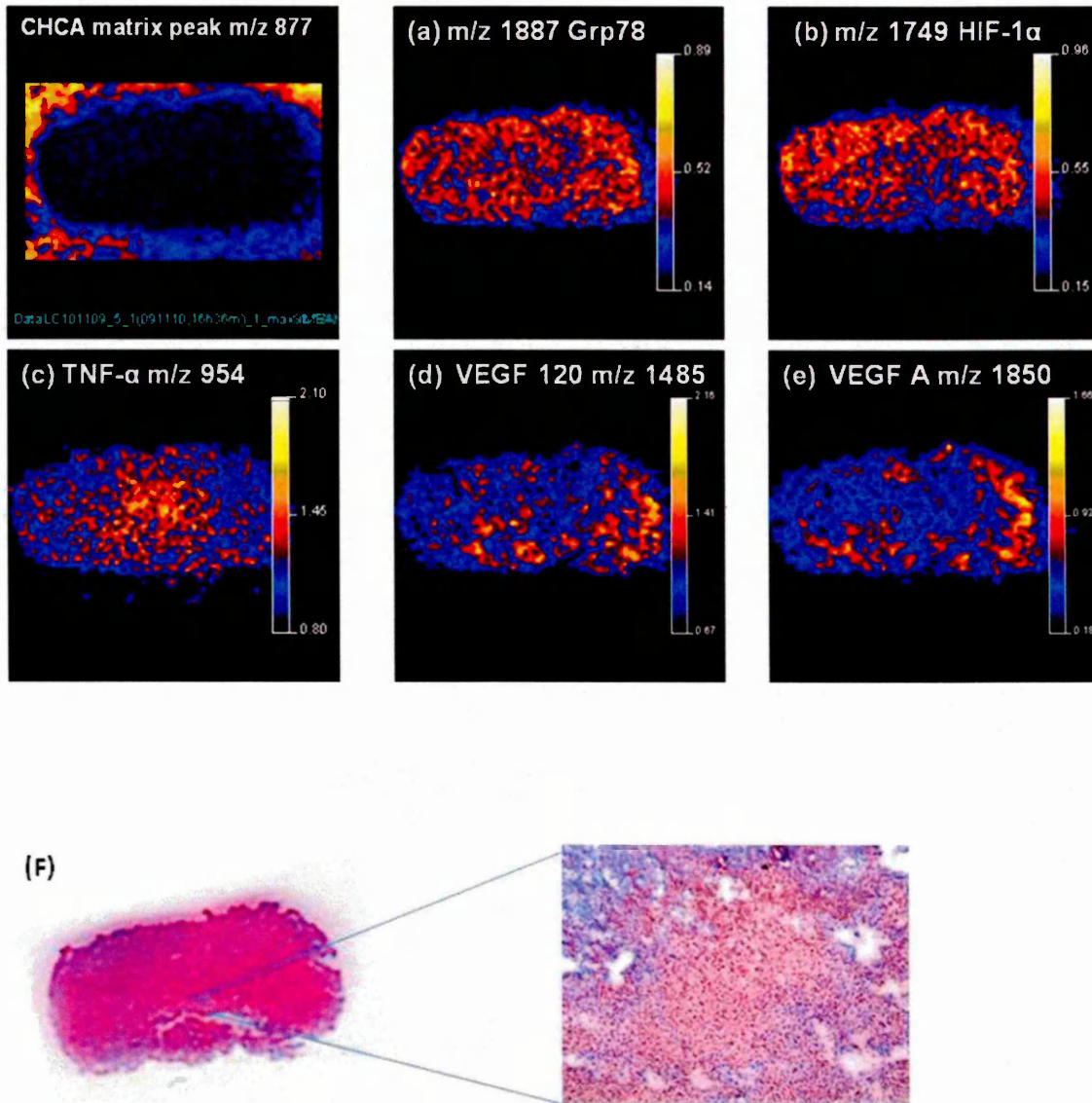


Figure 2. 6: MALDI-MSI of peptides from tumour 5:1 (24hrs CA-4-P). CHCA matrix peak m/z 877 used for normalisation, (a) m/z 1887 Grp78, (b) m/z 1749 HIF-1α, (c) TNF-α, (d) m/z 1485.7 VEGF 120, (e) m/z 1850.8 VEGF A (188), according to theoretical digests and (f) tumour 5:1 histological section after H&E staining with magnified insert showing necrotic tissue.

The ion signals shown in Figure 2.6 were generated according to predicted theoretical tryptic digests. Although at this stage protein identifications were not yet confirmed, it was fascinating to notice the differing spatial distribution of the potential peptides thus reflecting the heterogeneous nature of tumour tissue.

The possible detection and spatial distribution of proteins like glucose-regulated protein 78/Binding immunoglobulin protein (Grp-78/ BiP) (Figure 2.6a) could reveal vital information of how CA-4P can effect tumorigenesis thus inducing other pathological stimuli.

The image tentatively identified as belonging to VEGF A (188 isoform using UniProKB database (mouse) with 2 missed cleavages) in Figure 2.6 e is quite contradictory to the mouse model employed which had been genetically engineered to solely express the VEGF 120 isoform. The latter could be due to immune cell infiltration.

It was found however, that through further interrogation of peptide sequence databases i.e. Blast (<http://blast.ncbi.nlm.nih.gov/>) and reference to the article by Tischer *et al* (1991) that the peptide sequence given regarding the VEGF 120 ion at m/z 1485 is incorrect. The latter discovery came about whilst checking whether or not the sequence giving the ion signal (Figure 2.6 e) at m/z 1850 really matched part of the VEGF 188 protein sequence to support the theory of possible immune cell infiltration. It appeared that none of the VEGF 120 peptide 'RWQKIADELGNR' (2 missed cleavages) giving m/z 1485 provided by UniProKB theoretical digest is detectable in the original VEGF nucleotide sequences (Tischer *et al* 1991). The sequence in question when submitted to Blast database gave a result suggesting that the peptide could be a zinc finger protein. The VEGF 188 peptide 'FKSWSVHCEPCSERR' (although 2 missed cleavages) giving m/z 1850, matched with the nucleotide sequences detailed in UniProKB, Blast and original VEGF nucleotide sequences presented in Tischer *et al* (1991). Part of the VEGF 188 peptide sequence coincided with nucleotide sequences present in the VEGF exon 6, a region of the VEGF gene known exclusively to VEGF 188 (Figure 1.29), hence supporting the presence of VEGF 188 in the MALDI-MSI (Figure 6 e).

2.4.4 Principle component analysis – discriminant analysis (PCA-DA)

Multivariate analysis was chosen to statistically analyse the complex data sets which arise from *in situ* PMF's. PCA-DA was performed to try and correlate peptide induction with dose response and to provide a method of further analysing the PMF data.

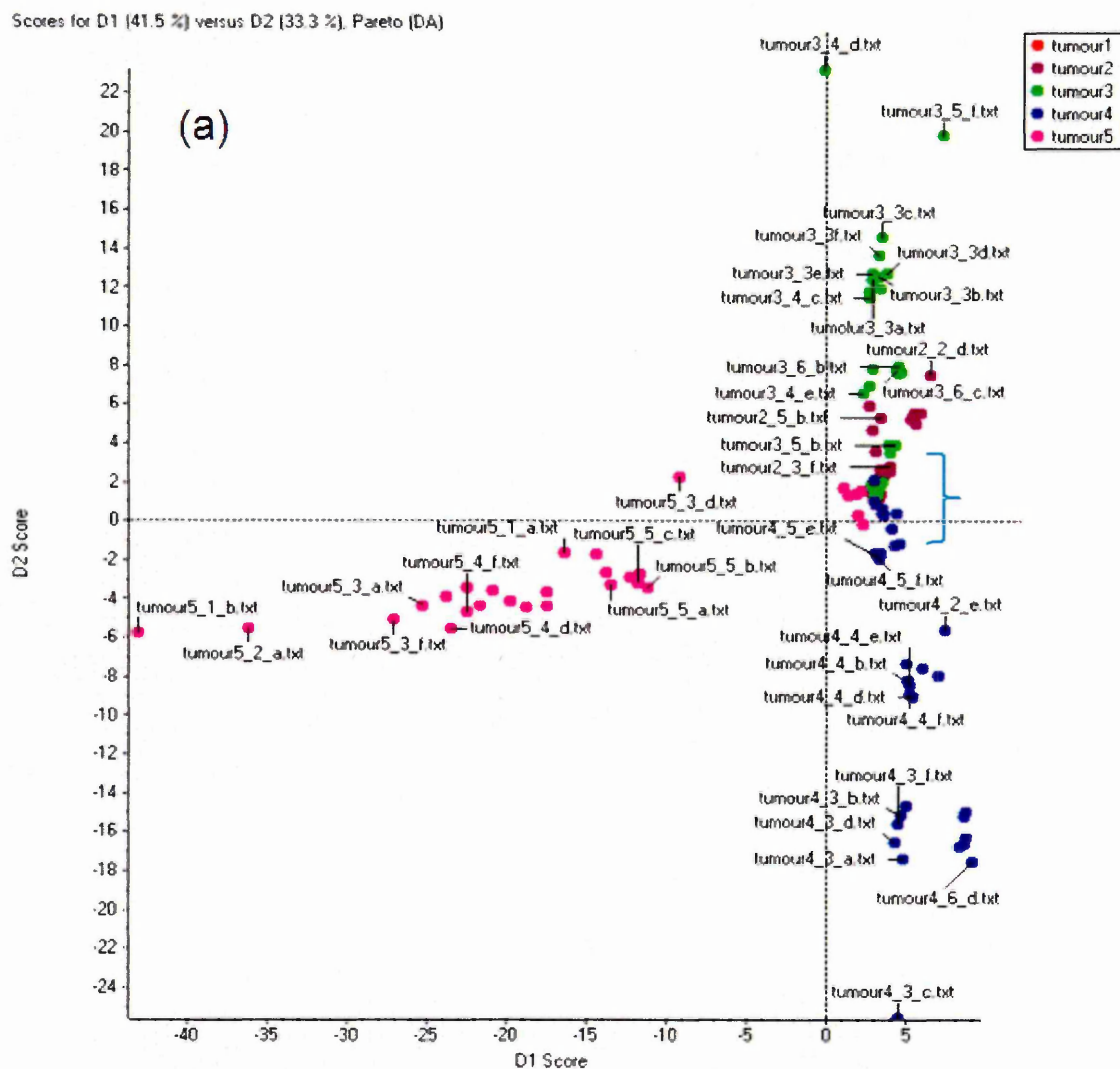


Figure 2. 7: PCA-DA of fibrosarcoma 120 tumour *in situ* tryptic digests.(a) The scores plot showing groupings and variability between tumour time point spectra, Tumour 1-5 indicates Saline/Control - 24h post CA-4-P (b) the loadings plot displaying the separation and spatial distribution of *m/z* values in relation to score plot positions, (c) illustrates the variability of two haemoglobin peptides within each tumour section. The red arrow on (b) indicates *m/z* 1274 (indicative of haemoglobin *b* chain) which is associated with the tumour 4 set (6 h post CA-4-P).

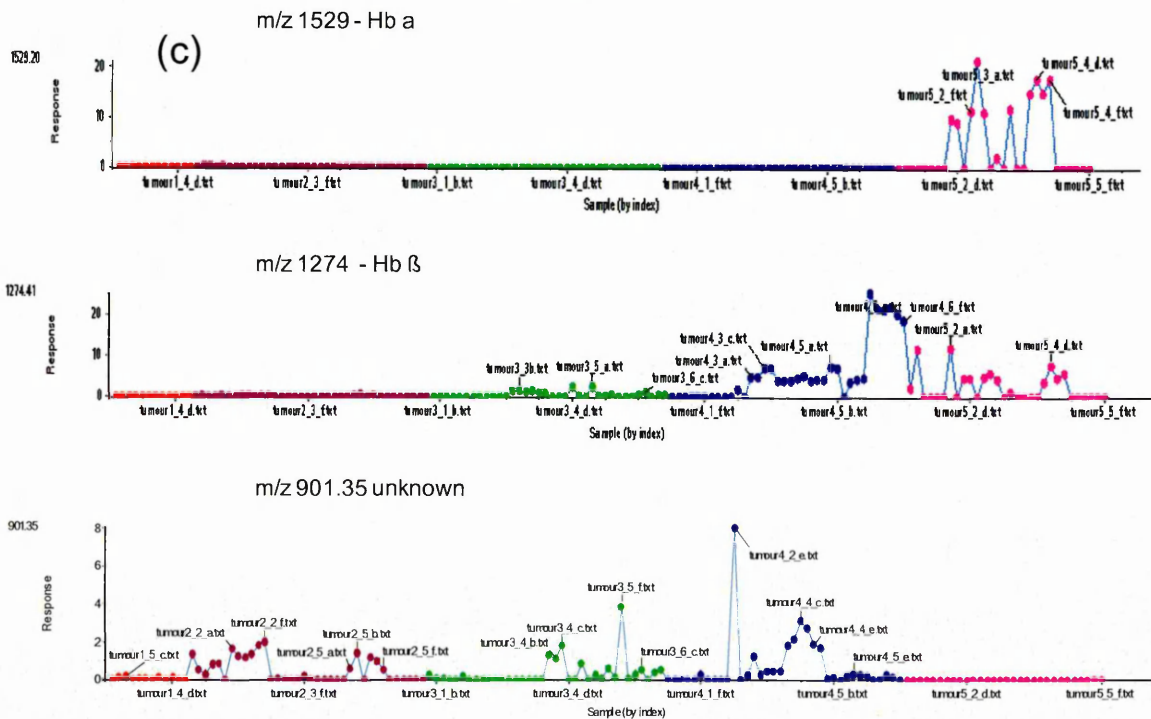
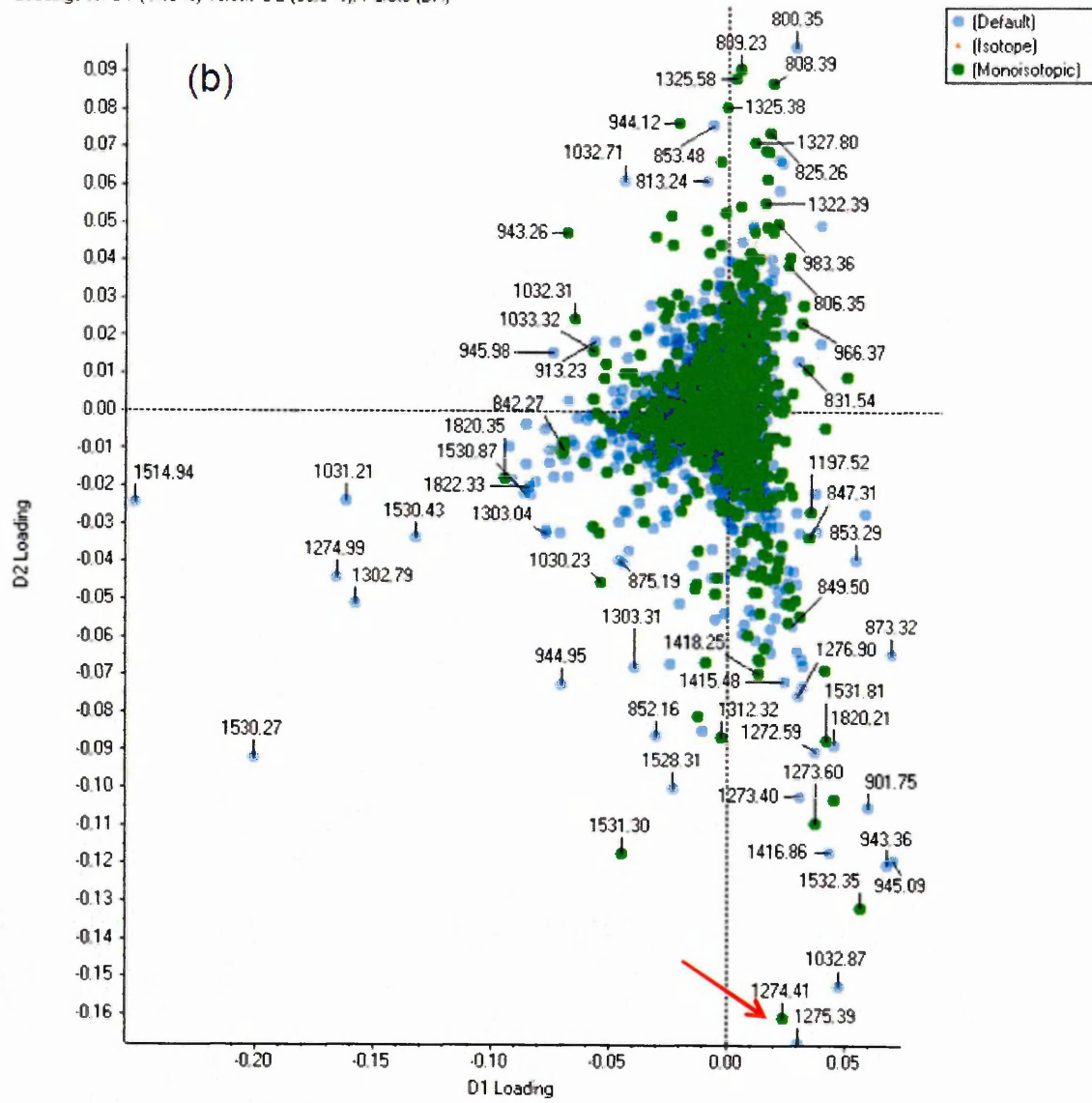


Figure 2.7 shows the results of PCA-DA of VEGF120 *in situ* tryptic digests: (a) the scores plot showing groupings and variability between tumour time point spectra, (b) the loadings plot displays the separation and spatial distribution of *m/z* values in relation to score plot positions, (c) illustrates the variability of two haemoglobin peptides within each tumour section and an unknown at *m/z* 901. The simple response present from the haemoglobin peptides was regarded as a standard for future time course results to aid validation of dose response relationships. The red arrow on Figure 2.7(b) indicates *m/z* 1274 (indicative of haemoglobin β chain) which is associated with the tumour 4 set (6 h after CA-4-P). In Figure 2.7(b) the green data points are peaks identified as monoisotopic by the Marker View 1.2 software and blue data points are peaks which have not been assigned as monoisotopic. These are termed "default" by the software.

For the chemometric investigation of the proteomics data reported here, multivariate analysis was deemed essential because of the large data sets thousands of signals can arise from just a single pixel due to the acquisition of full-range mass spectra (McCombie *et al* 2005). Comparisons of spectral signals are required between both biological and technical replicates throughout a time course experiment and multivariate analysis allows a better visualisation of the "vast data clouds". PCA-DA was chosen to provide preliminary insights into ion signals generated by *in situ* tryptic digestion using MALDI-MSI with the hypothesis that the samples should show separation of unique peptides due to known individual treatment time points.

The scores plot in figure 2.7a provides clear separation of tumour treatment groups 3, 4 and 5 which refer to 0.5 h, 6 h and 24 h post CA-4-P respectively. The earlier time points being tumour 1 (control/ saline) and 2 tumour (0 h) are not visible but can be seen if the region indicated is expanded. The peaks that appear on the loadings plot (Figure 2.7b) seem to be representative of high abundant peptides i.e. histones (*m/z* 944, *m/z* 1032, *m/z* 1325) and haemoglobin (*m/z* 1274, *m/z* 1416) which relate to the occurrence of haemorrhagic necrosis, DNA damage and hypoxic conditions within the tissue.

2.4.5. Employment of Ion Mobility MALDI-Mass Spectrometry to study *in situ* tryptic digestion in fibrosarcoma 120 models

Ion mobility enabled MALDI profiling and imaging describes a further separation method of isobaric species thus opening up another dimension to spectral analysis.

Protein	Accession number	Observed m/z with MALDI-MS	Sequence	Score	Mascot threshold score at 95% significance
Haemoglobin subunit alpha	P01942	2858.4	VADALASAAGHLDDLPGALSALSDLHAHK +21.9819 AT D14 Cation:Mg [II] (DE) [+21.9694], Cation:Na (DE) [+21.9819]	24	>20
		2836.4	VADALASAAGHLDDLPGALSALSDLHAHK	87	>20
		1819.8	TYFPHFDVSHGSAQVK	106	>36
		1529.7	IGGHGAEYGAEALER	98	>18
		1416.7	GGHGAEYGAEALER	87	>43
Histone H4	P62806	1325.7	DNIQGITKPAIR	76	>14
Haemoglobin beta chain	P02088	1302.6	VNSDEVGGEALGR	79	>38
		1161.6	LVVYPWTQR	29	>20
		1048.5	VVYPWTQR	32	>20
Histone H2A Type 1-F	Q8CGP5	1300.6	NDEELNKLGR	33	>21
Actin, aortic smooth muscle	P62737	1198.7	AVFPSIVGRPR	30	>13
		976.4	AGFAGDDAPR	64	>19
Histone H3	P68433	1032.6	YRPGTVALR	11	>10
		715.4	DIQLAR	19	>17
Histone H2A Type 1-F	Q8CGP5	944.5	AGLQFPVGR	24	>19
Rho GTPase-activating protein 2/ N-chimaerin	Q91V57	844.5	RLTSLVR	21	>18

Table 8: Identities and Mascot scores from the IMS-MS/MS analyses of peptide signals showing Mascot score of mouse protein identifications and corresponding threshold score at 95% confidence level.

A representative peptide mass fingerprint obtained from a tumour from an animal sacrificed 6 h after administration of CA-4-P (hereafter referred to as 6 h CA-4-P) using the Synapt instrument, is shown in Figure 2.8. These data illustrate the vast number of peptides that arise from an in situ tissue tryptic digest, as previously reported (Schwamborn *et al* 2007., Le maire *et al* 2007., Shimma *et al* 2006., Groseclose 2007).

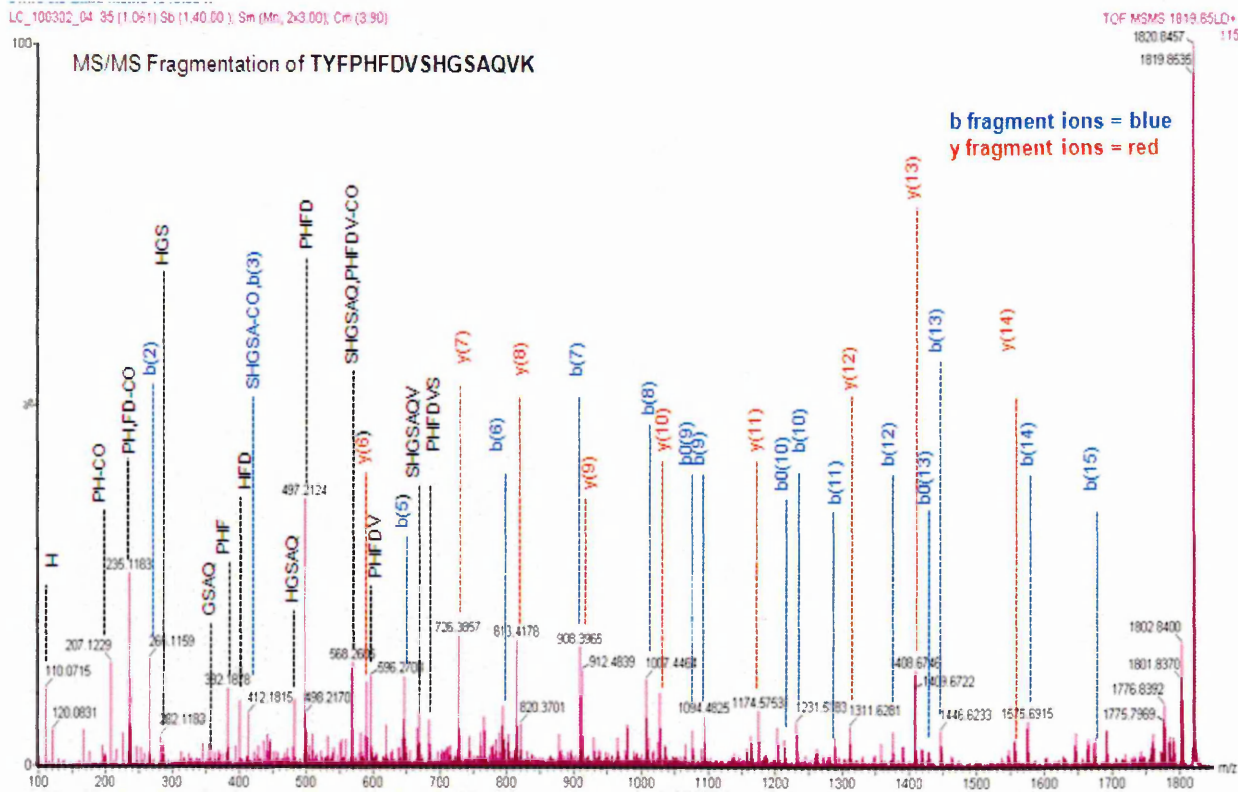


Figure 2. 9: IMS-MS/MS data obtained from the peak observed in Figure 2.8 at m/z 1819.3. This was identified by Mascot search as arising from Mouse HbAa 42-57 (TYFPHFVDVSHGSAQVK).

Figure 2.9 shows IMS-MS/MS data obtained from the peak at m/z 1819.8. This was identified by Mascot search as arising from Mouse HbAa 42-57 (TYFPHFVDVSHGSAQVK) (Table 1). These data are also a further indication of the advantages of IMS for the identification of “on-tissue” generated tryptic peptides. The complexity of the obtained data sets is shown in Figure 2.10a, where ions arising from doubly charged species and singly charged species are clearly separated by the use of ion mobility and further those singly charged ions arising from peptides, matrix adducts and lipids are also separated. Use of IMS separation prior to MS/MS yielded good quality MS/MS spectra for peptides that produced a high and significant Mascot score.

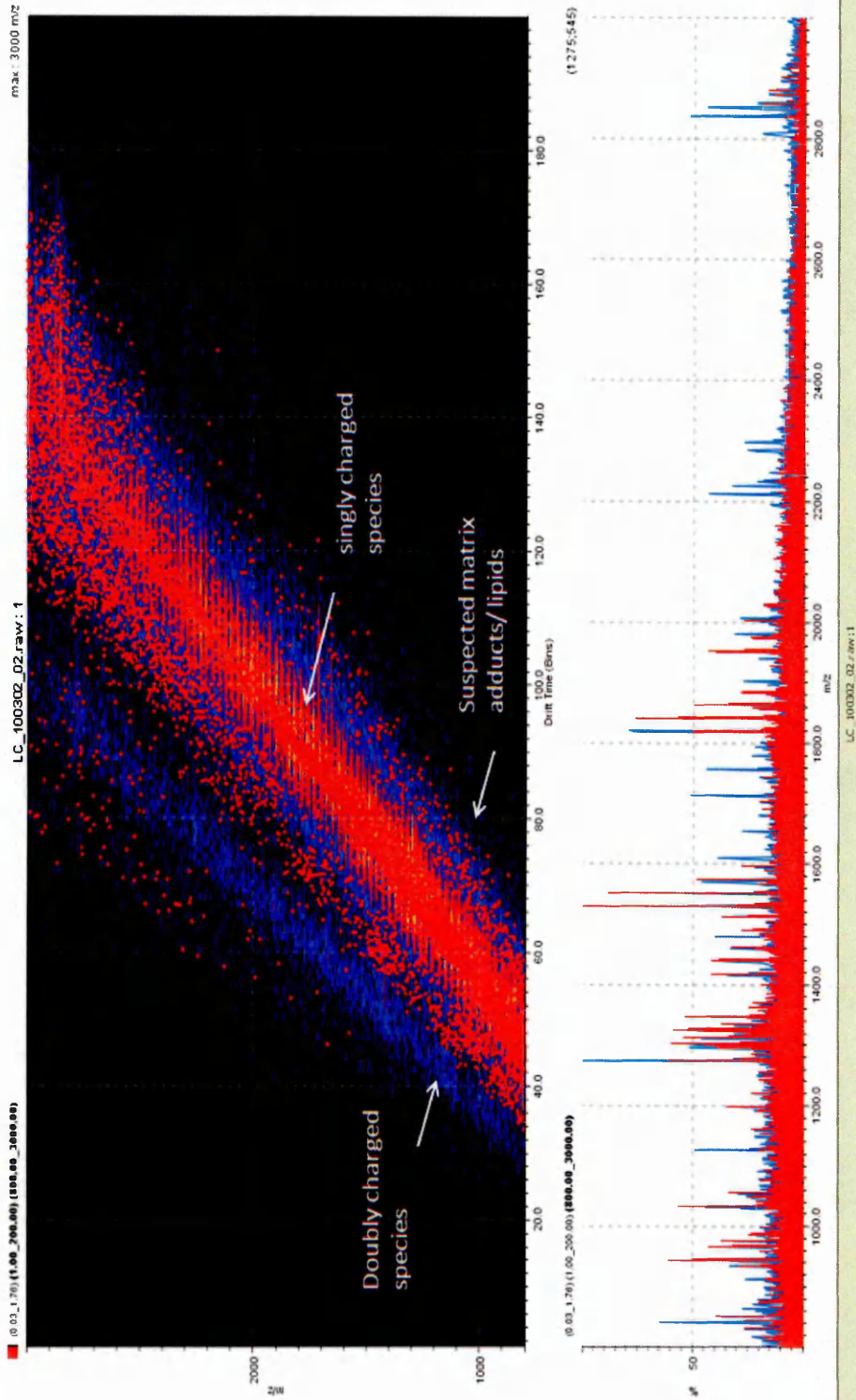


Figure 2. 10 a: A Drift scope plot of a tumour section 24 h post CA-4-P showing the ion mobility separation as a function of drift time. Possible trend lines of doubly charged singly charged and suspected matrix adduct ions/lipids are indicated.

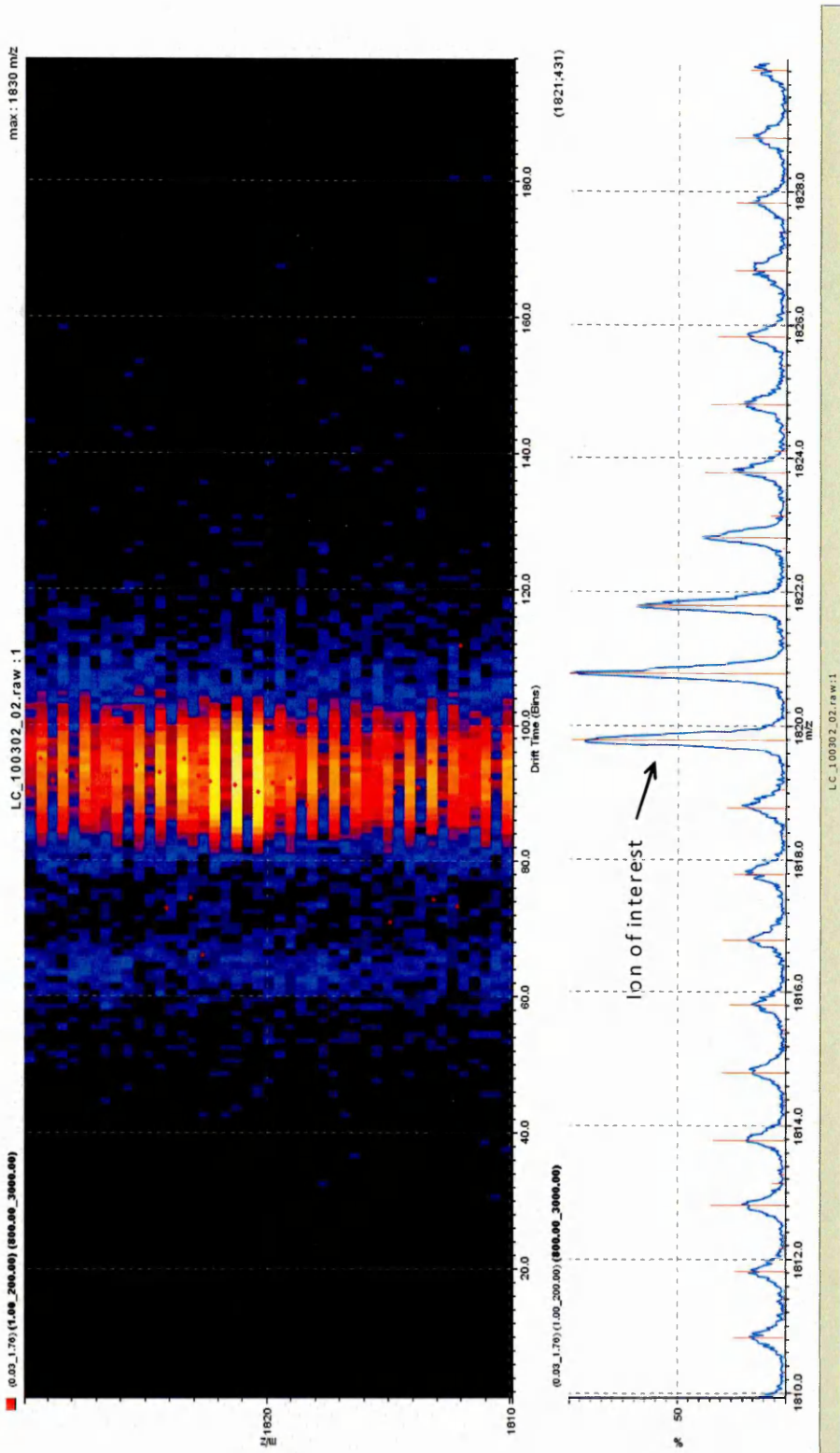


Figure 2.10 b: Zoomed in Drift scope plot shows ion mobility separation of ion of interest haemoglobin subunit alpha m/z 1819.8

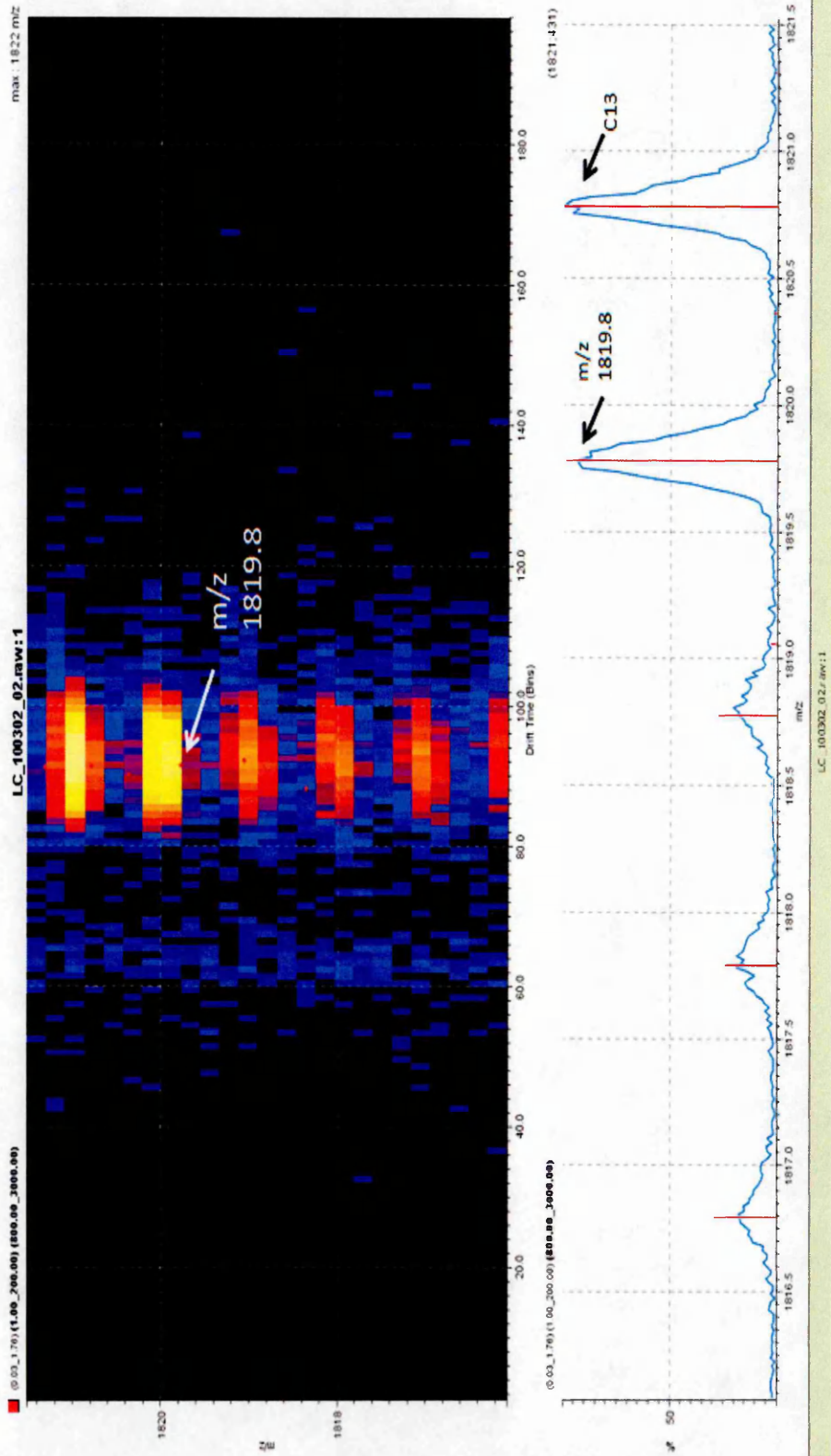


Figure 2.10 c: Drift scope plot shows ion mobility separation of ion of interest haemoglobin subunit alpha m/z 1819.8 and C13 as shown on mass spectrum directly below.

The additional specificity afforded by ion mobility that allows the selection of individual ion species can clearly be seen in Figure 2.10c . The white arrow indicates the ion of interest (m/z 1819.8) and the ion signal directly above depicts the isotope C13 which can be seen on the mass spectrum below the plot.

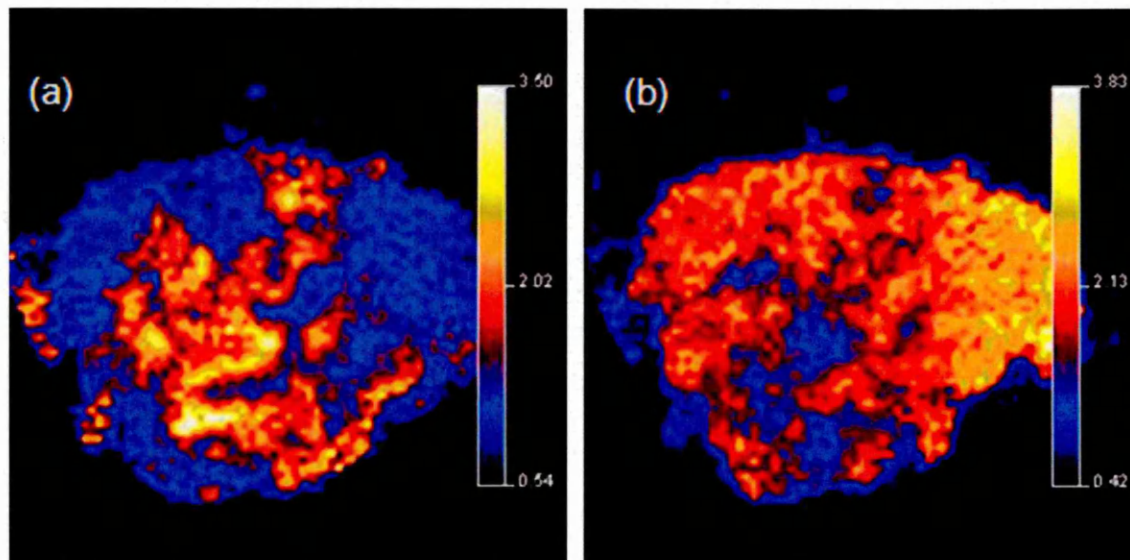


Figure 2. 11: The distribution of two known peptides in tumour 5_6, i.e. a tumour 24 h after treatment with CA-4-P (a) m/z 1416 from haemoglobin a chain depicting central necrotic haemorrhage and (b) m/z 1198 corresponding to actin.

The MALDI MSI images shown in Figure 2.11 show the distribution of two known peptides in tumour 5_6, i.e. a tumour 24 h after treatment with CA-4-P: (a) m/z 1416 from haemoglobin a chain depicting central necrotic haemorrhage and (b) m/z 1198 corresponding to actin. The inverse nature of their distribution is striking.

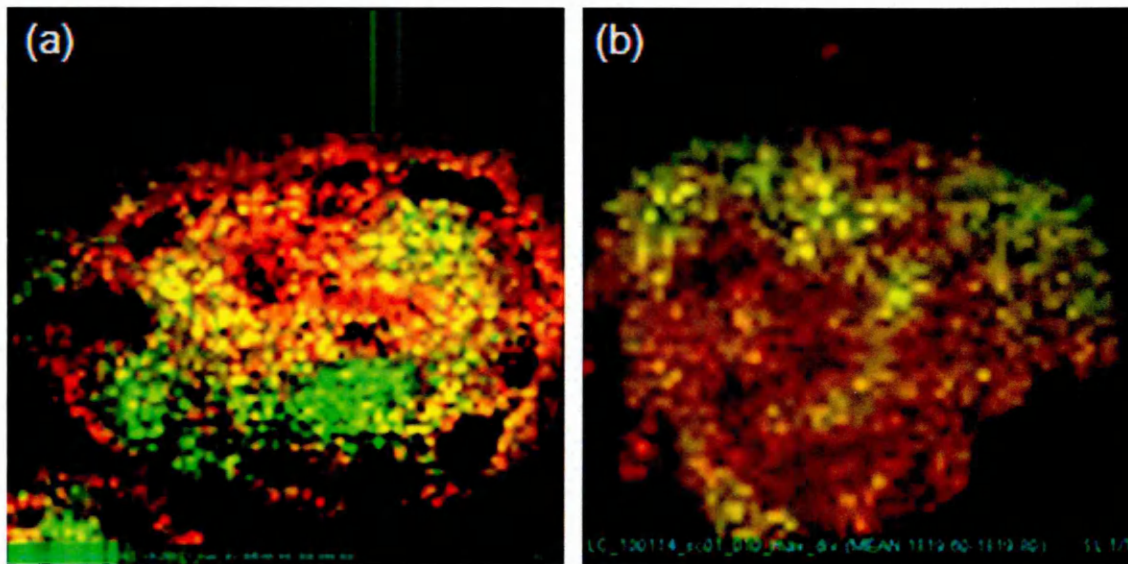


Figure 2. 12: Overlaid MALDI MSI images showing differing spatial distribution and co-registration of peptides. (a) m/z 944 Histone 2A in red and m/z 1274 Hb in solid green, (b) m/z 1819 Hb in red and m/z 944 Histone 2A in solid green.

Figure 2.12 shows examples of overlaid images to show differing spatial distribution and co-registration of peptides using MALDI MSI: (a) m/z 944 histone 2A in red and m/z 1274 Hb in solid green, (b) m/z 1819 Hb in red (from rainbow) and m/z 944 histone 2A in solid green. The Mascot scores for the IMS-MS/MS analyses of these peptides are given in Table 8.

2.4.6 Rho GTPases: a target to help understand resistance to CA-4-P?

The Rho GTPases are proteins known to be involved in cell permeability and actin/cytoskeleton dynamics. (Modolo et al 2012., Aznar and Lacal 2001., Aznar *et al* 2004., Schmitz *et al* 2002). Influence on extra cellular matrix (ECM) integrity, apoptosis, cell adhesion and proliferation, makes them potential targets in the comprehension of anti-tumour drug resistance.

A review by Vega and Ridley (2008) discusses the role of Rho GTPases in cancer cell biology and describes them as “*molecular switches*” which continuously revert from the active and inactive forms which are GTP-bound and GDP-bound respectively. In the activated state they can bind to many effectors which subsequently elicit a cascade of events leading to the processes mentioned previously.

Interestingly with relevance to the work reported here, some Rho proteins promote neovascularisation which could be as a result of association with angiogenic factors and drug resistance effectors (Vega and Ridley 2008).

Over a decade ago work by Kozma *et al* (1996) suggested that N-chimaerin (Rho GTPase activating protein 2) is implicated in morphological changes of the cytoskeleton when associated with cancer related protein Rac1 and cytoskeleton signalling protein Cdc42Hs (Kozma 1996). It is stated that n-Chimaerin induces the formation of the actin-based structures lamellipodia (actin projections) and filopodia in migratory mammalian cells and have pro-oncogenic properties. It has been suggested that Rho GTPases have strong influence not only on tumourigenesis but the migratory functionality of the cancer cell (Figure 2.13), therefore key players in the metastatic process (Karlsson et al 2009).

A potential combination therapy for colorectal cancer patients is administration of bevacizumab and cetuximab to target vascular endothelial growth factor (VEGF) and epidermal growth factor receptor (EGFR) (Leve and Morgado-Díaz 2012). It is known that in gastric cancer VEGF interacts with Rac1 whereas EGFR acts as a stimulatory factor of Rac to encourage the migratory process of colonic cells. Therefore the therapeutic likelihood of inhibiting cancer progression is evident. In an article by Leve and Morgado-Díaz (2012) it is suggested that it could be highly beneficial for the future of anti-cancer therapy to identify inhibitors of the Rho GTPase-associated functions.

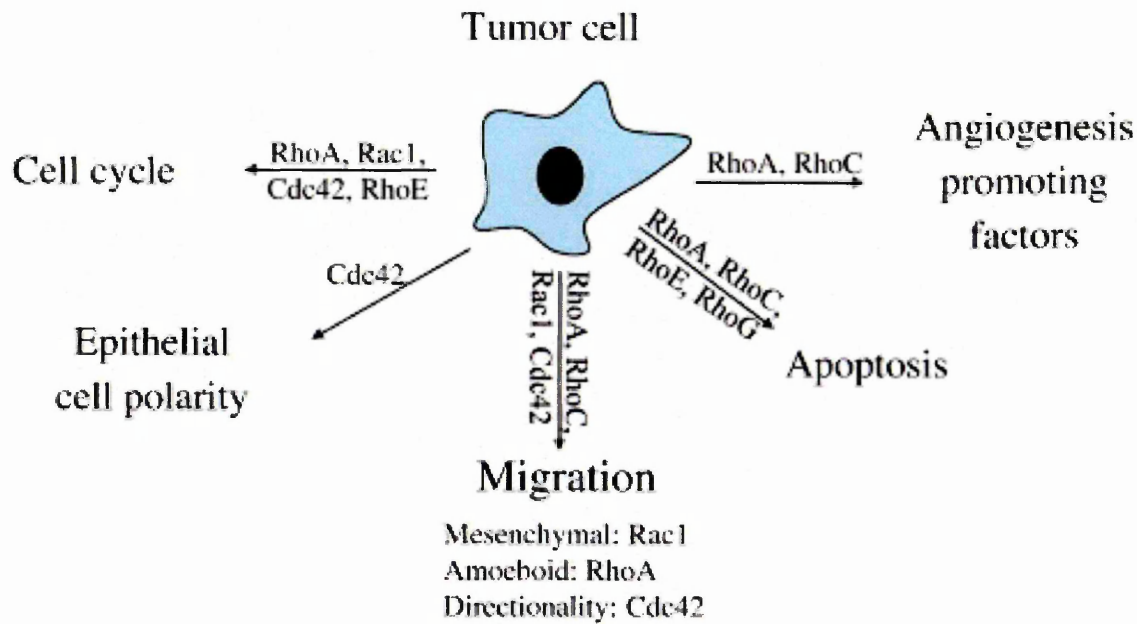
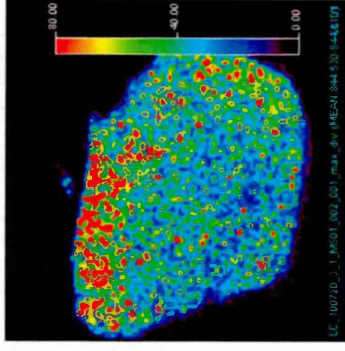


Figure 2. 13: Major Functions of Rho GTPases in vitro (Karlsson et al 2009).

A putative peptide assigned to the Rho protein N-chimaerin as mentioned earlier (Rho GTPase-activating protein 2) was identified in the following MALDI-IMS-MS/MS experimental work (Table 8). Mascot search results produced the peptide 183-189 (RLTSLVR) for the ion at m/z 844.5288.

The peak of interest is indicated in the PMF from fibrosarcoma 120 tissue 30min post CA-4-P administration (Figure 2.14). The corresponding MALDI image is featured showing the spatial distribution of the selected ion at m/z 844. The peptide appears to be located mostly around the periphery of the tumour possibly indicative of its involvement in resistant to CA-4-P. The IMS-MS/MS data obtained from the peak observed in Figure 2.14 at m/z 844.5 is shown in Figure 2.15, the mascot score histogram for the said results is featured in Figure 2.16.

Rho GTPase-activating protein 2
 TOF MS.LD+
 1.22e5



150µm MALDI image

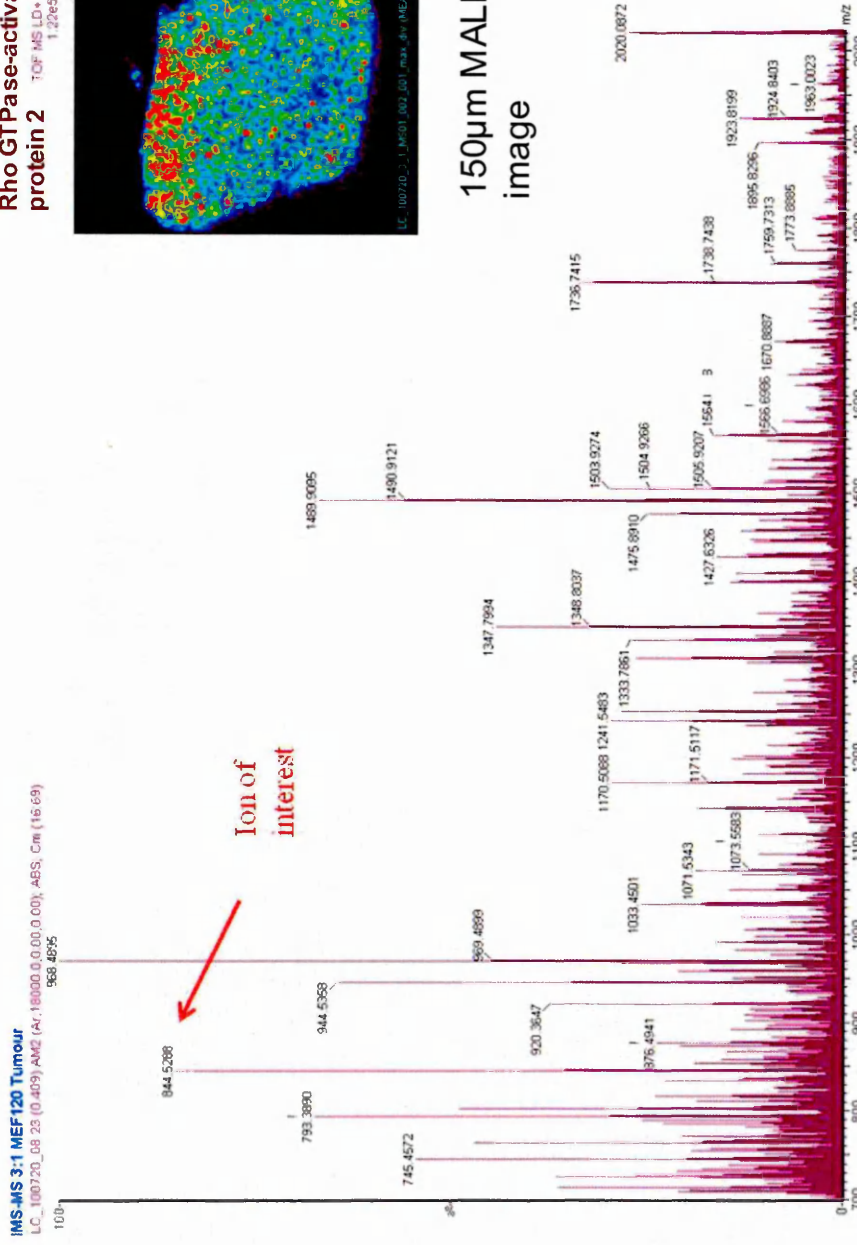


Figure 2. 14: Peptide mass fingerprints obtained from the fibrosarcom 120 tumour tissue 30min post CA-4-P(100 mg/kg i.p.) with peak of interest at m/z 844. The spectra in Figure 2.14 was acquired from an in situ tryptic digest of mouse fibrosarcoma 120 tissue, the peak associated with N-chimaerin (Rho GTPase activating protein 2) is indicated along with the corresponding MALDI image.

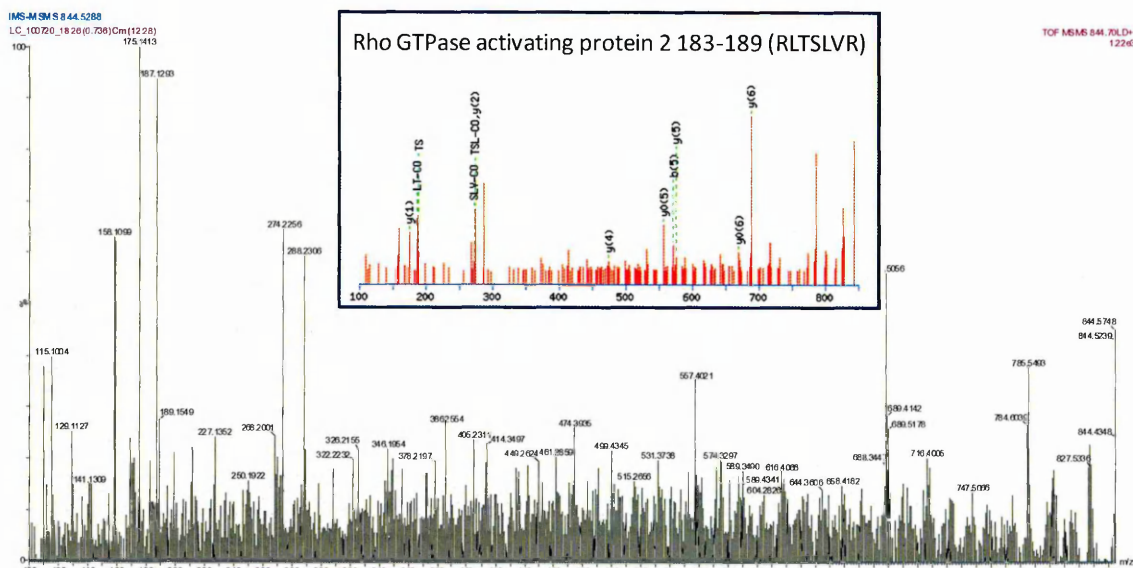


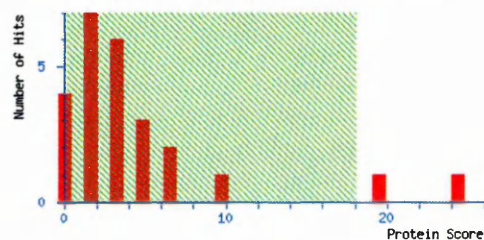
Figure 2. 15: IMS-MS/MS data obtained from the peak observed in Figure 2.14 at m/z 844.5. This was identified by Mascot search as arising from Mouse N-chimaerin (Rho GTPase activating protein 2) 183-189 (RLTSLVR), the insert features the matched MS/MS fragmentation pattern.

MASCOT Mascot Search Results

User : Laura Cole
 Email : lmcole@my.shu.ac.uk
 Search title :
 MS data file : all.pk1
 Database : SwissProt 2012_10 (538259 sequences; 191113170 residues)
 Taxonomy : Mus. (16624 sequences)
 Timestamp : 16 Nov 2012 at 11:25:09 GMT
 Protein hits : [H2A1F_MOUSE](#) Histone H2A type 1-F OS=Mus musculus GN=Hist1h2af FE=1 SV=3
 [CHIN_MOUSE](#) N-chimaerin OS=Mus musculus GN=Chn1 FE=1 SV=2

Mascot Score Histogram

Ions score is $-10 \cdot \log(P)$, where P is the probability that the observed match is a random event. Individual ions scores > 18 indicate identity or extensive homology ($p < 0.05$). Protein scores are derived from ions scores as a non-probabilistic basis for ranking protein hits.



Peptide Summary Report

Figure 2. 16: Mascot score histogram detailing the results in the identification of N-chimaerin.

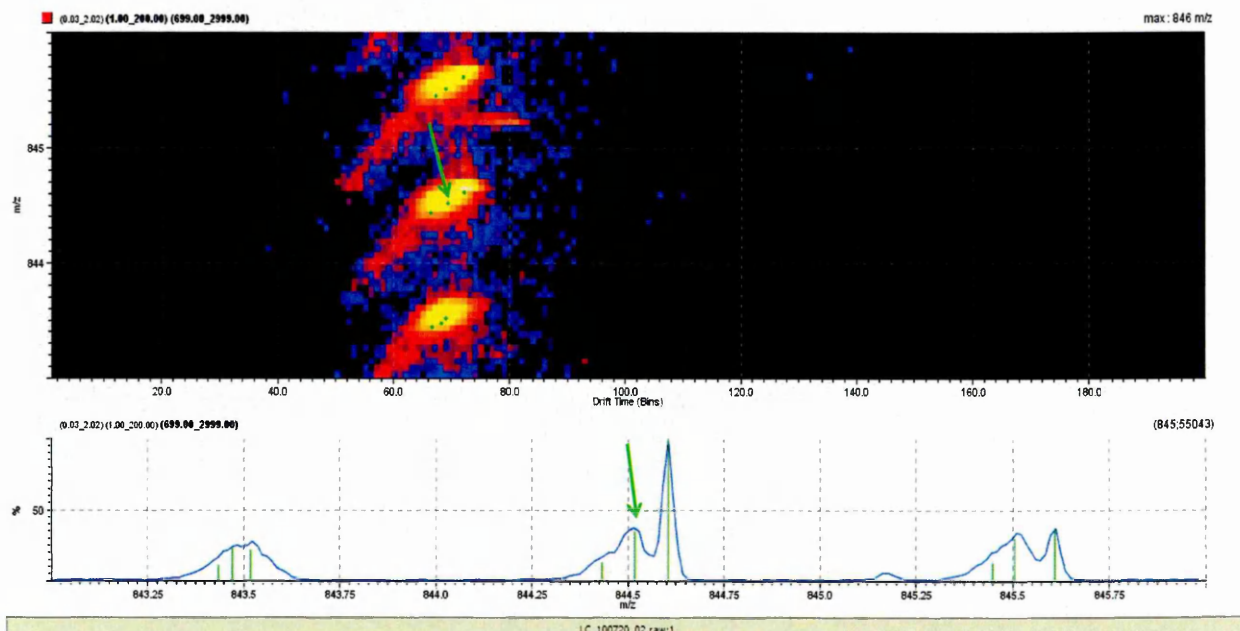
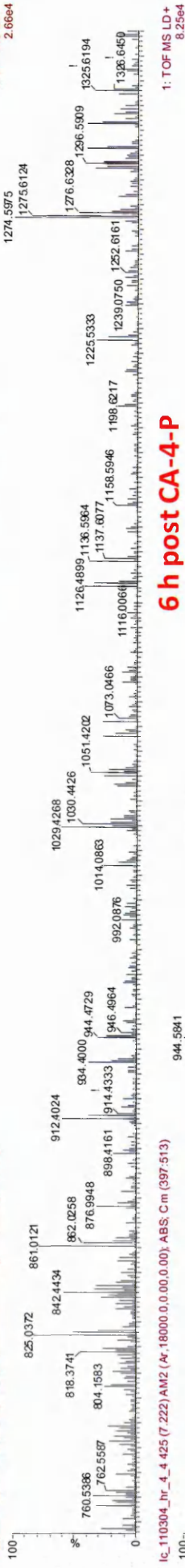


Figure 2. 17: Zoomed in Driftscope plot showing ion of interest, arrow indicating the peak originally selected.

It could be said that there are many overlapping signals in the tryptic peptide MS/MS spectrum shown in Figure 2.15 where both the arginine γ 1 ion (m/z 175) and evidence of potential hydroxy fatty acids (m/z 187) are visible. This is also evident in the Driftscope plot (Figure 2.17) where the arrows point to the actual peak that was selected for MS/MS fragmentation. The dominant peak to the left of the indicated peak in Figure 2.17 would be part of the MS/MS spectrum, despite this the peptide was matched and identified (Figure 2.15) having 1 missed cleavage from the fragments present in the data.

24 h post CA-4-P

MS 1:5 MEF120 turnour
 LC_100114_sc02_125 (5.351) AM2 (Ar: 9000.0.0.0.0.0.0); ABS; Cm (108:159)



6 h post CA-4-P

LC_110304_lr_4_425 (7.222) AM2 (Ar: 18000.0.0.0.0.0.0); ABS; Cm (397:513)



30min post CA-4-P

LC_100720_02_28 (0.495) AM2 (Ar: 18000.0.0.0.0.0.0); ABS; Cm (20:28)



Control/ Saline

LC_100720_01_23 (0.561) AM2 (Ar: 10000.0.0.0.0.0.0); ABS; Cm (22:35)

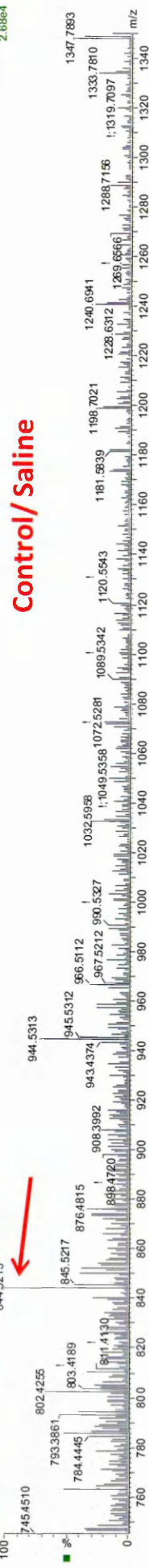


Figure 2. 18: PMF's throughout a fibrosarcoma 120 time course with putative peptide of interest N-chimaerin visible in early time points .Control (saline), 0.5 h post CA-4-P, 6 h post CA-4-P and 24 h postCA-4-P.

The apparent absence/ low abundance of the ion at m/z 844 (putative peptide, Rho GTPase activating protein 2) in the later time points post CA-4-P administration, could be indicative of how the drug effects the Rho protein's usual involvement in tumour progression and neo-genesis of the tumour vasculature. The latter response is evident in the following MALDI-MSI (Figure 2.19) of the ion found at m/z 844.5 corresponding to N-chimaerin.

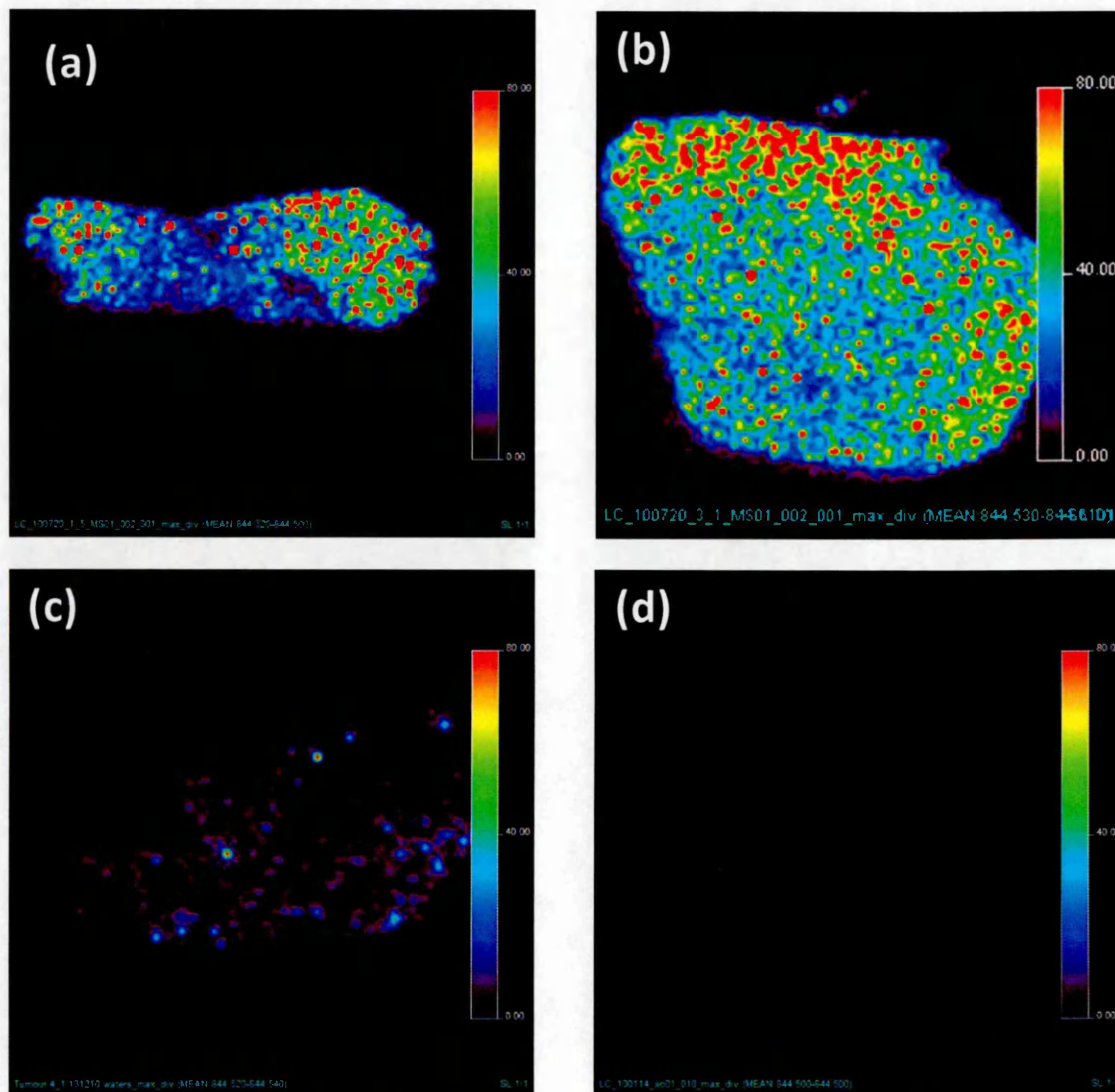


Figure 2. 19: MALDI-MSI throughout a fibrosarcoma 120 time course of the putative peptide Rho GTPase activating protein 2 m/z 844 (183-189, RLTSLVR). (a) control (saline), (b) 0.5 h post CA-4-P, (c) 6 h post CA-4-P and (d) 24 h post CA-4-P, the intensity scales are all set at 80 to aid observation of response.

As mentioned previously in this chapter the spatial distribution of this putative protein appears to be localised around the periphery of the tumour sections in the Control/ saline and 30min

post CA-4-P (Figure 2.19). The images mirror the spectra in Figure 2.18 with the peak of interest decreasing in abundance as the time course progresses.

2.4.7. Statistical analysis of mouse fibrosarcoma 120 tumour tissue using MATLAB®

Principle component analysis (PCA) is an unsupervised test to produce unbiased clustering of a data set, once confident that there were some differences emerging due to none discrimination of data then partial least squares discriminant analysis (PLSDA) was then chosen to provide a classification model.

MATLAB® (Matrix Laboratory) (MathWorks, Inc., Natick, MA 486USA) is used in many areas as a computational statistical tool for mass spectrometry multivariate data analysis, and also via the Bioinformatics Toolbox™ provides tools for spectral alignment and pre-processing.

Spectral data from both profiling and imaging experiments can be imported into MATLAB® in order to build predictive models. This allows the user a powerful means of understanding complex data sets. In addition to script writing using the usual MATLAB® command format, use of the Eigenvector PLS_Toolbox (<http://www.eigenvector.com>) enables access to a number of advanced statistical tools for the analysis of mass spectrometry (MS) data (Eigenvector Research Inc 2012). Recognition of trends within a data time course experiment can be detected via decomposition mathematical modelling i.e. principle component analysis (PCA). Classification studies of MS spectra were performed using PLSDA, where regression vector plots can illustrate presence of ions unique to a particular sample. MS results are imported into MATLAB® in .txt or .csv format either post “SpecAlign” or after application of “automatic peak detection” if using the instrument data processing software (Waters MassLynx™ Software). There are various pre-processing options available to aid linearization of variables within MS data with normalisation (2-Norm) and mean centre being frequently selected. 2-Norm refers to the sum of the squared value of all variables of the sample (Eigenvector Research Inc. 2012). During building of a PCA/PLSDA model the choice of cross validation is crucial to determine complexity of the data i.e. to consider data splits samples and/or latent variables/principle components. An example for a time course experiment would be selection of “contiguous blocks” which would look for assessing predictability between repeat blocks of spectra to circumvent the “replicate sample trap” which could lead to overly optimistic fitting of data.

In MATLAB® complex data clouds can be modelled with ease via the Eigenvector PLS_Toolbox allowing a deeper perception of variability throughout time course experiments.

Score Plot

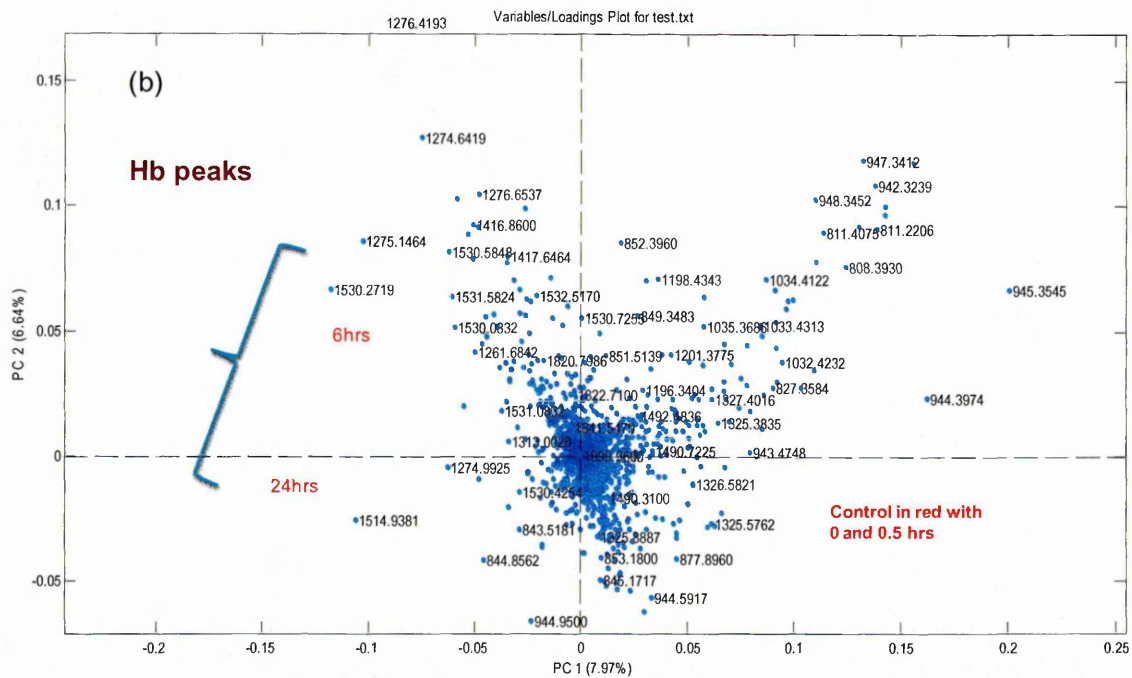
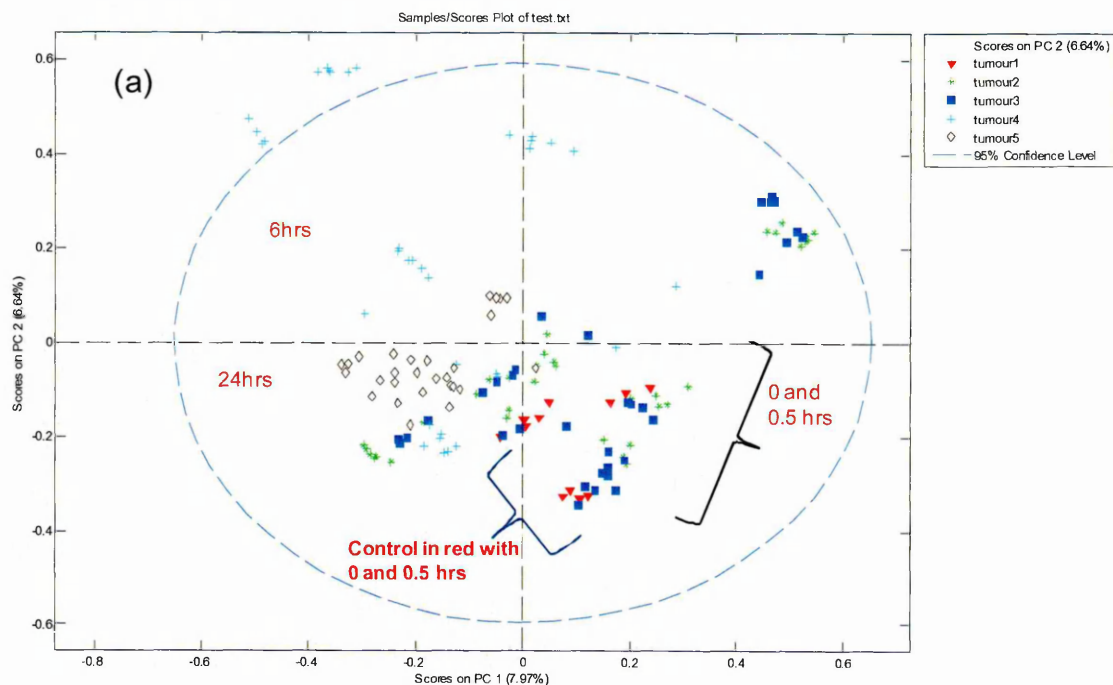


Figure 2. 20 : PCA of fibrosarcoma 120 tumour tissue in situ tryptic digests. The score plot (a) shows groupings between the tumour time points, the loading plot (b) contains the peak information which spatially relate to the groupings seen in (a) with dominant Hb peaks.

Figure 2.20a although not aesthetically pleasing as the PCA-DA model featured earlier in Figure 2.7 shows similar groupings shared by the earlier time points with separate regions assigned

for the 6h and 24h post CA-4-P. The Hb peaks are clearly visible in the later time points of the corresponding loadings plot (Figure 2.20b). This now, seemingly a characteristic of the CA-4-P susceptible fibrosarcoma model.

The conclusions that can be drawn from these data are fairly limited as the very intense haemoglobin and histone peaks appear to dominate the statistics. It could be argued that biomarker discovery requires supervised discriminant analysis i.e. PLSDA, opposed to non discriminant analysis. The rationale behind this idea is that non discriminant analysis could mask expected trends, an example of this scenario would be a treatment time course study. The treatment added throughout a time course experiment is a known factor that is expected to influence the data generated. Pre-grouping the data before building the statistical model could aid the separation of relevant peaks of interest.

PLSDA aimed to provide classification between tumour time points. The PLSDA data that follow are representative of the fibrosarcoma 120 data set as described in 2.3.5 Statistical analysis section.

An example of the clarity of the data possible from analysis using MATLAB® is shown in Figure 2.21. Here, the regression vector plots from PLSDA of “on-tissue” digests of fibrosarcoma 120 Control/Saline and 30 min post combretastatin-4-phosphate (CA-4-P) (a vascular disrupting agent), treatment tumour samples show the increased abundance of peaks at m/z 944 and 1032. This allows classification between data obtained from the control/saline and 30 min post treatment tumour samples based on the induction of Histone 2A and Histone H3. The latter could possibly be a reflection of DNA damage necrosis and hypoxia as a result of CA-4-P administration as discussed in a previous section.

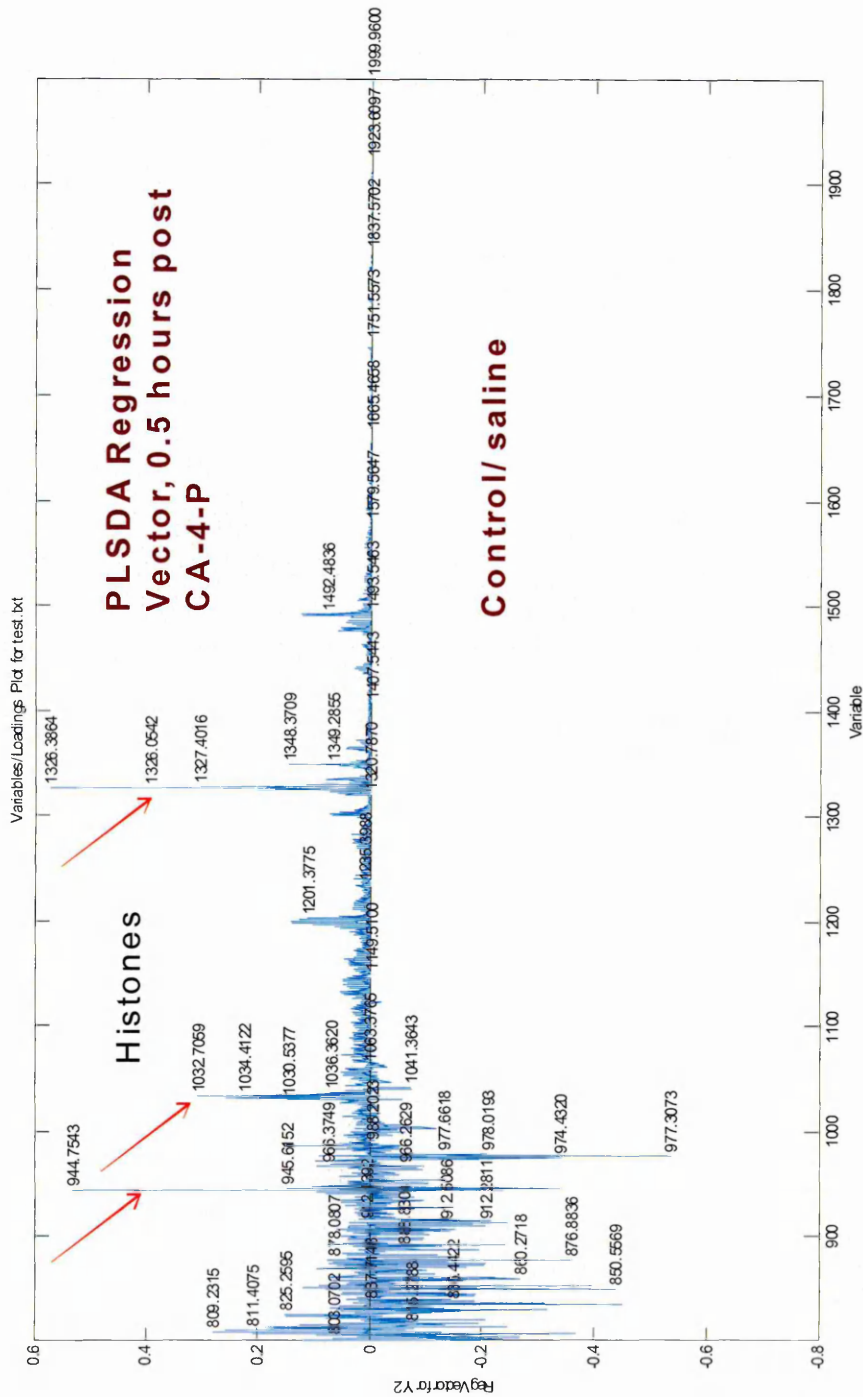


Figure 2. 21: Partial least squares discriminant analysis (PLSDA) regression vector plot comparing MALDI "on-tissue" digest data from samples of fibrosarcoma 120 Control/Saline and 30 min post combretastatin-4-phosphate (CA-4-P) (a vascular disrupting agent), treatment tumour samples. The increased abundance of peaks at m/z 944 and 1032 in the 30 min post treatment sample can be clearly seen.

The nature of this CA-4-P susceptible model could mean suppression of vital low abundant peptide information.

2.4.8 Region of interest (ROI) study for the analysis of tumour rim and necrotic regions within fibrosarcoma 120 tissue.

To enable further examination of tryptic digest spectra from MALDI images acquired using the fibrosarcoma 120 tumour set a ROI study was performed. ROI's were exported from the tumour rim and necrotic regions using the H&E tissue viable and necrotic areas for image co-registration. Straightforward selection of 'central necrosis' and 'viable rim' regions was not possible as the complex patterns of necrotic infiltration required a mixture of microscope and whole scanned image analysis.

Peptide induction was observed via PLSDA and Variable Importance in Projection (VIP) scores were used from PLSDA regression modelling to determine the importance of variables within the data time course.

HDI software (Waters Corporation, Manchester, UK) was used to view the MALDI-MSI for the following statistics. ROI's were selected according to areas either being necrotic or directly on the tumour rim for export to WatersMassLynx™ Software. After using the automatic peak detection processing option the text files were then imported into MATLAB® where predictive statistical models were built.

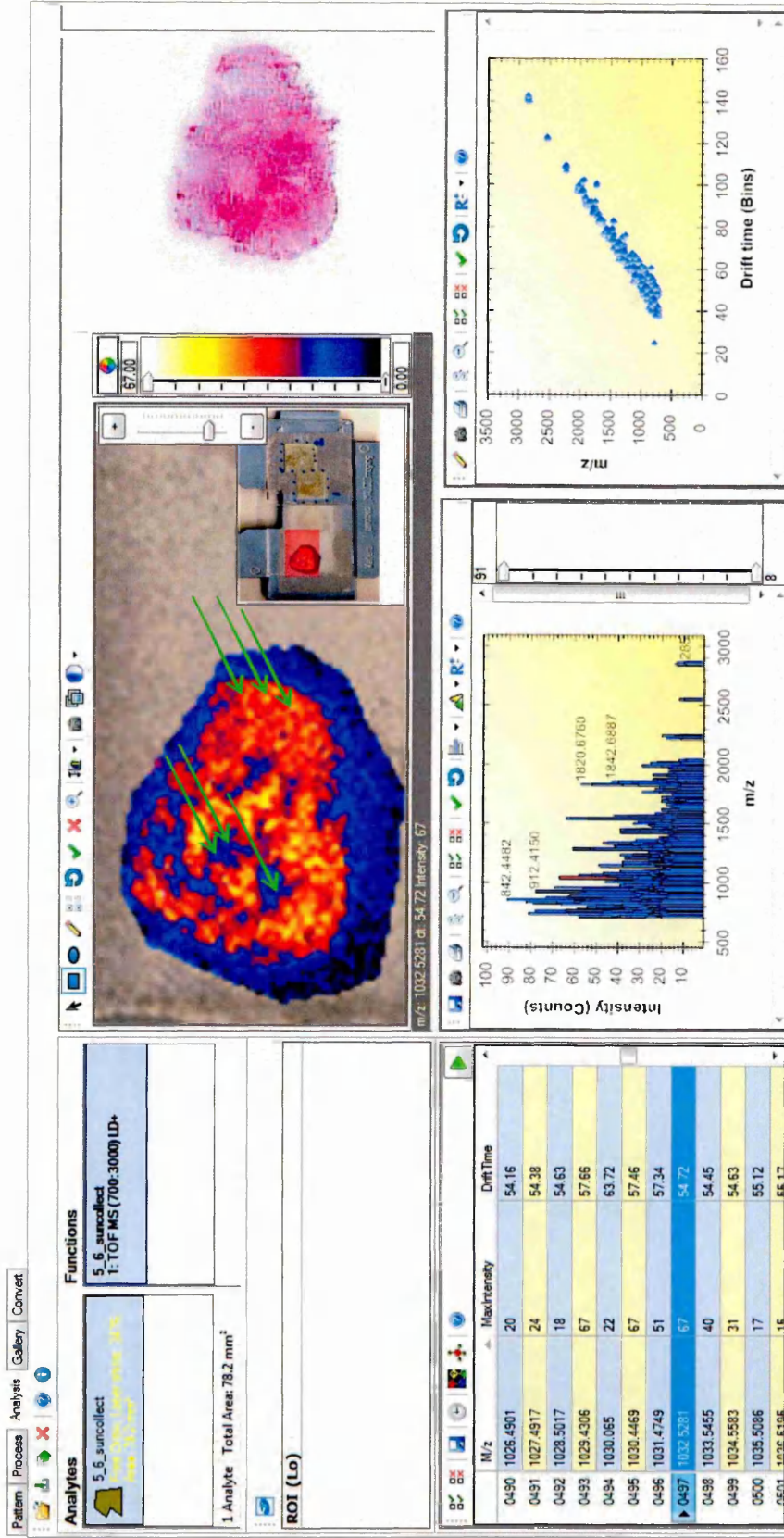


Figure 2. 22: HDI software (Waters Corporation, Manchester, UK) displaying MALDI-MSI from a fibrosarcoma tumour section 24h post CA-4-P. Shown in Figure 2.22 is an example of the regions taken for export according to H&E histological optical image registration.

The zoomed insert in Figure 2.24 shows a clear separation between control and 24h post CA-4-P.

To examine this data further the following VIP scores show the variables within the fibrosarcoma 120 ROI study that are deemed most important.

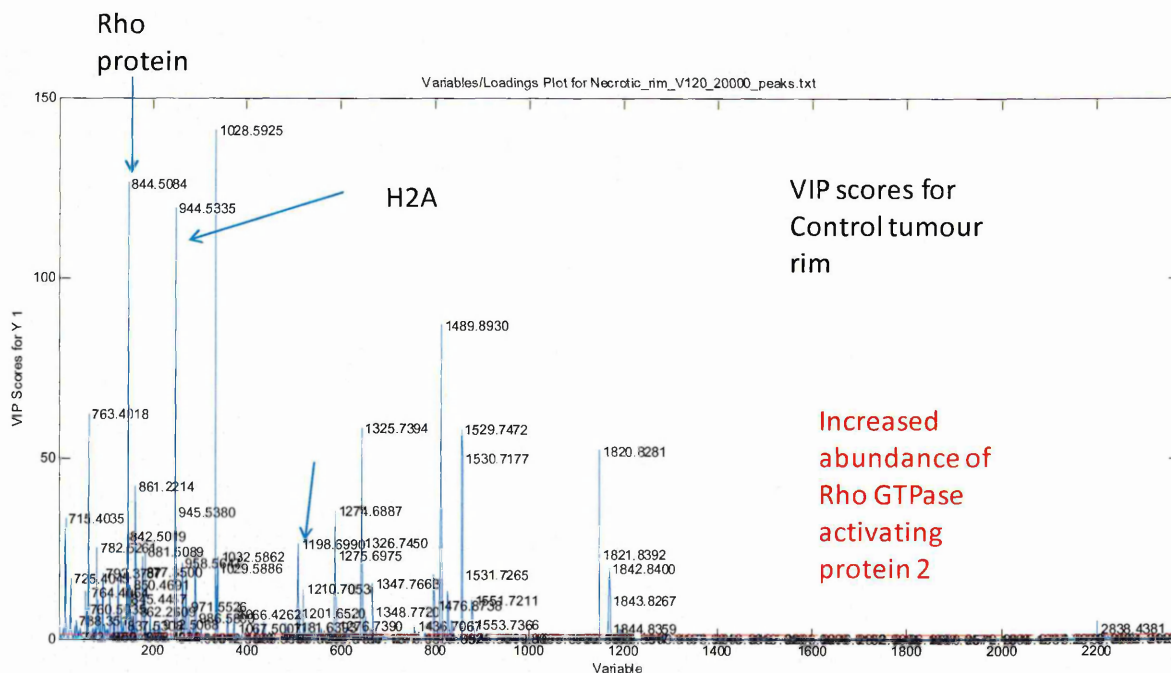
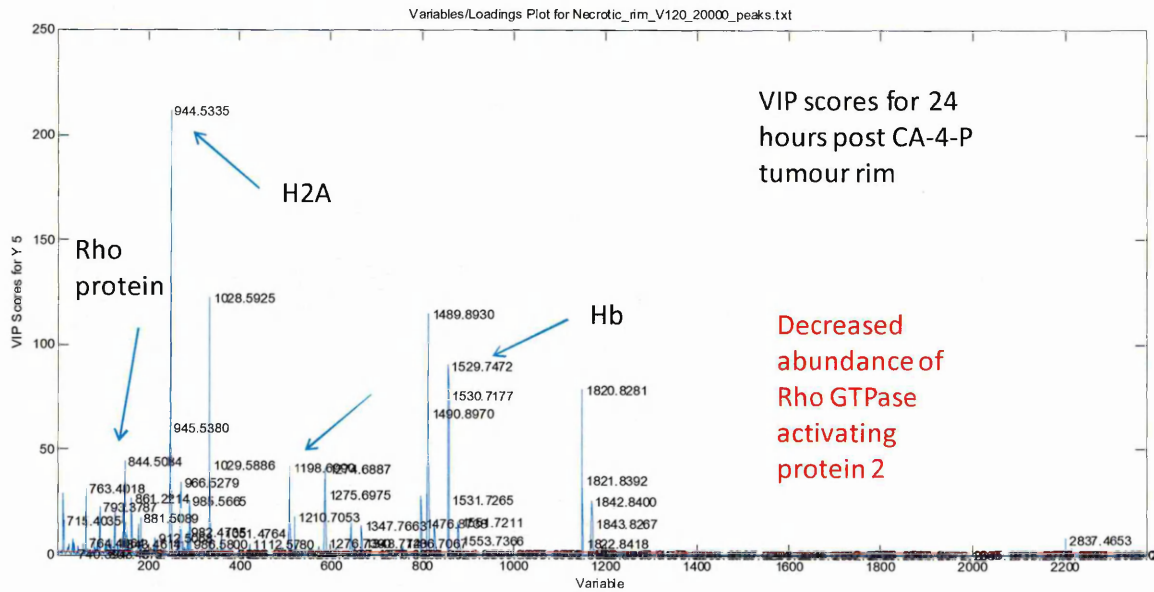


Figure 2.25: VIP scores for the Control fibrosarcoma 120 tumour rim regions. The Rho protein N-chimaerin is indicated at m/z 844, Histone 2A at m/z 944 and actin aortic smooth muscle at m/z 1198. These data is in good agreement with the increased ion signal for m/z 844.5 displayed in earlier results for this protein.



2.4.9 Concluding Remarks

The potential for investigations into protein induction following drug treatment strategies is phenomenal. Currently one major challenge is the management and analysis of the large amounts of data generated. Considering each of the peptide mass fingerprints (Figures 2.2 and 2.8), on first inspection these seem to be very noisy, however this could be a signature of a successful tryptic digestion. Therefore the many low-abundance peptide signals contained in the apparent noise could house evidence of significant proteins such as heat shock proteins in addition to the expected and readily visible abundant peptide signals (actin, histones etc.). Due to the nature of these results one has to question whether or not each peak is worthy of further scrutiny, or should the vast amount of peaks be simply treated as noise/interference. The use of ion mobility separation and its associated data extraction software certainly appears to ease this dilemma making many more signals visible for subsequent examination by MS/MS. In this work the suspected pharmacological response of haemorrhaging to treatment with CA-4-P was investigated (Figure 2.3). The MALDI-MS images generated from m/z 1274 in Figure 2.3 show a clear increase in Hb with time after treatment with CA-4-P. The latter is then confirmed in Figure 2.4 in the H&E sections. At 6 h after CA-4-P treatment, the tumour in Figure 2.4 was partially necrotic and Hb was evident in both necrotic and viable tumour regions. The tumour excised at 24 h was almost completely necrotic. The increase in haemoglobin is also clearly visible in Figure 2.7(c), the time course plot extracted from the PCA-DA data, where again the increase in m/z 1274 and m/z 1820 can be clearly observed. Many other peptides were observed in this work, including some tentatively identified as arising from VEGF isoforms other than VEGF120 Figure 2.6e. This mostly likely could be due to infiltration of immune cells (McDonnell *et al* 2012) especially after further investigation into the VEGF 188 peptide 'FKSWSVHCEPCSERR' which confirmed that it was present in the exon 6 region known exclusively to VEGF 188. This influx and subsequent induction of certain chemokines is a studied response to tumour vascular targeted therapy. In the case of the VEGF 120 signal at m/z 1485, it was found to be vital to cross check protein database outputs and refer back to the original publication detailing the sequencing of that particular gene to be sure analysis of the correct peptide sequence information.

In PCA-DA of complex data sets, the scores plot (in this case Figure 2.7a) represents the variance of the original variables, i.e. the obtained sample groups. The loadings plot (in this case Figure 2.7b) describes the variable behaviour and differences between the observed groups. The PCA-DA of tryptic digest spectra from fibrosarcoma 120 tumour tissue reported here shows good grouping of the tumour time points (Figure 2.7a). Confirmation of the

increase in haemoglobin due to CA-4-P treatment is given by the association of haemoglobin ions with the 24 h tumour in the loadings plot (Figure 2.7b) and this is shown further in Figure 2.7(c). Further analysis of this large data was required. The aim of this was to examine whether changes in signals arising from proteins of lower abundance provided an insight into other pharmacodynamic responses to the treatment.

After the discovery via Mascot search of protein N-chimaerin (Figure 2.16) (Rho GTPase activating protein 2), spectra in Figure 2.18 and MALDI images in Figure 2.19 depicted the proteins decreased expression over time and peripheral spatial distribution in the early time points. The latter could be due to interference by CA-4-P. Driftscope plots (Figure 2.17) helped to build evidence of its response throughout the time course of experiments. Statistical analysis using MATLAB® confirmed the earlier findings from this chapter namely reflecting haemorrhaging, necrosis and N-chimaerin responses.

MALDI MSI has been used to study the effect of treatment with CA-4-P, a vascular disrupting agent in late stage clinical trials, on mouse VEGF120 tumours. A strategy incorporating “on-tissue” tryptic digestion, MS/MS identification peptides and ion mobility separation to improve specificity was employed. By taking tumour samples at a number of time points after treatment, gross effects were clearly visible through changes in the expression of certain peptides. These were identified as arising from haemoglobin and indicated the disruption of the tumour vasculature. It was hoped that the use of PCA-DA, PCA and PLSDA would reveal more subtle changes taking place in the tumour samples however at present these are masked by the dominance of the changes in the haemoglobin signals and other proteins of high abundance.

The MALDI-IMS-MS/MS reported here was performed manually by direct peptide/ protein profiling. The numerous signals from the PMF's generated most likely contain many peaks which have been post translationally modified thus hampering peptide identifications. The MS/MS spectrum in Figure 2.15 is an example of this, clearly containing overlapping MS/MS fragmentation patterns. Therefore the experimental work reported in the following chapters which describes similar experiments conducted using a CA-4-P resistant mouse model explores not only MALDI-MSI but the use of conventional proteomic techniques to compliment and aid interpretation of the MALDI-MSI data.

References

Abdollahi A and Folkman J (2010) *Evading tumour evasion: Current concepts and perspectives of anti-angiogenic cancer therapy*. Drug Resistance Updates. **13**. 16-28

Aznar S, Fernández-Valerón P, Espina Carolina, Lacal Juan Carlos (2004) *Rho GTPases: potential candidates for anticancer therapy*. Cancer Letters. **206**. 181-191

Aznar S and Lacal JC (2001) *Searching new targets for anticancer drug design: the families of Ras and Rho GTPases and their effectors*. Progress in Nucleic Acid Research and Molecular Biology. **67**. 193-234.

Djidja M-C, Claude E, Snel MF, Scriven P, Francese S, Carolan V, Clench MR (2009) *Maldi-ion mobility separation-mass spectrometry imaging of glucose-regulated protein 78 kDa (Grp78) in human formalin fixed paraffin-embedded pancreatic adenocarcinoma tissue sections*. Journal of Proteome Research. **8**. (10) 4876-4884

Eigenvector Research Inc (2012) *About PLS Toolbox and Solo*, available at URL: <http://wiki.eigenvector.com>, Last accessed 18/11/12

Galbraith SM, Maxwell RJ, Lodge MA, Tozer GM, Wilson J, Taylor NJ, et al. (2003) *Combretastatin A4 phosphate has tumor antivascular activity in rat and man as demonstrated by dynamic magnetic resonance imaging*. Journal of Clinical Oncology. **21**. 2831–2842

Groseclose MR, Andersson M, Hardesty WM, Caprioli RM (2007) *Identification of proteins directly from tissue: in situ tryptic digestions coupled with imaging mass spectrometry*. Journal of Mass Spectrometry. **42**. (2) 254–262.

Kanthou C and Tozer GM (2007) *Selective destruction of the tumour vasculature by targeting the endothelial cytoskeleton*. Drug discovery today: Therapeutic strategies. **4**. (4) 237-243

Kanthou C and Tozer GM (2009) *Microtubule depolymerizing vascular disrupting agents: Novel therapeutic agents for oncology and other pathologies*. International Journal of Experimental Pathology **90** (3) 284-294

Karlsson R, Pederson ED, Wang Z, Brakebush C (2009) *Rho GTPase function in tumorigenesis*. Biochimica et Biophysica Acta – Reviews on cancer. **1796**.(2), 91–98

Kozma R, Ahmed S, Best A, Lim L (1996) *The GTPase-Activating Protein n-Chimaerin Cooperates with Rac1 and Cdc42Hs To Induce the Formation of Lamellipodia and Filopodia*. Molecular and Cellular Biology **16**.(9) 5069–5080

Lemaire R, Desmons A, Tabet JC, Day R, Salzet M, Fournier I (2007) *Direct analysis and MALDI imaging of formalin-fixed, paraffin-embedded tissue sections*. Journal of Proteome Research **6**. (4) 1295–1305.

Lemaire R, Menguellet SA, Stauber J, Marchaudon V, Lucot J, Collinet P, Farine M, Vinatier D, Day R, Ducoroy P, Salzet M, Fournier I (2007) *Specific MALDI Imaging and Profiling for*

Biomarker Hunting and Validation: Fragment of the 11S Proteasome Activator Complex, Reg Alpha Fragment, Is a New Potential Ovary Cancer Biomarker. Journal of Proteome Research.**6.** (11) 4127–4134.

Leve F and Morgado-Díaz JA(2012) *Rho GTPase Signalling in the Development of Colorectal Cancer.*Journal of Cellular Biochemistry Volume.**113.** (8)

Li X, Zhang K, Li Z (2011) *Unfolded protein response in cancer: the Physician's perspective.* Journal of Hematology & Oncology.**4.** (8) 1-10.

Lord CJ and Ashworth A (2010) *Biology-driven cancer drug development: back to the future.* BMC Biology.**8.** (38) 1-12

McCombie G, Staab D, Stoeckli M, Knochenmuss R (2005) *Spatial and spectral correlations in MALDI mass spectrometry images by clustering and multivariate analysis.* Analytical Chemistry.**77.** (19) 6118-6124

McDonnell LA, Corthals GL, Willems SM, Remoortere van A, Zeijl van RJM, Deelder AM (2010) *Peptide and protein imaging mass spectrometry in cancer research.* Journal of Proteomics.**73.** (10) 1921–1944.

Modolo MF, Tillmann Biz M, Machado de Sousa S, Fachinelli RL, Crema VO (2012) *Immunohistochemical expression of Rho GTPases inameloblastomas.* Journal of Oral Pathology and Medicine.**41.** (5) 400-407

Prise VE, Honess DJ, Stratford MRL, Wilson J, Tozer GM (2002) *The vascular response of tumor and normal tissues in the rat to the vascular targeting agent, combretastatin A-4-phosphate, at clinically relevant doses.* International Journal of Oncology. **21.** 717–26.

Schmitz AAP, Govek EE, Bottner B, Aelst LZ (2000) *Rho GTPases: Signaling, Migration, and Invasion.*Experimental Cell Research. **261.** (1) 1–12

Schwamborn K, Krieg RC, Reska M, Jakse G, Knuechel R, Wellmann A (2007) *Identifying prostate carcinoma by MALDI-Imaging.*International Journal of Molecular Medicine.**20.** (2) 155–159.

Shimma S, Furuta M, Ichimura K, Yoshida Y, Setou M, (2006) *A Novel Approach to in situ Proteome Analysis Using Chemical Inkjet Printing Technology and MALDI-QIT-TOF Tandem Mass Spectrometer.* Journal of Mass Spectrometry Society Japan.**54.** (4) 133–140.

Siemann DW (2010) *The unique characteristics of tumour vasculature and preclinical evidence for its selective disruption by tumour-vascular disrupting agents.* Cancer Treatment Reviews.**37.** (1) 63-74

Siemann DW and Horsman MR (2009)*Vascular targeted therapies in oncology.* Cell and Tissue Research.**335.**(1) 241-248

Thorpe PE, Chaplin DJ, Blakely DC (2003) *The first international conference on vascular targeting: Meeting overview.* Cancer Research.**63.** 1144-1147

Tozer GM, Kanthou C, Lewis G, Prise VE, Vojnovic B, Hill A (2008) *Tumour vascular disrupting agents: combating treatment resistance*. The British Journal of Radiology.**81**. S12-S20

Trim PJ, Djidja MC, Muharib T, Cole LM, Flinders B, Carolan VA, Francese S, Clench MR (2012) *Instrumentation and software for mass spectrometry imaging—Making the most of what you've got*. Journal of Proteomics.**75**. (16) 4931–4940

Vega FM and Ridley AJ (2008) *Rho GTPases in cancer cell biology*. FEBS Letters.**582**. 2093-2101

Zhi-chao SI, Jie L (2008) *What 'helps' tumours evade vascular targeting treatment?* Chinese Medical Journal.**121**. (9) 844-84

Chapter 3

Protein induction post CA-4-P
administration in a resistant
fibrosarcoma 188 mouse model

3.1 Introduction

In this Chapter data from the analysis of a mouse fibrosarcoma model tumour genetically engineered to solely express the insoluble matrix bound VEGF 188 isoform is described. In contrast to the soluble VEGF 120 isoform type that were the focus of Chapter 2, which have been found to be susceptible to VDA, the VEGF188 isoform type have been reported to be resistant to treatment with VDA (Tozer *et al* 2008). In bone development, VEGF 120 and VEGF 188 both have different roles in vascularisation (Maers *et al* 2004). VEGF 188 is amongst the matrix bound isoforms thought to be involved in vascularisation of the metaphyseal bone regions, whereas the soluble VEGF components are concerned with the epiphyseal area. It is stated that the various isoforms of VEGF all play unique roles in the proliferation and chondrocyte survival in a hypoxic environment (Maers *et al* 2004).

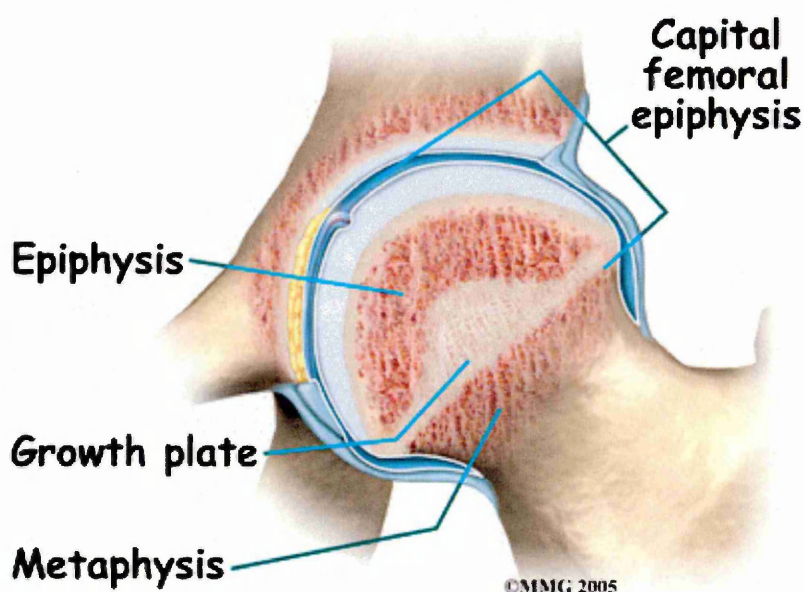


Figure 3. 1: Diagrammatical cross section of the region present at the end of growing long bones showing the areas involved in epiphysis and metaphysis. (Ortho paediatrics group (2012) (http://www.orthopaedics.com/docs/Guides/slipped_CFE.html))

The term fibrosarcoma describes a malignant fibrous mesenchymal neoplasm which is said to be found in the femur, humerus, jaw bone and is sometimes present in organs/ soft tissues (Encyclopædia Britannica Inc 2013),. Angiero *et al* 2007).

In tumours VEGF is known to be a potent angiogenic stimulator and levels are found to be elevated in both the tumour cells and stroma (Harris *et al* 2012, Saharinen *et al* 2011). The tumour microenvironment is said to promote the recruitment of inflammatory cells due to chemoattractants. These actions are said to result in such cells becoming a major component

of the actual tumour mass (Saharinen *et al* 2011). Pro- and/or antitumorigenic functions can result as a consequence of immune cell infiltration which is largely tissue/ tumour dependant. Tumour associated myeloid cells (TAMs) are known to secrete numerous factors which favour angiogenesis some of which include; VEGFs, TNF- α , interleukin (IL)-1 β , matrix metalloproteinases, PDGFB, basic fibroblastgrowth factor.

In the data to follow using fibrosarcoma 188 tumours, a further time point of 72h post CA-4-P was added based on the more resistant nature of this matrix bound VEGF isoform model (Tozer *et al* 2008). The rationale for this decision was to try to observe any response which could be indicative of drug resistance and a potential switch back to tumour viability.

The use of CA-4-P treatment could enhance knowledge of the proteins induced in tumours expressing either fibrosarcoma 188/ 120 isoforms under hypoxic conditions. The following data aims to provide proteomic comparisons throughout a treatment time course using fibrosarcoma 188 models, and allow observational differences to be made between the expression of proteins in the resistant fibrosarcoma 188 and susceptible 120 tumour models.

3.2 Materials and Samples

3.2.1 Chemicals and Materials

α -Cyano-4-hydroxycinnamic acid (CHCA), aniline (ANI), ethanol (EtOH), chloroform (CHCl₃), acetonitrile (ACN), octyl- α / β -glucoside (OcGlc), tri-fluoroacetic acid (TFA), ammonium bicarbonate, haematoxylin, eosin, xylene and DPX mountant were from Sigma–Aldrich (Dorset, UK). Modified sequence grade trypsin (20 μ g lyophilised) was obtained from Promega (Southampton, UK).

3.2.2 Tissue samples

Mice were injected sub-cutaneously in the flank with a 50 μ l tumour cell suspension containing 1×10^6 cells in serum-free medium. The cells employed in this study were from the mouse fibrosarcoma cell line, VEGF188. This has been engineered to express only the VEGF188 isoform. Tumours were allowed to grow to approximately 500 mm³, before CA-4-P treatment (a single dose of 100 mg/kg i.p). The dosage for CA-4-P are consistent with animal studies performed at clinically relevant doses (Galbraith 2003., Prise 2002). Mice were sacrificed and tumours excised at various times after treatment. All animal work carried out documented herein was performed by Dr. J. E. Bluff, Tumour Microcirculation Group, University of Sheffield, UK. Samples were provided as frozen excised tumours and stored at -80°C.

3.2.3. Experimental groups

Controls (no treatment, saline i.p), n = 4 (labelled tumour 6_1 – tumour 6_4), C-A4-P (0.5 h after treatment), n = 5, (labelled tumour 7_1 – tumour 7_5), C-A4-P (6 h after treatment), n = 5, (labelled tumour 8_1 – tumour 8_5), C-A4-P (24 h after treatment), n = 5, (labelled tumour 9_1 – tumour 9_5), C-A4-P (72 h after treatment) n = 4, (labelled tumour 10_1 – tumour 10_4).

3.2.4 Tissue preparation

Frozen tissue sections were cut to give approximately 10 μ m sections, using a Leica CM3050 cryostat (Leica Microsystems, Milton Keynes, UK) (Djidja *et al* 2009). The sections were then freeze thaw mounted on poly-lysine glass slides. Mounted slides were either used immediately or stored in an airtight tube at -80 °C for subsequent use.

3.2.5 In situ tissue digestion and trypsin deposition

The tissue samples in triplicate to undergo MALDI-MS/MSI were washed initially with 70% and then 90% ethanol for 1 min then left to dry, subsequently slides were immersed in chloroform for 10 s. Prior to matrix application, in situ tissue digestion was performed with trypsin solution prepared (from lyophilised trypsin) at 20 µg/ml by addition of 50 mM ammonium bicarbonate (NH₄HCO₃) pH 8, containing 0.5% octyl-a/b-glucoside (OcGlc) based on a protocol by Djidja *et al* (2009).

The “Suncollect” (SunChrom, Friedrichsdorf, Germany) automatic pneumatic sprayer was used to spray trypsin in a series of layers. The sections for MALDI-MS and MALDI-MSI were incubated overnight in a humidity chamber containing H₂O 50%: methanol 50% overnight at 37°C and 5% CO₂.

3.3 Methods and instrumentation

3.3.1 Matrix deposition

The matrix, α-cyano-4-hydroxycinnamic acid (CHCA) and aniline in acetonitrile:water:TFA (1:1:0.1 by volume), was applied using either the Suncollect (at 5 mg/ml) or the Portrait™ 630 Multispotter (at 10 mg/ml), as described above. Identical coordinate settings were used as with the trypsin deposition, to ensure sample uniformity. Equimolar amounts of aniline were added to the CHCA solution, i.e. 1 ml of 5 mg/ml CHCA solution contained 2.4 µl of aniline. These matrix deposition parameters were based on methods from Djidja *et al* (2009).

3.3.2 Instrumentation

MALDI-IMS/MS, MALDI-IMS/MSI and MALDI-IMS-MS/MS were performed using a HDMS SYNAPT™ G2 system (Waters Corporation, Manchester, UK) and Drift scope 2.1 software (Waters Corporation, UK). Instrument calibration was performed using standards consisting of a mixture of 217 polyethylene glycol (Sigma-Aldrich, Gillingham, UK) ranging between m/z 100 to 218 3000 Da prior to MALDI-IMS-MSI analysis. In order to achieve good quality MS/MS spectra, they were acquired manually moving the laser position and adjusting the collision energy to achieve good signal to noise for product ions across the full m/z range of the spectrum. Collision energies were adjusted from 70 to 100 eV during acquisition and acquisition times were generally of the order of 5–10 s per spectrum. MS/MS spectra were uploaded to perform a Mascot (Matrix Science, London, UK) search which used the UniProt database in order to generate a sequence match. Image acquisition was performed using raster imaging mode at 30-100 µm spatial resolution, Biomap 3.7.5.5 software (<http://www.maldi->

msi.org/) was used for image generation. To enable simple visual comparison between images all data were normalised to m/z 877/ m/z 1066 (peaks arising from the α CHCA matrix).

The LC-ESI-MS/MS analysis of prepared tissue digests was performed by Adam Dowle at the Proteomics Technology Facility, Department of Biology (Area 15), University of York. LC-ESI-MS/MS analyses were performed with a Bruker nanoESI source fitted with a steel needle using ion spray voltage of 1500V. MS/MS was acquired using the following Auto MSMS settings: MS: 0.5 s (acquisition of survey spectrum), MS/MS (CID with N₂ as collision gas): ion acquisition range: m/z 300-1,500, 0.1 s acquisition for precursor intensities above 100,000 counts, for signals of lower intensities down to 1,000 counts acquisition time increased linear to 1s, the collision energy and isolation width settings were automatically calculated using the AutoMSMS fragmentation table; 5 precursor ions, absolute threshold 1,000 counts, preferred charge states: 2 – 4, singly charged ions excluded. 1 MS/MS spectrum was acquired for each precursor and former target ions were excluded for 30 s. The data obtained from the University of York was in the MASCOT .data file format. The .dat files selected used the following modification searches and parameters using the MASCOT Mus (Musculus) protein database:

Fixed modification: Carbamidomethyl (C) and variable modifications: Acetyl (Protein N-term), Gln->pyro-Glu (N-term Q), Glu->pyro-Glu (N-term E), Oxidation (M).

Mass values: Monoisotopic, protein Mass : Unrestricted, peptide Mass Tolerance : \pm 10 ppm, fragment Mass Tolerance: \pm 0.1 Da and max Missed Cleavages : 1

These data were then processed using Scaffold 3 proteomic software tool for visualisation and analysis of the LC-ESI-MS/MS data (<http://www.proteomesoftware.com/>). The data files (.dat) produced from MASCOT which corresponded to each digested analysed, were uploaded individually. Analysis with X! Tandem was selected in order to improve protein identifications with searching through an additional database.

3.3.3 Haematoxylin and eosin staining

Slides were immersed in haematoxylin for 1 min, rinsed in tap water until the water ran clear, immersed in 1% eosin for 30 s and rinsed in tap water until the water ran clear. They were then dehydrated as follows: 50% ethanol for 2 min, 70% ethanol for 2 min, 80% ethanol for 2 min, 95% ethanol for 2 min and 4 changes of xylene applied to each slide for 1 min at a time. Finally, they were mounted with DPX mountant and left to dry in the fumehood overnight.

3.3.4 Statistical analysis

PCA and PLSDA was performed using MATLAB® (Matrix Laboratory) (MathWorks, Inc., Natick, MA 486 USA). The PCA/ PLSDA data that follows is representative of the fibrosarcoma 188 data where either n= 4/5 biological replicates per time point with up to 6 technical replicates for each. (control – 72 hours). PLSDA Data for ROI study using HDI software (Waters Corporation, Manchester, UK) was analysed using one tumour per time point with 9 technical replicates per ROI. Variable Importance in Projection (VIP) scores were used from PLSDA regression modelling to determine the importance of variables within the data time course.

3.3.5 Data pre-processing using Waters MassLynx™ Software and MATLAB®

MS results were imported into MATLAB® in .txt or .csv format after application of “automatic peak detection” using the instrument data processing software (Waters MassLynx™ Software). Normalisation (2-Norm) and mean centre were selected, “contiguous blocks” was used for cross validation.

3.3.6 Protein network analysis

Accession lists generated by results from the LC-ESI-MS/MS Mascot searches were imported into the STRING 9.0 database (from Mus (Musculus) MASCOT protein database). Observations of the relationships were made between the proteins identified throughout a fibrosarcoma 188 time course. The sample data was used to build predictive proteomic pathways and study the predicted functional partners of known protein-protein interactions (<http://string-db.org/>).

3.3.7 Immunohistochemical staining

3.3.7.1 Chemicals and Materials

Methanol, Acetone, Hydrogen peroxide solution 30% wt., Xylene, Ethanol, Gill's Haematoxylin and DPX mountant were all purchased from Sigma Aldrich UK. Phosphate buffer saline tablets (Dulbecco 'A' Tablets) were from Oxoid Ltd. Normal goat serum, ImmEdge hydrophobic barrier pen, 10X Casein solution, Avidin/Biotin horseradish peroxidase complex blocking kit, ABC solution kit, Diaminobenzidine (DAB) substrate kit were from Vector Laboratories Ltd UK. HSP-90 (ab13494, 16F1) and Plectin (ab32528, E398P) antibodies were from Abcam, Cambridge UK. Macrophage cell surface marker F4/80 (MCA497GA, Cl:A3-1) antibody was from AbD Serotec.

3.3.7.2 Immunohistochemical methods

Mounted frozen tissue sections were allowed to equilibrate to R.T for 5 min. Slides were then fixed in ice cold acetone for 20 min then rinsed in PBS. Endogenous peroxidases were blocked using 30% H₂O₂ and Methanol. After rinsing in PBS, tissues were blocked for 1hr using Goat sera containing 10% Casein. After PBS washes, Primary Ab was added and left O.N at 4°C. To aid optimisation of immunohistochemistry, Ab's were first diluted using dilutions ranging from 1:50 – 1:1600 depending on Ab and manufacturer's guidelines. Primary antibody dilutions were; 1:400 for both Plectin and F4/80 and 1:2000 for HSP-90. Isotype IgG controls were used for F4/80 and for Plectin and HSP-90 primary antibody was just omitted a negative control. After overnight incubation and subsequent PBS washes, Secondary Ab was added diluted (1:200) in 2% Goat sera and left for an incubation time of 1h at R.T. After this period, ABC solution was added after rinsing in PBS and left to incubate for 45min at R.T. After PBS washing, DAB solution was applied and left to allow development of the staining. Slides were rinsed in tap water prior to immersion in Gill's Haematoxylin for 2min. After slide dehydration using 70% - 100% EtOH tissue was immersed in 2 changes of Xylene for 5 min each. Slides were mounted using DPX mountant.

3.3.8 Protein precipitation and digestion

3.3.8.1 Chemicals and materials

Chloroform (CHCl₃), methanol (MeOH), acetonitrile (ACN), hydrochloric acid (HCl), tri-fluoroacetic acid (TFA), ammonium bicarbonate, DL-Dithiothreitol solution, Iodoacetamide, urea, potassium di-hydrogen phosphate (KH₂PO₄), TRIzol were from Sigma–Aldrich (Dorset, UK). Modified sequence grade trypsin (20 µglyophilised) was obtained from Promega (Southampton, UK).

3.3.8.2 Tissue homogenisation and precipitation of protein

The fibrosarcoma 188 tumour tissue was homogenised in 800µl of TRIzol solution using a micro-homogeniser (Kline and Wu 2009). Homogenised solution was centrifuged (1,500 rpm) for 5 min to pellet out nuclei/ unbroken cells. Post-nuclear supernatant was then centrifuged (14,000 rpm) for 30 min. Resulting supernatant was discarded and cellular membrane pellet was retained for protein precipitation. 200µl of MeOH and 50µl of CHCl₃ were then added to each protein pellet sample. After vortexing, 150µl HPLC H₂O was added with further vortexing. After centrifugation (14,000 rpm) for 2 min, the bottom CHCl₃ layer was removed. A further 50µl CHCl₃ was added, removal of the bottom CHCl₃ layer was repeated following

centrifugation (14,000 rpm) for 2 min. Subsequent removal of the H₂O layer resulted in the remaining protein precipitate layer. CHCl₃ (50µl) and MeOH (150µl) were added directly to the protein precipitate, after vortexing solution was centrifuged (14,000 rpm) for 2 min. Supernatant was removed and protein pellet was then allowed to air dry for 2 min.

3.3.8.3 Protein Digestion

100µl of 0.1% RapiGest in 50mM NH₄HCO₃ buffer (pH 7.8) was added to the air dried protein pellet. Each sample pellet/ solution was consecutively vortexed, incubated at -80°C (~ 1hr) and heated to 70°C (1 min) until solubilised. Once fully solubilised the sample was heated to 100°C (2 min) and then left to reach room temperature. Each sample was reduced with DTT (final concentration 5mM) for 30 min at 60°C the left to reach room temperature. Solutions were then alkylated with iodoacetamide (final concentration 15mM) in the dark for 30 min at room temperature. Sequence grade modified trypsin was added (20µg/ml) to 80µg of protein following the BCA Protein Assay (see 3.3.9) used for protein determination. In-solution digests were incubated over night at 37°C with shaking.

3.3.8.4 Preparation of samples for column loading

Fibrosarcoma 188; HCL (final concentration 100mM) was added to the overnight digest, solution was then incubated for a further 45 min at 37°C. After this step the sample was then centrifuged (14,000 rpm, 4°C) for 10 min, the supernatant removed for analysis. This remaining solution was lyophilised and stored at -80°C until further use.

3.3.9 Protein estimation – BCA assay

3.3.9.1 Chemicals and materials

BCA protein assay reagent (bicinchoninic acid), copper (II) sulfate pentahydrate 4% solution, protein standard solution, 1.0 mg/mL bovine serum albumin (BSA) were from Sigma Aldrich UK. RapiGest detergent solution was purchased from Waters (UK).

3.3.9.2 BCA method

Solubilised protein pellets were thawed, vortexed and centrifuged ready for the BCA assay. BSA standards were prepared within an analytical range of 0-4 mg/ml. BCA reagent was added to BCA standards and tumour tissue solution samples and left to incubate at R/T for 30min. BCA standards were measured in triplicate and Samples were measured in duplicate in a 96 well plate using a Wallac plate reader (spectrophotometer) at 570nm.

3.4 Results and Discussion

3.4.1 MALDI-MSI of fibrosarcoma 188 CA-4-P treated tumour tissue

The MALDI spectra from both fibrosarcoma 188 and 120 *on tissue* digests contain numerous peaks, the challenge so far has been exploration and identification of the low abundant species present.

One of the main aims at this point of the project was to develop a system of techniques that could be used in collaboration with each other in order to co-validate proteomic responses observed within a treatment time course.

Proteins of interest possibly induced as a result of CA-4-P treatment were firstly visualised by MALDI-MSI as putative protein targets. These responses therefore could then be supported by immunohistochemical staining. Similarly protein responses observed employing conventional proteomic techniques i.e. Liquid Chromatographic methods coupled with ESI or MALDI, were then used to relate back to MALDI-MSI.

3.4.1.1 Trypsin application for the avoidance of protein delocalisation

One of the main potential pitfalls of *in situ* tissue tryptic digestion is protein delocalisation. A factor which when occurs eliminates the analysis of spatial protein distribution. To ensure good tryptic digest MALDI-MSI, a homogeneous coating is essential during trypsin application.

Other issues to consider would be the tissue type, section size and to ensure a suitable flow rate is employed when using a pneumatic sprayer for trypsin deposition. Too much trypsin sprayed per cycle could lead to 'over wetting' of the tissue and subsequent protein delocalisation. The following images were as a result of initial trypsin application optimisation involving flow rates, cycles and gas pressure in order to avoid any issues previously mentioned.

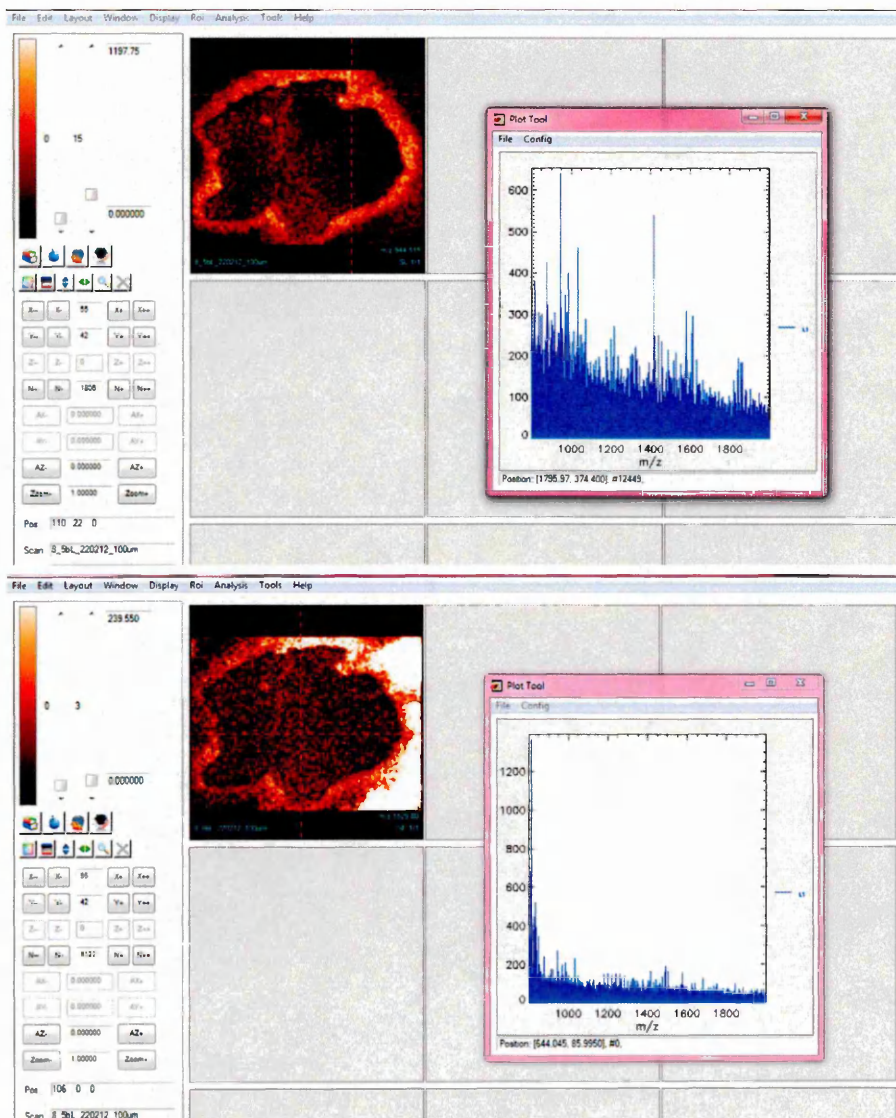


Figure 3. 2: Screen shot of protein delocalisation in MALDI-MSI, visualised using BioMap imaging software. Figure 3.2 displays a screen shot of MALDI-MSI of an on tissue tryptic

digest where trypsin applied using a pneumatic sprayer has caused delocalisation of proteins as a result of an incorrect spraying speed. The trypsin therefore, has not had sufficient drying time and over wetting of the tissue has occurred. The cross hairs which map the ion signals in the top MALDI-MSI in Figure 3.2, show lots of tryptic peptide signals outside of the tissue, indicative that the spatial distribution of the proteins have changed. The signals given from the cross hairs in the bottom image in Figure 2 show a substandard tryptic spectrum as a result.

The MALD-MSI featured in Figure 3.3 can be regarded as an exemplar of *on tissue* tryptic digestion. The characteristic contrast of discreet CHCA matrix clusters seen in the left hand MALDI-MSI, compared to the tryptic PMF evident from the cross hair mapping on the tissue image shown to the right.

The most suitable parameters for spraying trypsin were found to be the employment of a series of 5 layers at a flow rate of 2.5 μ l/ minute. To avoid protein delocalisation and ensure sample spray uniformity the regions set for trypsin application allowed enough drying time between each spray pass. A fine spray was found to be essential with a view to maintain protein positioning within the tissue and the nitrogen gas pressure used was ~15 psi for spraying trypsin.

For matrix application, the same principles were applied but the gas pressure was decreased to ~10 psi. The flow rate was adjusted to 4 μ l/ minute to take into account of solvent evaporation and aid sample coverage and co-crystallisation.

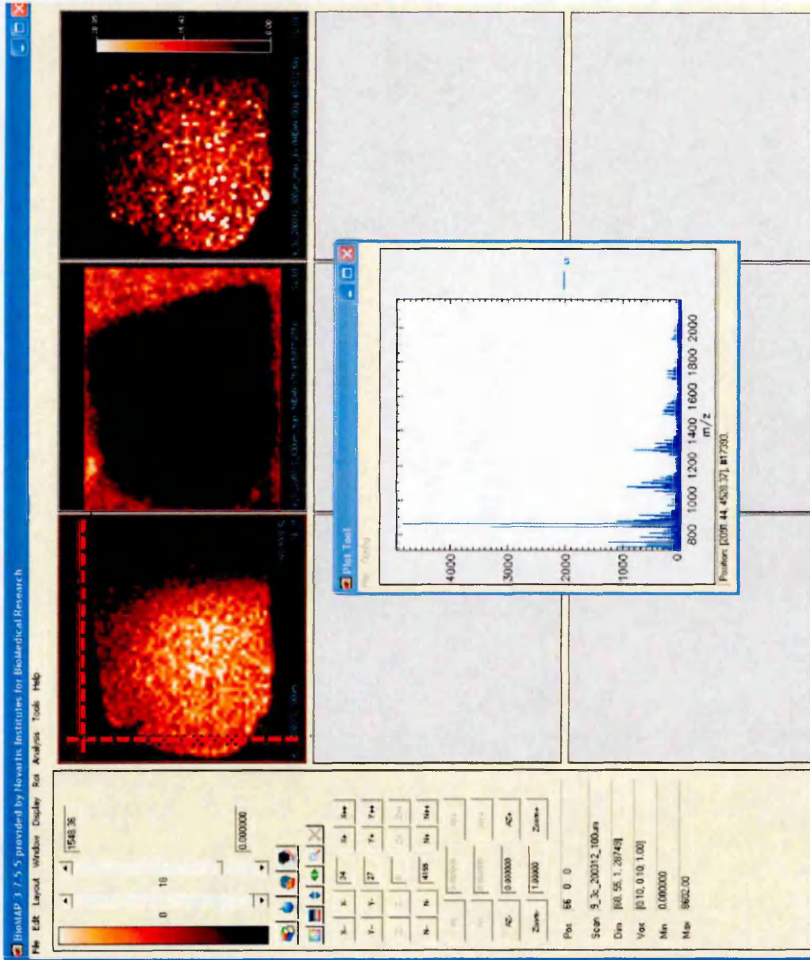
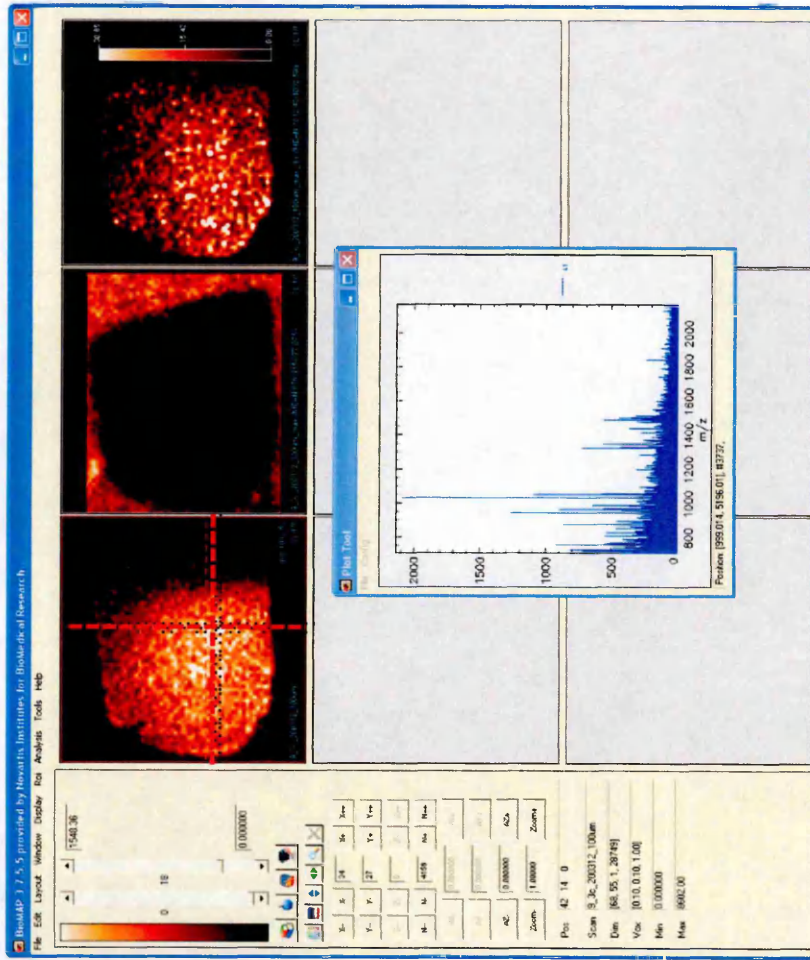


Figure 3. 3: Screen shot of an on tissue tryptic digest using MALDI-MSI, visualised using BioMap imaging software.

The spectra in Figure 3.4 are typical representations of fibrosarcoma 188 peptide mass fingerprints (PMF) throughout the CA-4-P treatment time course studied.

The spectra within the time course of Figure 3.4 all appear to be quite similar upon first inspection. The zoomed in regions of the fibrosarcoma 188 time course now shown in Figure 3.5 shows subtle differences of the appearance of Hb at m/z 1416 and appearance of an unknown at m/z 1577. The high abundant Hb peaks (m/z 1274, m/z 1302, m/z 1529 and m/z 1819) which are evident in the spectra from Figures 2.1 and 2.2 in Chapter 2, do not dominate the fibrosarcoma 188 spectra. This could be due to the CA-4-P resistant nature of this tumour mouse model.

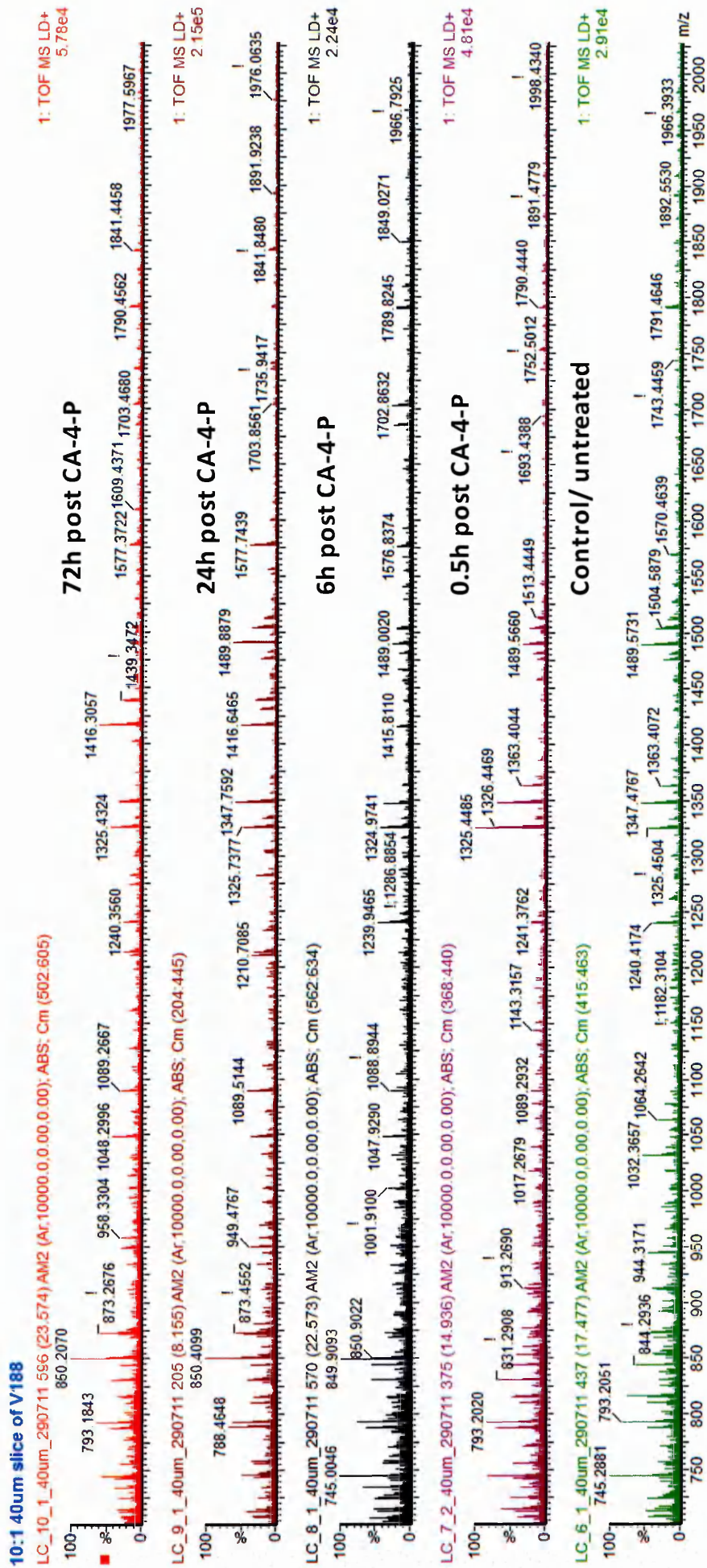


Figure 3. 4: PMF's of a fibrosarcoma 188 time course study. Spectra shown are Control, 0.5h, 6h, 24h and 72h post CA-4-P treatment.

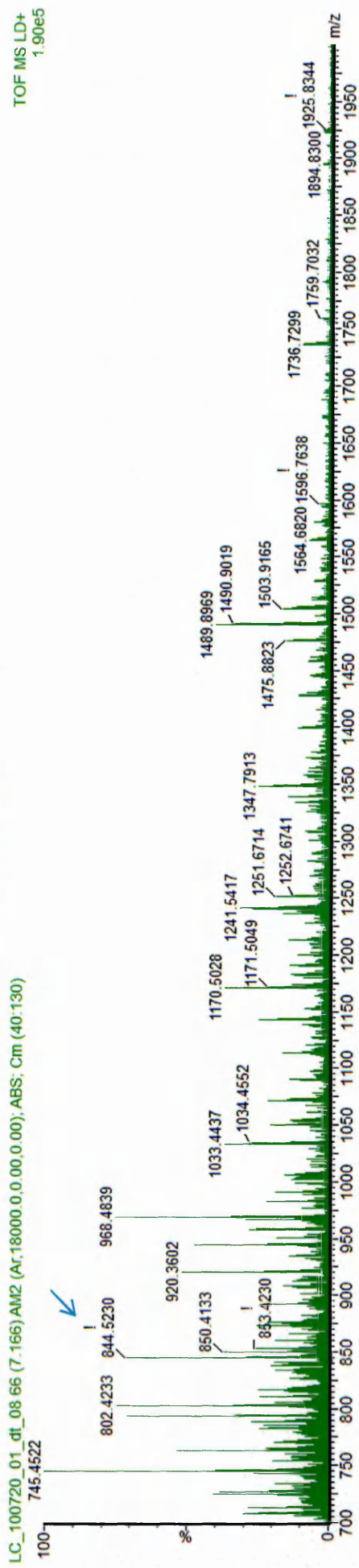
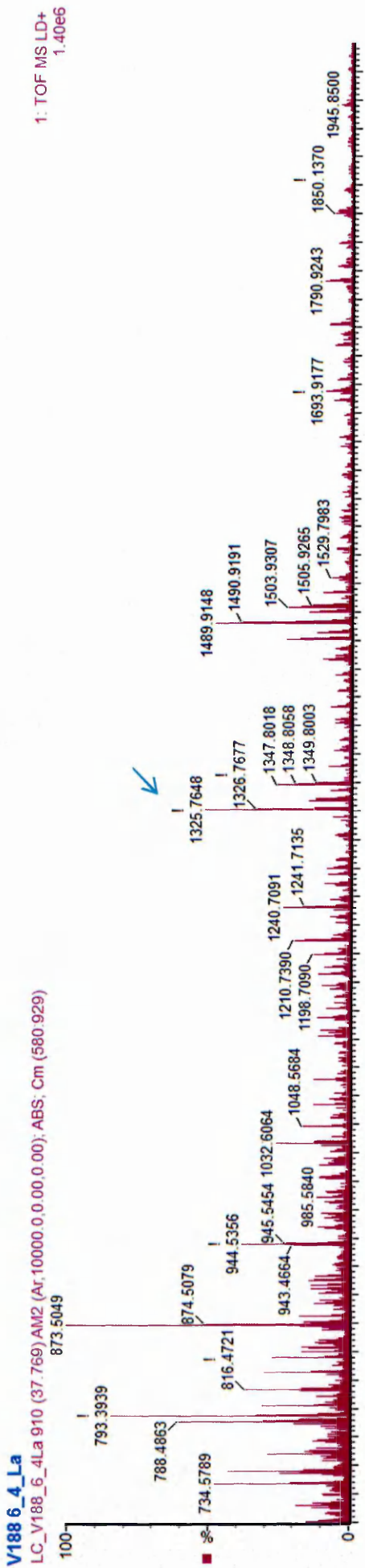


Figure 3. 6: Comparison control tissue peptide mass fingerprints from fibrosarcoma 120 and 188 on tissue digests. The blue arrows indicate Histone H4 (m/z 1325) and N-Chimaerin (m/z 844).

3.4.1.2. Spectral comparison of peptide mass fingerprints

Figure 3.6 displays the spectra from examples of control tumour tissue from each tumour model, fibrosarcoma 120 and 188. The peak tentatively relating to the Rho GTPase protein discussed in Chapter 2 can be seen in the fibrosarcoma 120 spectra (indicated by an arrow), but not at the same intensity in the spectra corresponding to fibrosarcoma 188. Similarly, the same can be deduced for the ion at m/z 1325 relating to Histone H4 seen in the 188.

Although further work is required to determine the relevance of increased Histone H4 intensity seen here, there have been many studies on the analysis of Histone H4 acetylation/deacetylation with the premise of histone deacetylase inhibitors as potential anti-cancer treatment (Advani *et al* 2010). It is stated that expression of Histone acetylation in cancers can influence patient prognosis. Reports claim that increased levels of acetylated Histone H4 in patients with esophageal squamous cell cancer can correlate with an encouraging clinical outcome (Toh *et al* 2007).

Ultimately, histones are said to be key in gene regulation (Grunstein 1997). In the 188 Control spectra seen here (Figure 3.6), the prominent Histone H4 could be a characteristic of this more drug resistant fibrosarcoma 188 tissue.

3.4.1.3 MALDI-MSI and immunohistochemistry to analyse a fibrosarcoma 188 treatment course

Initial MALDI-MSI using the fibrosarcoma 188 tissue was carried out at a resolution of 100 μ m employing a spot to spot laser pattern with the SYPNAT G2 HDMS system (Waters, UK). The gross haemorrhagic pharmacological response that already has been shown in Chapter 2 using the fibrosarcoma 120 tumours was considered a good place to start when validating responses seen by other ions. Figure 3.7 shows a multi time point MALDI image of a fibrosarcoma 188 time course ranging from Control – 72 hours post CA-4-P. The MALDI images were taken from a slide containing multiple samples.

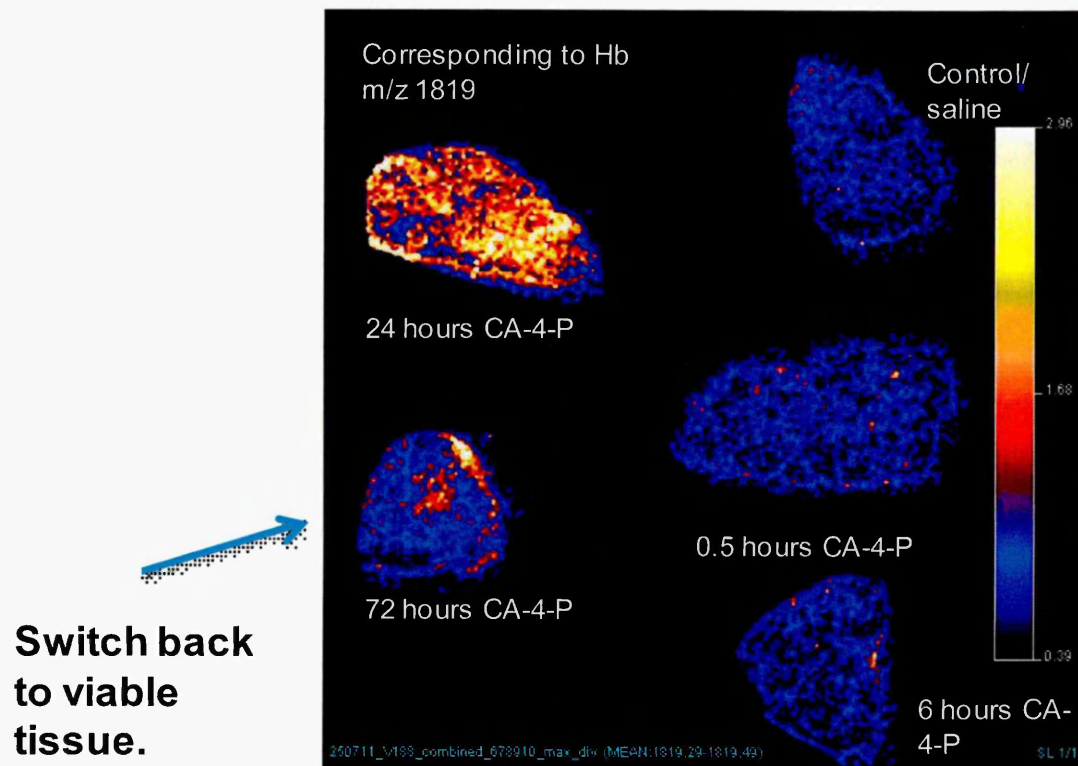


Figure 3. 7: MALDI-MSI multi image of a fibrosarcoma 188 time course. The images show the spatial distribution of a peptide of haemoglobin subunit alpha at m/z 1819 throughout a treatment time course from Control – 72 hours post CA-4-P administration.

The MALDI-MSI shown in Figure 3.7 of the matrix bound VEGF 188 model shows a different response to that seen of a Hb peptide in Figure 2.3 (Chapter 2). The haemorrhagic response is observed much later in the 24h tissue opposed to the 6h sample in the fibrosarcoma 120 MALDI-MSI. In contrast to the evidence of complete necrosis and vascular disruption in the last time point of the fibrosarcoma 120 (Figure 2.3 – 24h), here the 72h time point exhibits a very different response. There appears to be evidence of a switch back to viable tissue in this more resistant tumour model.

Heat shock protein 90 (HSP-90) is ubiquitous in all normally functioning cells and serves to prevent the misfolding of proteins by helping to retain the correct structural format of the protein (Neckers 2007). The characteristic tumour microenvironment renders cancer cells to anoxia, alterations in pH and attack via pharmacological anticancer agents. HSP-90 has been suggested as a potential target protein for anticancer therapy due to the dependence on structural conformity by the cancer cell (Den and Lu 2012).

It is known that inhibition of HSP-90 results in the degradation of the HSP-90 stabilised protein (client protein) via the proteasome.

Elevated levels of HSP-90 in breast cancer patients have been found to correlate with poor patient survival due to the conserving effect of HSP-90 on human epidermal growth factor receptor 2 (Jameel *et al* 1992). It is also stated that HSP-90 is highly expressed in solid tumours and it is suggested that HSP-90 plays a key role in the evasion of apoptosis thus promoting tumour cell survival (Den and Lu 2012).

There are over 20 known clinical trials taking place which currently involve the use of HSP-90 inhibitors (Den and Lu 2012). A review article by Den and Lu (2012) poses the question of which tumour type is the most suitable for HSP-90 inhibition study and whether or not the anticancer target should be the HSP-90 '*client protein*' i.e. epidermal growth factor receptor in non-small cell lung cancer/ human epidermal growth factor receptor 2 in breast cancer.

The MALDI images in Figure 3.8 display the spatial distribution and relative abundance of an ion at m/z 1168 corresponding to HSP-90. The optical scans shown in Figure 3.6 show the immunohistochemical staining of HSP-90.

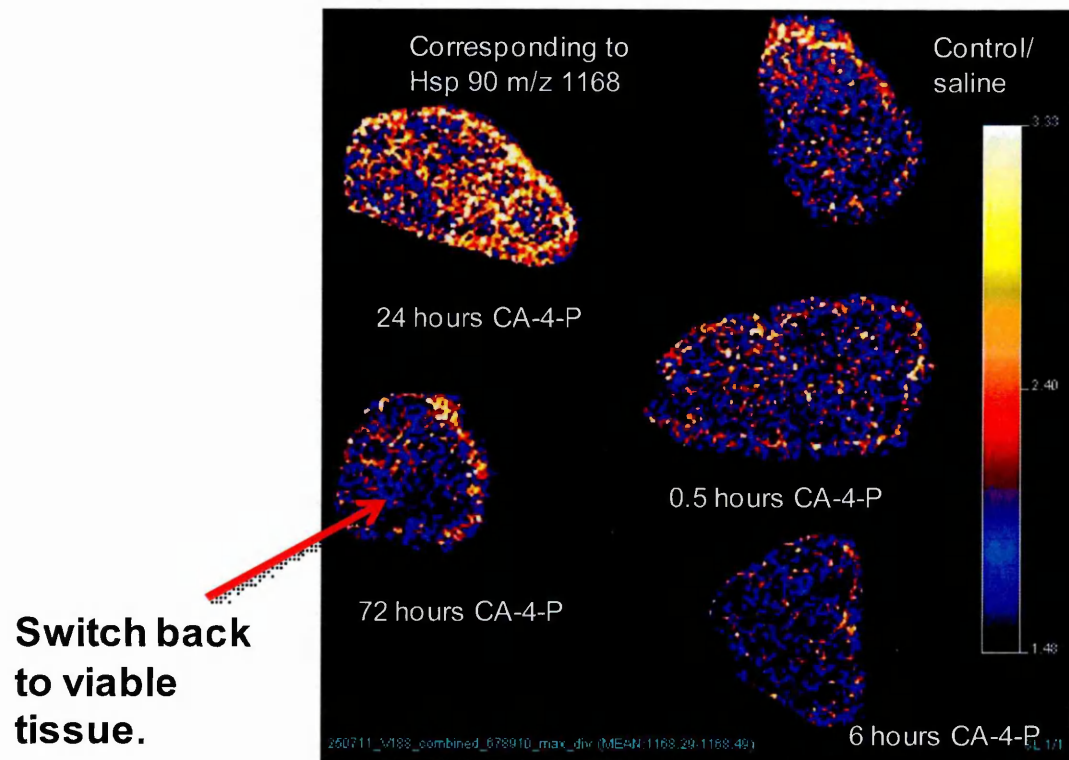


Figure 3. 8: Fibrosarcoma 188 MALDI-MSI multi image showing spatial distribution of HSP-90. MALDI images showing spatial distribution of HSP-90 alpha at m/z 1168.

The presence of HSP-90 is shown throughout the fibrosarcoma 188 time course. The MALDI image corresponding to 24hr post CA-4-P is indicative of complete HSP-90 saturation. This response is matched by HSP-90 immunohistochemical staining seen in Figure 3.8.

The possible 'switch back to viable tissue' is also exhibited by the 72h time point in Figure 3.8. This potential evidence of tumourigenesis can also be seen in the immunohistochemical equivalent in Figure 3.9.

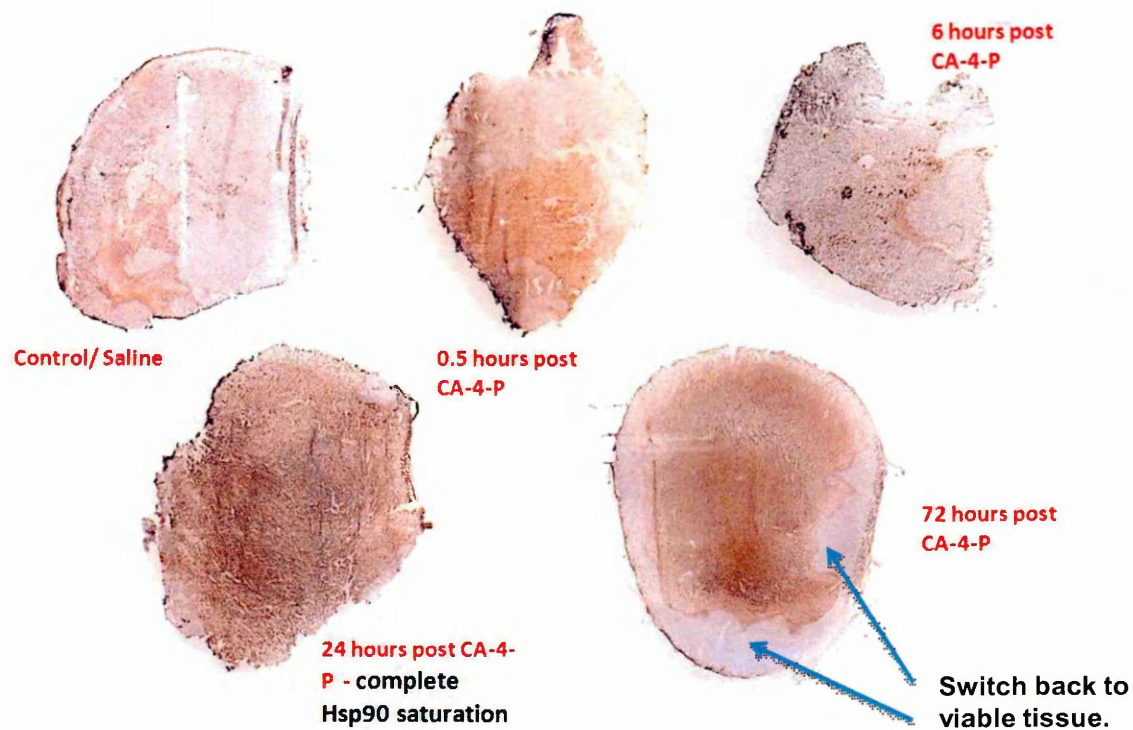


Figure 3. 9: Immunohistochemical staining of a fibrosarcoma 188 time course. Evidence of complete HSP-90 saturation can be observed in the 24h optical scan with the indication of tumour tissue rejuvenation in the 72h tumour time point.

The microscopic images in Figure 3.10 were captured in brightfield 10X to enable closer inspection of the immunohistochemical staining seen here in Figure 3.9.

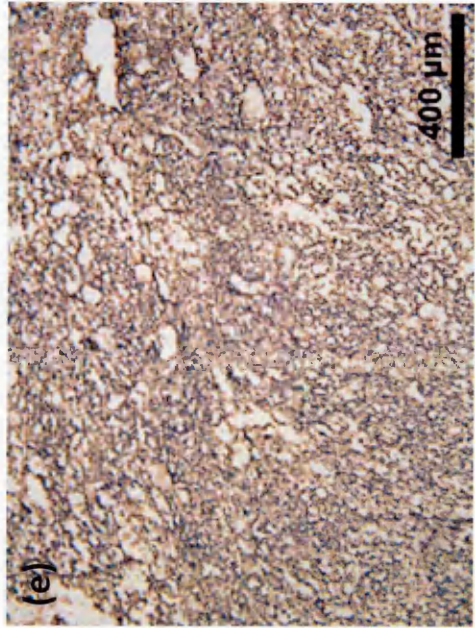
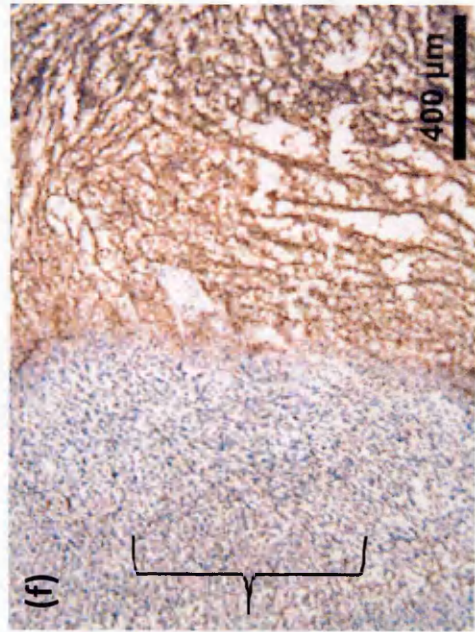
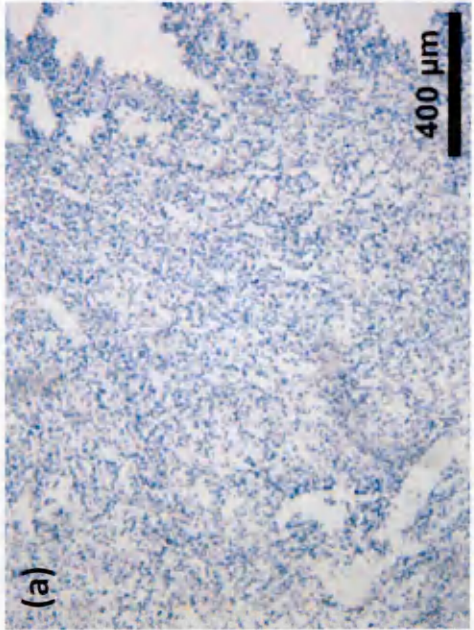
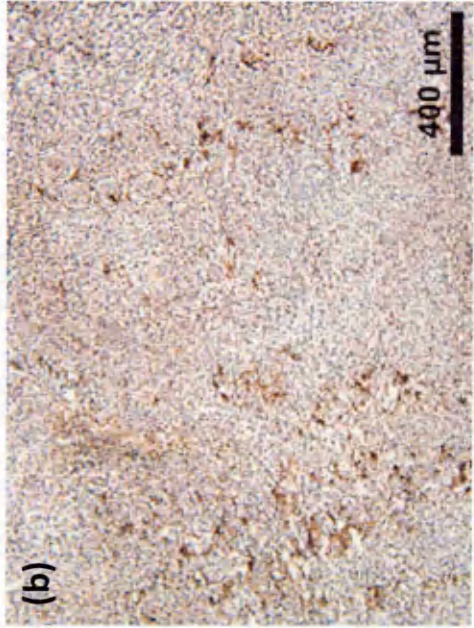


Figure 3. 10: Immunohistochemical staining of HSP-90 in Fibrosarcoma 188 tissue (continued overleaf)

Figure 3.10; (a) displays the negative Control for HSP-90, the time point used was 24h post CA-4-P, (b) HSP-90 staining using fibrosarcoma 188 Control tissue, (c) HSP-90 staining of 0.5h post CA-4-P, (d) 6h post CA-4-P, (e) HSP-90 staining of 24h post CA-4-P showing HSP-90 tissue saturation status and (f) HSP-90 of the saturated necrotic central region and viable tissue regional indicated by the bracket.

The HSP-90 immunohistochemical staining in Figure 3.10 was captured at 10X magnification to allow closer inspection of the HSP-90 optical scans previously shown. The apparent saturation of HSP-90 in the 24h time point visible in the MALDI-MSI and in Figure 3.9 can be seen in Figure 3.10(e). The 10x image of HSP-90 showing the regional switch back to viability can be clearly observed in Figure 3.10(f), the viable tumour cells are highlighted by the bracket.

3.4.1.4 High resolution MALDI-MSI using fibrosarcoma 188 tumour tissue

The MALDI-MSI featured here employed high resolution imaging with a view to focus down on the tumour rim regions.

Tissue was imaged using vertical sliced regions which encompassed both the tumour rim and central area.

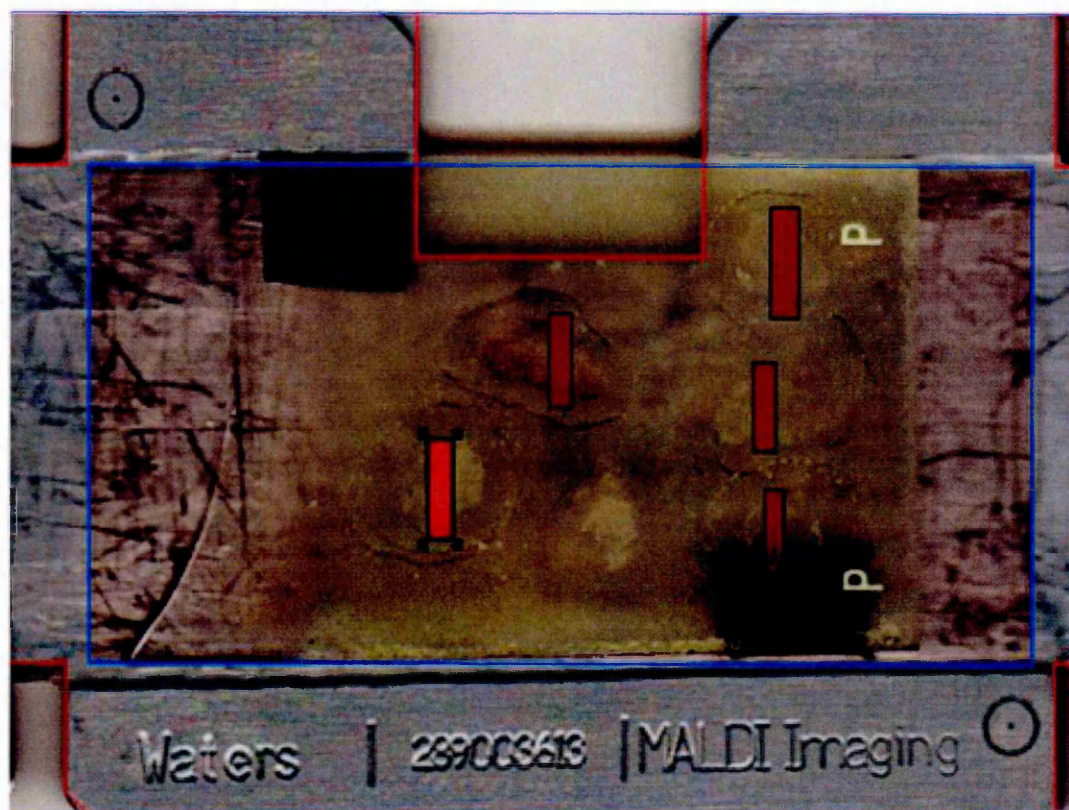


Figure 3. 11: SYNAPT G2 MALDI imaging plate indicating tissue image regions. The regions selected for MALDI-MSI analysis have been superimposed over the histological tissue sections.

The 40 μ m resolution image show in Figure 3.12 shows the spatial distribution of m/z 844.5 which corresponded to the putative Rho GTPase activating 2 protein mentioned earlier in Chapter 2. Although not a dominant peak within the fibrosarcoma 188 spectra, the spatial distribution of this ion is shown to be localised around the periphery of the tumour tissue in the following MALDI-MSI of a 72hr treatment time point.

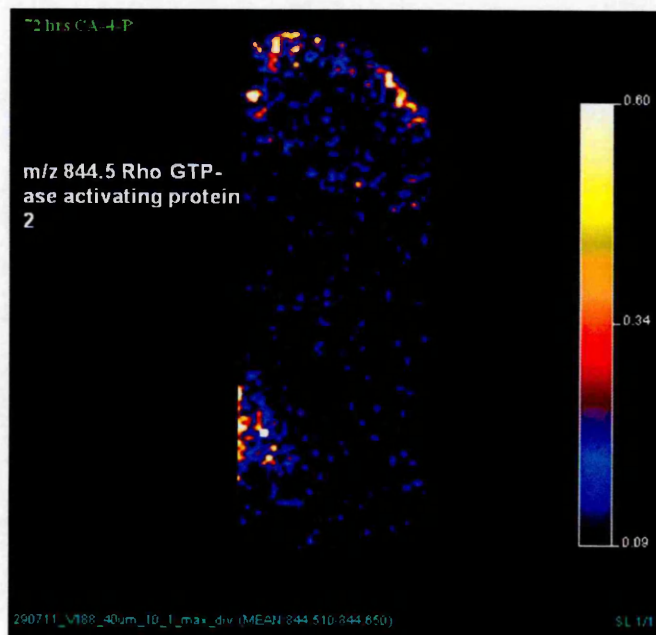


Figure 3. 12: 40µm MALDI-MSI of 24h post CA-4-P fibrosarcoma 188 tumour tissue. Peripheral localisation of n-Chimaerin at m/z 844.5.

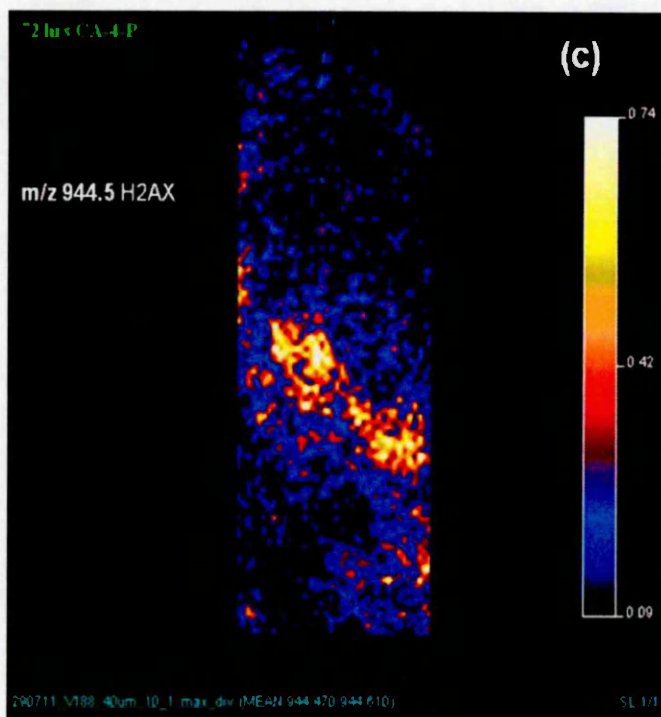


Figure 3. 13: 40µm MALDI-MSI of m/z 944.5 in fibrosarcoma 188 tumour tissue. The differing spatial distribution of an ion is shown here corresponding to Histone 2A.

An image from the same acquisition shown in Figure 3.12 is displayed in Figure 3.13. The ion at m/z 944.5 (Histone 2A) is located in the necrotic region of the tissue, emphasising the distinction in spatial distribution between m/z 844.5 and 944.5. The necrotic region is indicated by the H and E in Figure 3.14.

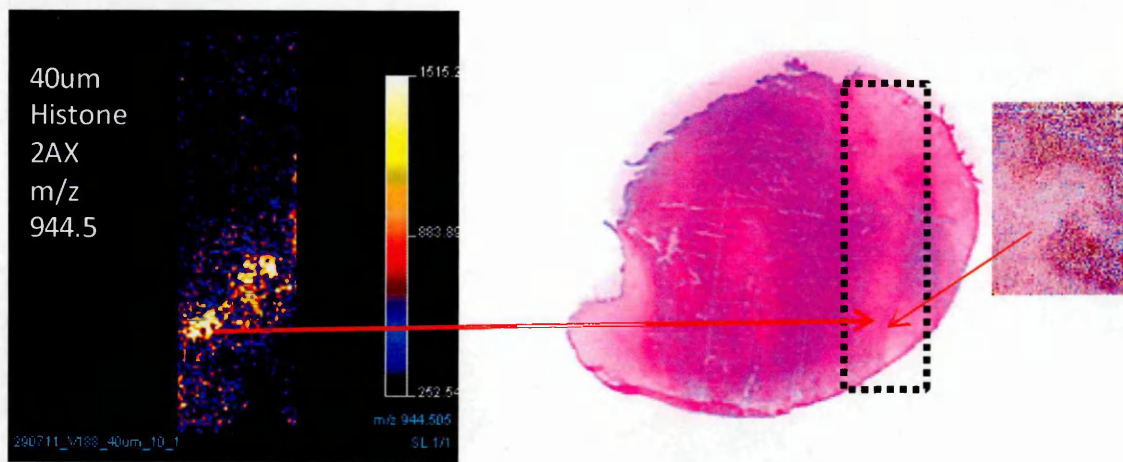


Figure 3. 14: 40µm MALDI-MSI of a on tissue tryptic digest and corresponding H and E histological section. A necrotic region is seen here to correlate with the spatial distribution of Histone 2A.

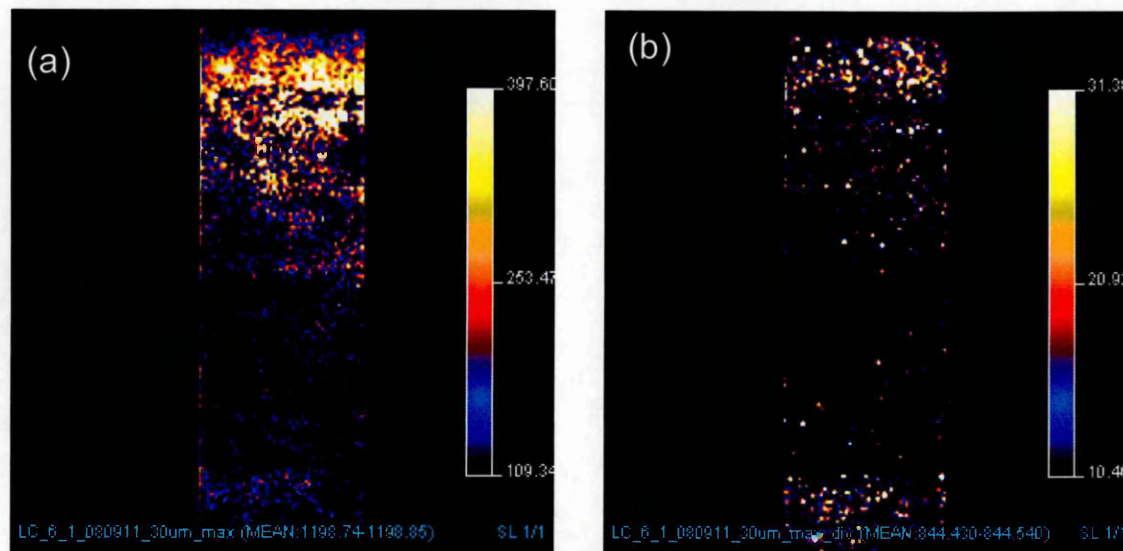


Figure 3. 15: 30 µm MALDI-MSI of a Control fibrosarcoma 188 tumour on tissue tryptic digest. The spatial distribution of Actin (a) and Rho GTPase activating protein 2 (b) is shown in the 30µm MALDI-MSI.

30µm images (Figure 3.15) were performed to investigate the tumour rim and although images appear slightly 'grainy', distribution of known peptides could still be visualised. This 'grainy' appearance of the MALDI-MSI here could be an artefact of 'over sampling' due to the laser spot size measuring ~60-70µm teamed with the 30µm high resolution laser spot to spot pattern.

3.4.2 Statistical analysis of mouse fibrosarcoma 188 tumour tissue using MATLAB®

Initial statistical analysis on the fibrosarcoma 188 tryptic digest spectra was performed using Principle component analysis (PCA) via MATLAB® through the Eigen Vector tool box, to produce an unbiased clustering of spectra acquired from MALDI-MSI of the fibrosarcoma188 data. As discussed in Chapter 2, there is a requirement for an element of discrimination in a statistics model for known time course data. This considered, a preliminary PCA test was done to predict potential groupings between time points. This PCA consisted of 9 technical replicates from MALDI images acquired in triplicate to include an example of each CA-4-P treatment time point. The results are shown in Figures 3.16 and 3.17.

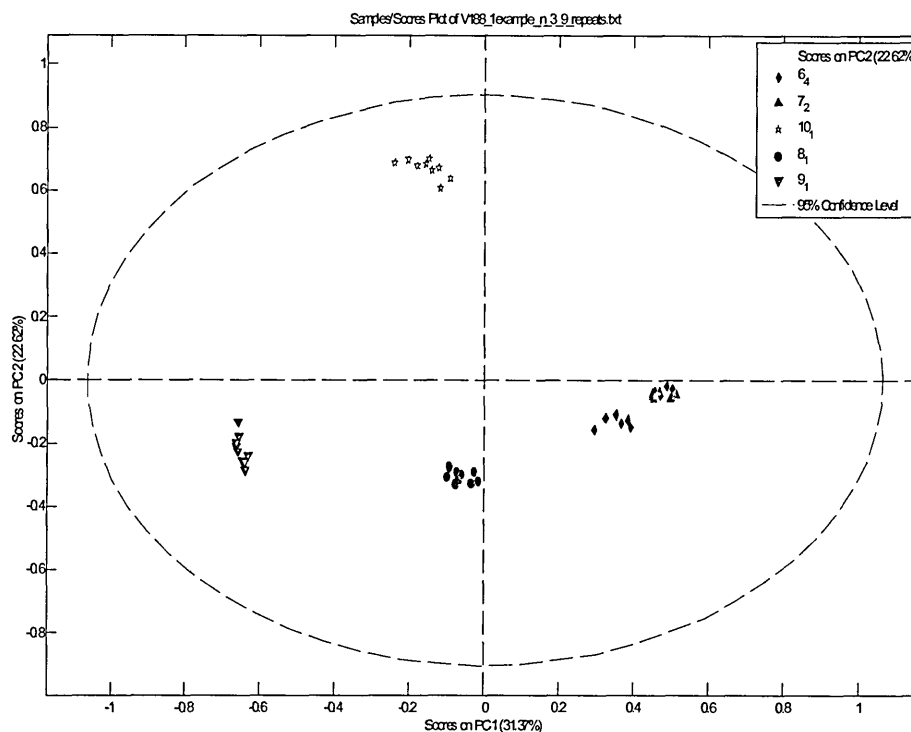


Figure 3. 16: PCA score plot of fibrosarcoma 188 tumour tissue in situ tryptic digests. The score plot in Figure 3.16 shows the potential groupings between the tumour time points in this fibrosarcoma 188 study. From this preliminary PCA test there does appear to be a separation between tumour treatment groups with an apparent overlap observed here in the Control (6:4) and 0.5h post CA-4-P (7:2)

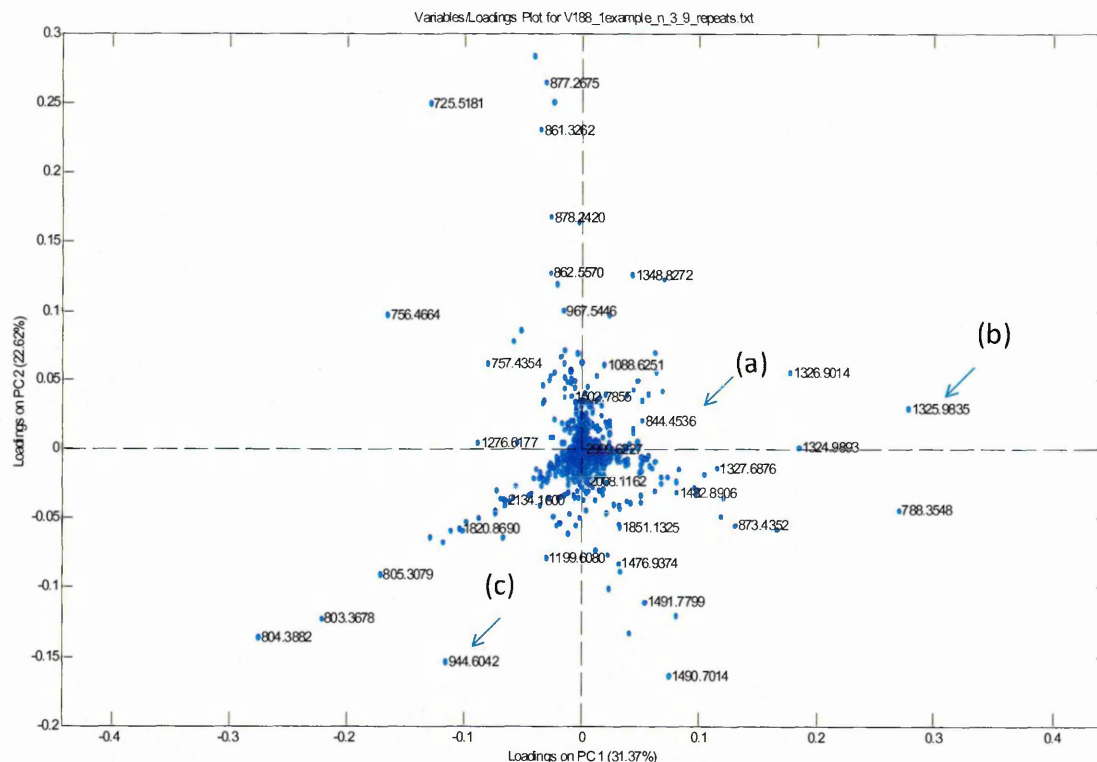


Figure 3. 17: PCA loadings plot fibrosarcoma 188 tumour tissue in situ tryptic digests. (a) corresponds to a peak relating to N-Chimaerin mentioned earlier, (b) Histone H4 and (c) Histone 2A.

The loadings plot contains the peak information which spatially relate to the groupings seen in Figure 3.17. The loadings plot seen here does not appear to exhibit the Hb dominance that was visible in the PCA loadings plot featured in Figure 2.20, Chapter 2.

The region in Figure 3.17 that spatially relates to the 72h post CA-4-P tissue contains many unknown peaks between the mass range of 700-800 Da. Further confirmation is required to elucidate peak identifications here as to whether the peaks are indicative of the viable tissue switch discussed previously, or due to matrix/ lipid peak signals.

PLSDA was then carried out on a larger data set then the VIP scores for each time point were then analysed. For the PLSDA analysis, 3 biological repeats per tumour time point were used via MALDI-MSI acquisitions and 6 technical spectral repeats were taken from each biological replicate.

PLSDA models were built to compare the treatment time points against the Control tumour tissue.

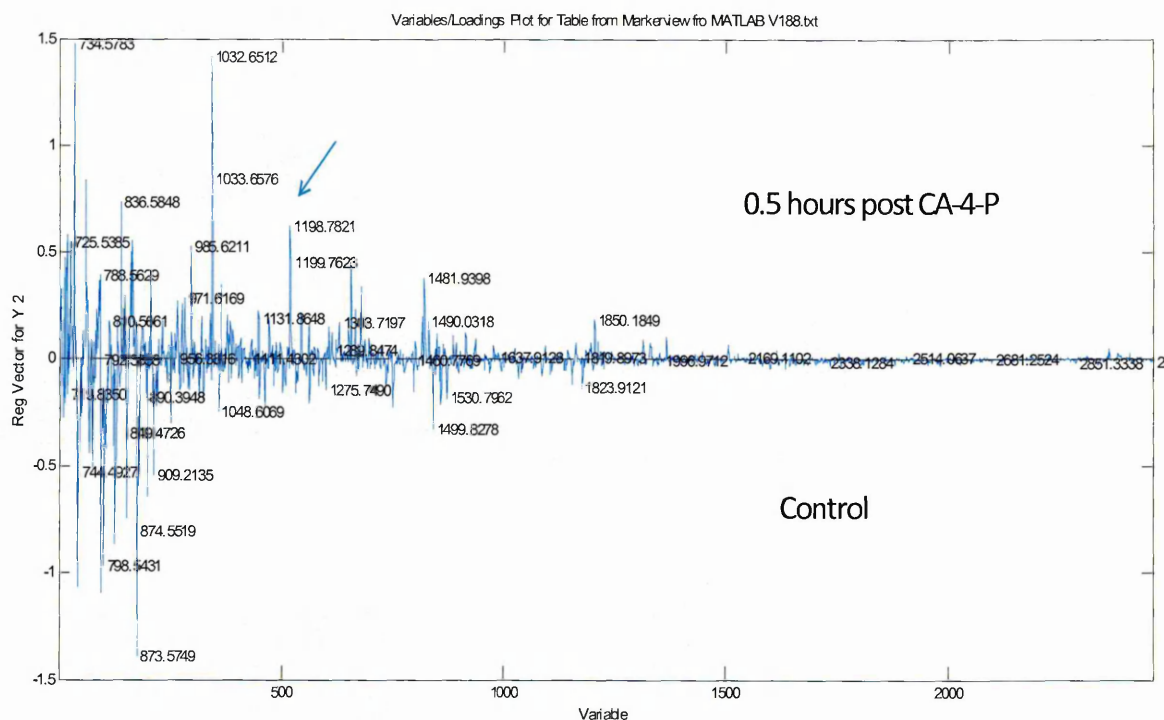


Figure 3. 18: Partial least squares discriminant analysis (PLSDA) regression vector plot comparing MALDI “on-tissue” digest data from samples of fibrosarcoma 188 Control and 0.5h post combretastatin-4-phosphate (CA-4-P), treatment tumour samples. The increased abundance of Actin at m/z 1198.7 in the 0.5h post treatment sample can be clearly seen.

As previously mentioned, there are numerous peaks in the low mass range seen here in the regression vector plot especially in the Control tissue. The peptide corresponding to Actin is seen to be increased in the 0.5h treatment. A similar treatment response was reported by Kanthou and Tozer (2002) (discussed in the Introduction) with fluorescent staining of Human umbilical vein endothelial cells, Control and post CA4P administration. The results from this study showed an increase of filamentous Actin overtime after treatment.

The following regression vector plot generated using PLSDA is between Control and 6h post CA-4-P treatment.

VIP scores were then observed which considered 0.5h, 6h, 24h and 72h time points based on the PLSDA predictive models in Figures 3.18-3.21. Inspection of these data aimed to observe the variables within the fibrosarcoma 188 study that are considered most important to that time point.

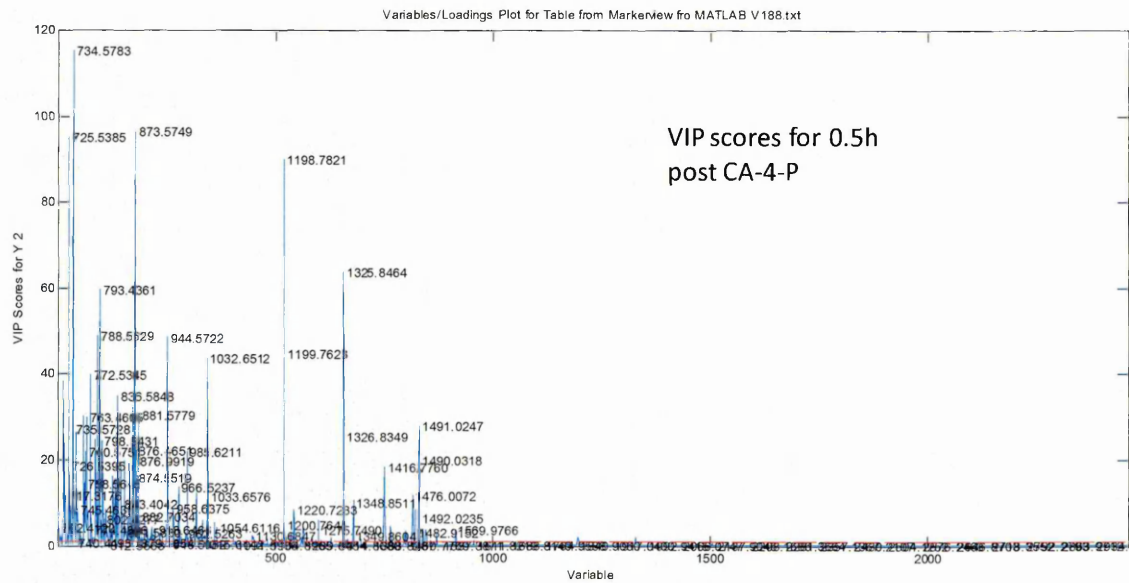


Figure 3. 22: VIP scores for the 0.5h post CA-4-P fibrosarcoma 188 on tissue digest.

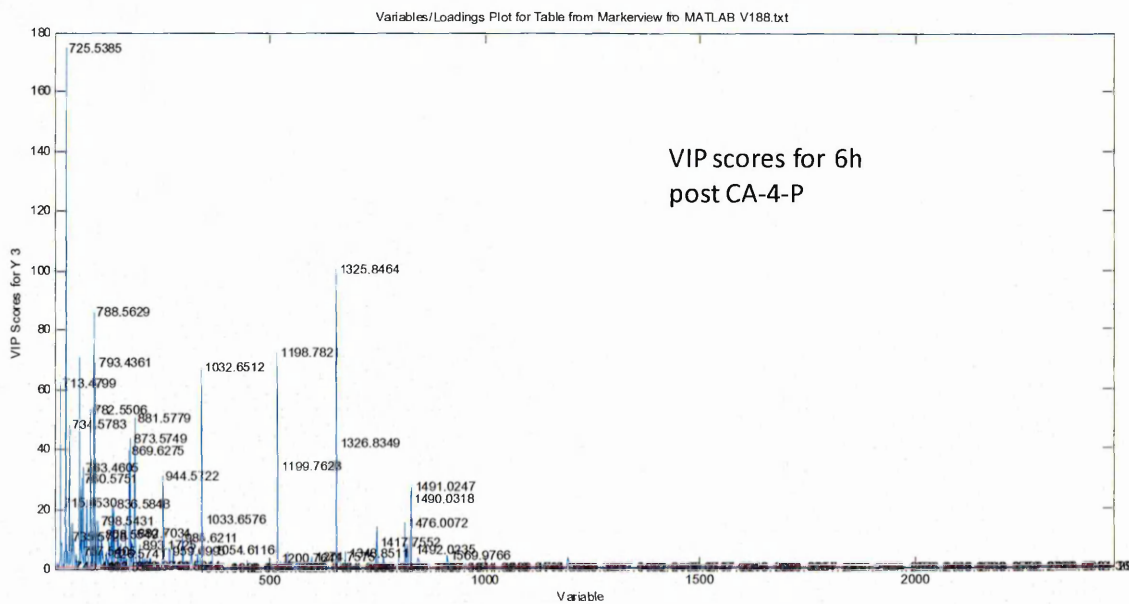


Figure 3. 23: VIP scores for the 6h post CA-4-P fibrosarcoma 188 on tissue digest.

Histone H4 (m/z 1325) is deemed to have a key position in the time points apart from in the 24h samples which could be indicative of CA-4-P interference before the regenerative tumour action commences, seen in the 72h treatment.

3.4.3 Label free LC-ESI-MS/MS for the identification of proteins in a CA-4-P treated fibrosarcoma 188 mouse model

Recognition of proteins via label free MS/MS peptide identification describes the widely used technique of Bottom Up shotgun proteomics. As mentioned earlier (see Introduction), this methods uses enzymatic digestion of proteins prior to data-dependent mass spectrometric analysis (Old *et al* 2005). MS/MS fragmentation spectra are matched against a proteomic database in order to achieve a unique, rank 1 peptide identification.

The method reported here is based on multidimensional protein identification technology (MudPIT) involving reversed-phase (RP) HPLC (Kline and Wu 2009,. McCormack *et al* 1997,. Link *et al* 1999,. Wolters *et al* 2001).

Label free LC-ESI-MS/MS was employed to study protein response throughout the fibrosarcoma 188 treatment time course. Control, 0.5h, 6h, 24h and 72h post CA-4-P treatments were used for analysis.

Scaffold 3 proteomics software tool was used for the analysis of the following Label free LC-ESI-MS/MS. Time course protein responses were plotted using normalised spectral counting calculated and presented via Scaffold 3. Gene ontology pie charts were included in the experimental output from Scaffold to aid understanding of biological function of the protein identified.

Figure 3.26 displays a screenshot from the fibrosarcoma 188 Label free LC-ESI-MS/MS data list. After importing of data, 201 proteins were listed which included those which have a minimum of 2 peptides assigned per protein, 99% minimum protein and 90% minimum peptides.

The data options for exportation to excel are; protein identification probability, percentage of total spectra, number of assigned spectra, number of unique peptides, number of unique spectra, percentage coverage, un-weighted spectrum count and quantitative value.

The Control/ CA-4-P protein response bar graphs to follow use the quantitative value based on normalised spectrum counts.

Figures 3.27 – 3.33 show the entire Scaffold 3 protein list and corresponding normalised spectrum counts that were generated. Figure 3.34 features a response bar graph of selected proteins of interest.

Load Data | Samples | Proteins | Similarity | Quantity | Publish | Statistics

Display Options: Quantitative Value | Min Protein: 99.0% | Min Peptides: 2 | Min Peptide: 90% | Search: | No Filter | Req Mods: |

Probability Legend:
 over 95% (green)
 80% to 94% (yellow-green)
 50% to 79% (yellow)
 20% to 49% (orange)
 0% to 19% (red)

Identified Proteins (201)
 Including 0 Decoys

Visible?	Starred?	Accession Number	Molecular Weight	Protein Grouping Ambiguity	Quantitative Variance (Variance)	Taxonomy	Biological Process	Cellular Compartment	Molecular Function	1 Con... 2 30 ... 3
<input checked="" type="checkbox"/>	<input checked="" type="checkbox"/>	Reclname: Full=Serum albumin; FL... IP100131695	69 kDa	20% LK3 tra...	26% unkn...	unkno...	growth	plasma membrane	transporter activity	Biosample 1
<input checked="" type="checkbox"/>	<input checked="" type="checkbox"/>	Tax_Id=10090 Gene_Symbol=Fn... IP100652813	?	5% LK3 tra...	5% LK3 tra...	unkno...	cellular process	plasma membrane	transcription regulator activity	Biosample 2
<input checked="" type="checkbox"/>	<input checked="" type="checkbox"/>	Reclname: Full=Actin, cytoplasmic... IP100110850	42 kDa	43% LK3 tra...	43% LK3 tra...	LK3 tra...	cellular process	plasma membrane	transcription regulator activity	88 86
<input checked="" type="checkbox"/>	<input checked="" type="checkbox"/>	Reclname: Full=Myosin-9; Althiam... IP100788324	226 kDa	27% LK3 tra...	27% LK3 tra...	LK3 tra...	cellular process	plasma membrane	transcription regulator activity	55 122
<input checked="" type="checkbox"/>	<input checked="" type="checkbox"/>	Reclname: Full=Vimentin... IP100227299	54 kDa	28% LK3 tra...	28% LK3 tra...	LK3 tra...	cellular process	plasma membrane	transcription regulator activity	14 75
<input checked="" type="checkbox"/>	<input checked="" type="checkbox"/>	Reclname: Full=Tubulin beta-5 ch... IP100117352	50 kDa	14% LK3 tra...	14% LK3 tra...	LK3 tra...	cellular process	plasma membrane	transcription regulator activity	28 59
<input checked="" type="checkbox"/>	<input checked="" type="checkbox"/>	Reclname: Full=Pyruvate kinase is... IP100407130	58 kDa	33% LK3 tra...	33% LK3 tra...	LK3 tra...	cellular process	plasma membrane	transcription regulator activity	93 60
<input checked="" type="checkbox"/>	<input checked="" type="checkbox"/>	Reclname: Full=Heat shock cognat... IP100323357	71 kDa	36% LK3 tra...	36% LK3 tra...	LK3 tra...	cellular process	plasma membrane	transcription regulator activity	38 53
<input checked="" type="checkbox"/>	<input checked="" type="checkbox"/>	Reclname: Full=Tubulin alpha-1B C... IP100117348	50 kDa	51% LK3 tra...	51% LK3 tra...	LK3 tra...	cellular process	plasma membrane	transcription regulator activity	21 37
<input checked="" type="checkbox"/>	<input checked="" type="checkbox"/>	Reclname: Full=Hemoglobin subun... IP10031649...	16 kDa	170% LK3 tra...	170% LK3 tra...	LK3 tra...	cellular process	plasma membrane	transcription regulator activity	73 43
<input checked="" type="checkbox"/>	<input checked="" type="checkbox"/>	Tax_Id=10090 Gene_Symbol=Ah... IP100553798	?	25% unkn...	25% unkn...	unkno...	cellular process	plasma membrane	transcription regulator activity	19 38
<input checked="" type="checkbox"/>	<input checked="" type="checkbox"/>	Reclname: Full=Alpha-actinin-4; AL... IP100118899	105 kDa	47% LK3 tra...	47% LK3 tra...	LK3 tra...	cellular process	plasma membrane	transcription regulator activity	5 35
<input checked="" type="checkbox"/>	<input checked="" type="checkbox"/>	Reclname: Full=Myosin-9; Althiam... IP100788324	226 kDa	27% LK3 tra...	27% LK3 tra...	LK3 tra...	cellular process	plasma membrane	transcription regulator activity	94 30

Sample Information:
 Biological Sample: | Sample Category: | Sample Description: | MS/MS Sample: | MS/MS Sample Notes:

Gene Ontology:
 cellular process
 cellular component organization
 cellular component assembly
 cell junction assembly
 cell-substrate junction assembly
 hemidesmosome assembly

Protein Information:
 Lookup Accession Number In: NCBI (e.g. |1351907|ALBU_BOVIN,P02769)
 IP100229509 | IP100230061 | IP100400214 | IP100400215
 Preferred Accession Number: IP100229509
 Protein Name: Reclname: Full=Plectin; Short=PCN; Short=PLTN; AltName:

201 Proteins
 0.0% Prot FDR
 8387 Spectra
 0.0% Pept FDR

Figure 3. 26: Scaffold proteomic tool software used for LC-ESI-MS/MS analysis. An example is shown of the protein list from the LC-ESI-MS/MS fibrosarcoma 188 data with information regarding biological process, cellular compartment and molecular function.

Graph A - Label free quantitative comparison of the expression of proteins showing response to treatment post CA-4-P

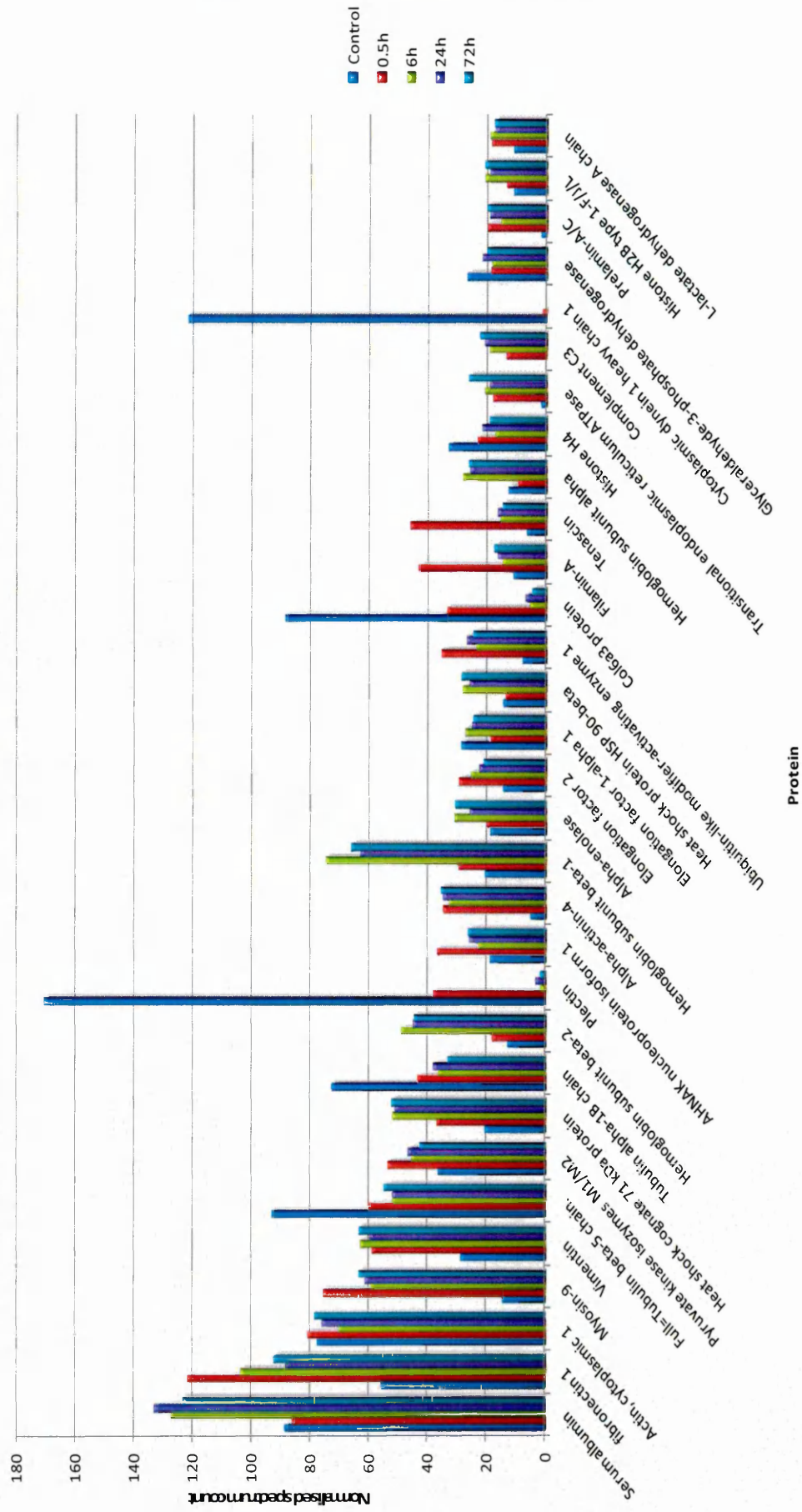


Figure 3. 27: Graph A - Fibrosarcoma 188 treatment time course results, exported from Scaffold 3.

Graph B - Label free quantitative comparison of the expression of proteins showing response to treatment post CA-4-P

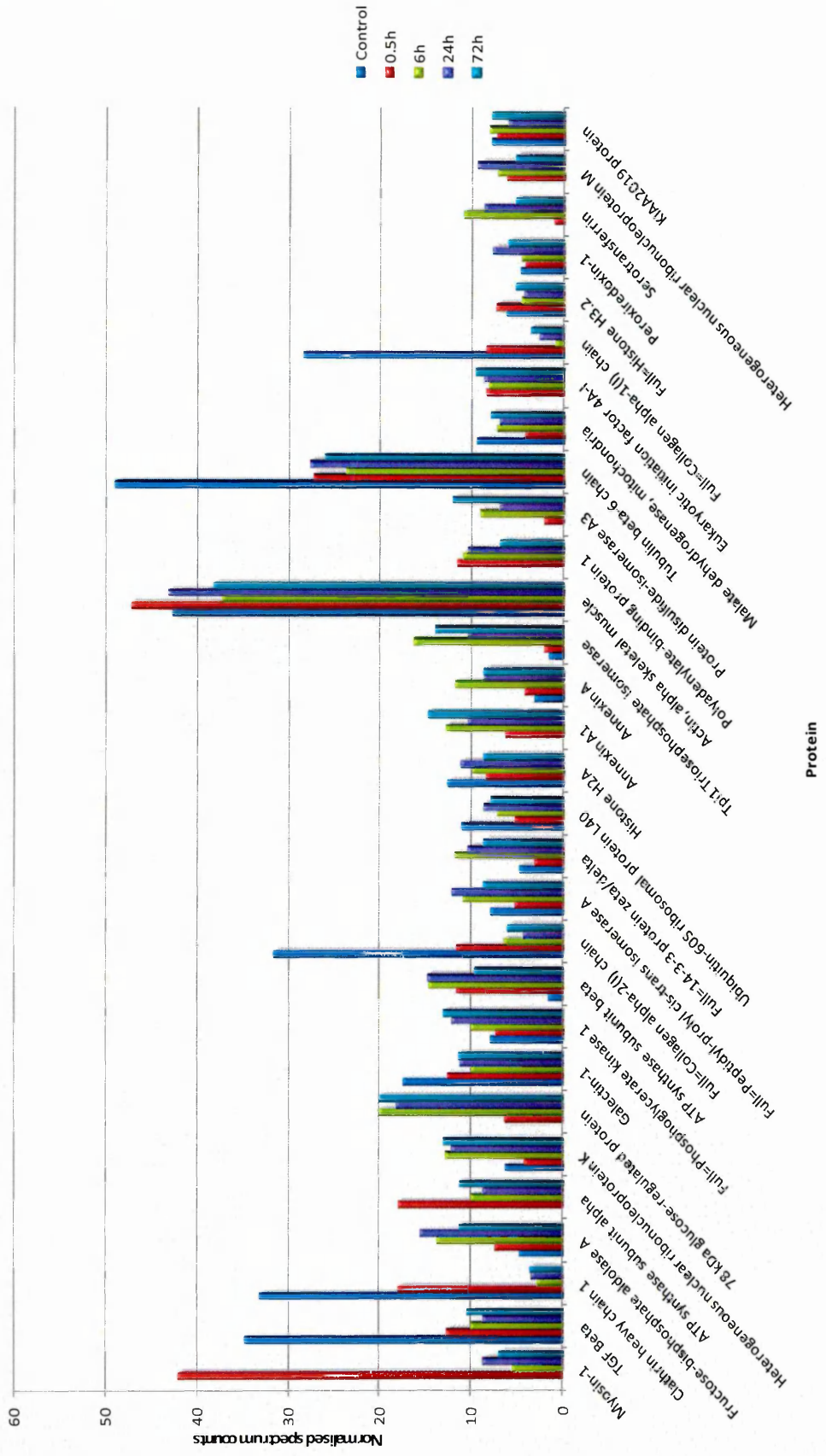


Figure 3. 28: Graph B - Fibrosarcoma 188 treatment time course results, exported from Scaffold 3.

Graph C - Label free quantitative comparison of the expression of proteins showing response to treatment post CA-4-P

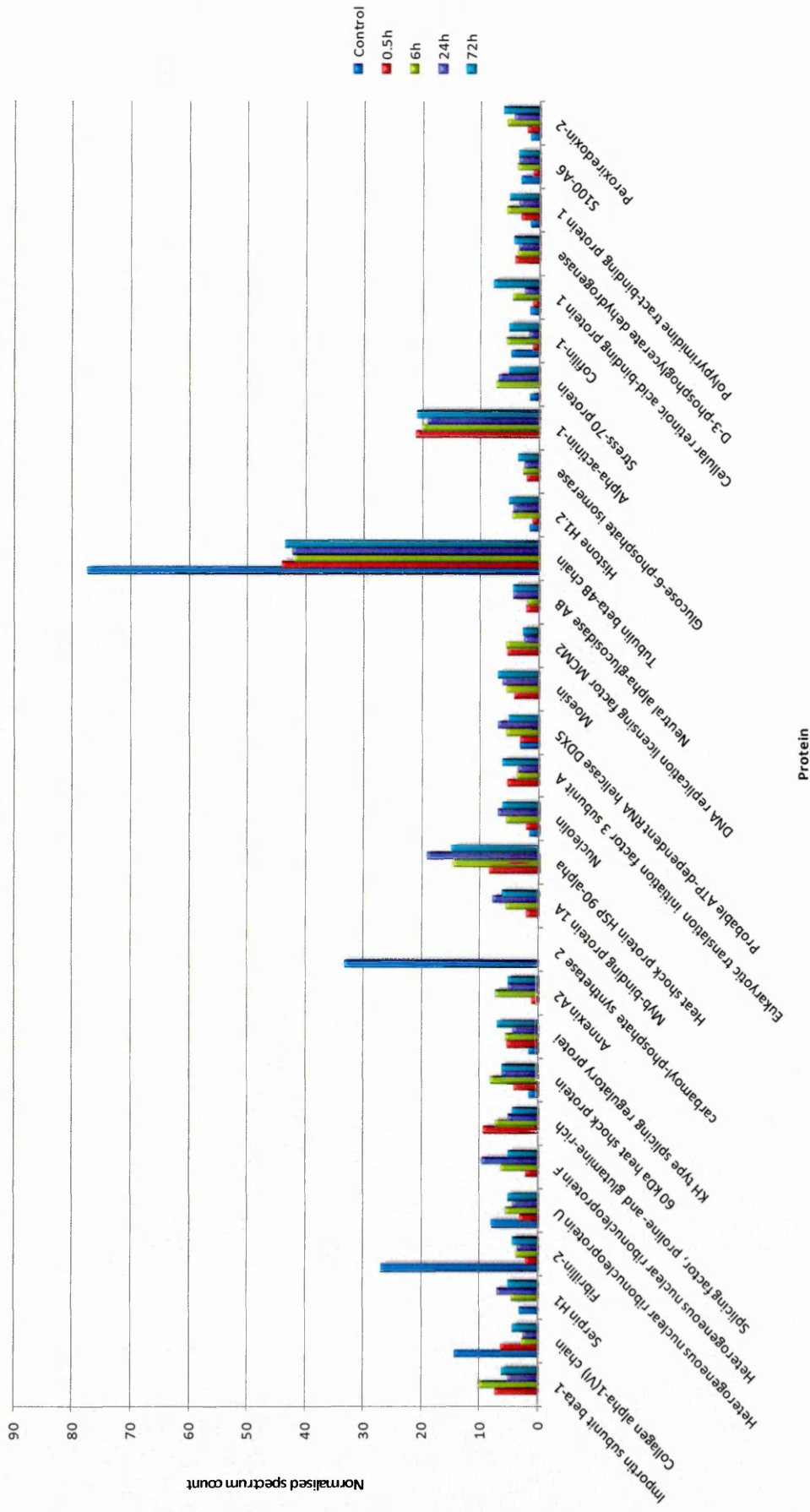


Figure 3. 29: Graph C - Fibrosarcoma 188 treatment time course results, exported from Scaffold 3.

Graph E - Label free quantitative comparison of the expression of proteins showing response to treatment post CA-4-P

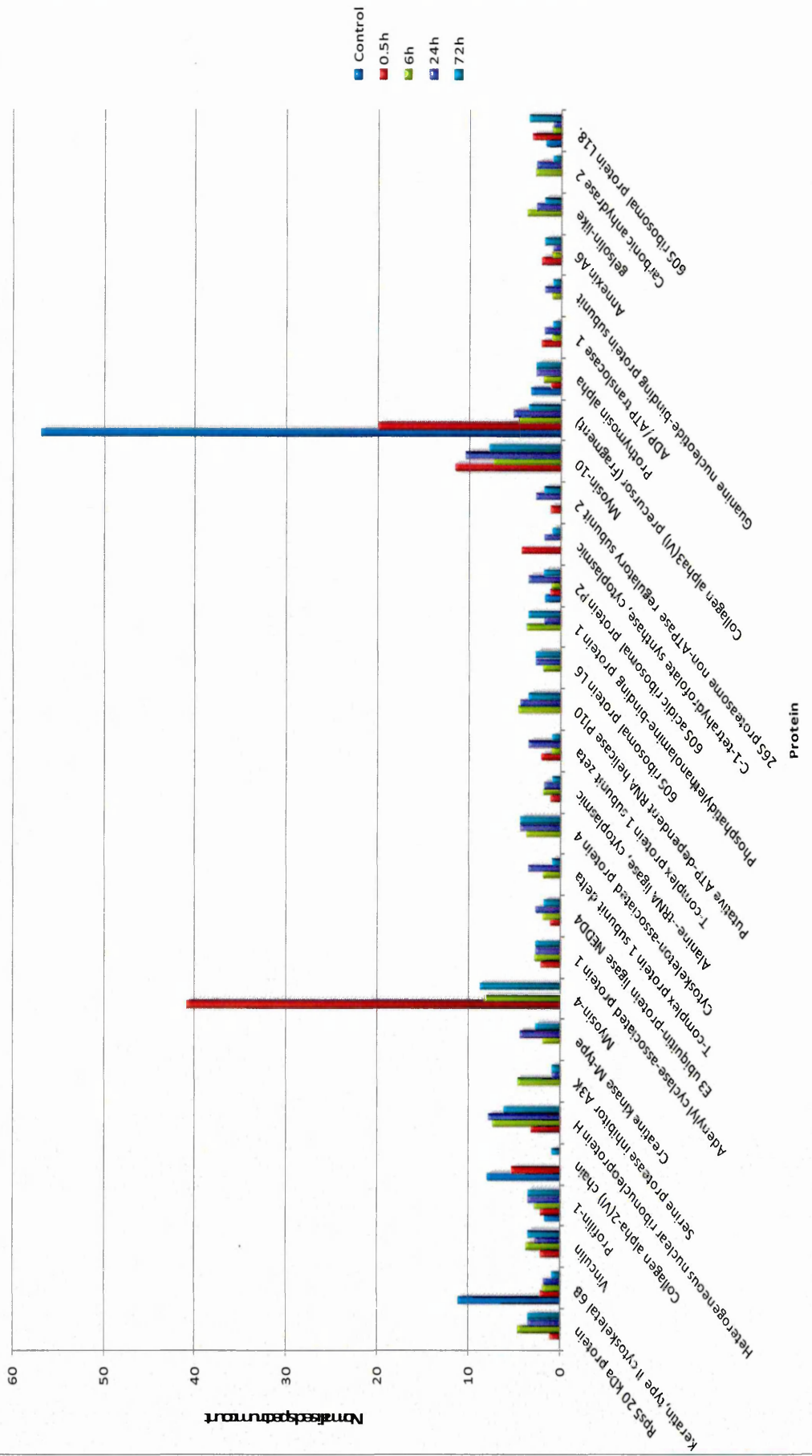


Figure 3. 31: Graph E - Fibrosarcoma 188 treatment time course results, exported from Scaffold 3.

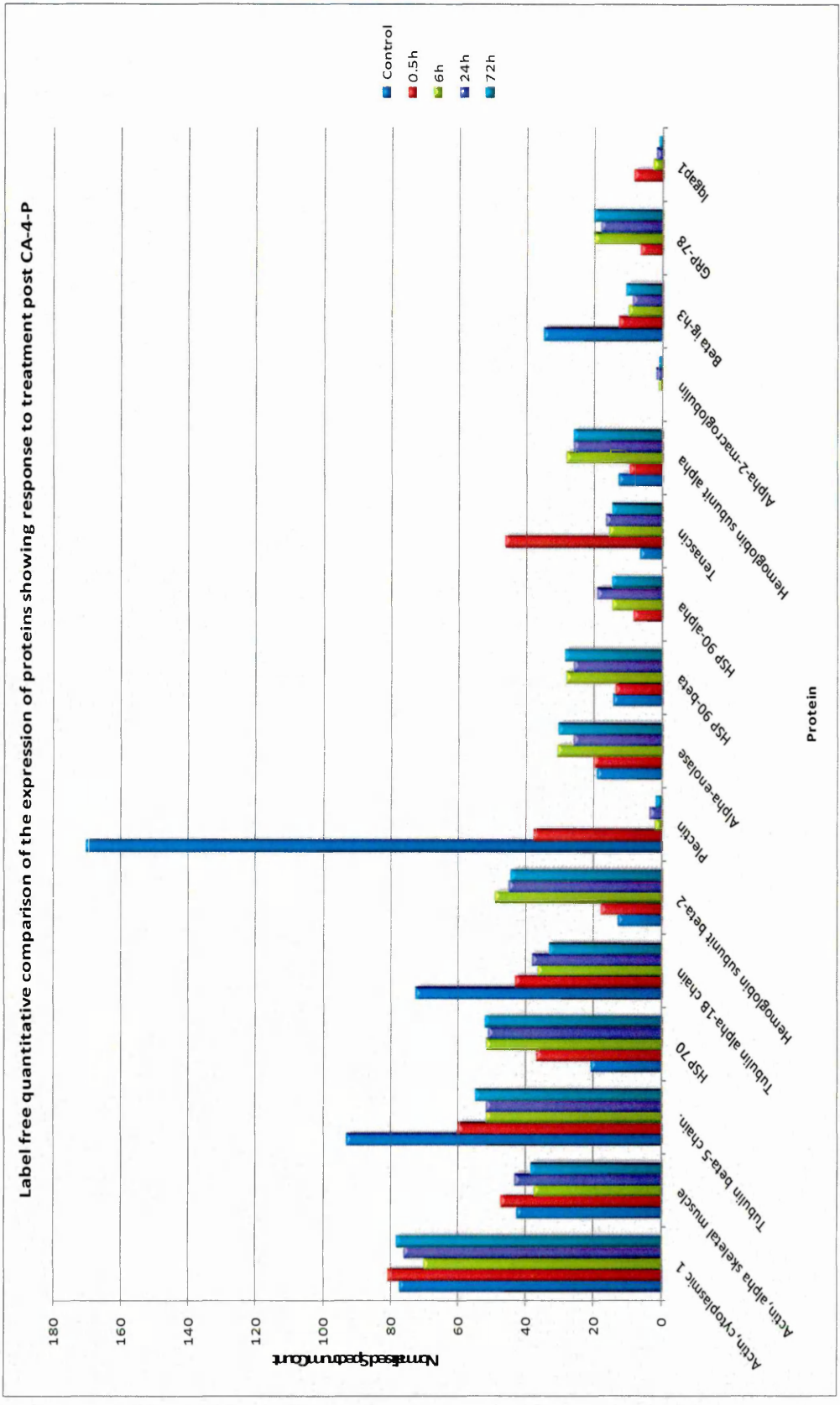


Figure 3. 34: Fibrosarcoma 188 time course results post CA-4-P treatment using LC-ESI-MS/MS.

The rationale for selection of the proteins included in Figure 3.34 was from proteins that either had a high percentage of co-variance throughout the time course (as seen in Scaffold 3), provided a known validating response or may be of relevance to the stress response and could be characteristic of tumour biology.

The increases in Figure 3.34 from both Haemoglobin subunit alpha and Haemoglobin subunit beta-2 exhibit the distinctive gross pharmacological response from administration of a vascular disrupting agent.

Disruption in the architectural integrity of the vasculature is indicated by decreases in structural Tubulin beta-5 chain and Tubulin alpha-1B chain compared to the Control tumour tissue.

Actin, cytoplasmic 1 (Beta-actin) and Actin, alpha skeletal muscle precursor (Alpha-actin-1) appear to show different trends throughout the LC-ESI-MS/MS data here in Figure 3.34.

It is known that the reorganisation and/or disruption of the cytoskeleton results in stress fibre formation (Kanthou and Tozer 2007). Administration of CA-4-P elicits such a response on the tumour cells thought to be induced by stress activated apoptosis.

Overtime the tumour appears to 'retaliate' favouring actin polymerisation after a brief decrease of Beta-actin in the 6h time point with increased levels evident in the 24h and 72h time points.

An overall decrease of alpha skeletal muscle precursor (Alpha-actin-1) towards 72h post CA-4-P is visible from Figure 3.34. This decline could be due to disruption by CA-4-P, further shotgun proteomics and immunohistochemical studies could ascertain the trend in the decreased seen here of Alpha-actin-1. An article by Hemingway *et al* (2012) reports of a study looking at the expression of Alpha isoform of smooth muscle actin (SMA) in primary, benign and malignant bone tumours. It was found that SMA was differentially expressed in the primary tumours and although findings were inconclusive, interestingly SMA expressing pericytes (peri-vascular cells) present in bone marrow/ were also mentioned as a source of SMA levels.

The concept of progenitor cells, infiltrating immune cells or indeed a full stromal cell population could be regarded as a key factor to consider when analysing protein dose response relationships.

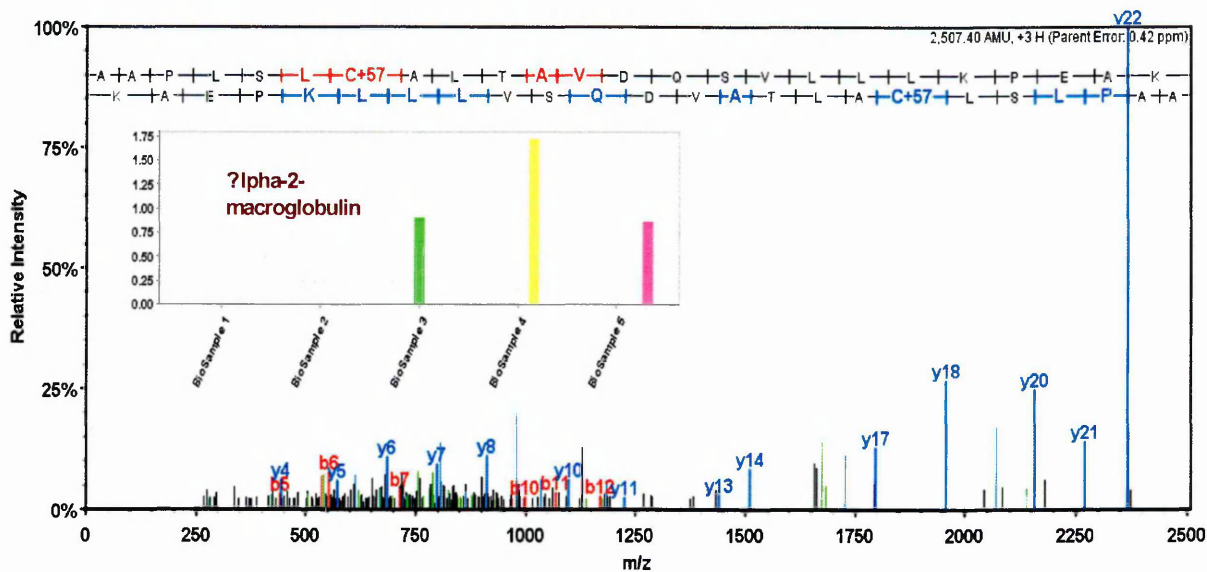
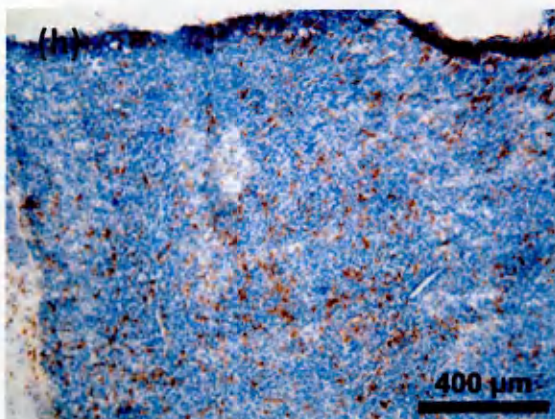
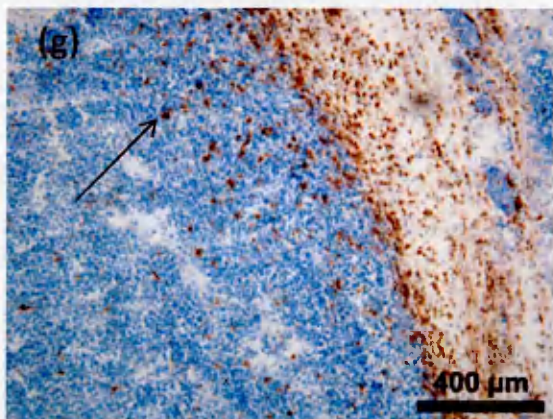
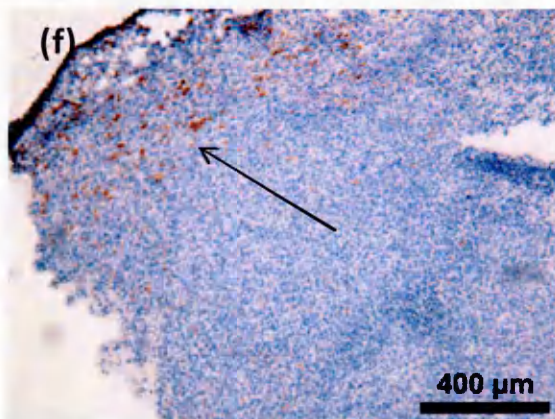
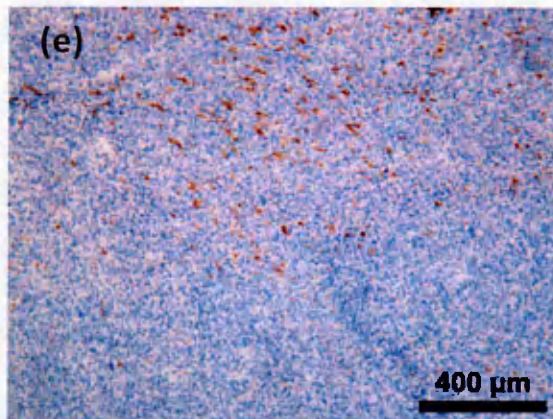
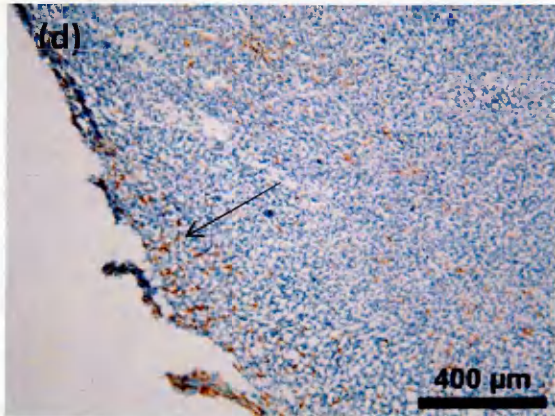
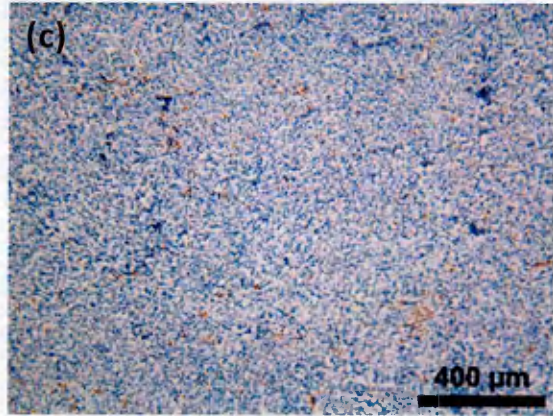
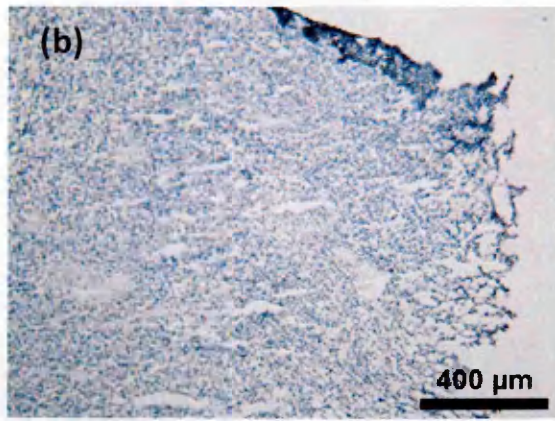
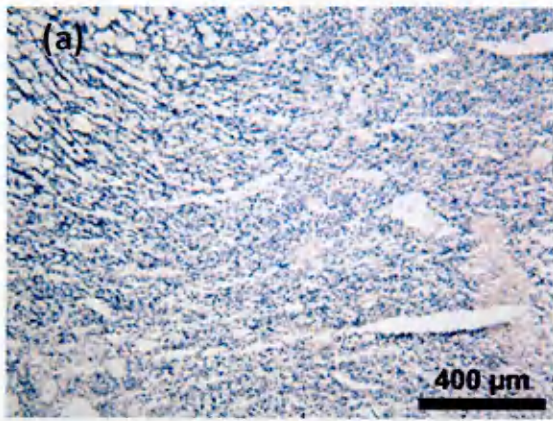


Figure 3. 35: MS/MS spectrum and normalised intensity graph of Alpha-2-macroglobulin in fibrosarcoma 188 LC-ESI-MS/MS results. Insert displays the normalised spectral counts for Alpha-2-macroglobulin throughout the time course post CA-4-P.

Alpha-2-macroglobulin is a carrier protein and is known to have strong associations with growth factors and cytokines i.e. basic fibroblast growth factor, Interleukin 1- β (IL-1 β) and transforming growth factor beta (as seen in Figure 3.34) (Feige et al 1996,. Wellcome trust Sanger Institute 2012). Alpha-2-macroglobulin is also known to be synthesised locally in tissues by infiltrating macrophages.

The dose response relationship of this protein from the LC-ESI-MS/MS results can be observed in Figure 3.35 via the Scaffold 3 viewer proteomics tool. Levels here appear to be undetected by this technique in the early fibrosarcoma 188 treated time points but a sudden increase is evident from the 6h treated sample, a surge in the 24h time point with the 72h representing a drop in expression.

With aim to study this response further, immunohistochemical staining was performed on F4/80, a macrophage cell surface marker to see whether or not this response could be studied indirectly as a reflection of infiltrating immune cells in response to CA-4-P treatment.



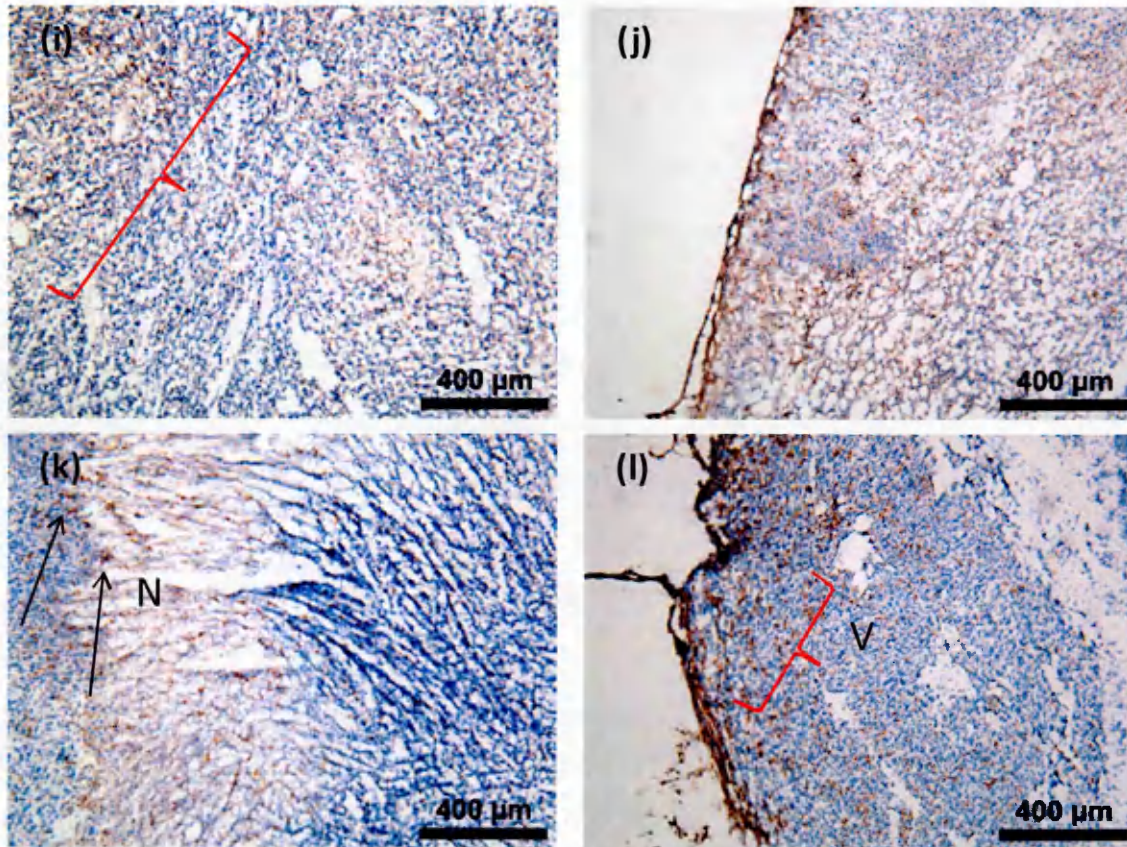


Figure 3.36: Immunohistochemical staining of macrophage cell surface marker F4/80 using fibrosarcoma 188 tissue 10x. (a) negative F4/80 isotype control using 72h post CA-4-P fibrosarcoma tissue – central region, (b) negative F4/80 isotype control using 72h post CA-4-P fibrosarcoma tissue – rim region, (c) F4/80 staining of Control – central region, (d) F4/80 staining of Control – rim region, (e) F4/80 staining of 0.5h post CA-4-P – central region, (f) F4/80 staining of 0.5h post CA-4-P – rim region, (g) F4/80 staining of 6h post CA-4-P – central region, (h) F4/80 staining of 6h post CA-4-P – rim region, (i) F4/80 staining of 24h post CA-4-P – central region with bracketed region showing macrophage population within the necrotic tissue, (j) F4/80 staining of 24h post CA-4-P – rim region, (k) F4/80 staining of 72h post CA-4-P – central region, the arrows indicate evidence of macrophages still present and an example of a necrotic region is labelled with N (l) F4/80 staining of 72h post CA-4-P – rim region, the bracket indicates a macrophage population with the V labelling an example of viable tissue.

There appears to be few macrophages present mainly around the periphery of the tumour in the Control tissue (Figure 3.36 c and d) as indicated by the arrow with a meagre presence visible within the central region shown. Similar staining is evident in the 0.5h treatment (Figure 3.36 e and f) central and rim areas. The latter could explain the undetected presence of Alpha-2-macroglobulin in the equivalent Scaffold 3 LC-ESI-MS/MS results.

An army of macrophages are now seen to be infiltrating the 6h post CA-4-P rim and central tissue regions in Figure 3.36 (g) and (h) with populations still present in the 24h treatment fibrosarcoma tissue.

The isotype controls for the immunohistochemical staining of F4/80 are shown in Figure 3.36(a)-(b) using the same tissue from 72h images in 3.36 (k) and (l). There appears to be macrophages still present in the necrotic and viable tissue as indicated.

The engulfing of cellular debris due to the phagocytic nature of the macrophage could explain the decrease at 72h following the surge at 24h. The steep increase could be as a result of the widespread necrosis observed at 24h post CA-4-P and influx of debris clearing immune cells overtime between 6h/24h time points hence Alpha-2-macroglobulin accumulation in the tissue. The decreased levels of Alpha-2-macroglobulin at 72h could be indicative of an efflux in macrophage cell populations.

The tumour associated macrophages (TAM's), known to stimulate angiogenesis undoubtedly play a major role in drug resistance (Welford *et al* 2011., Ey *et al* 2006., Bingle *et al* 2002). The complex tumour microenvironment can result in the promotion of anti-tumour T cells yet conversely studies have shown that biological events within the tumour can 're-programme' TAM's to possess pro-oncogenic, assisting tumour growth and progression. The F4/80 staining in the 72h could suggest a possible pro-tumourigenic action via the macrophage population considering their presence in the viable tissue region.

The HSP-90 beta levels in the label free quantitation graph (Figure 3.34) show a steady increase in response to CA-4-P administration. The HSP-90 alpha however is in close agreement with the earlier MALDI-MSI in Figure 3.8 and HSP-90 immunohistochemical staining in Figure 3.9 mirroring the 24h HSP-90 saturation prior to a slight decrease in the 72h due to the switch back to viable tissue concept.

Plectin (Figure 3.34) was found to have a high value of percentage co-variance (170%) throughout the sample time course so this effect was investigated in order to relate the response to the biological action of tumour tissue. The graph of Fibrosarcoma 188 time course results post CA-4-P treatment using LC-ESI-MS/MS (Figure 3.34), indicates a marked abundance of Plectin in the Control then levels dramatically decrease overtime.

Figure 3.37 displays an example of a Plectin MS/MS spectra visualised through Scaffold 3 software.

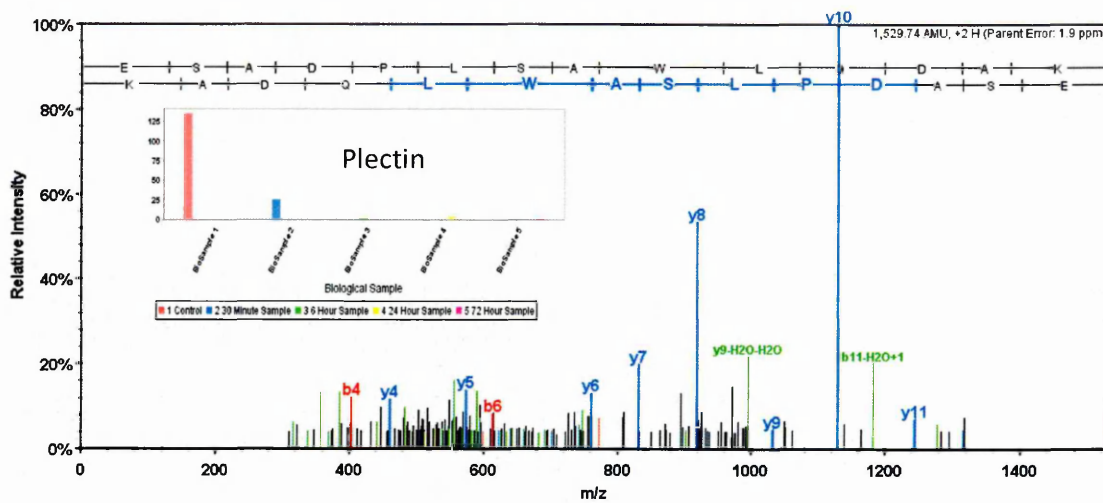


Figure 3. 37: MS/MS spectrum and normalised intensity graph of Plectin in fibrosarcoma 188 LC-ESI-MS/MS results. Insert displays the normalised spectral counts for Plectin throughout the time course post CA-4-P.

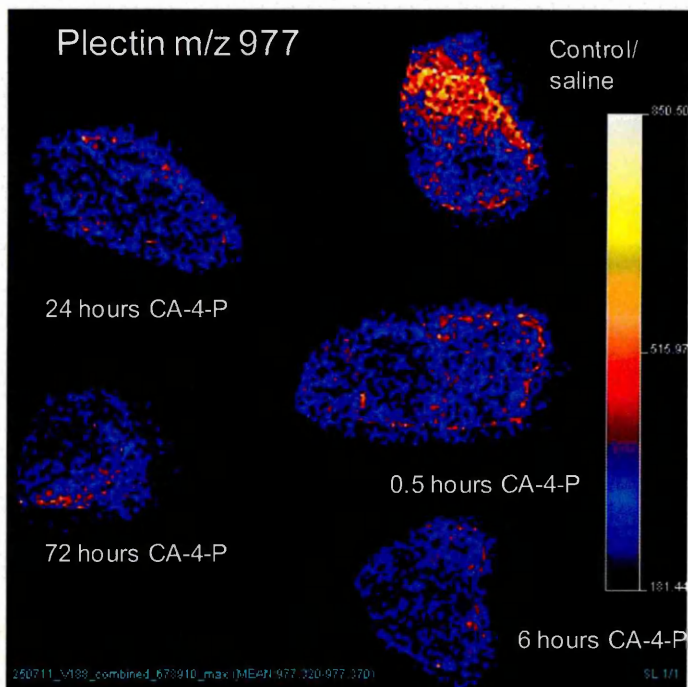


Figure 3. 38: Fibrosarcoma 188 MALDI-MSI multi image showing spatial distribution of Plectin. MALDI images showing spatial distribution of Plectin at m/z 977.

The MALDI-MSI shown here in Figure 3.38 are in good agreement with the LC-ESI-MS/MS label free quantitative results with an apparent abundance of Plectin in the Control with the reduction in levels overtime post CA-4-P.

Immunohistochemical studies using anti-Plectin were performed to visualise this response in histological tumour sections.

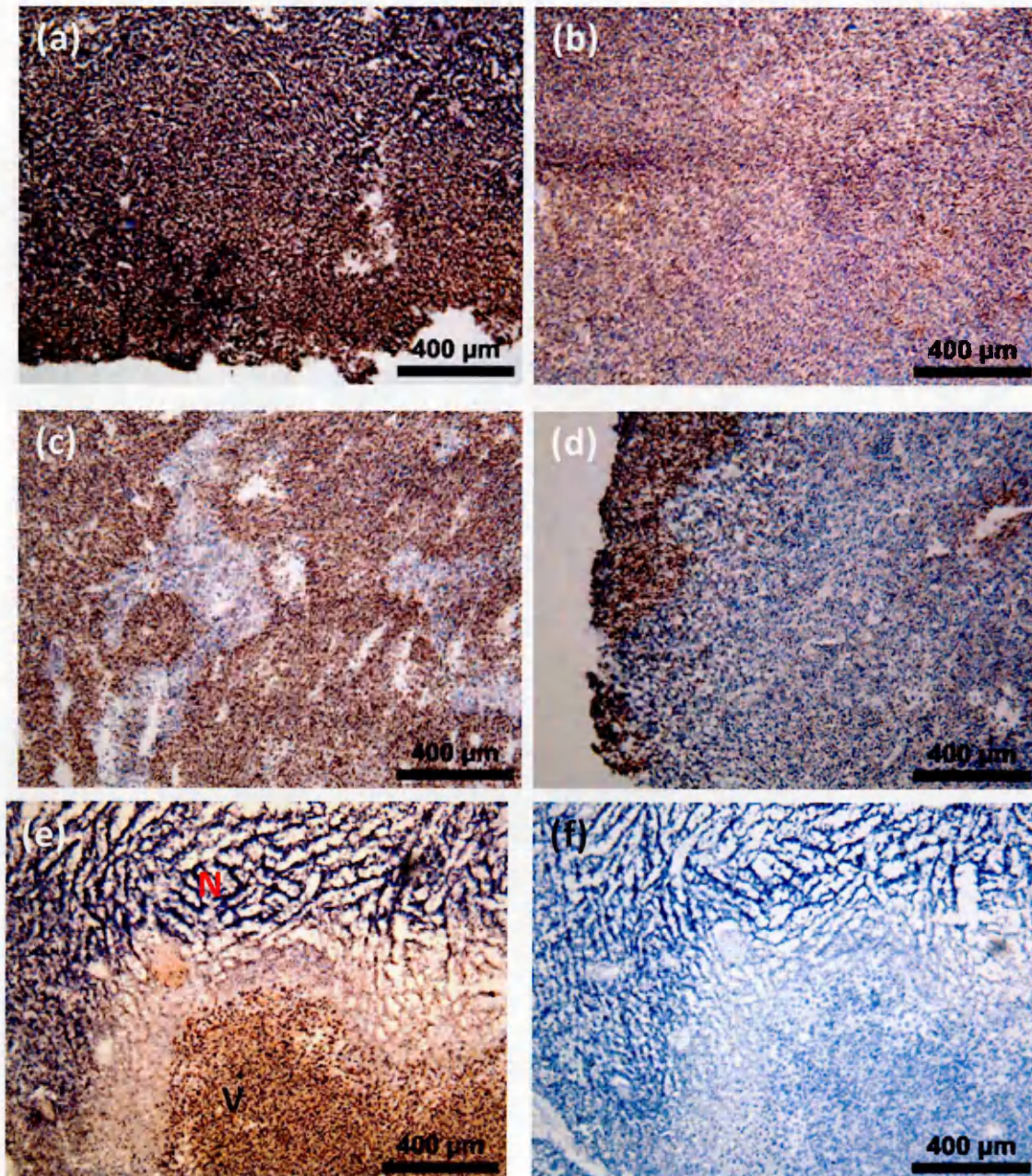


Figure 3.39: Immunohistochemical staining of Plectin in Fibrosarcoma 188 tissue post CA-4-P treatment. Figure 3.39- (a) anti-Plectin staining of fibrosarcoma 188 Control tissue, (b) anti-Plectin staining of fibrosarcoma 188 tissue 0.5h post CA-4-P, (c) anti-Plectin staining of fibrosarcoma 188 tissue 6h post CA-4-P, (d) anti-Plectin staining of fibrosarcoma 188 tissue 24h post CA-4-P, (e) anti-Plectin staining of fibrosarcoma 188 tissue 72h post CA-4-P, the 'V' is indicative of the viable tissue stained here using anti-Plectin and the 'N' relates to the necrotic area which remained unstained and (f) the negative control using fibrosarcoma 188 tissue 72h post CA-4-P.

The anti-Plectin staining in Figure 3.39 (a) suggests that Plectin is highly expressed in the Control tissue which correlates with both MALDI-MSI and LC-ESI-MS/MS data seen earlier (Figure 3.38 and 3.37 respectively). In addition to this, there is also evidence of a reduction in Plectin expression as the time course progresses as seen in Figures 3.39 (b)-(e).

From the anti-Plectin immunohistochemistry it is also apparent that Plectin is distributed in the viable tissue regions.

Plectin is described as a 'cytolinker' and has a key role in the stabilisation of the cytoskeleton via the formation of a mesh-like scaffold (Liu *et al* 2011, Wiche 1998). An article by Katada *et al* (2012) suggested that Plectin could be a 'novel prognostic marker' for head and neck squamous cell carcinoma. The article concluded that Plectin had a strong influence on tumour survival and metastatic processes and further work would elucidate how Plectin mediates cancer migration and invasion. Plectin is amongst the proteins said to be increased in tumour tissue and studies have found elevated levels of in colorectal cancer, prostate cancer and pancreatic ductal adenocarcinoma (Winter and Wiche 2013, Nagel *et al* 1995, Lee *et al* 2004, Katada *et al* 2012).

The response reported here using CA-4-P treated fibrosarcoma 188 tissue suggested that Combretastatin greatly interferes with Plectin expression. In addition to this, the decrease in Plectin expression overtime could be an indication of apoptosis and/or necrosis within the tumour tissue. It is known that initiator caspase 8 translocates to Plectin after apoptotic induction leading to remodelling of actin/ microfilaments (Stegh *et al* 2000).

Remodelling and degradation of proteins occurs via the intrinsic and extrinsic apoptotic pathways (Elmore 2007). Executioner caspases (i.e. caspases 3, 6, 7) supersede initiator caspases (caspases 2, 8, 9, 10) to then play a role in protein degradation.

Gelsolin, a known substrate for executioner caspase 3 will then go on (after itself being cleaved by caspase 3) to cleave Actin to essentially destroy the architectural integrity of the cytoskeleton (Elmore 2007).

Interestingly, from the immunohistochemistry reported here there is strong evidence of an inverse correlation between the HSP-90 and Plectin. This enabled visualisation of regions associated with tumour stress response versus those exhibiting tumour survival, growth and progression. This inverse correlation is displayed in Figure 3.40.

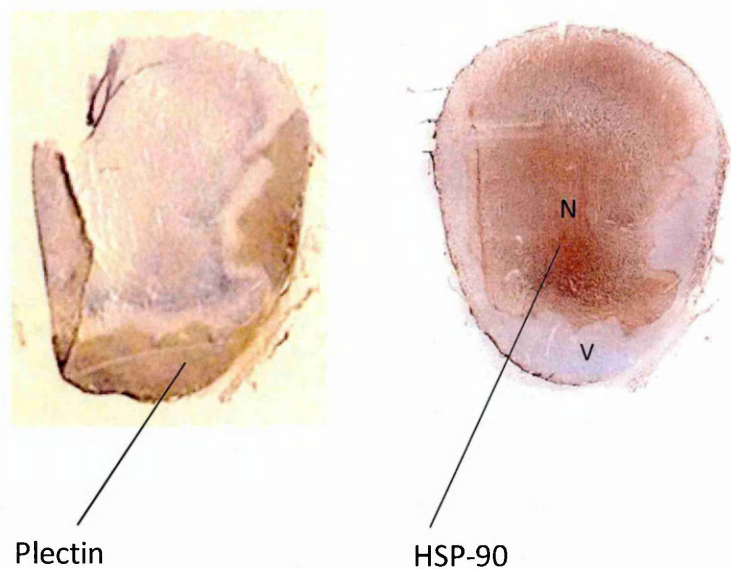


Figure 3. 40: Optical scans of anti-Plectin and HSP-90 Immunohistochemical staining in fibrosarcoma 188 serial sections, 72h post CA-4-P treatment. The necrotic (N) and viable (V) tissue regions are indicated.

A clear inverse correlation is displayed between the viable Plectin stained tissue and the necrotic HSP-90 stained regions in Figure 3.40.

In Chapter 2 a Rho GTPase activating protein 2 was identifiable from the MALDI-MSI-MS/MS of fibrosarcoma 120 tissue, here in the fibrosarcoma 188 samples Ras GTPase-activating-like protein (IQGAP1) has been matched.

IQGAP1 is said to be a multimodal scaffolding protein and is implemented in actin dynamics, tubulin multimerisation, cell motility and migration via numerous signalling pathways (Malarkannan *et al* 2012). There are that studies report that increased expression of IQGAP1 resulted in disruption of cell-cell junctions thus promoting a migratory, invasive phenotype (Mataraza *et al* 2003). In Figure 3.34 IQGAP1 is undetected in the Control but visible from the graph in the 0.5h from which point levels decrease in an 'L' trend through to the 72h treatment, suggesting possible CA-4-P pharmacological action.

An example of an MS/MS spectrum corresponding to IQGAP1 and normalised spectrum time course graph is featured in Figure 3.41.

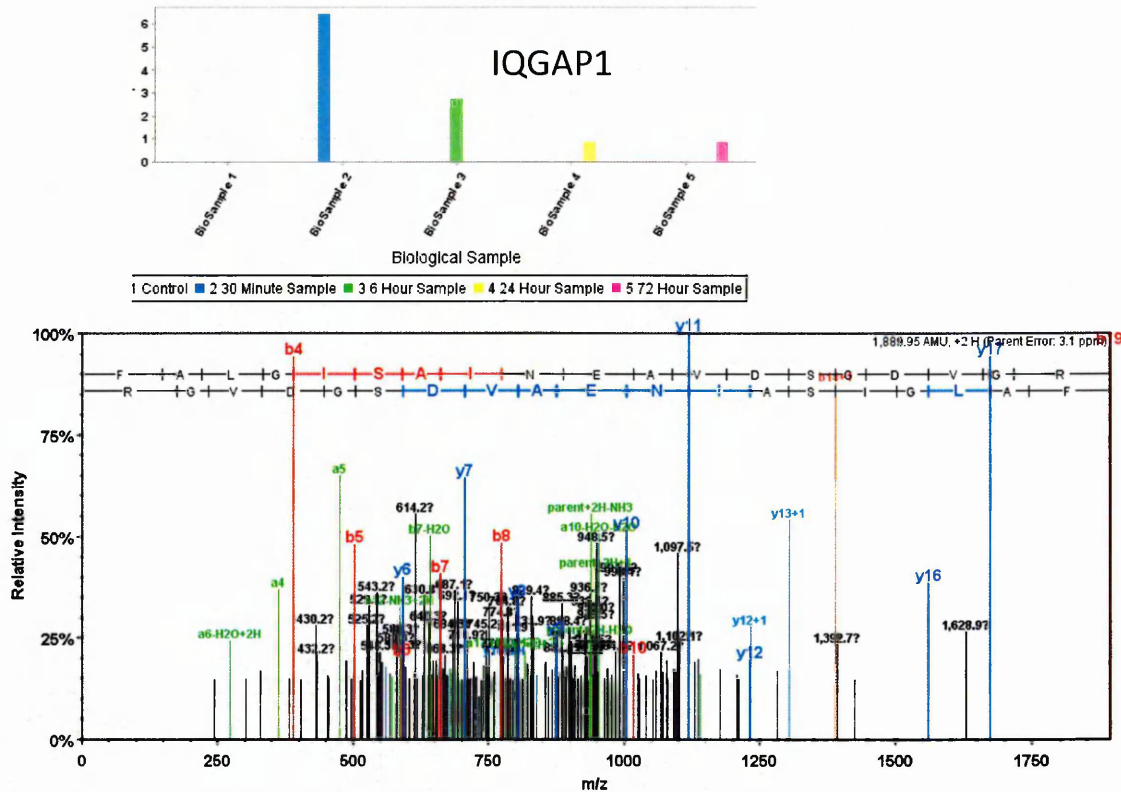


Figure 3. 41: Example MS/MS spectrum and normalised intensity graph of IQGAP1 in fibrosarcoma 188 LC-ESI-MS/MS results. Insert displays the normalised spectral counts for IQGAP1 throughout the time course post CA-4-P.

It can be said that the glycoprotein Tenascin (C), has similar functions to those of IQGAP1 having involvement in tumour survival and the outgrowth of circulating cancer cells (Oskarsson et al 2011).

The levels seen in Figure 3.34 show a marked increase in the 0.5h compared to the Control with decreases evident in the later time points to follow, a similar response to that observed from IQGAP1 .

An example MS/MS spectra with intensity graph is shown in Figure 3.42.

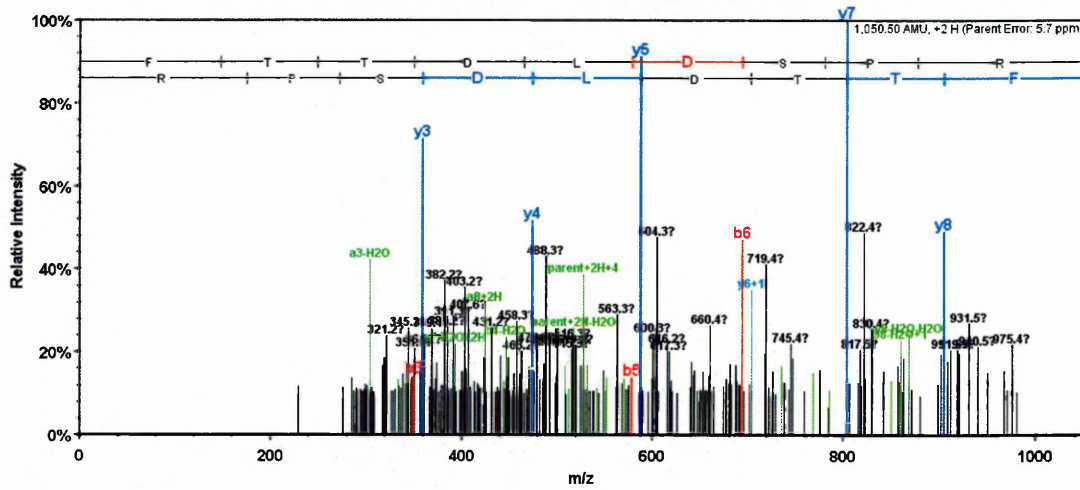
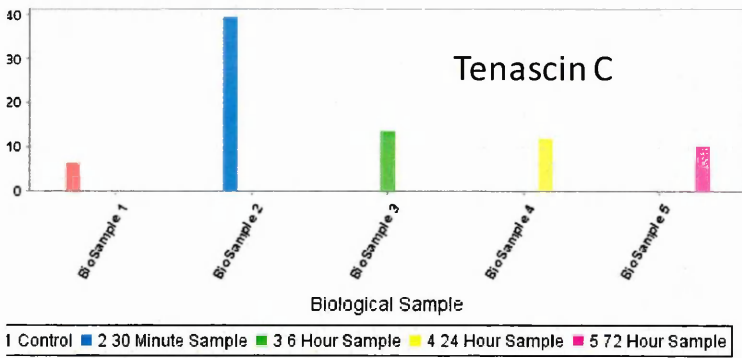


Figure 3. 42: Example MS/MS spectrum and normalised intensity graph of Tenascin C in fibrosarcoma 188 LC-ESI-MS/MS results. Insert displays the normalised spectral counts for Tenascin C throughout the time course post CA-4-P.

The action of CA-4-P does appear to have an inhibitory effect on Tenascin C however there is literature to suggest that its fellow glycoprotein, Tenascin W could prove to be a more suitable marker in solid tumours (Brellier *et al* 2012). This article reports that the expression of Tenascin W is more specific in tumours compared to healthy tissues therefore facilitating the grading/ scoring of diseased tissue. Future studies involving Mass spectrometric techniques could help to ascertain this claim.

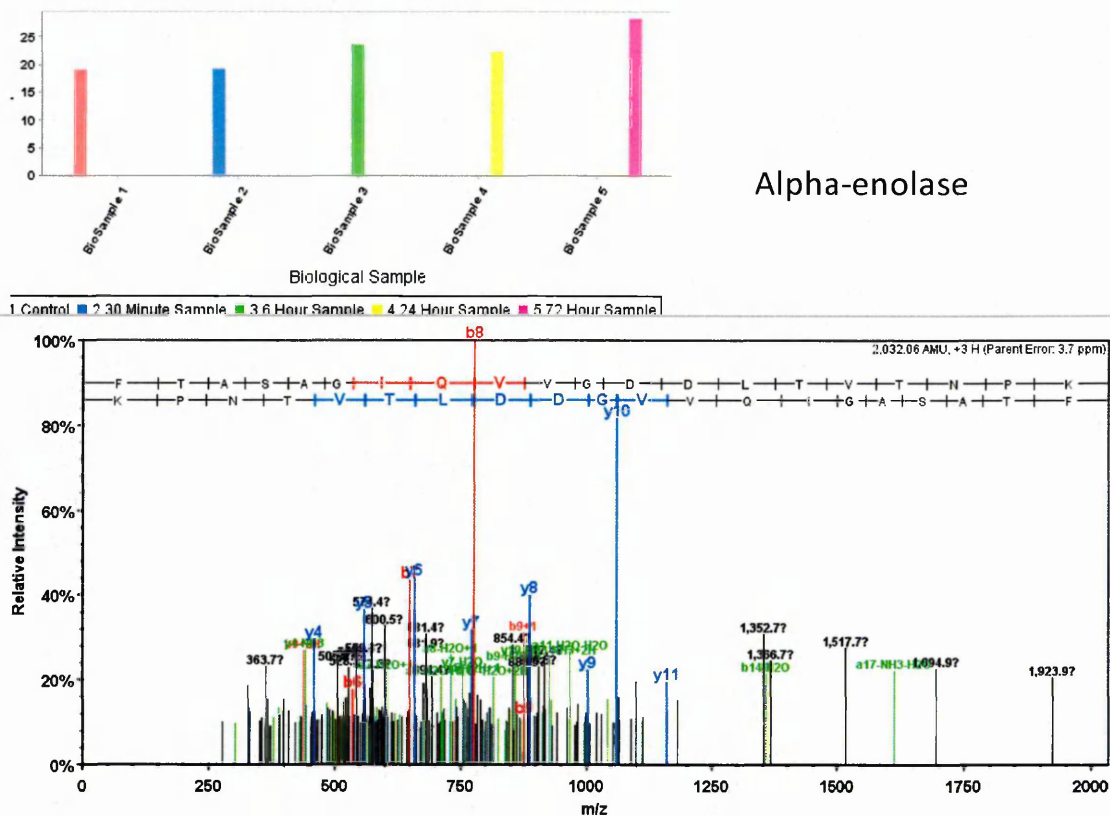


Figure 3.43: Example MS/MS spectrum and normalised intensity graph of Alpha-enolase in fibrosarcoma 188 LC-ESI-MS/MS results. Insert displays the normalised spectral counts for Alpha-enolase throughout the time course post CA-4-P.

Alpha-enolase is thought to be implemented in many processes. In addition to its role as a glycolytic enzyme it is known to have transcriptional capacity and molecular chaperone capabilities (Pancholi 2001, Kang *et al* 2008). The overall reaction to CA-4-P treatment by Alpha-enolase is a steady increase from Control – 72h. Alpha-enolase is regarded as a tumour associated antigen (TAA) and when elevated levels are present in tumour tissue activation of immune responses occur in patients with cancer (Capello *et al* 2011). Increased expression of Alpha-enolase is also indicative of aggressive tumour progression.

The response seen here by Alpha-enolase in Figures 3.34 and 3.43 could be a reflection of this CA-4-P resistant tumour type which is now shown to have regenerative capability.

Transforming growth factor-beta-induced protein ig-h3 (Tgfb1) is featured in the following Figure (3.41).

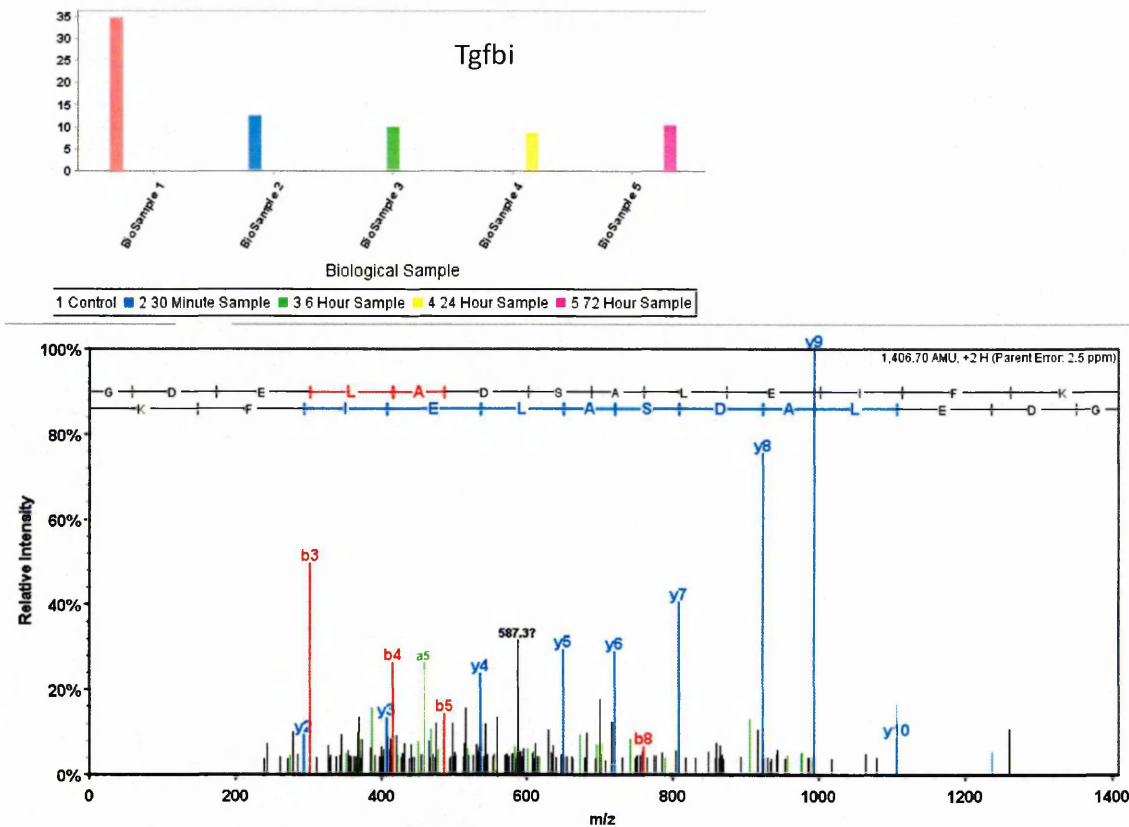


Figure 3.44: Example MS/MS spectrum and normalised intensity graph of Transforming growth factor-beta-induced protein ig-h3 (Tgfb1) in fibrosarcoma 188 LC-ESI-MS/MS results. Insert displays the normalised spectral counts for Tgfb1 throughout the time course post CA-4-P.

From the LC-ESI-MS/MS time course results in Figure 3.34/ 3.44, Tgfb1 is shown to demonstrate a ‘L’ shape trendline similar to that seen from Plectin (Figure 3.34) with high levels in the Control compared to the samples post treatment.

The latter response is a trend similar to the results documented in an article by Li *et al* (2012) entitled ‘*The role of TGFBI in mesothelioma and breast cancer: association with tumor suppression*’. It is stated that Tgfb1 is a known tumour suppressor and expression of TGFBI is reported to be greatly reduced in many tumour cell lines (Kim *et al* 2000, Zhao *et al* 2004, Shao *et al* 2006). However a dual role is suggested for Tgfb1 which proposes an anti-tumourigenic function in early tumour growth and as a pro-oncogenic supporter in late stage tumours.

It is hard to ascertain whether the response seen here is solely by Tgfb1 in this resistant tumour type or as a result of a synergistic effect from Tgfb1-CA-4-P interaction.

3.4.4 Protein relationship mapping of fibrosarcoma 188 LC-ESI-MS/MS data using String 9.0

Visualisation of the complex protein pathways and networks that govern tumour biological function could help the understanding of protein dose response relationships.

The following protein-protein interactions visualised by String 9.0, are depicted by spatial positioning and linear connections with thicker lines representing stronger associations between proteins.

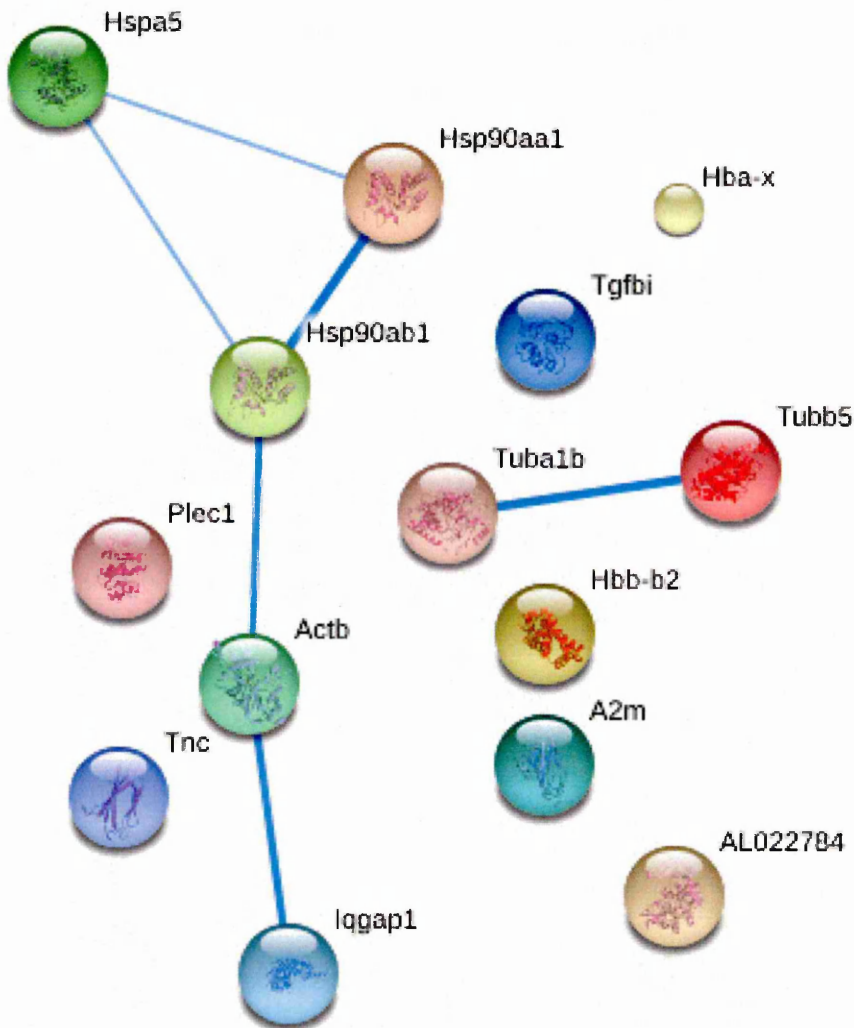


Figure 3. 45: LC-ESI-MS/MS proteins of interest from fibrosarcoma 188, visualised through proteomic pathway software STRING 9.0.

The String 9.0 association network in Figure 3.45 consisted of the proteins chosen in the LC-ESI-MS/MS proteins of interest graph (Figure 3.34).

The focal pathway association seen here (Figure 3.45) within this group of proteins is the linkage between the heat shock proteins; HSP-90 α , HSP-90 β , GRP-78 (Hspa5) and Actin, cytoplasmic 1 and Ras GTPase-activating-like protein (IQGAP1).

The stronger association within this pathway runs directly from HSP-90 α through to IQGAP1 encompassing Actin, cytoplasmic 1. The latter is characteristic of an active tumour micro-environment incorporating the morphological changes exhibited by architectural remodelling of Actin due to CA-4-Administration.

Although not directly linked Plectin and Tenascin display close positioning to IQGAP1 all of which as previously mentioned, are known to be involved with promoting tumour survival, cellular migration and metastatic invasion.

A strong link is visible between fellow tubulin proteins and interestingly ALO22784 (Alpha-enolase) is in close proximity to carrier protein Alpha-2-macroglobulin (A2m). Close positioning of ALO22784 to macrophage related protein A2m is indicative of allergic stress response which remains true to the pharmacological intervention here. Haemoglobin subunit beta positioned above (A2m and ALO22784) supports the haemorrhagic theory.

Tumour suppressing adhesion protein Transforming growth factor-beta-induced protein ig-h3 (Tgfb1), is joined in this structural reorganisational milieu, as mentioned earlier the protein has involvement in cell-collagen interactions.

The full pathway from the LC-ESI-MS/MS results recognised by String 9.0 is featured in Figure 3.46.

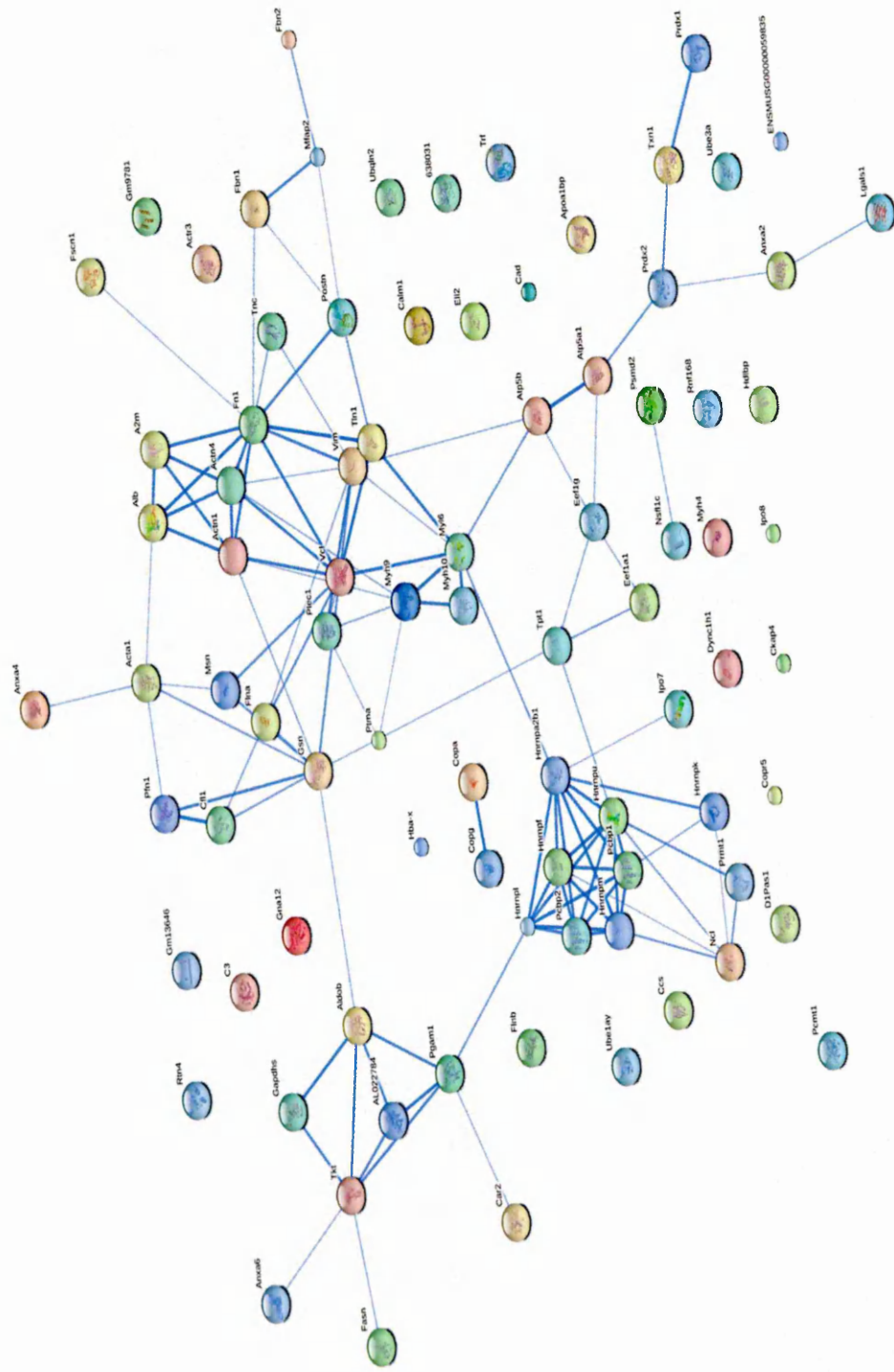


Figure 3. 46: Proteomic network from LC-ESI-MS/MS fibrosarcoma 188 data.

The proteomic network association tool String 9.0 is featured in more detail in Chapter 4 in the iTRAQ proteomic analysis section.

3.4.5 Concluding remarks

The data reported here in this Chapter appears to be suggestive of an active tumour microenvironment possibly relating to this resistant nature of this fibrosarcoma 188 model.

The VIP scores (Figures 3.22-3.25) based on the PLSDA results gave the impression of transcriptionally active tumour tissues. Structural modifications were apparent via the Actin and Hb peaks present teamed with increases in hypoxia related Histone H3. As mentioned earlier, Histone H4 (m/z 1325) is believed to have a chief position in all time points apart from in the 24h samples. Further work would be required to confirm if this is due to CA-4-P interference before the regenerative tumour action commences, seen in the 72h treatment.

Collectively the results from the LC-ESI-MS/MS comprise of proteins connected with necrosis, cell structural reorganisation, polymerisation, tumour survival and stress induced molecular chaperones. The inverse correlation of molecular chaperone HSP-90 and survival promoting Plectin is evidence of this showing the distinct regional differences in the MALDI-MSI, immunohistochemistry and LC-ESI-MS/MS results.

Overall the levels of the proteins involved in heat shock response i.e. GRP-78, HSP-90 β , HSP-70 are increased overtime, but interestingly HSP-90 α displays the reduction in the 72h treatment, possibly highlighted the switch back to tumour viability. Mentioned previously in the introductory chapter regarding the concept of '*repeatedly identified differentially expressed proteins*' (RIDEPs). A few were also seen in the full list of proteins identified which included HSP-70, enolase protein and peroxiredoxin.

Future studies could also consider the potential pharmacological interactions with the tumour suppressor Tgfb1, to clarify whether a dual role is undertaken, dependant on dose response relationships.

Combination anticancer therapy is a known route of choice in the treatment of patients. The future of disease diagnostics could include MALDI imaging as a diagnostic tool in combination with conventional imaging and proteomics. A novel and exciting approach was reported by Balog *et al* (2010) which described how mass spectrometry could be incorporated directly into the surgical theatres to identify tumour tissue boundaries and proximal metastases via Rapid Evaporative Ionization Mass Spectrometry. The latter subsequently substituting the wait for histological confirmation.

Label free LC-ESI-MS/MS shotgun proteomics is a powerful technique with the potential to identify thousands of proteins. Like all methodologies in science it can be said that optimisation is key when performing shotgun proteomics. Further optimisation not only during

sample preparation but throughout data-dependent acquisition mode could prove invaluable to advance proteome analysis and coverage (Kalli and Hess 2012).

References

Advani AS, Gibson SE, Douglas E, Jin T, Zhao X, Kalaycio M, Copelan E, Sobecks R, Sekeres M, Sungren S, Hsi ED (2010) *Histone H4 acetylation by immunohistochemistry and prognosis in newly diagnosed adult acute lymphoblastic leukemia (ALL) patients*. BMC Cancer. **10**. (387) 2-7

Angiero F, Rizzuti T, Crippa R, Stefani M (2007) Fibrosarcoma of the Jaws: Two Cases of Primary Tumors with Intraosseous Growth. Anticancer Research. **27**. 2573-2582

Balog J, Szaniszló T, Schaefer K-C, Denes J, Lopata A, Godorhazy L, Szalay D, Balogh L, Sasi-Szabo L, Toth M, Takats Z (2010) *Identification of Biological Tissues by Rapid Evaporative Ionization Mass Spectrometry* Analytical Chemistry. **82**. 7343–7350

Bingle L, Brown NJ, Lewis CE (2002) The role of tumour associated macrophages in tumour progression: implications for new anticancer therapies. The Journal of Pathology. **196**. (3) 254–265

Brellier F, Martina E, Degen M, Heuzé-Vourc'h N, Petit A, Kryza T, Courty Y, Terracciano L, Ruiz C, Chiquet-Ehrismann C (2012) *Tenascin-W is a better cancer biomarker than tenascin-C for most human solid tumours*. BMC Clinical Pathology. **12**. (14) 1-10

Capello M, Ferri-Borgogno S, Cappello P, Novellia (2011) *F-enolase: a promising therapeutic and diagnostic tumortarget*. FEBS Journal. 1064–1074

Den RB and Lu B (2012) *Heat shock protein 90 inhibition: rationale and clinical potential*. Therapeutic Advances in Medical Oncology. **4**. (4) 211–218

Elmore S (2007) *Apoptosis: A Review of Programmed Cell Death*. Toxicol Pathol. **35**. (4): 495–516.

Encyclopædia Britannica Inc (2013) *"fibrosarcoma."* Encyclopædia Britannica. Encyclopædia Britannica Online Academic Edition.) Available at URL: <http://www.britannica.com/EBchecked/topic/205941/fibrosarcoma>. Last accessed 04/01/13

Ey L, Li J, Gnatovskiy L, Deng Y, Zhu L, Grzesik DA, Qian H, Xue XN, Pollard JW (2006) *Macrophages regulate the angiogenic switch in a mouse model of breast cancer*. Cancer Research. **66** (23) 11238–11246

Feige JJ, Negoescu A, Keramidas M, Souchelnitskiy S, Chambaz EM (1996) *Alpha 2-macroglobulin: a binding protein for transforming growth factor-beta and various cytokines*. Hormone research. **45**. 227-32.

- Grunstein M (1997) *Histone acetylation in chromatin structure and transcription*. NATURE. **389**. 349-352
- Harris S, Craze M, Newton J, Fisher M, Shima DT, Tozer GM, Kanthou C (2012) *Do Anti-Angiogenic VEGF (VEGFxxx) Isoforms Exist? A Cautionary Tale*. PLoS ONE **7**. (5) 1-14
- Hemingway F, Kashima TG, Mahendra G, Dhongre A, Hogendoorn PCW, Mertens F, Athanasou NA (2012) *Smooth muscle actin expression in primary bone tumours*. Virchows Arch. **460**.525–534
- Jameel A, Skilton RA, Campbell TA, Chander SK, Coombes RC, Luqmani YA (1992) *Clinical and biological significance of HSP89 alpha in human breast cancer*. International Journal of Cancer **50** 409–415.
- Jin Kang HJ, Jung S-K, Kim SJ, Chung SJ (2008) *Structure of human α -enolase (hENO1), a multifunctional glycolytic enzyme*. Acta Crystallographica Section D. **D64**. 651–657
- Kanthou C, Tozer GM (2002) *The tumor vascular targeting agent combretastatin A-4-phosphate induces reorganization of the actin cytoskeleton and early membrane blebbing in human endothelial cells*. BLOOD. **99**. (6) 2060-2069
- Kanthou and Tozer (2007) *Selective destruction of the tumour vasculature by targeting the endothelial cytoskeleton*. Drug discovery today: Therapeutic strategies. **4**. (4) 237-243
- Kalli A and Hess S (2012) *Effect of mass spectrometric parameters on peptide and protein identification rates for shotgun proteomic experiments on an LTQ-orbitrap mass analyzer*. Proteomics, **12**.21–31
- Katada K, Tomonaga T, Satoh M, Matsushita K, Tonoike Y, Koderad Y, Hanazawa T, Nomura F, Okamoto Y (2012) *Plectin promotes migration and invasion of cancer cells and is a novel prognostic marker for head and neck squamous cell carcinoma*. Journal of Proteomics. **1803**-1815
- Kenneth NS, Rocha S (2008) *Regulation of gene expression by hypoxia*. Biochemical Journal. **414**. 19–29
- Kim JE, Kim EH, Han EH, Park RW, Park IH, Jun SH, Kim JC, Young MF, Kim IS (2000) *A TGF- β -inducible cell adhesion molecule, β 1g-h3 is downregulated in melorheostosis and involved in osteogenesis*. Journal of Cellular Biochemistry. **77**. 169–178

Kline KG and Wu CC (2009) *MudPIT Analysis: Application to human heart tissue*. *Methods in Molecular Biology*.**528**. 281-293

Li B, Wen G, Zhao Y, Tong J, Hei TK (2012)*The role of TGFBI in mesothelioma and breast cancer: association with tumor suppression*. *BMC Cancer*.**12**. (239) 1-12

Lee KY, Liu YH, Ho CC, Pei RJ, Yeh KT, Cheng CC, Lai YS (2004) An early evaluation of malignant tendency with plectin expression in human colorectal adenoma and adenocarcinoma. *Journal of Medicine*. 35. 141–149

Link, AJ, Eng J, Schieltz DM, Carmack E, Mize GJ, Morris DR, Garvik BM, Yates JR (1999) *Direct analysis of protein complexes using mass spectrometry*. *Nature Biotechnology*.**17**. 676–682

Liu Y-H, Ho C-C, Cheng C-C, Chao W-T, Pei RJ, Hsu Y-H, Lai Y-S(2011) *Cytokeratin 18-mediated disorganization of intermediate filaments is induced by degradation of plectin in human liver cells*. *Biochemical and Biophysical Research Communications*.**407**. 575–580

Maes C, Stockmans I, Moermans K, Van Looveren R, Smets N, Carmeliet P, Bouillon R, Carmeliet G (2004) *Soluble VEGF isoforms are essential for establishing epiphyseal vascularization and regulating chondrocyte development and survival*. *The Journal of Clinical Investigation*.**113**. (2) 188-199

Malarkannan S, Awasth A, Rajasekaran K, KumarP, Schuldt KM, Bartoszek A, Manoharan N, Goldner NK, Umhoefer CMr, Thaka MS (2012)*IQGAP1: A Regulator of Intracellular Spacetime Relativity*.*The Journal of Immunology*.**188**. (5) 2057-2063

Mataraza JM, Briggs MW, Zhigang L, Entwistle A, Ridley AJ, Sacks DB (2003)*IQGAP1 Promotes Cell Motility and Invasion*. *The Journal of Biological Chemistry*.**278**. (42) 41237–41245

McCormack, AL, Schieltz, DM, Goode B, Yang S, Barnes G, Drubin D, Yates JR (1997) *Direct analysis and identification of proteins in mixtures by LC/MS/MS and database searching at the low-femtomole level*. *Analytical Chemistry*.**69**. 767–776

Nagle RB, Hao J, Knox JD, Dalkin BL, Clark V, Cress AE (1995) *Expression of hemidesmosomal and extracellular matrix proteins by normal and malignant human prostate tissue*. *American Journal of Pathology*. **146**. 1498–507

Neckers L (2007)*Heat shock protein 90: The cancer chaperone*. *Journal of Biosciences*.**32**. (3) 517–530

- Old WM, Meyer-Arendt K, Aveline-Wolf L, Pierce KG, Mendoza A, Sevinsky JR, Resing KA, Ahn NG (2005) *Comparison of Label-free Methods for Quantifying Human Proteins by Shotgun Proteomics*. *Molecular and Cellular Proteomics*.**4**. 1487–1502
- Ortho paediatrics group (2012) *A Patient's Guide to Slipped Capital Femoral Epiphysis*. Available at URL: http://www.orthopediatrics.com/docs/Guides/slipped_CFE.html. Last accessed 28/12/12
- Oskarsson T, Acharyya S, Zhang X H-F, Vanharanta S, Tavazoie S, Morris PG, Downey RJ, Manova-Todorova K, Brogi E, Massague J (2011) *Breast cancer cells produce Tenascin C as a metastatic niche component to colonize lungs*. *Nature Medicine*.**17**. (7) 867-874
- Pancholi V (2001) *Multifunctional -enolase: its role in diseases*. *CMLS Cellular and Molecular Life Sciences*.**58**. 902–920
- Saharinen P, Eklund L, Pulkki K, Bono P, Alitalo K (2011) *VEGF and angiopoietin signaling in tumor angiogenesis and metastasis*. *Trends in Molecular Medicine*.**17**. (7) 347-362
- Shao G, Berenguer J, Borczuk AC, Powell CA, Hei TK, Zhao Y (2006) *Epigenetic inactivation of Betaig-h3 gene in human cancer cells*. *Cancer Research*.**66**. 4566–4573
- Stegh AH, Herrmann H, Lampel S, Weisenberger D, Andra K, Seper M, Wiche G, Krammer PH, Peter ME (20000000) *Identification of the Cytolinker Plectin as a Major Early In Vivo Substrate for Caspase 8 during CD95- and Tumor Necrosis Factor Receptor-Mediated Apoptosis*. *Molecular and Cellular Biology*. **20**. (15). 5665-5679
- Toh Y, Ohga T, Endo K, Adachi E, Kusumoto H, Haraguchi M, Okamura T, Nicolson GL (2007) *Expression of the metastasis-associated MTA1 protein and its relationship to deacetylation of the histone H4 in esophageal squamous cell carcinomas*. *International Journal of Cancer*.**110**. 362-367
- Tozer GM, Kanthou C, Lewis G, Prise VE, Vojnovic B, Hill A (2008) *Tumour vascular disrupting agents: combating treatment resistance*. *The British Journal of Radiology*.**81**. S12-S20
- Welford AF, Biziato D, Coffelt SB, Nucera S, Fisher M, Pucci F, Di Serio C, Naldini L, De Palma M Tozer GM, Lewis CE (2011) *TIE2-expressing macrophages limit the therapeutic efficacy of the vascular-disrupting agent combretastatin a4 phosphate in mice*. *The Journal of Clinical Investigation*.**121**.(5) 1-5

Wellcome trust Sanger Institute (2012) Available at URL:
<http://pfam.sanger.ac.uk/family/PF01835>. Last accessed 22/01/13.

Wiche G (1998) *Role of plectin in cytoskeleton organization and dynamics*. Journal of Cell Science. **111**. 2477–2486.

Winter L and Wiche G (2013) *The many faces of plectin and plectinopathies: pathology and mechanisms*. Acta Neuropathologica. **125**. 77–93

Wolters DA, Washburn MP, Yates J R (2001) *An automated multidimensional protein identification technology for shotgun proteomics*. Analytical Chemistry. **73**. 5683–5690

Zhou X, Sun H, Chen H, Zavadil J, Kluz T, Arita A, Costa M (2010) *Hypoxia Induces Trimethylated H3 Lysine 4 by Inhibition of JARID1A Demethylase*. Cancer Research. **70**. (10) 4214-4786

Zhao Y, Shao G, Piao CQ, Berenguer J, Hei TK (2004) *Down-regulation of Betaig-h3 gene is involved in the tumorigenesis in human bronchial epithelial cells induced by heavy-ion radiation*. Radiation Research. **162** 655–659

Chapter 4

LC-MALDI-MS/MS using iTRAQ
labelling to investigate protein
induction in CA-4-P treated
fibrosarcoma 120 and 188 mouse
models

4.1 Introduction

It is known that potential disease biomarkers are of relative low abundance thus making data validation a challenge (Ye *et al* 2010). The 'matrix suppression effect' is considered to exacerbate analysis of low abundant species (Knochenmuss and Zenobi 2003). An article by Knochenmuss and Zenobi (2003) states that in MALDI, matrix ions can be suppressed if sufficient analyte is present. In *on tissue* tryptic digestion, this is seldom the scenario for ions of interest. Suppression from high abundant Hb/ histones within MALDI-MS spectra is another example of ion suppression. Such ion suppression by high abundant Hb and histone species was evident in Figure 2.1 in Chapter 2.

iTRAQ labelling coupled with LC-MALDI is a technique which aims to provide relative absolute quantitation of fractionated samples to give protein response information using the reporter ions generated (Chen *et al* 2012). Up to 8 samples can be combined for analysis and the method is described as a robust labelling technique implemented by N-hydroxysuccinimide (NHS) ester chemistry (Evans *et al* 2012, Noirel *et al* 2011). Sensitivity is improved as the mass spectra displays summed peptide ion signals from the isobaric labelled sample combination. The principles of iTRAQ multiplex chemistry are shown in Figure 4.1 (Ross *et al* 2004).

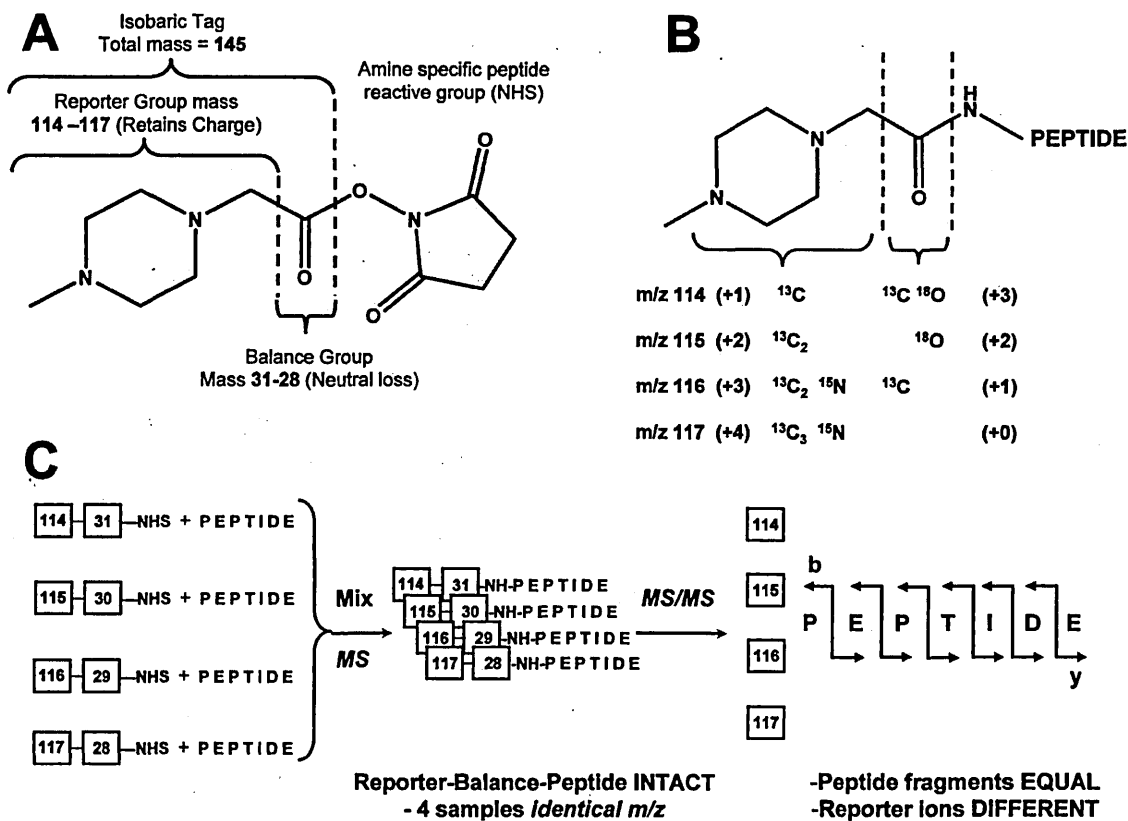


Figure 4. 1: The principles of multiplex tagging chemistry. (Ross *et al* 2004). A, illustrates the 3 main components of the isobaric tag molecule, reporter, balancer and reactive group. B, shows the formation of an amide linkage created with a peptide amine, CID induces fragmentation here similarly to that of the peptide backbone. C, depicts the individually labelled peptides which when combined cannot be resolved by MS intact analysis, upon CID

the reporter ions emerge as separate masses retaining the b-/y- ion information. The intensity of the corresponding reporter ions determines the concentration of the peptides.

The technique of iTRAQ is a recognised method widely used throughout Oncology (Sutton *et al* 2010). Ruppen *et al* (2010) studying KiSS-1 (a metastasis suppressor gene) in bladder cancer reported the use of iTRAQ to help predict the involvement of proteins in biological disease. iTRAQ analysis was performed on protein extracts from transfected (vector containing KiSS-1 gene) bladder cancer cells (EJ138). iTRAQ comparisons were done of the transfected, mock, and empty vector-exposed cells. A recent paper by McMahon *et al* (2012) employed iTRAQ to study global changes in protein expression in a regional analysis experiment using multicell tumour spheroids. The article also used immunohistochemistry, Western blotting and enzyme assays to complement the iTRAQ findings. The aim of the work reported in this Chapter was to support/validate the results found using MALDI-MSI, LC-ESI-MS/MS and immunohistochemistry described in Chapter 3.

4.2 Materials and Samples

4.2.1 Chemicals and Materials

a-Cyano-4-hydroxycinnamic acid (CHCA), aniline (ANI), ethanol (EtOH), chloroform (CHCl₃), methanol (MeOH), acetonitrile (ACN), hydrochloric acid (HCl), tri-fluoroacetic acid (TFA), ammonium bicarbonate, BCA protein assay reagent (bicinchoninic acid), copper (II) sulfate pentahydrate 4% solution, protein standard solution, 1.0 mg/mL bovine serum albumin (BSA), DL-Dithiothreitol solution, Iodoacetamide, urea, potassium di-hydrogen phosphate (KH₂PO₄), TRIzol were from Sigma–Aldrich (Dorset, UK). Modified sequence grade trypsin (20 μg/lyophilised) was obtained from Promega (Southampton, UK). Modified sequence grade trypsin (1 mg/lyophilised) was obtained from Roche (Roche Products Limited Pharmaceuticals, UK). iTRAQ reagents (AB Sciex, Warrington, UK). Isolute C18 RP LC column (Kinesis Ltd., St. Neots, UK). RapiGest SF Surfactant was from Waters (UK). Peptide Calibration Standard II (Bruker Daltonics, Bremen, Germany).

4.2.2 Tissue samples

Mice were injected sub-cutaneously in the flank with a 50 μl tumour cell suspension containing 1 x 10⁶ cells in serum-free medium. The cells employed in this study were from the mouse

fibrosarcoma cell lines, VEGF120 and VEGF188. These have been engineered to express either the VEGF120 or VEGF188 isoforms only. Tumours were allowed to grow to approximately 500 mm³, before CA-4-P treatment (a single dose of 100 mg/kg i.p). The dosage for CA-4-P are consistent with animal studies performed at clinically relevant doses (Galbraith 2003., Prise 2002). Mice were killed and tumours excised at various times after treatment. All animal work carried out documented herein was performed by Dr. J. E. Bluff, Tumour Microcirculation Group, University of Sheffield, UK. Samples were provided as frozen excised tumours and stored at -80°C.

4.2.3. Experimental groups

Fibrosarcoma 120 tumour samples: Controls (no treatment, saline i.p), n = 6 (labelled tumour1_1 – tumour 1_6), C-A4-P (0 h after treatment), n = 6, (labelled tumour2_1 – tumour 2_6), C-A4-P (0.5 h after treatment), n = 6, (labelled tumour 3_1 – tumour 3_6), C-A4-P (6 h after treatment), n = 6, (labelled tumour 4_1 – tumour 4_6), C-A4-P (24 h after treatment) n = 6, (labelled tumour 5_1 – tumour 5_6).

Fibrosarcoma 188 tumour samples: Controls (no treatment, saline i.p), n = 4 (labelled tumour 6_1 – tumour 6_4), C-A4-P (0.5 h after treatment), n = 5, (labelled tumour 7_1 – tumour 7_5), C-A4-P (6 h after treatment), n = 5, (labelled tumour 8_1 – tumour 8_5), C-A4-P (24 h after treatment), n = 5, (labelled tumour 9_1 – tumour 9_5), C-A4-P (72 h after treatment) n = 4, (labelled tumour 10_1 – tumour 10_4).

4.2.4 Tissue preparation

The following preparation was performed on sections from fibrosarcoma 120 and 188 tissue with one example used from each tumour treatment time point. Frozen tissue sections were cut to give approximately 10 x 10 µm sections per sample for digestion, using a Leica CM3050 cryostat (Leica Microsystems, Milton Keynes, UK) (Djidja *et al* 2009). Sample sections were stored in airtight tubes at -80°C until further use.

4.2.5 Tissue homogenisation and precipitation of protein

The tissue as described in 4.2.4 was homogenised in 800 µl of TRIzol solution using a micro-homogeniser (Kline and Wu 2009). Homogenised solution was centrifuged (1,500 rpm) for 5 min to pellet out nuclei/ unbroken cells. Post-nuclear supernatant was then centrifuged (14,000 rpm) for 30 min. Resulting supernatant was discarded and cellular membrane pellet was retained for protein precipitation. 200 µl of MeOH and 50 µl of CHCl₃ were then added to each protein pellet sample. After vortexing, 150 µl HPLC H₂O was added with further vortexing.

After centrifugation (14,000 rpm) for 2 min, the bottom CHCl_3 layer was removed. A further 50 μl CHCl_3 was added, removal of the bottom CHCl_3 layer was repeated following centrifugation (14,000 rpm) for 2 min. Subsequent removal of the H_2O layer resulted in the remaining protein precipitate layer. CHCl_3 (50 μl) and MeOH (150 μl) were added directly to the protein precipitate, after vortexing solution was centrifuged (14,000 rpm) for 2 min. Supernatant was removed and protein pellet was then allowed to air dry for 2 min.

4.2.6 Protein Digestion

100 μl of 0.1% *RapiGest* in 50mM NH_4HCO_3 buffer (pH 7.8) was added to the air dried protein pellet. Each sample pellet/ solution was consecutively vortexed, incubated at -80°C ($\sim 1\text{hr}$) and heated to 70°C (1 min) until solubilised. Once fully solubilised the sample was heated to 100°C (2 min) and then left to reach room temperature. Each sample was reduced with DTT (final concentration 5mM) for 30 min at 60°C the left to reach room temperature. Solutions were then alkylated with iodoacetamide (final concentration 15mM) in the dark for 30 min at room temperature. The fibrosarcoma 120 samples were then lyophilised and re-suspended in 5 μl of 8M urea in 400mM NH_4HCO_3 buffer prior to tryptic digestion. Sequence grade modified trypsin was added (20 $\mu\text{g}/\text{ml}$ or 1mg/ml) to 80 μg (fibrosarcoma 188) / 100 μg of protein (fibrosarcoma 120), a BCA Protein Assay Reagent (bicinchoninic acid) was used for protein determination. In-solution digests were incubated over night at 37°C with shaking.

4.2.7 Preparation of samples for column loading

Fibrosarcoma 120; after overnight digestion the solution was centrifuged (1,500 rpm) for 1 min and reaction stopped by placing samples on ice where 10 μl of 10% TFA was added. Each sample for analysis was de-salted using C18 Bond-elute columns and subsequently lyophilised until required.

Fibrosarcoma 188; HCL (final concentration 100mM) was added to the overnight digest, solution was then incubated for a further 45 min at 37°C . After this step the sample was then centrifuged (14,000 rpm, 4°C) for 10 min, the supernatant removed for analysis. This remaining solution was lyophilised and stored at -80°C until further use.

4.2.8 C18 bond-elute preparation

The C18 columns were wetted with 1ml MeOH, equilibrated with (x2) 1ml solvent A (2% ACN, 0.05% TFA), after the addition of the sample two wash steps were performed with (x2) 1ml solvent A (2% ACN, 0.05% TFA) and peptides were collected in a fresh tube after 1ml solvent B (80% ACN, 0.05% TFA).

4.2.9 Sample re-suspension

Each lyophilised sample was re-suspended in 10µl of TEAB, 0.1% SDS, vortexed and centrifuged (14,500 rpm) for 1 min at room temperature.

4.2.10 iTRAQ labelling

The iTRAQ reagents (AB Sciex, Warrington, UK) were removed from -20°C storage and allowed to equilibrate to room temperature. After brief centrifugation (bench top), 40µl of isopropanol was added to each iTRAQ vial, vortexing and brief centrifugation followed. Transfer of each individual iTRAQ vial to each corresponding sample tube was as follows:

8-plex Fibrosarcoma 120; (a)Control - sample 1 – iTRAQ 113, (b)Control- sample 2 – iTRAQ 114, (c)0h post CA-4-P - sample 3 – iTRAQ 115, (d)0.5h post CA-4-P - sample 4 – iTRAQ 116, (e) 0.5h post CA-4-P - sample 5 – iTRAQ 117, (f)6h post CA-4-P - sample 6 – iTRAQ 118, (g)6h post CA-4-P - sample 7 – iTRAQ 119, (h)24h post CA-4-P - sample 8 – iTRAQ 121.

All iTRAQ ratios were calculated relative to the control labelled 113.

(a)Control - sample 1 – iTRAQ 113, (c)0h post CA-4-P - sample 3 – iTRAQ 115, (d)0.5h post CA-4-P - sample 4 – iTRAQ 116,(f)6h post CA-4-P - sample 6 – iTRAQ 118,(h)24h post CA-4-P - sample 8 – iTRAQ 121 combinations are shown here for comparison to fibrosarcoma 188.

5-plex Fibrosarcoma 188;(a)Control - sample 1 – iTRAQ 113, (b)0.5h post CA-4-P - sample 2 – iTRAQ 114, (c)6h post CA-4-P - sample 3 – iTRAQ 115, (d) sample 4 – iTRAQ 116, (e)24h post CA-4-P - sample 5 – iTRAQ 117.

All iTRAQ ratios were calculated relative to the control labelled 113.

To ensure maximum iTRAQ reagent transfer a further 10µl of isopropanol was added to each iTRAQ reagent tube to then vortex and centrifuge. The contents were transferred to the corresponding iTRAQ/ sample contents. Each sample with iTRAQ reagent was then thoroughly vortexed and centrifuged (1 min) (NB – no turbidity observed). The pH was tested for each sample and adjusted to pH 7.0 – 10.0 with 1M TEAB (maintain organic concentration of 60%). 50µl of HPLC H₂O was added to each reaction, vortex followed by bench top centrifugation. The corresponding samples were all combined into 1 reaction tube. A further 25µl of HPLC H₂O was added to the combined reaction tube before lyophilisation (50°C aqueous and then stored overnight at 4°C).

4.2.11 SCX

The SCX column was washed/wetted using 1ml HPLC grade H₂O (assisted by a syringe) followed by 1ml (x2) of loading buffer. The combined sample was re-suspended in 1ml loading buffer (25% ACN: 75% HPLC H₂O) and pH checked to adjust to approximately pH 2.5-3 with 10% TFA. The sample was added to the SCX column by passive hydrostatic pressure and the flow through collected (FT1). A further 1ml of was added directly to the SCX column and flow through collected (FT2). For the elution of peptides varying concentrations of 500µl 60mM – 1000mM KCL were added to the column resulting in fractions E1 – E6. Fractions were de-salted with C18 Isolute columns. Prior to de-salting 1.5ml HPLC solvent A was added (2% ACN, 0.05% TFA) to the fractions. After de-salting the samples were lyophilised and stored at -20°C until further use. As required, each eluate was re-suspended in 13µl of 10% ACN.

4.3 Methods and instrumentation

4.3.1 Sample fractionation and matrix deposition

The Bruker PROTEINEER fc LC-MALDI Fraction Collector (Bruker Daltonics, GmbH Bremen, Germany) was used to deposit the LC separated peptide fractions in a combination of CHCA matrix and peptide solution. Fractions were automatically spotted onto MALDI AnchorChip targets. The matrix, α -cyano-4-hydroxycinnamic acid (CHCA) was used, in EtOH: Acetone (2:1), 100mM ammonium phosphate, 10% TFA.

4.3.2 Instrumentation

Liquid chromatography was performed with LC Packings/Dionex Ultimate 3000 capillary HPLC system (Dionex, Camberley, Surrey, UK). Samples were injected onto a C18, 300µm x 5mm, 5µm diameter, 100Å PepMap pre-column (LC Packings, Sunnyvale, CA) on an LC Packings UltiMate 3000 (McMahon *et al* 2012, Montgomery *et al* 2012). The sample was washed with mobile phase A for 3.5 minutes at a flow rate of 300 nl/min on the pre-column before being switched onto a C18, 75µm x 15cm, 3µm diameter, 100Å PepMap column (LC Packings) equilibrated with mobile phase A at a flow rate of 300 nl/min. Mobile phase B (80% acetonitrile, 0.05% TFA) was increased to 10% and then increased with a linear gradient to either 30% - 40% over 105 minutes. The fractions after HPLC were coeluted with 1.2 µL of saturated α -cyano-4-hydroxy cinnamic acid (CHCA) matrix solution. Peptide Calibration Standard II (Bruker Daltonics, Bremen, Germany) was as listed; Angiotensin I, Angiotensin II, Substrate P, Bombesin, ACTH clip 1-17, ACTH clip 18-39, Somatostatin 28, Bradykinin fragment 1-7 and Renin Substrate Tetradecapeptide porcine. The calibrant covered a mass of

range 700–3200 Da. Peptide mass fingerprints and MALDI-MS/MS were acquired by using a MALDITOF/ TOF UltraFlex II instrument (Bruker Daltonics, Bremen, Germany) with a 200 Hz smartbeam laser (>250 $\mu\text{J}/\text{pulse}$) in reflectron positive ion mode. WarpLC software (v1.2) was used in automated mode which comprised of data acquisition (FlexControl version 3.0) and peak detection (FlexAnalysis version 3.0, using the Snap peak detection algorithm), initially in MS mode screening LC fractions between 700 and 3000 Da to generate a list of peptides. External calibration was carried out for each during MS analysis. For Each peptide MS/MS analysis was performed using LIFT mode (FlexControl 3.0). Mass lists (FlexAnalysis 3.0, using TopHat baseline subtraction, Savitzky- Golay smoothing and Snap peak detection algorithms) from each MS/MS spectrum were compiled into a batch file for exportation to perform protein database searching.

4.3.3 Data pre-processing

Mascot software version 2.2 (Matrix Science, U.K.) was used for protein identification searching, comparisons of the MS fragmentation data were made against the Swiss-Prot 2010 Mus (Musculus) protein database. The Mascot search parameters included used Mudpit scoring with the following post translational modification parameters for both tumour types;

Fixed modifications : Carbamidomethyl (C) **(fixed)**

Fixed modifications : Carbamidomethyl (C) with a filter of protein score ≥ 28 **(fixed filtered)**

Variable modifications : Carbamidomethyl (C), Acetyl (Protein N-term),Gln->pyro-Glu (N-term Q),Glu->pyro-Glu (N-term E),Oxidation (M) **(variable - fixed)**

Variable modifications : Carbamidomethyl (C), Acetyl (Protein N-term),Gln->pyro-Glu (N-term Q),Glu->pyro-Glu (N-term E),Oxidation (M) with a filter of protein score ≥ 28 **(variable filtered - fixed)**

The confidence threshold selected was 95% ($p < 0.05$) for MS/MS data mining. Proteinscape software v2.1 (Bruker Daltonics, Bremen, Germany) was used to collate the total 7 LC–MALDI runs in each case (fibrosarcoma 120 / fibrosarcoma 188) into a single nonredundant protein list (comprising at least one unique peptide and in the filtered search cases with a Mascot score of ≥ 28) (McMahon *et al* 2012,. Montgomery *et al* 2012). The protein lists generated by ProteinScape was manually filtered to flag proteins iTRAQ labelled/ un-labelled, peptides that were not ranked first were discarded.

4.3.4 Statistical analysis

Excel spreadsheets were generated via exportation of data lists generated by ProteinScape for both fibrosarcoma 120 and fibrosarcoma 188 tumours analysed. The ratios were all quantified relative to the control at time zero and normalised to the average of 1. Thus allowing the study of quantitative information from the iTRAQ reporter ions throughout the time course of samples, post CA-4-P administration. Scaffold 3Q+ was used for additional visualisation and analysis of the iTRAQ data (<http://www.proteomesoftware.com/>). The data files (.dat) produced from ProteinScape which corresponded to each fraction analysed, were uploaded individually selecting 'iTRAQ 8-plex' and 'MudPit Experiment (combine samples)'. The .dat files selected were using a fixed modification search. Analysis with X! Tandem was selected in order to improve protein identifications with searching through an additional database.

4.3.5 Protein network analysis

Accession lists generated by ProteinScape were imported into the STRING 9.0 database to observe the relationships between the proteins identified and study the predicted functional partners of known protein interactions (<http://string-db.org/>).

4.4 Results and discussion - Fibrosarcoma 120

4.4.1. HPLC UV profiles of fibrosarcoma 120 tumour fractions

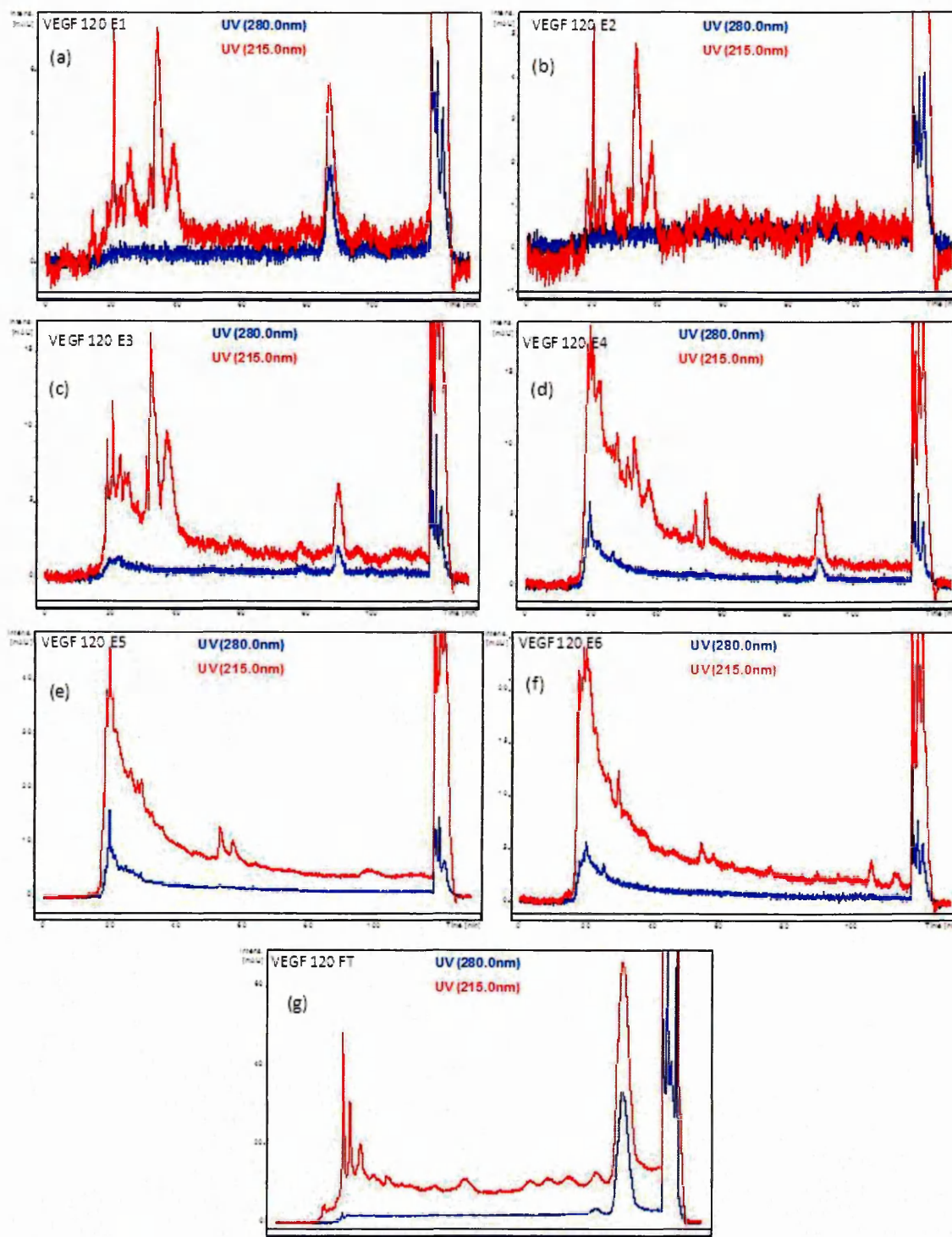


Figure 4.2: UV profiles from the fibrosarcoma 120 fractions after SCX. (a) shows the UV profile from the first eluant (E1) after 60mM KCl following the flow through (FT) fraction from strong cation exchange, (b) 120mM KCl (E2), (c) 180mM KCl (E3), (d) 300mM KCl (E4), (e) 500mM KCl (E5), (f) 1000mM KCl (E6) and (g) (FT) after addition of the combined iTRAQ labelled sample. The FT UV profile (Figure 4.2 (g)) does not show many peptide peaks which could be a sign of good binding of the sample to the CSX column. It appears from the UV profiles that the most of the peptides are present in fractions E3-E6. For these HPLC runs the gradient was reduced to 30% to maximise peptide elution from the column.

4.4.2 Frequency of unique peptides identified

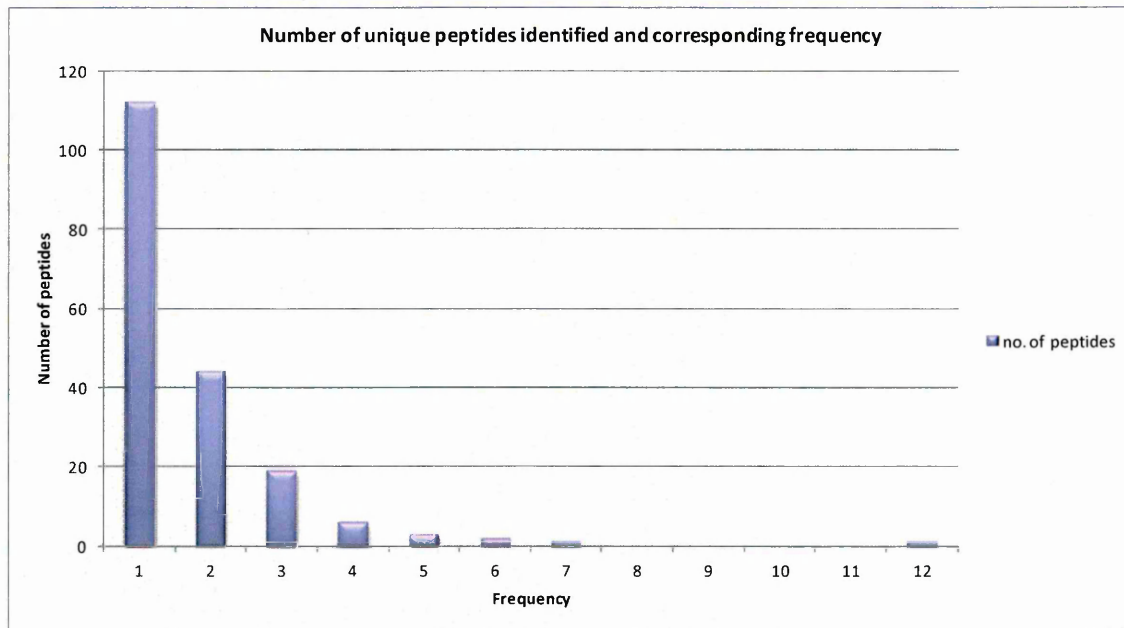


Figure 4. 3: Frequency of detection of unique peptides by LC-MALDI-MS/MS. The graph shows the range of unique peptides detected, for example 112 unique peptides were only seen once with only 1 peptide having 12 unique peptides assigned to it.

4.4.3. Analysis using excel

Spreadsheets were prepared which featured exported lists generated from ProteinScape. Figure 4.4 displays a screen shot of an excel spreadsheet used for protein analysis and ratio comparison. This relevance of this data output was to observe the full protein list supplied by MASCOT (using the 'mus' search database) prior to importing into Scaffold proteomic tool software using a simple colour coded thresholds shown in Figure 4.4. The thresholds were determined for each column by using the standard deviation (SD) value. To depict down regulation values lower than the SD were coloured red, up regulation was determined by values of $1 + SD$ and values that fell between the thresholds were coloured yellow.

A	B	C	D	E	F	G	H	I	J	K	L	M	N	O	P	Q	R	S	T
1	Row	User Flag	OK	Accession	Protein	MW [kDa]	pI	#Alt. Prote Scores	#Peptides	SC [%]	RMS90 [pt Rank]	Median [11 Normaliser#(115/113)]	CV [%]	Normaliser#(116/113)	Normaliser#(116/113)	CV [%]	Median [11 Normaliser#(115/113)]	Normaliser#(116/113)	Normaliser#(116/113)
7	16	Green	true	ALDOA_MOUSE	Fructose	39.3	9.2	1	72.2	2	18.64	16	0.72	0.846029	2	2.68	1.63	1.835016	2
8	24	Green	true	LEG1_MOUSE	Galectin-	14.9	5.2	1	53.6	2	11.9	24	0.6	0.705024	2	41.02	0.59	0.645232	2
9	25	Green	true	G3P_MOUSE	Glycerak	35.8	9.2	1	53.2	1	11.15	25	0.87	1.022285	1	30.72	1.52	1.71116	1
10	7	Green	true	HSP7C_MOUSE	Heat sho	70.8	5.2	5	237.9	10	16.96	10	0.74	0.86953	10	30.72	0.7	0.788043	10
11	13	Green	true	HS90B_MOUSE	Heat sho	83.2	4.8	3	107.2	5	8.3	13	0.71	0.834279	5	87.8	1	1.125776	5
12	8	Green	true	HBA_MOUSE	Hemoglo	15.1	9.1	2	202.6	5	28.2	8	0.72	0.846029	5	53.26	0.76	0.95559	5
13	4	Green	true	HBB1_MOUSE	Hemoglo	15.8	8	1	273.3	5	15.08	4	0.94	1.104538	5	20.21	0.97	1.092003	5
14	5	Green	true	HBB2_MOUSE	Hemoglo	15.9	9	1	262.9	6	15.72	5	0.79	0.928282	6	21.99	0.91	1.024457	6
15	27	Green	true	H12_MOUSE	Hemoglo	21.3	11.5	4	37.1	1	5.2	27	1.36	1.598055	1	23.61	0.75	0.844332	1
16	15	Green	true	H2AV_MOUSE	Histone H	13.5	11	12	78.8	2	12.5	15	0.76	0.893031	2	50.25	0.54	0.679319	2
17	28	Green	true	H2B1C_MOUSE	Histone H	13.9	10.8	8	36.4	1	7.1	15	0.85	0.998784	1	50.25	0.8	0.900621	1
18	14	Green	true	H4_MOUSE	Histone H	11.4	11.8	1	96.5	2	21.4	14	0.77	0.904781	2	60.89	0.67	0.75427	2
19	12	Green	true	K2C1_MOUSE	Keratin, t	65.6	9.2	5	123.6	2	3.6	12	3.82	4.488655	2	60.89	2.6	2.927019	2
20	20	Green	true	K22O_MOUSE	Keratin, t	62.8	9.5	1	61.3	2	2.7	20	1.12	1.316045	2	98.6	1.5	1.698695	2
21	17	Green	true	LDHA_MOUSE	L-lactate	36.5	8.8	1	71.6	3	8.1	17	0.62	0.728525	3	6.71	0.84	0.945652	3
22	18	Green	true	PRDX1_MOUSE	Peroxirec	22.2	9.2	1	71.2	2	4	18	0.85	0.998784	2	18.16	0.82	0.923137	2
23	25	Green	true	PDI3_MOUSE	Protein d	56.6	5.8	1	42.3	2	4	18	0.78	0.918532	2	27.33	0.85	0.95691	2
24	23	Green	true	S10A6_MOUSE	Protein S	10	5.2	1	56.2	2	16.9	24	0.5	0.59752	2	34.96	0.66	0.743012	2
25	10	Green	true	KPYM_MOUSE	Pyruvate	57.8	7.9	2	148.2	5	8.5	10	0.95	1.18288	5	12.95	0.88	0.990683	5
26	3	Green	true	ALBU_MOUSE	Serum al	68.6	5.7	1	396.8	10	16.3	3	0.41	0.481753	10	52.23	0.4	0.452311	10
27	29	Green	true	TMPSD_MOUSE	Transmer	59.8	10.3	1	33.8	1	1.5	29	0.7	0.822528	1	14.41	0.64	0.720497	1
28	21	Green	true	TBA1C_MOUSE	Tubulin a	49.9	4.8	4	58	2	3.8	21	0.77	0.904781	2	14.41	0.56	0.532475	2
29	22	Green	true	TBB5_MOUSE	Tubulin b	49.6	4.6	1	56.8	2	5	22	0.41	0.481753	2	16.84	0.56	0.532475	2
30	1	Green	true	VIME_MOUSE	Vimentin	53.7	4.9	9	584.5	16	32.6	1	0.61	0.716775	16	48.2	0.74	0.833075	16
31											Ave	0.851034		1			0.888276		1
32											St Dev	0.60695					0.442534		
33													0 Hours						
34																			
35																			

Figure 4. 4: iTRAQ results from fibrosarcoma 120 fixed filtered search. The above excel spreadsheet provides an example of the format used to process iTRAQ ratios relative to the control (113), values were normalised to an average of 1 for comparison. The normalised values highlighted in either green, yellow or red indicate response relative to the control either increased, no change or decreased respectively.

iTRAQ ratios showing response relative to the control, normalised to the average .1

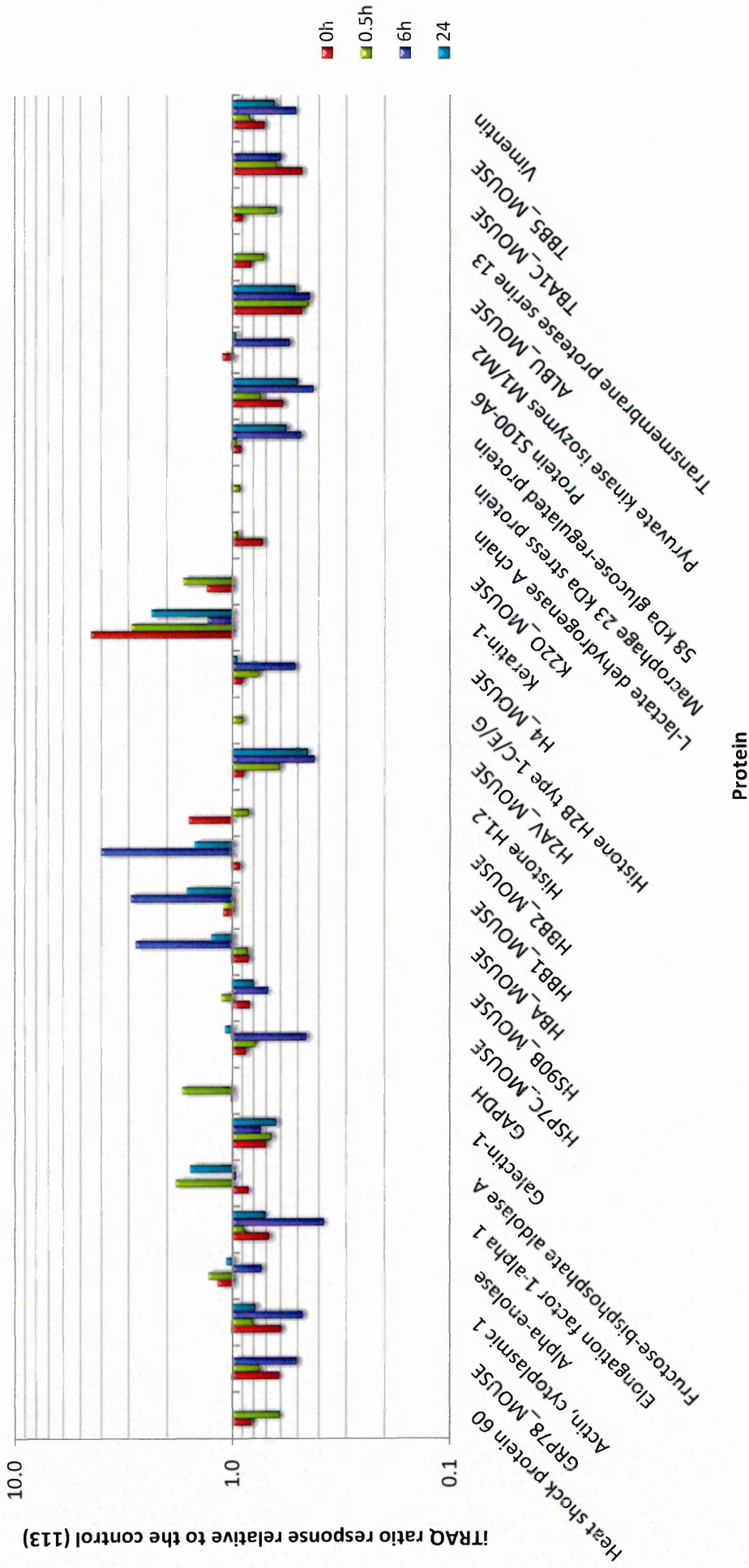


Figure 4. 5: iTRAQ ratio response in fibrosarcoma 120 samples relative to the control (113), normalised to an average of 1. The proteins shown here are from a fixed filtered Mascot search using a mouse database employing MudPit scoring, the peptides used to compile these data had a Mascot score ≥ 28 with fixed modification Carbamidomethyl (C).

The results featured in Figure 4.5 are from the complete excel spreadsheet in Figure 4.4.

The iTRAQ ratio response relative to the control (113) shown in Figure 4.5, displays various outcomes throughout the tumour time course post CA-4-P. Due to the CA-4-P susceptible nature of the fibrosarcoma 120 model the dominant factors apparent from the bar graph (Figure 4.5) appear to be from the Hb peptides Haemoglobin subunit alpha, Haemoglobin subunit beta-1 and Haemoglobin subunit beta-2.

Keratin-1 (KRT1) also produced an increased response compared to the control tumour tissue and it is difficult to explain the increase seen here in the 0h time point. Further work is therefore required to validate such a response so soon after treatment. Interestingly, an article by Tang *et al* (2012) proposes Keratin 1 as cis-diamminedichloroplatinum-resistant (cDDP) protein in nasopharyngeal carcinoma cell lines. The data from this Nasopharyngeal carcinoma study concluded that the expression of KRT1 was related to the issue of drug resistance in this particular cancer and suggested KRT1 as a potential biomarker and key player in the mechanism of multidrug resistance in Nasopharyngeal carcinoma (Tang *et al* 2012).

It is known that the type I and II keratins (polypeptides of the non-hair category) are co-expressed during the differentiation of tumours, consist of either acidic or basic proteins and are found mostly in epithelial cells (Karantza 2011). KTR1 is present in normal endothelia, benign and malignant tumour tissue (Remotti *et al* 2001). It is also suggested that KRT1 has a key role in the architectural integrity of the cytoskeleton in tumour cells (Reichelt *et al* 2004).

The increased response found in Figure 4.5 (0h-24h post CA-4-P) relative to the control tumour tissue could be evidence of the need to maintain epithelial cellular architecture as KRT1 levels are still elevated in the later time points (Karantza 2011).

In contrast to the latter, type 3 mesenchymal intermediate filament Vimentin, is shown to be greatly decreased in response to CA-4-P administration (Figure 4.5). Vimentin is expressed in normal mesenchymal tissue and considered to have involvement in migratory, adhesive and cell survival mechanisms (Lahat *et al* 2010).

Vimentin is said to play a role in mesenchymal transition in cancerous tissues with a study by Handra-luca *et al* (2011) reporting a three-fold higher expression of vimentin in pancreatic neoplasms. Increased expression of Vimentin is not seen in the time points following the control, possibly suggesting an inhibitory action due to CA-4-P. However due to the results here (Figure 4.5) being n=1 then further repeats would clarify the response from Vimentin.

Glyceraldehyde-3-phosphate dehydrogenase (GAPDH) is commonly used as a housekeeping gene in quantitative experimental studies (protein/ RNA analysis) where expression levels are used for normalisation purposes (Barber *et al* 2005). GAPDH levels therefore are renowned for consistency throughout various tissues strengthening its use as an internal standard. Reports by Said *et al* (2009) revealed that under hypoxic conditions GAPDH in hepatocellular

carcinoma, human lung adenocarcinoma epithelia and colon cancer cell lines (*in vitro*) remains unregulated by hypoxia. The article concludes that a GAPDH-hypoxia study is not a suitable strategy for future anti-cancer therapeutics in hepatocellular carcinoma, human lung or human colon cancer. The GAPDH results in Figure 4.5 are in opposition to this hypothesis. A considerable increase in the 0.5h post CA-4-P time point is evident whilst the 0h post CA-4-P remains consistent with the control tissue. Unfortunately the protein remained undetected in the later time points therefore making it impossible to deduce the complete response throughout the time course. The other assumption could be that the absence of GAPDH in the 6h and 24h (post CA-4-P) samples is due to the effects of CA-4-P induced hypoxia.

With a view to validate the uncharacteristic alteration in GAPDH response in the later time fibrosarcoma time points, the responses exhibited by Hb could be considered. GAPDH showed a marked increase relative to the control as a result of treatment with the vascular disrupting agent CA-4-P. Peptides relating to GAPDH were absent from the 6h and 24h samples. The internal standard in the case of this iTRAQ experiment validating the GAPDH reaction post CA-4-P could be the characteristic haemorrhagic response evident from Haemoglobin subunit alpha, Haemoglobin subunit beta-1 and Haemoglobin subunit beta-2.

The protein lists reported here were generated using ProteinScape applying fixed modification Carbamidomethyl (C), and filtered using a Mascot score ≥ 28 which yielded 29 protein identifications.

The protein lists generated using the alternative modification parameters; fixed, variable filtered and variable gave the following proteomics outcomes:

fixed – 99 protein identifications, variable filtered - 31 protein identifications, variable – 352 protein identifications.

4.4.4. Analysis with Scaffold Q+

A screen shot of a protein list generated in Scaffold proteomic software from the LC-MALDI-MS/MS results is shown in Figure 4.6. The corresponding list generated after applying iTRAQ quantitative 3Q+ using the parameters above is displayed in Figure 4.7.

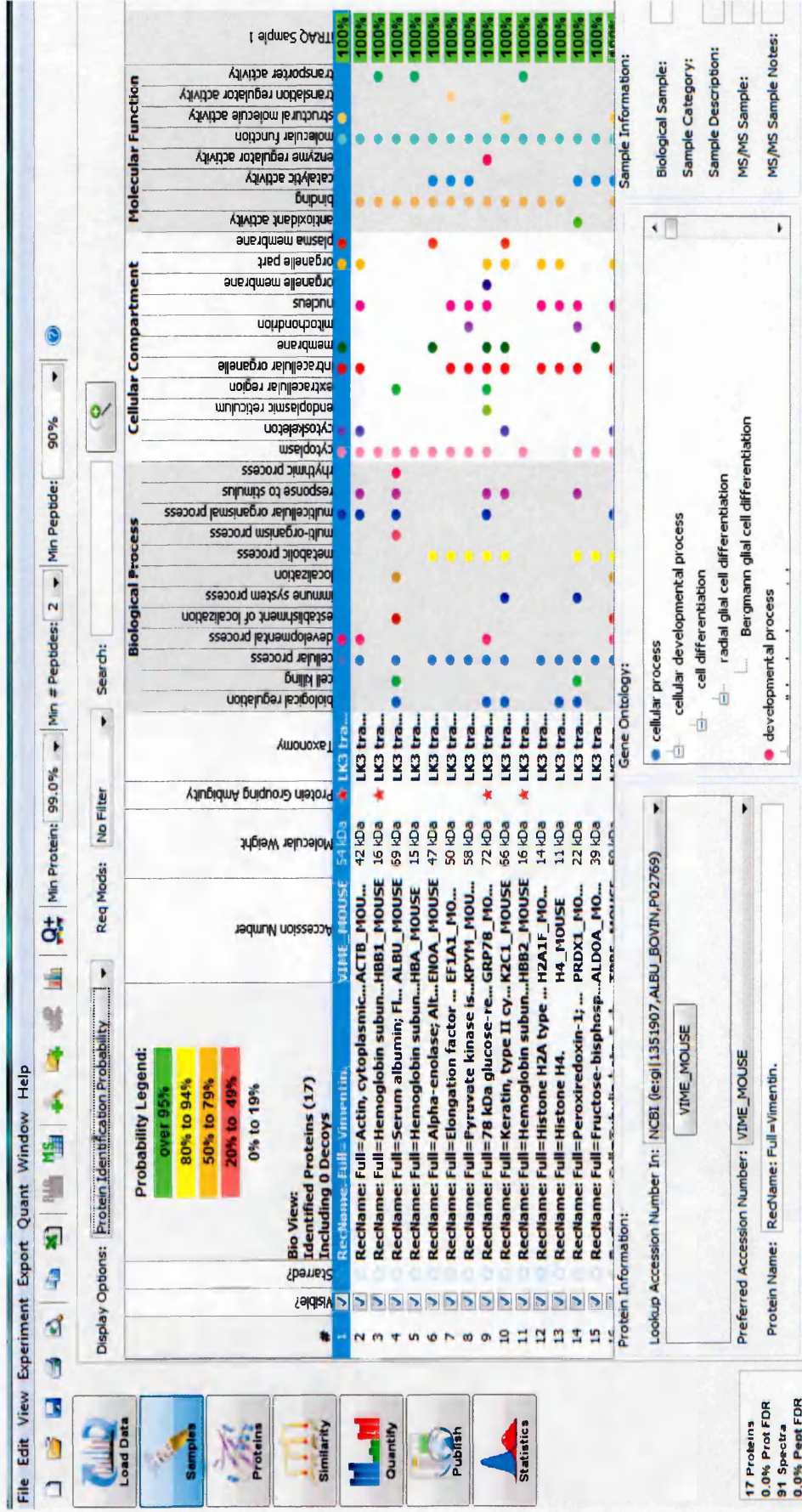


Figure 4. 6: Scaffold proteomic software used for iTRAQ analysis. An example is shown of the protein list from the LC-MALDI-MS/MS fibrosarcoma 120 data with information regarding biological process, cellular compartment and molecular function using Scaffold proteomic software.

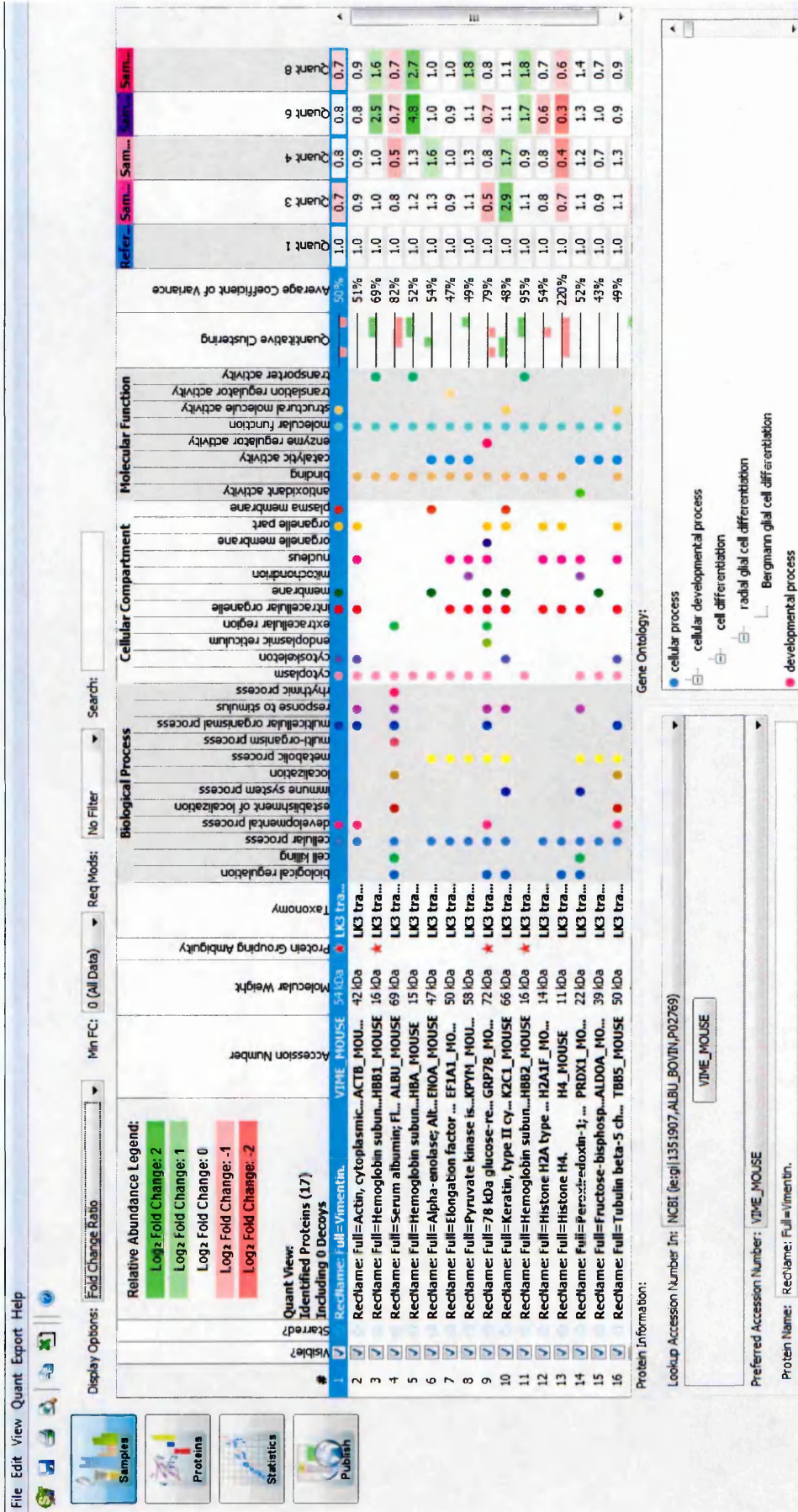


Figure 4. 7: Scaffold proteomic software with the employment of 'Q+' function for iTRAQ ratio analysis. In addition to gene ontology information the fold change ratio throughout the time course samples can be observed; Quant 1 (Control) - Quant 8 (24h post CA-4-P, fibrosarcoma 120).

iTRAQ fold change ratios of proteins identified from fibrosarcoma 120 tumours

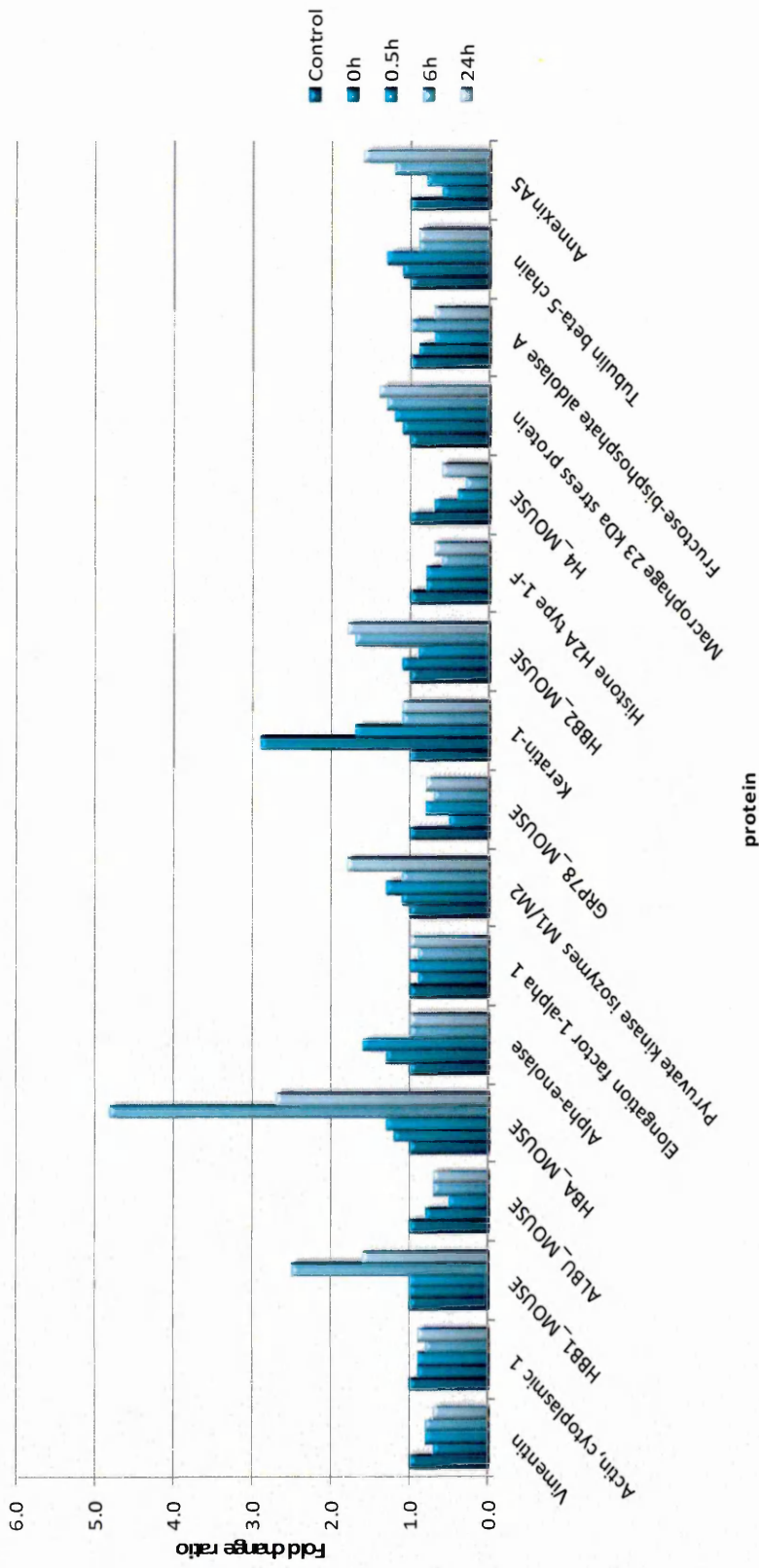


Figure 4. 8: iTRAQ fold change ratio using fibrosarcoma 120 tumour digest samples. Proteins response throughout the fibrosarcoma time course, Control – 24h post CA-4-P.

The fold change ratios which can be seen in Figure 4.7 are displayed in Figure 4.8.

The search parameters applied by Scaffold proteomic software using the .dat file from fibrosarcoma fixed search gave information for 17 proteins (Figure 4.8). The subsequent data shows examples of protein sequences found and spectra used for protein identification and relative quantitation by Scaffold 3 Q+ using LC-MALDI-MS/MS. The following proteins detailed are; Vimentin, Hb subunit beta, Peroxiredoxin-1 (Macrophage 23kDa stress protein), Tubulin beta-5 chain, Annexin A5 and Keratin -1 (type II skeletal-1).

Vimentin (Figure 4.9), Hb subunit beta (Figure 4.10), Tubulin beta-5 chain (Figure 4.12) and Keratin -1 (type II skeletal-1) (Figure 4.14) are portrayed similarly to the excel analysis in Figure 4.5 as previously discussed. The employment of an unfiltered fixed modification search (proteins ≥ 10 Mascot score) yielded Annexin A5 and the missing peptides for 6h and 24h post CA-4-P corresponding to Peroxiredoxin-1 (Macrophage 23kDa stress protein). The Log_2 of normalised intensity in Figure 4.11 shows an initial decrease of Peroxiredoxin-1 with levels recovering during the 6h and 24h time points. The latter matches the iTRAQ ratio initial response of Peroxiredoxin-1 shown in Figure 4.5 evident in the Control and 0h time points. Peroxiredoxin-1 is thought to be involved in hypoxia/ reoxygenation process and levels appear elevated in a number of cancers (Park *et al* 2007). A recent study by Kalinina *et al* (2012) looking at cisplatin resistance formation in cancer cells using peroxiredoxin genes included *PRDX1*. It was found that elevated levels of *PRDX1* was found in 3 cisplatin resistant cell lines. Over expression of the *PRDX1* gene is said to act as a protective mechanism against H_2O_2 induced apoptosis (Kalinina *et al* 2012). Could this be an explanation for the regenerative response seen here by Peroxiredoxin-1?

The biological role of Annexin A5 has yet to be fully determined however it is commonly used as a marker of apoptosis (Rand *et al* 2012). This is due to the favourable binding affinity of Annexin A5 to phosphatidylserine which is expressed on the cell surface of cells undergoing programmed cell death. Expression levels of Annexin A5 are known to be increased in vascular endothelium cells. Interestingly the results in Figure 4.13 show an increase in Annexin A5 as the time course progresses fitting in with the increase in necrotic tissue postulated by CA-4-P administration.

VIME_MOUSE (100%) 53.688.7 Da
 ReName: Fvl=Vimentin.

MSTRVSSSSS
 YVTRSSAARL
 YRLEQQN
 DIMRLREKIQ
 EIQELQDAQIQ
 AANRNLNDALR
 TIGRLQDEIQ
 LNLRETNLES
 YRRMFGSSGT
 RSSVPGVRL
 LAELEQLK
 EEMLQREAE
 EQHVQIDVDY
 QAKQESNEYR
 NMKKEEMARHL
 LPLVDTHSR
 SSSRPSSNRSY
 QDSVDFSLAD
 GGKSRLLGDL
 STLQSFRC
 SKPDLTAAALR
 RQVQD
 TLLIKTVETR
 VTTSTRTYSL
 AINTEFKNT
 EEMRELR
 DNASLARLDL
 DVRQYESVA
 DALKGTNESL
 MALDIEIATY
 DGQVINETSQ
 GSALRPSSTR
 TNEKVELQEL
 VDQLTNDKAR
 ERKVESLQEE
 AKMLQEAEEW
 ERQMRMEEN
 RMLLEGEESR
 HHHDDLE
 SLYSSSSPPGGA
 NDRFANYIDK
 VEVERDNLAE
 IAFLLKLLHDE
 YRASKFIADLSE
 FALFAANYQD
 ISLPLPTFSS

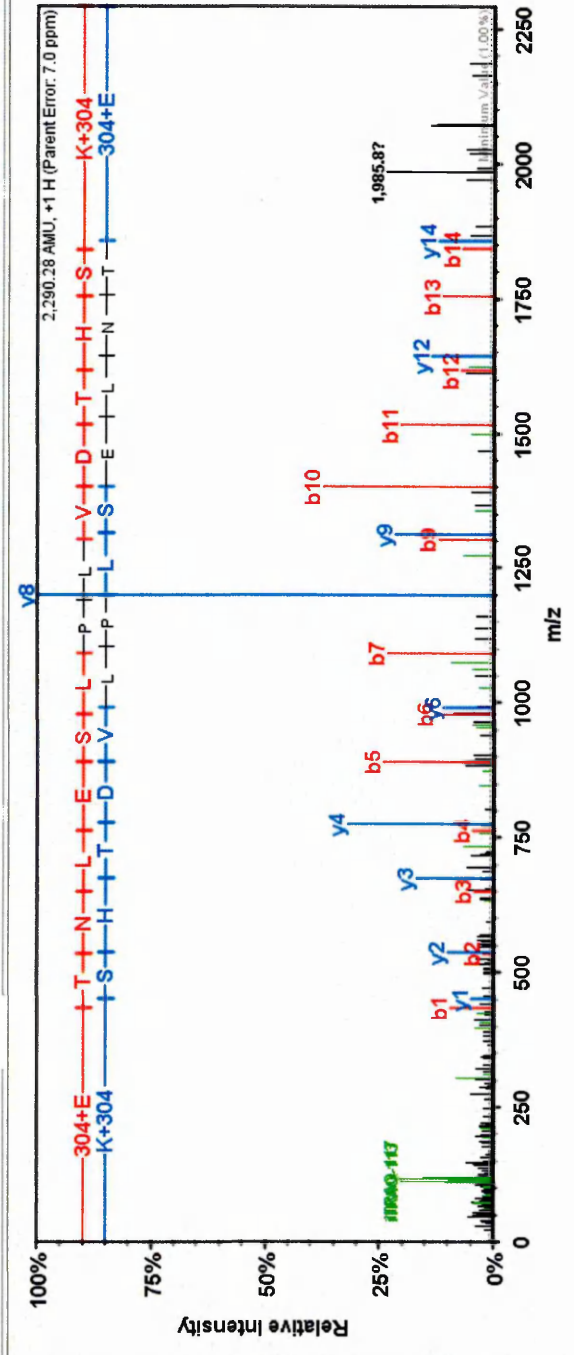


Figure 4. 9: Vimentin peptides identified, response bar graph and related MS/MS spectrum from iTRAQ LC-MALDI-MS/MS Fibrosarcoma 120 tissue. iTRAQ 113-121 refers to iTRAQ labelled control-24h post CA-4-P.

HBB1_MOUSE (100%) 15,840.2 Da
 RecName: Full=Hemoglobin subunit beta-1; AltName:

M V H L T D A E K A A V S C L W G K V N R L L V V Y P W T Q R Y F D S F G D L S S A S A I M G N A K
 V K A H G K K V I T A F N D G L N H L D S L K K G T F A S L S E L H C D K L L H V D P E N F R L L G N M I V I V L G H H L L G
 K D F T P A A Q A A F Q K V V A G V A T A L A H K K Y H

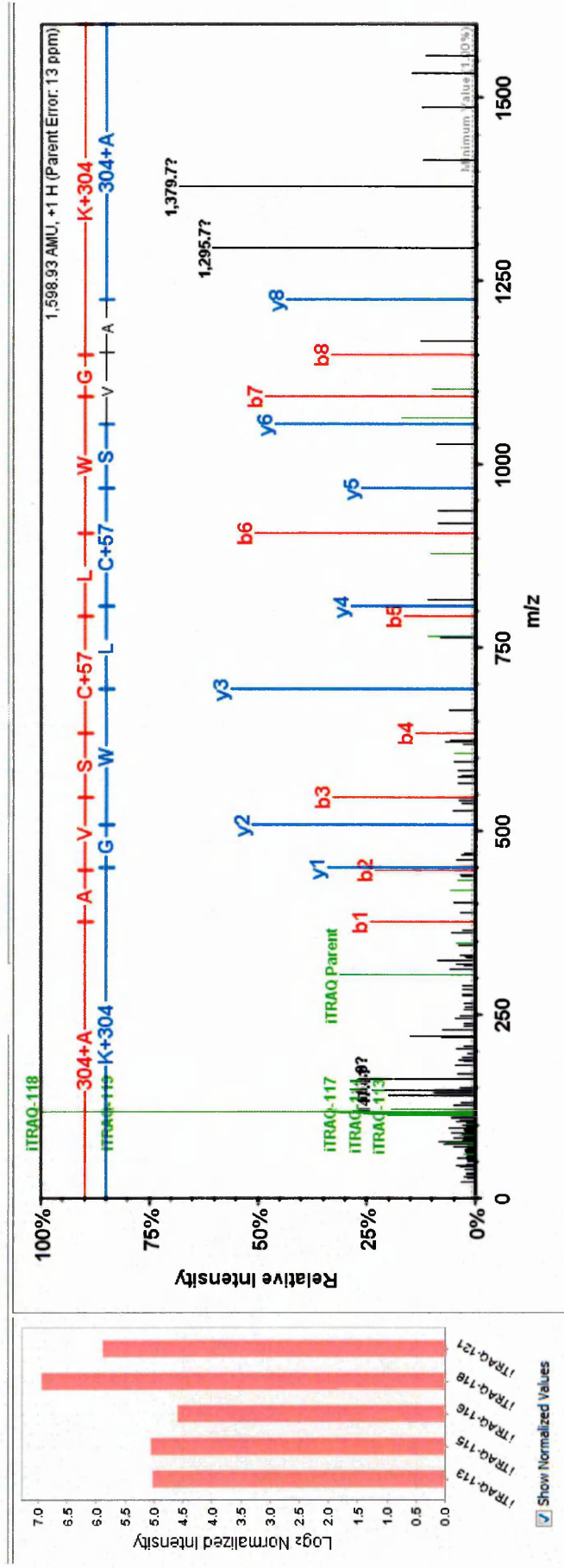


Figure 4. 10: Haemoglobin subunit beta-1 peptides identified, response bar graph and related MS/MS spectrum from iTRAQ LC-MALDI-MS/MS Fibrosarcoma 120 tissue. iTRAQ 113-121 refers to iTRAQ labelled control-24h post CA-4-P.

PRDX1_MOUSE (100%) 22,177.5 Da

RecName: Full=Peroxiredoxin-1; AltName: Full=Macrophage 23 kDa

M S S G N A K **I G Y** P A P N F **K** A T A V M P D G Q F K D I S L S E Y K G K Y V V F F F Y P L D F T F V C P T E I I A F S
 D R A D E F K K L N C Q V I G A S V D S H F C H L A W I N T P K K Q G G L G P M N I P L I S D P K R **T I A Q D Y G V L K**
 A D E G I S F R G L F I I D D K G I L R Q I T I N D L P V G R S V D E I I R L V Q A F Q F T D K H G E V C P A G W K P G
 S D T I K P D V N K S K E Y F S K Q K

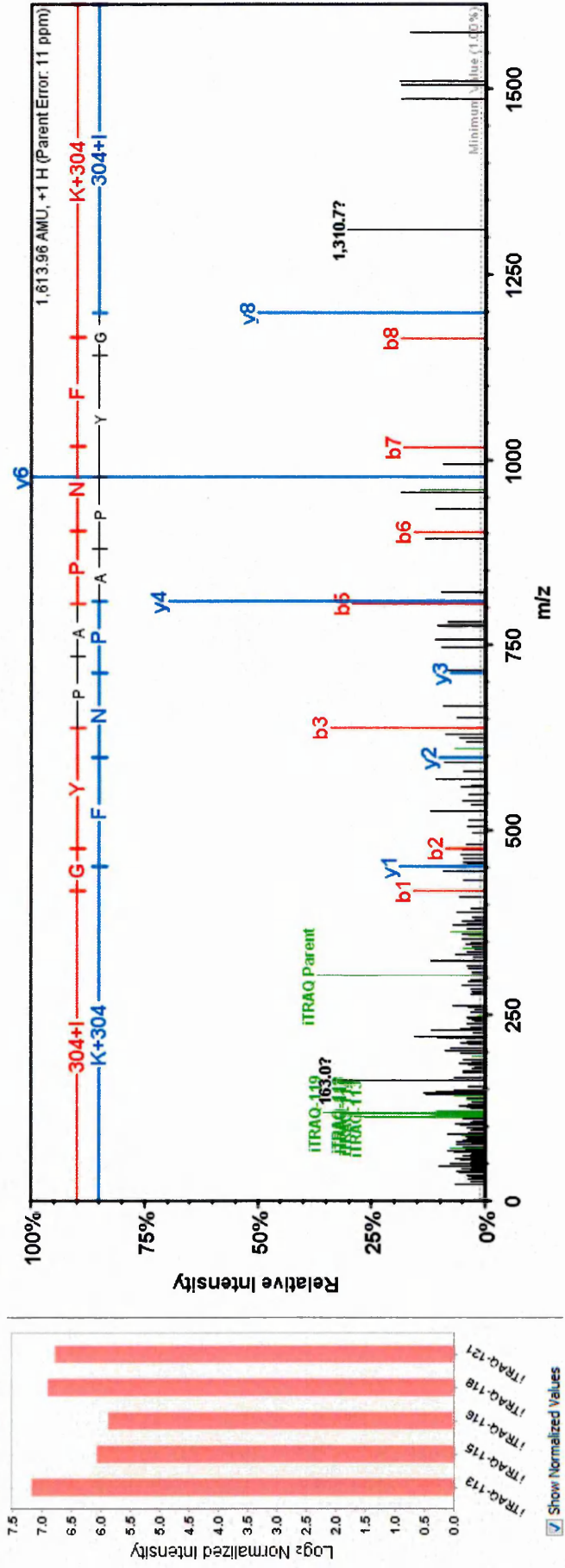


Figure 4. 11: Peroxiredoxin-1 (Macrophage 23kDa stress protein) peptides identified, response bar graph and related MS/MS spectrum from iTRAQ LC-MALDI-MS/MS Fibrosarcoma 120 tissue. iTRAQ 113-121 refers to iTRAQ labelled control-24h post CA-4-P.

TBB5_MOUSE (100%) 49,670.6 Da
 RecName: Full=Tubulin beta-5 chain.

MR E I V H I Q A G Q C G N Q I G A K F W E V I S D E H G I D P T G T Y H G D S D L Q L D R Y T E G A Y N E A T G G R Y V
 P R A I L V D L E P G T M D S V R S G P F G Q I F R P D N F V F G Q S G A G N N W A K G H Y T E G A E L V D S V L D V V
 P K A E S C D C L Q G F Q L T H S L G C G T G S G M G T L L I S K I R E E Y P L I M N T F S V V P S P K V S D T V V
 E P Y N A T L S V H Q L V E N T D E T Y C I D N E A L Y D I C F R T L K L T T P T Y G D L N H L V S A T M S G V T T C L
R P G Q L N A D L R K L A V N M V P F P R L H F F M P G F A P L T S R R G S Q Q Y R A L T V P E L T Q Q V F D A K N M M
 A A C D P R H G R Y L T V A A V F R G R M S M K E V D E Q M L N V Q N K N S Y F V E W I P N N V K T A V C D I P P R G
 L K M A V T F I G N S T A I Q E L F K R I S E Q F T A M F R R K A F L H W Y T G E G M D E M E F T E A E S N M M N D L V S
 E Y Q Q Y Q D A T A E E E E D F G E E A E E E A

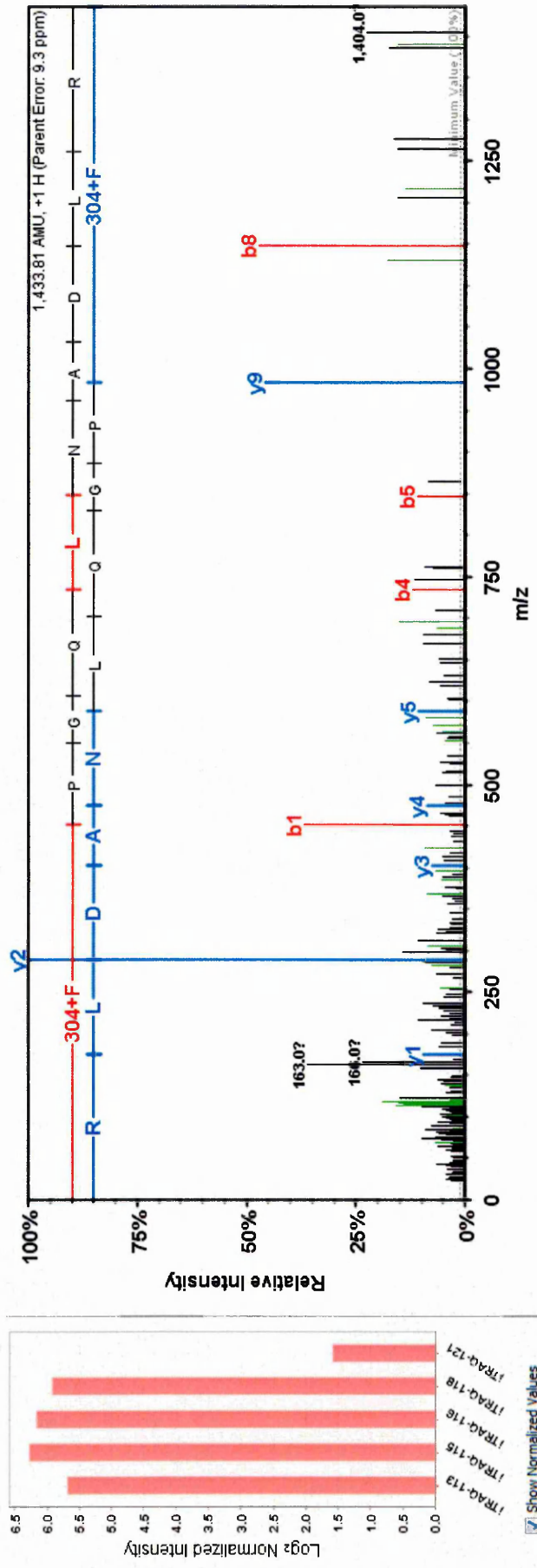


Figure 4. 12: Tubulin beta-5 chain peptides identified, response bar graph and related MS/MS spectrum from iTRAQ LC-MALDI-MS/MS Fibrosarcoma 120 tissue. iTRAQ 113-121 refers to iTRAQ labelled control-24h post CA-4-P.

ANXA5_MOUSE (99%) 35,754.2 Da
 RecName: Full=Annexin A5; AltName: Full=Anchorin CII; AltName:

M A T R G T V T D F P G F D G R A D A E V L R K A M K G L G T D E D S I L N L L T S R S N A Q R R **D E** I A Q E F K T L F G
 R D L V D D L K S E L T G K F E K L I V A M M K P S R L Y D A Y E L K H A L K G A G T D E K V L T E I I A S R R **T P E E L**
S A I M Q V Y E E E Y G S N L E D D V V G D T S G Y Y Q R M L V V L L Q A N R D P D T A I D D A Q V E L D A Q A L F Q A
 G E L K W G T D E E K F I T I F G T R S V S H L R R V F D K Y M T I S G F Q I E E T I D R E T S G N L E Q L L L A V V K
 S I R S I P A Y L A E T L Y Y A M K G A G T D D H T L I R V V Y S R S E I D L F N I R K E F R K N F A T S L Y S M I K G
 D T S G D Y K K A L L L L C G G E D D

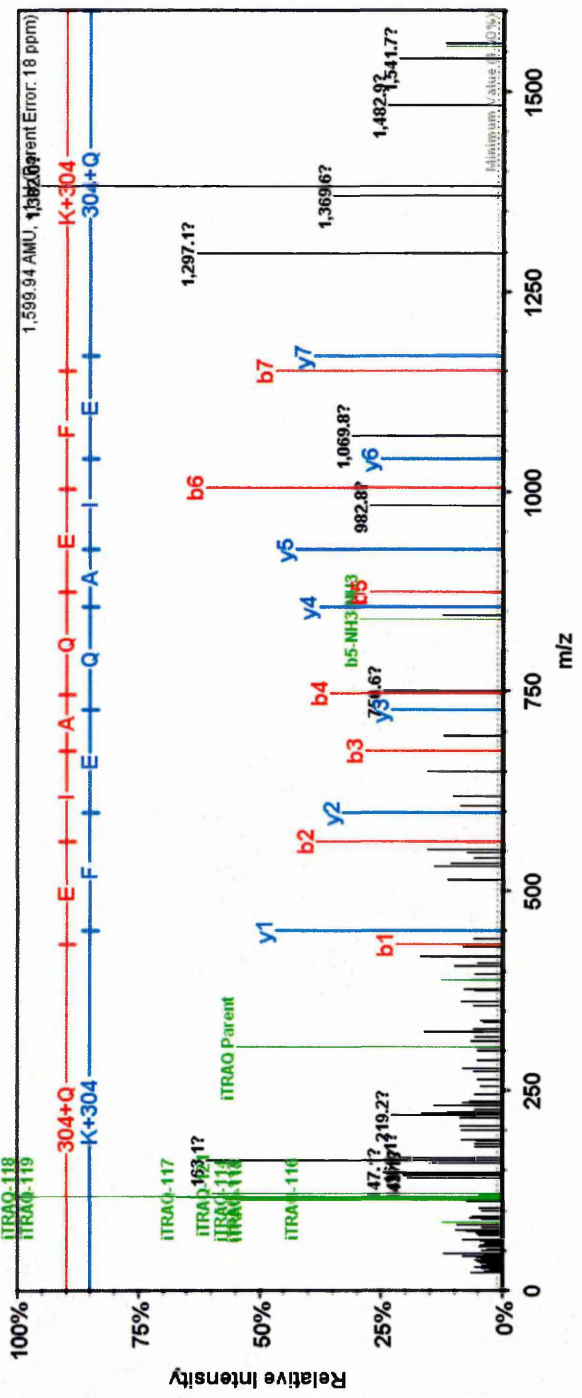


Figure 4. 13: Annexin A5 peptides identified, response bar graph and related MS/MS spectrum from iTRAQ LC-MALDI-MS/MS Fibrosarcoma 120 tissue. iTRAQ 113-121 refers to iTRAQ labelled control-24h post CA-4-P.

4.4.5 Protein relationship mapping of fibrosarcoma 120 data using STRING

9.0

Observation of protein relationship maps facilitates the analysis of complex proteomic data sets. Understanding known protein-protein interactions could provide an insight into potential biomarkers. The proteomic pathway software STRING 9.0 proposed known protein pathways and networks with an additional predicted functional partners feature (<http://string-db.org/>).

The following proteomic networks generated by STRING 9.0 will feature zoomed in sections of the original networks shown in Figures 4.15 and 4.16 to ease interpretation. Evidence and confidence views are included which depict evidence of association and strength of association respectively. To relate to the fixed unfiltered search list imported into Scaffold 3 Q+ the same list will be used for compilation of the following protein relationship maps.

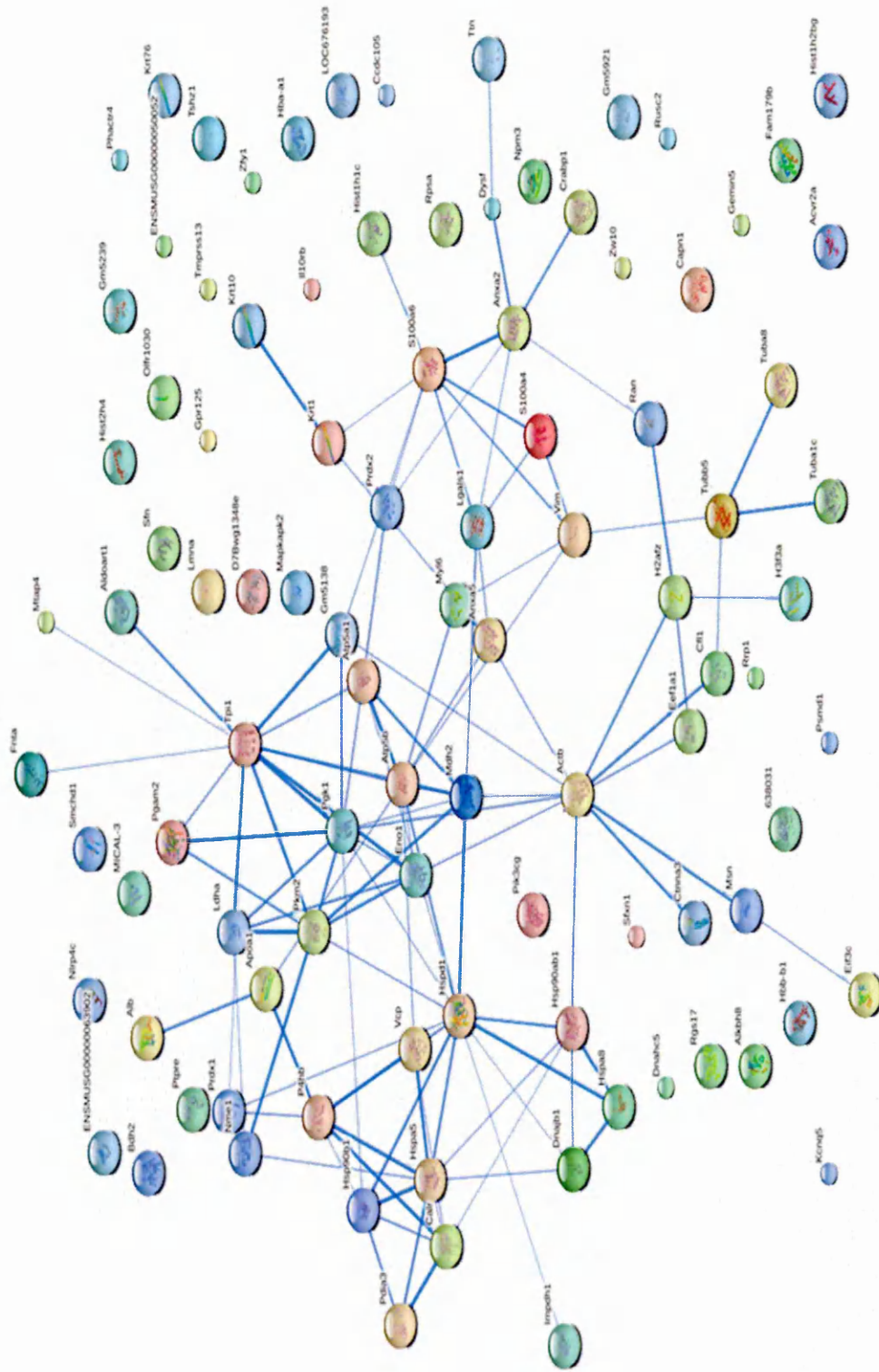


Figure 4. 15: Fixed modification search showing proteins from iTRAQ using Fibrosarcoma 120 tumours, visualised by STRING 9.0 (Confidence view).

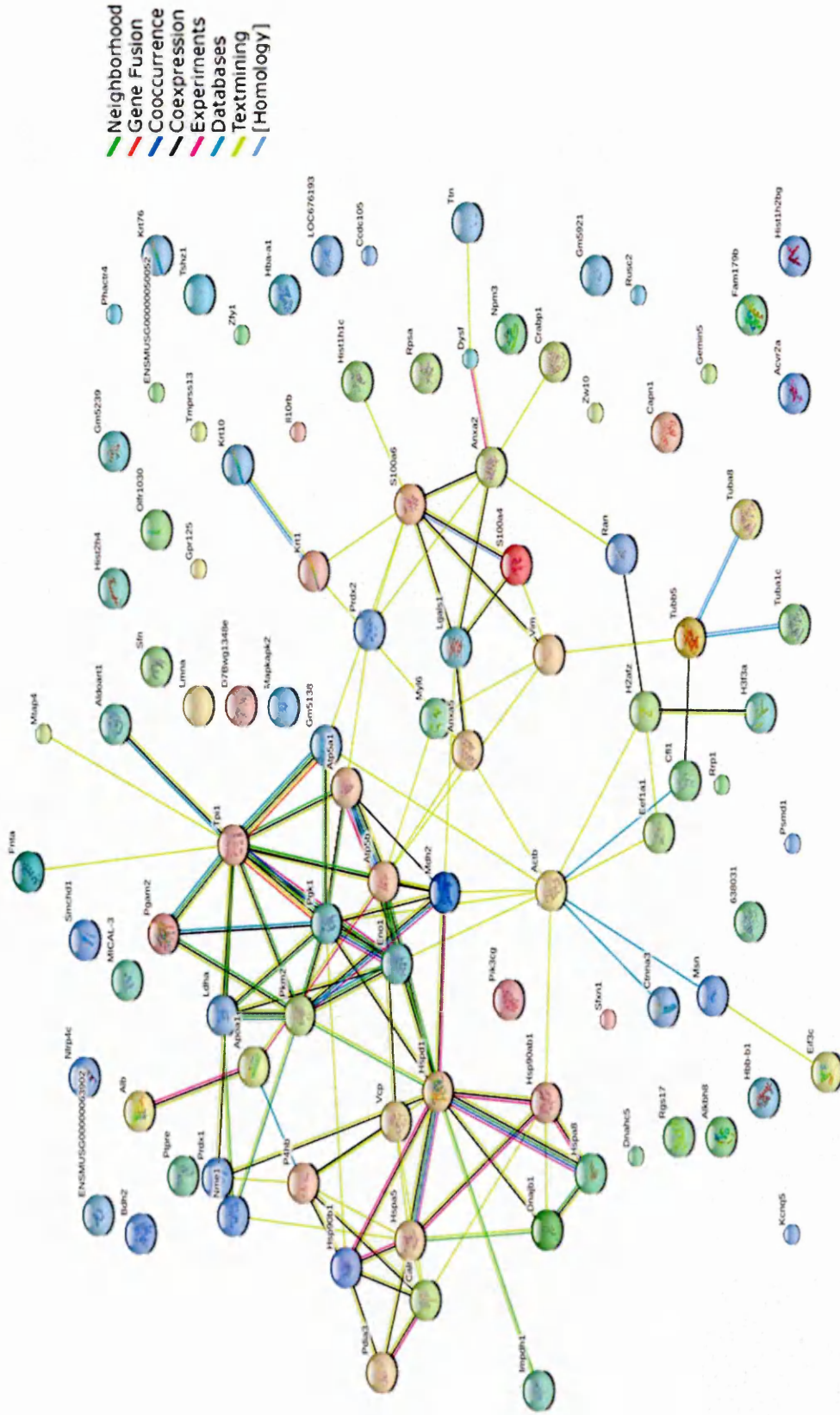


Figure 4. 16: Fixed modification search of iTRAQ fibrosarcoma 120 proteomic data, compiled using STRING 9.0, evidence view.

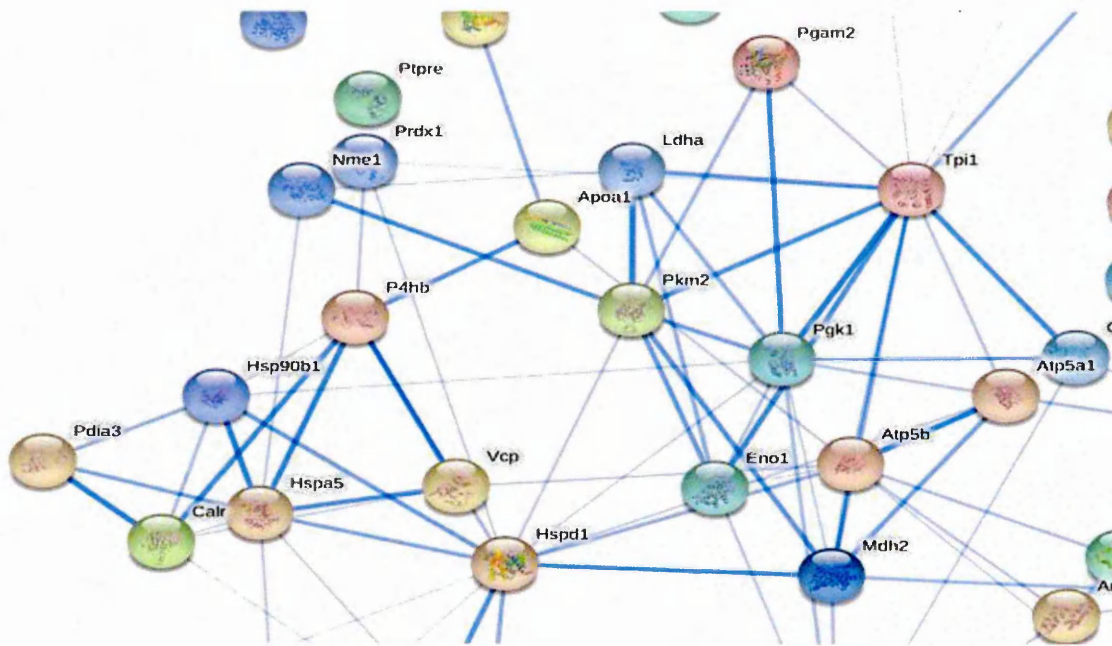


Figure 4. 17: Zoomed in region of a fixed modification search, iTRAQ fibrosarcoma 120 samples.

There is a link suggested in Figure 4.17 between Peroxiredoxin-1 (Prdx1) and prolyl 4-hydroxylase beta (P4hb). Considering Prdx1 potential involvement in reoxygenation and anti-apoptosis, a link with P4hb fits. P4hb function includes the inhibition of aggregated malformed proteins (<http://string-db.org/>). P4hb protein then has strong associations with Hspa5 (78 kDa glucose-regulated protein) and Hsp90b1. Hsp90b1 was mentioned earlier in Chapter 3 along with its relevance to tumour biology and the stress response. Calreticulin (Calr) is also included to have strong associations with P4hb. Trace levels of Calr are found on normal lung cells but highly expressed in lung cancer cells (Liu *et al* 2012). Alpha Enolase 1 (Eno1, 8 peptides found, collective Mascot score of 241) can be seen in the zoomed region in Figure 4.17, it also features in iTRAQ ratio response graph (Figure 4.5) and the iTRAQ fold change graph (Figure 4.8). Both graphs display an early increase in the 0h and 0.5h post CA-4-P with levels decreasing towards Control levels in the 6h and 24h samples. Eno1 is known to be involved in tumourigenesis, proliferation and cancer cell metastasis due to its role as a plasminogen receptor (Capello *et al* 2011). It could be suggested that its sudden decrease in the later time points maybe as a result of increased necrosis by CA-4-P affecting the role of hypoxia tolerance by Eno1 (<http://string-db.org/>).

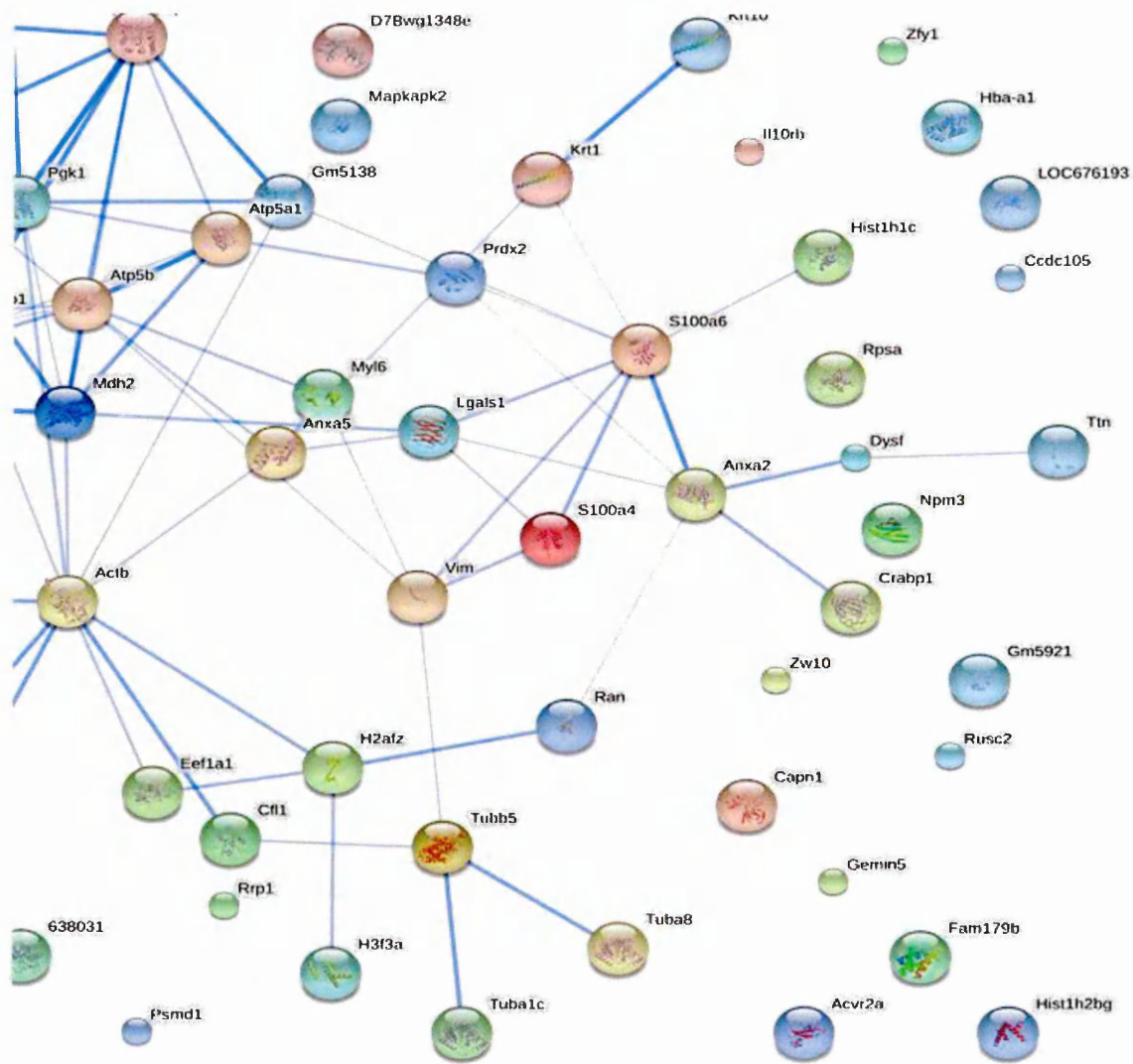


Figure 4. 18: Zoomed in region of a fixed modification search, iTRAQ fibrosarcoma 120 samples.

Annexin A5 (Anxa5) where functional properties are mentioned earlier in this chapter, has several associations. Galectin-1 (Lgals1 – 2 peptides identified with a collective Mascot score of 54) is one such protein and is thought to have functional influence on cell proliferation, apoptosis and differentiation, therefore enhancing tumour progression (Banh 2011). Figure 4.5 displays a contradictory trend to this where all the other time points relative to the control are notably decreased, again suggesting an inhibitory effect by CA-4-P.

The same response exhibited by Galectin-1 is true for S100 calcium binding protein A6 (see Figure 4.5) (Calcylin -2 peptides identified with a collective Mascot score of 56). Functions of Calcylin include an indirect role in cell motility and cytoskeleton restructuring (Ning *et al* 2012).

The Tubulin proteins (Tuba1c, Tubb5, Tuba 8) are shown with associations feeding into Vimentin with branching from Tubb5 to Cofilin 1, a protein which too intervenes in the regulation of morphological cell changes and cytoskeletal architecture.

Actin cytoplasmic 1 (Actb) is positioned prominently linking the proteins relevant in structural integrity, necrosis and heat shock molecular chaperones expressed due to malformed unglycosylated proteins.

4.5 Results and discussion - Fibrosarcoma 188

4.5.1. HPLC UV profiles of fibrosarcoma 188 tumour fractions

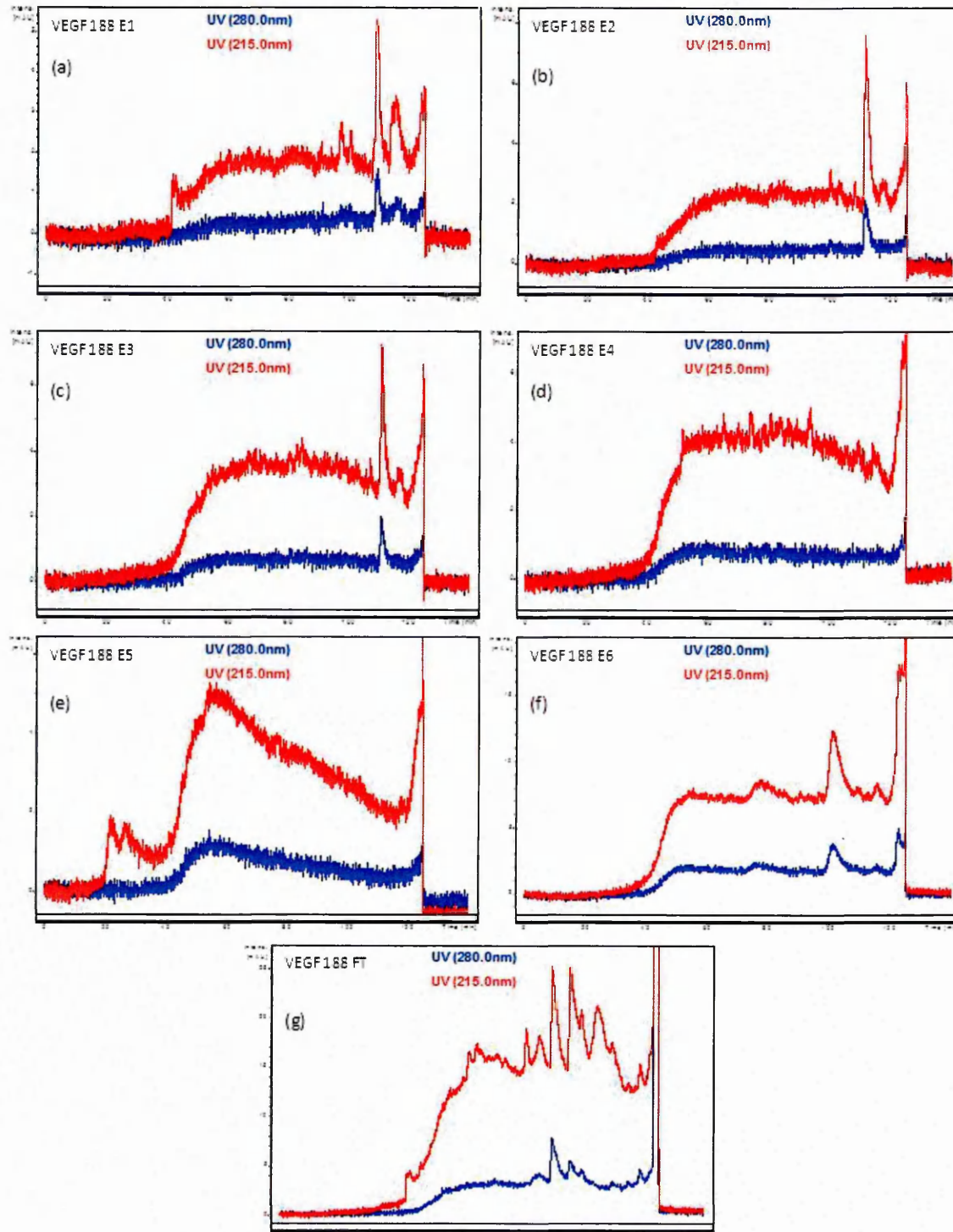


Figure 4. 19: UV profiles from the fibrosarcoma 188 fractions after SCX. (a) shows the UV profile from the first eluant (E1) after 60mM KCl following the flow through (FT) fraction from strong cation exchange, (b) 120mM KCl (E2), (c) 180mM KCl (E3), (d) 300mM KCl (E4), (e) 500mM KCl (E5), (f) 1000mM KCl (E6) and (g) (FT) after addition of the combined iTRAQ labelled sample.

The UV profiles in Figure 4.19 appear to indicate a greater protein elution compared to those in Figure 4.2 with a more even spread of UV signal, possibly indicating improved separation of peptides.

4.5.2 Frequency of unique peptides identified

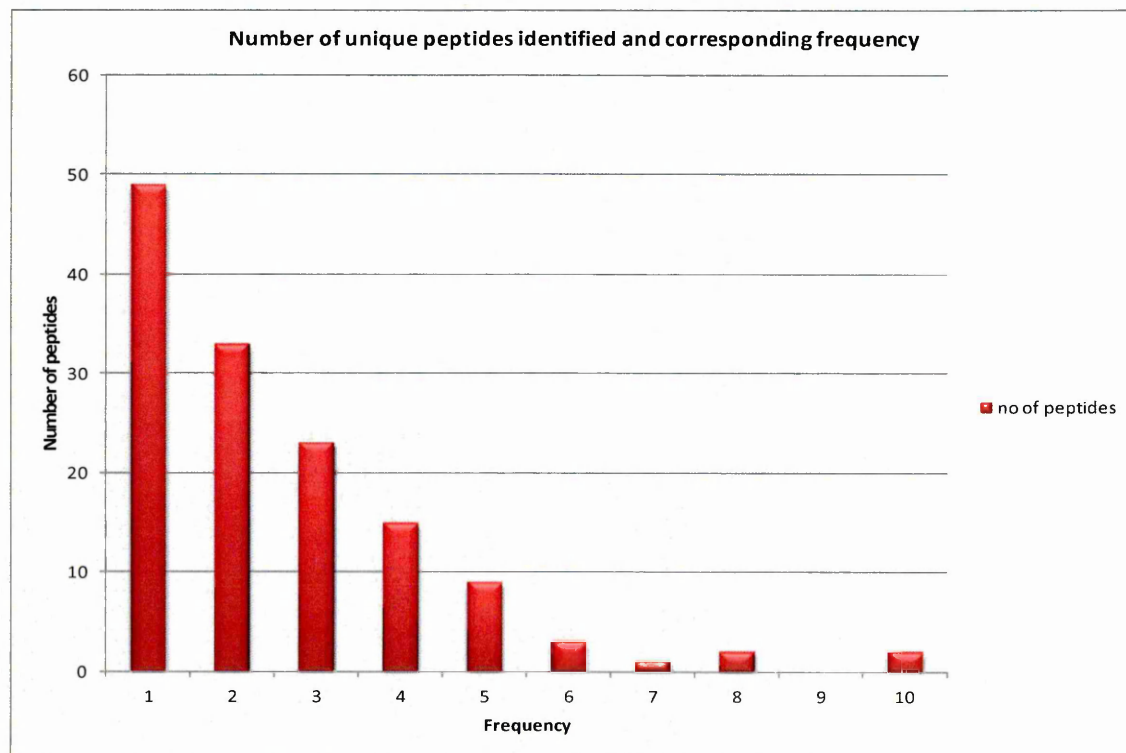


Figure 4. 20: Frequency of detection of unique peptides by LC-MALDI-MS/MS. The graph shows the range of unique peptides detected. Here 49 unique peptides were only seen once whereonly 2 proteins had 10 unique peptides assigned to them.

4.5.3. Analysis using excel

Spreadsheets were prepared employing the methods described in section 4.43. Figure 4.21 displays a screen shot of an excel spreadsheet containing the fibrosarcoma 188 iTRAQ samples used for protein analysis and ratio comparison.

1	Row	A	B	C	D	E	F	G	H	I	J	K	L	M	N	O	P	Q	R			
		Accession Protein	MW [kDa]	pI	#Alt. Prote Scores	#Peptides	SC [%]	RMS90 [p]	Rank	Median	Normaliser#	CV [%]	Median	Normaliser#	CV [%]	Median	Normaliser#	CV [%]	Median	Normaliser#	CV [%]	
23	31	Green	HBE_MOL Hemoglobin subunit epsilon-Y2 OS=H	16.1	9.1	1	60.9	2	12.9	15.67	31	0.87	0.803736	3	27.69	8.32	1					
24	29	Green	HNRH1_M Heterogeneous nuclear ribonucleoprotein	49.2	5.9	3	62.8	2	5.8	19.04	29	1.48	1.367276	2	33.17	3.2	0					
25	16	Green	HNRPU_IV Heterogeneous nuclear ribonucleoprotein	87.9	5.9	1	123	4	4.6	9.05	16	1.42	1.311846	6	82.11	8.51	1					
26	34	Green	ROA2_MC Heterogeneous nuclear ribonucleoprotein	37.4	9.3	1	49.6	2	7.1	11.99	34	0.96	0.886882	4	49.04	5.12	0					
27	39	Green	H12_MOU Histone H1.2 OS=Mus musculus GN	21.3	11.5	4	37.5	1	4.2	13.13	39	1.95	1.801478	1	16.03	2						
28	20	Green	H2AV_MO Histone H2A.V OS=Mus musculus G	13.5	11	12	89.6	3	20.3	7.03	20	0.89	0.822213	7	48.68	6.13	1					
29	24	Green	H32_MOU Histone H3.2 OS=Mus musculus GN	15.4	11.9	3	82.8	3	16.9	8.96	24	1.22	1.127079	7	18.8	4.79	0					
30	22	Green	H4_MOUS Histone H4 OS=Mus musculus GN=H	11.4	11.8	1	88.7	2	19.4	6.79	22	0.59	0.545063	3	37.91	6.42	1					
31	27	Green	PRDX1_MI Peroxiredoxin-1 OS=Mus musculus C	22.2	9.2	1	68.9	2	13.1	20.82	27	0.56	0.517343	2	6.14	3.47	0					
32	10	Green	PLEC_MO Plectin OS=Mus musculus GN=Plec	533.9	5.7	1	175.8	9	2	12.82	10	0.88	0.812975	10	38.63	2.89	0					
33	38	Green	PDC6L_MC Programmed cell death 6-interacting l	96	6.1	1	43.3	1	1.7	16.57	38	1.09	1.00698	1	5.38	0						
34	42	Green	MCM10_M Protein MCM10 homolog OS=Mus m	98.3	9.9	1	30	1	1	16.57	42	0.46	0.424964	2	37.1	1.83	0					
35	35	Green	S10A6_MC Protein S100-A6 OS=Mus musculus	10	5.2	1	28.1	1	9	5.67	44	0.79	0.72983	1	3.27	1						
36	8	Green	KPYM_MC Pyruvate kinase isozymes M1/M2 OS	57.8	7.9	2	220.1	6	10.9	7.21	8	1.33	1.2287	13	46.12	6.87	1					
37	2	Green	ALBU_MO Serum albumin OS=Mus musculus G	68.6	5.7	1	366.8	9	16.8	6.66	2	0.93	0.859166	17	60	6.88	1					
38	40	Green	TCPB_MO T-complex protein 1 subunit beta OS-	57.4	6	1	37.1	1	2.2	17.3	40	3.29	3.039417	1	11.45	2						
39	17	Green	TENA_MO Tenascin OS=Mus musculus GN=Ten	231.7	4.6	1	107.2	3	1.5	7.15	17	1.95	1.801478	4	25.67	3.96	0					
40	36	Green	BGH3_MC Transforming growth factor-beta-induc	74.5	6.7	1	47.4	2	2.5	6.59	36	0.87	0.803736	2	32.57	3.4						
41	33	Green	TERA_MO Transitional endoplasmic reticulum A	89.3	5	1	51.3	1	2.4	4.51	33	1.98	1.829193	1	4.73	0						
42	41	Green	TPIS_MO Triosephosphate isomerase OS=Mus	32.2	5.5	1	32.5	1	4	10.28	41	0.59	0.545063	1	2.15	0						
43	32	Green	TBA1C_MI Tubulin alpha-1C chain OS=Mus mus	49.9	4.8	4	55.3	1	2.2	10.36	32	0.86	0.794498	5	28.28	5.93	1					
44	19	Green	RL40_MO Ubiquitin-60S ribosomal protein L40 C	14.7	10.7	4	94.8	4	21.9	8.18	19	1.03	0.95155	4	22.75	4.85	0					
45	35	Green	UBA1_MO Ubiquitin-like modifier-activating enzy	117.7	5.3	1	47.6	2	2.2	18.78	35	0.87	0.803736	3	13.31	3.65	0					
46	7	Green	VIME_MO Vimentin OS=Mus musculus GN=Vir	53.7	4.9	17	232.9	5	8.8	7.89	7	1.48	1.367276	8	82.31	8.89	1					
47																						
48																						
49																						
50																						
51																						

Figure 4. 21: iTRAQ results from fibrosarcoma 188 fixed filtered search.iTRAQ ratios relative to the control (113), values were normalised to an average of 1 for comparison. The normalised values highlighted in either green, yellow or red indicate response relative to the control either increased, no change or decreased respectively (individual figures were still considered in addition to colour coded threshold).

iTRAQ ratios showing response relative to the control, normalised to the average. 1

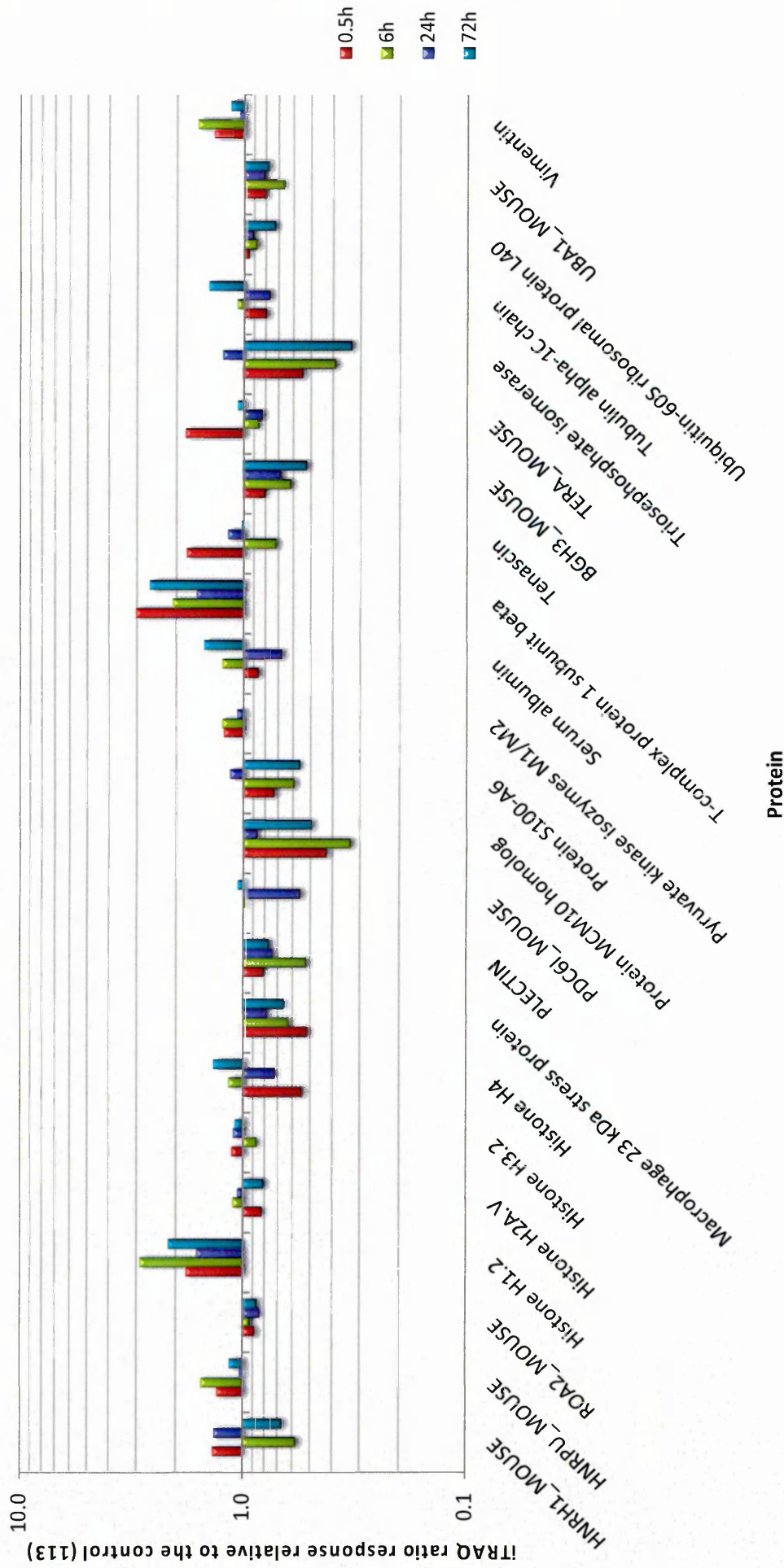


Figure 4.22: b Fibrosarcoma 188 iTRAQ samples showing ratio response relative to the control (113), normalised to an average of 1.

The proteins seen in Figures 4.22a and 4.22b are from the same excel spreadsheet separated into two bar graphs to aid interpretation. These data has been generated via ProteinScape and exported to excel for analysis employing the same parameters prior to examination as detailed in the previous section entitled '*4.3.4 Statistical analysis*'.

The fixed filtered search performed on the fibrosarcoma 188 samples resulted in a greater peptide yield in comparison to the fibrosarcoma 120 results. 45 proteins were identified, opposed to 29 proteins in the fibrosarcoma 120 data set. The latter could be due to differing factors during the tissue digestion, SCX or LC fractionation. Another factor to consider could be the more CA-4-P resistant nature of the fibrosarcoma 188 tumour where different peptides identified could be as a result of decreased suppression from high abundant proteins i.e. Haemoglobin/ Histones.

The discussion that follows aims to highlight key responses from Figures 4.22a and 4.22b.

The haemoglobin peptides (Haemoglobin subunit alpha, Haemoglobin subunit beta-1, Haemoglobin subunit beta-2 and Haemoglobin subunit epsilon-Y2) are consistently present in Figure 4.22a to aid validation of the other protein responses however even with the fixed filtered search parameters many different proteins are observable.

Heat shock protein HSP 90-beta is increased in the 6h-72h time points with what appears to be a saturation point achieved in the 24h. This response by Heat shock protein HSP 90-beta was discussed in Chapter 3 where evidence of the switch back to viable tissue was observed both in the MALDI-MSI and immunohistochemistry.

A similar surge pattern of GAPDH levels (Figure 4.22a) seen previously in Figure 4.5 can be observed. The sudden increase appears in the 0.5h fibrosarcoma 120 time point (Figure 4.5) whereas in the fibrosarcoma 188 samples the surge is seen 6h post CA-4-P with decreased levels apparent in the 24h and 72h samples. An explanation of the delayed response in the Fibrosarcoma 188 data could be indicative of more resistant tumour model.

Tumour enhancing protein Galectin-1 (Figure 4.22a) is shown to be decreased relative to the control but later on in the 72h sample a small increase is observable possibly indicative of tumour regeneration.

Elongation factor 1-alpha 1 is a protein giving very different responses in the two tumour models. In the fibrosarcoma 188 samples levels are elevated throughout the time points in Figure 4.22b relative to the control. In contrast to this, levels in the fibrosarcoma 120 iTRAQ results are all decreased relative to the control. Elongation factor 1-alpha 1 is a known

regulator of the cytoskeleton (Shiina *et al* 1994, Veremieva *et al* 2010). One explanation could be that the elevated levels seen in the fibrosarcoma 188 samples maybe due to some form of pharmacological conflict elicited by this CA-4-P resistant tumour model.

The Complement system exhibits regulatory influences on host immune, inflammatory processes. Activation of this complex cascade of biological events is triggered via 3 main activation routes; the alternative, classic, and lectin pathways. (Nunez-Cruz *et al* 2012) Complement C3 is the key activator of the 3 main routes previously mentioned. Studies have shown that increased Complement anaphylatoxin levels have been detected in the peritoneal cavity fluid of ovarian cancer patients (Bjorge *et al* 2005). In vivo studies by Nunez-Cruz *et al* (2012) used complement deficient mouse models crossed with epithelial ovarian cancer susceptible mice. One of the key findings in this article was that tumour growth was either absent or greatly retarded in the offspring, compared to the wild- type. Thus indicating the importance of Complement C3 in tumour progression. Figure 4.22a shows that the iTRAQ ratio responses from 0.5h, 6h and 24h are reduced after CA-4-P treatment with a slight increase emerging from the 72h time point.

Plectin, not identified in the fibrosarcoma 120 data set is shown to have a greatly reduced response relative to the control in Figure 4.22b. Plectin is has been shown to be present in high levels in cancers such as head and neck squamous carcinoma and correlates with poor patient survival (Katada *et al* 2012). The ITRAQ data presented here show good agreement with the findings presented in Chapter 3 where MALDI-MSI and LC-ESI-MS/MS label free results displayed increased Plectin levels in the Control fibrosarcoma 188 samples with a dramatic decrease evident over the 0.5h-72h time course. Hence a decrease in Plectin expression, a protein associated with tumour aggressiveness, does therefore appear to be a response to CA-4-P dosage.

The protein lists reported here were generated using ProteinScape applying fixed modification Carbamidomethyl (C), and filtered using a Mascot score ≥ 28 which yielded 45 protein identifications. The protein lists generated using the alternative modification parameters; fixed, variable filtered and variable gave the following proteomics outcomes:

fixed – 318 protein identifications, variable filtered - 51 protein identifications, variable – 1088 protein identifications.

4.5.4. Analysis with Scaffold Q+

A screen shot of a protein list generated in Scaffold proteomic software from the LC-MALDI-MS/MS results is shown in Figure 4.23. The corresponding list generated after applying iTRAQ quantitative 3Q+ using the parameters detailed in section 4.4.4.

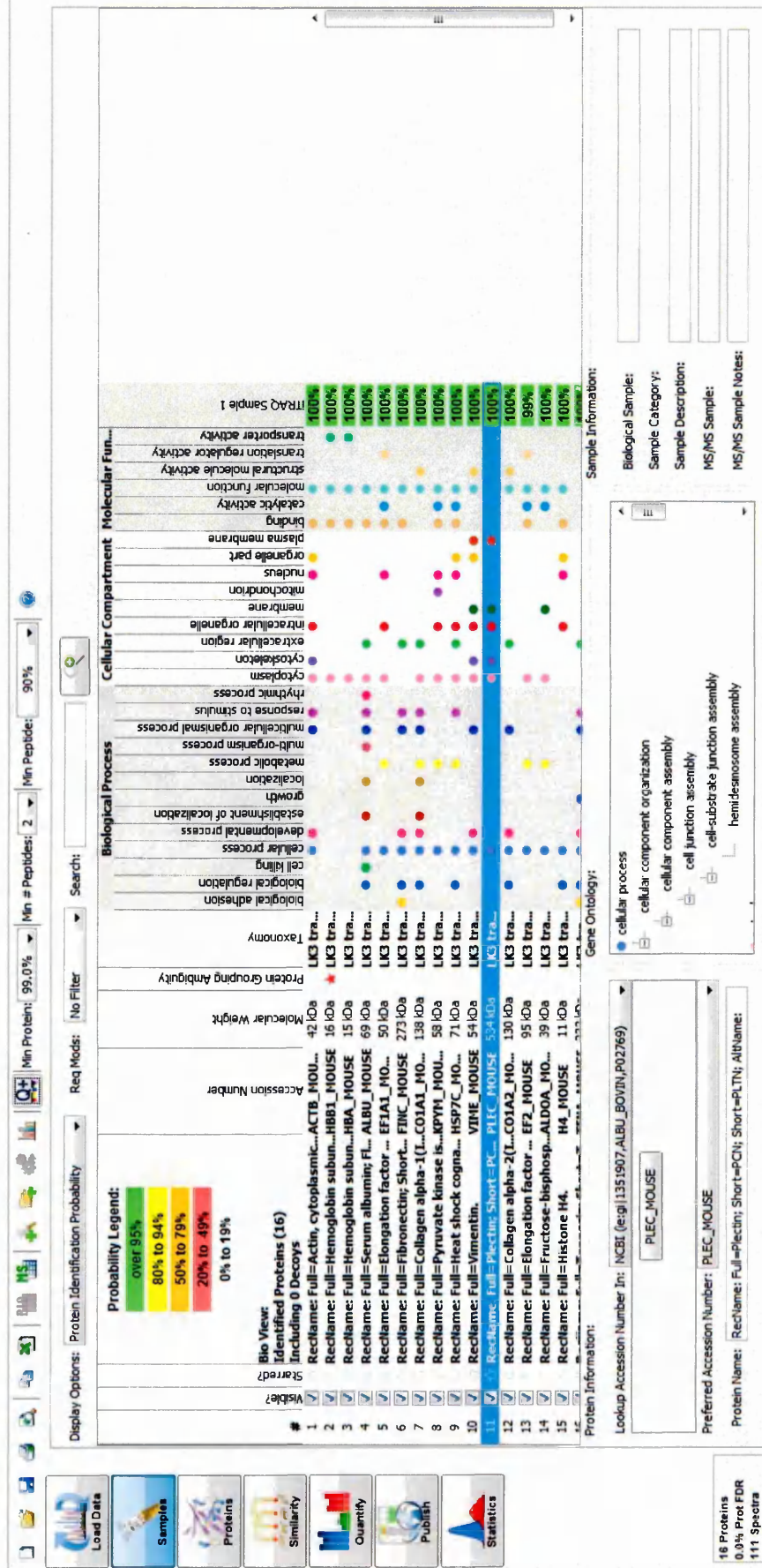


Figure 4. 23: Scaffold proteomic software used for ITRAQ analysis. An example is shown of the protein list from the LC-MALDI-MS/MS fibrosarcoma 188 data, shownis information regarding biological process, cellular compartment and molecular function.

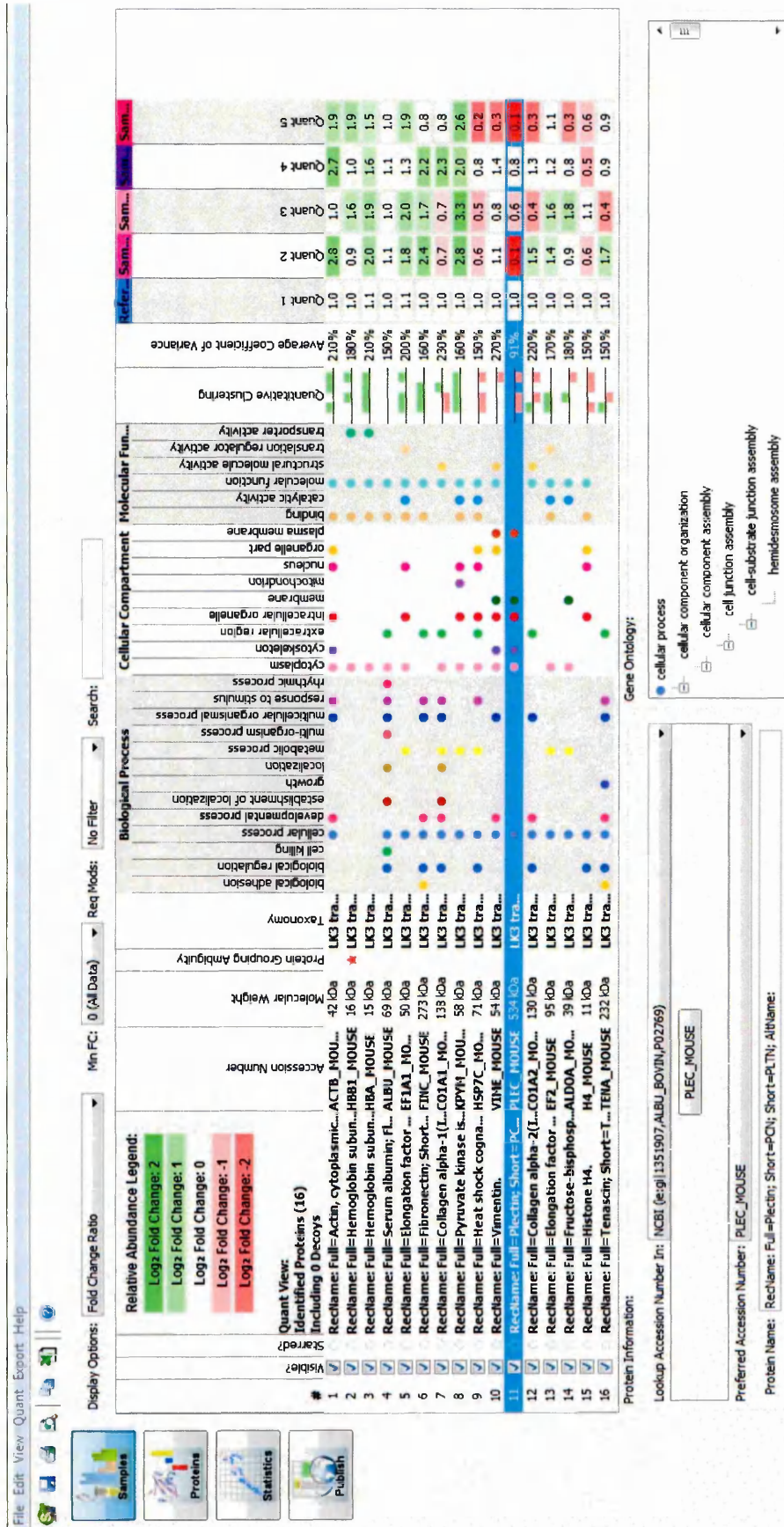


Figure 4. 24: Scaffold proteomic software with the employment of 'Q+' function for iTRAQ ratio analysis. In addition to gene ontology information the fold change ratio throughout the time course samples can be observed; Quant 1 (Control) - Quant 5 (72h post CA-4-P, fibrosarcoma 188).

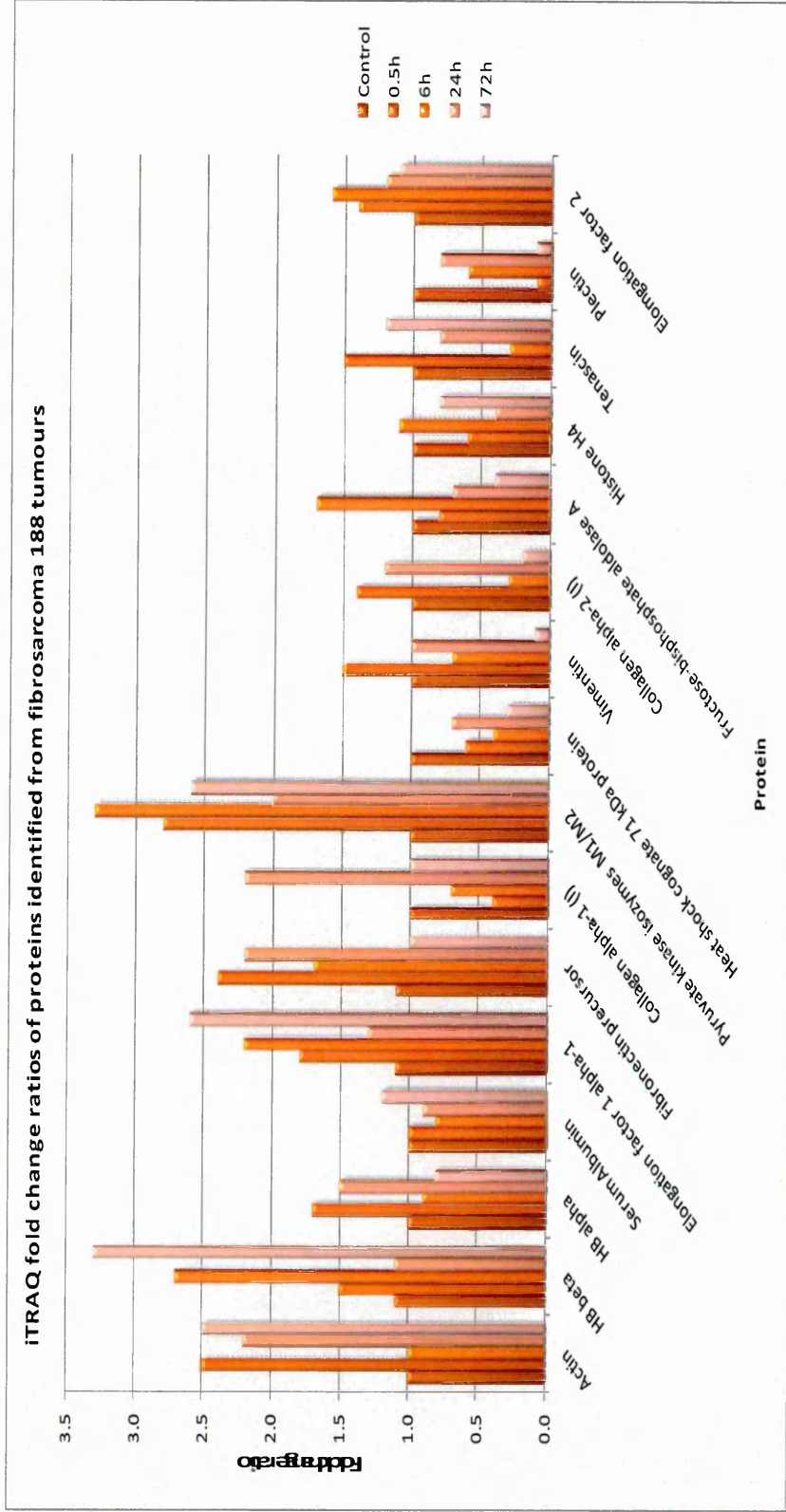


Figure 4. 25: iTRAQ fold change ratio using fibrosarcoma 188 tumour digest samples. Proteins response throughout the fibrosarcoma time course, Control – 72h post CA-4-P.

The fold change ratios which can be seen in Figure 4.24 are displayed in Figure 4.25.

To analyse the data from fibrosarcoma 188 models the search parameters applied by Scaffold proteomic software using the .dat file from fibrosarcoma fixed search gave information for 16 proteins (Figure 4.25). The subsequent data shows examples of protein sequences found and spectra used for protein identification and relative quantitation by Scaffold 3 Q+ using LC-MALDI-MS/MS. The following proteins detailed are; Vimentin, Hb subunit beta, Pyruvate kinase isozymes M1/M2, Tenascin and Fibronectin precursor. The rationale for selection of these proteins was to assess differences and similarities in the Scaffold 3 Q+ results in the fibrosarcoma 120 model and observe proteins which did not appear in the VEGF 120 samples.

The Vimentin response observed by the resistant 188 model in Figure (4.26) bears some similarity to the study mentioned by Handra-luca et al (2011) reporting elevated Vimentin in pancreatic neoplasms. Although levels are still low in the 72h post CA-4-P sample a considerable increase is evident from the 6h and 24h time points, not observed in the earlier Vimentin VEGF 120 Log₂ normalised intensity graph (Figure 4.9).

Hb subunit beta in Figure 4.26 does not exhibit a steady haemorrhagic response but levels still remain increased toward the final 72h time point.

Results displayed in Figure 4.25 of Pyruvate kinase isozymes M1/M2 show greatly increased fold change ratios when compared to the equivalent fibrosarcoma 120 graph in Figure 4.8. The fibrosarcoma 188 6h value shows over a 3 fold increase along with a 2.5 fold increase in the 72h for Pyruvate kinase isozymes M1/M2, opposed to the 120 model which only shows a 1.8 fold in the 24h. Pyruvate Kinase isozyme M2 is found in tumour cell and proliferating tissues alike and hypoxia-inducible factor 1 is said to play a role in its induction (Ye *et al* 2012).

Glycoprotein Tenascin, is seen in the fold change ratio graph (Figure 4.25). Tenascin appears to exhibit a 'peak-trough-peak' response throughout the timecourse. Due to the non identification of this protein in the fibrosarcoma 120 data set, it is difficult to validate or comment on this reaction. Tenascin is reported to promote metastasis (Minn *et al* 2005, Oskarsson *et al* 2011). Studies by Oskarsson *et al*(2011) link Tenascin expression to the aggressiveness of breast cancer cells and their ability to further produce lung metastases. Considering the latter could the last 'peak' previously mentioned be a feature supportive of the 'switch back to viability concept' overtime after treatment.

Fibronectin precursor is known to bind to Tenascin, interestingly when comparing the fold change responses (Figure 4.25), both proteins appear to have an inverse fold change

relationship; Tenascin 'peak-trough-peak', Fibronectin 'trough-peak-trough'. Further study is needed to confirm and comprehend this trend of protein-protein interaction.

HBB1_MOUSE (100%) 15,840.2 Da

RecName: Full=Hemoglobin subunit beta-1; AltName:

M V H L T D A E K A A V S C L W G K V N S D E V G G E A L G R L L V V Y P W T Q R Y F D S F G D L S S A S A I M G N A K
 V K A H G K K V I T A F N D G L N H L D S L K G T F A S L S E L H C D K L H V D P E N F R L L G N M I V I V L G H H L G
 K G F T P A A Q A A F Q V V A G V A T A L A H K Y H

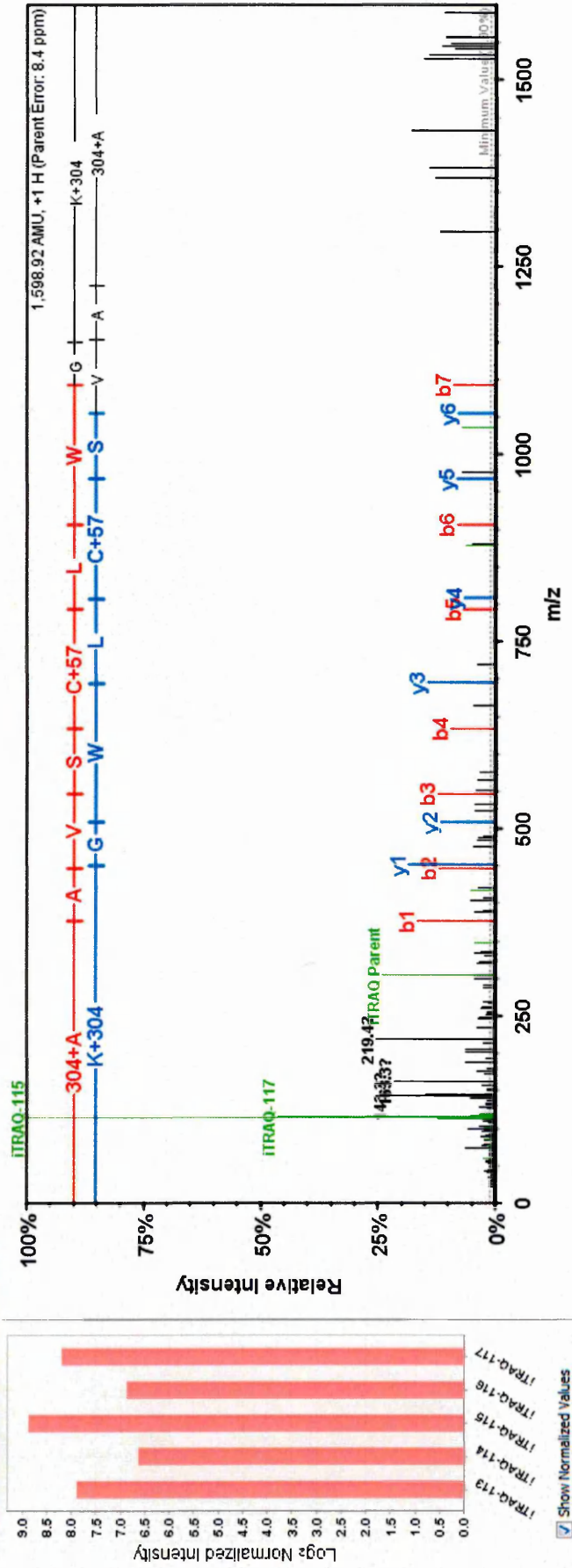
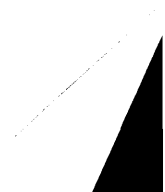


Figure 4. 27: Haemoglobin subunit beta-1 peptides identified, response bar graph and related MS/MS spectrum from iTRAQ LC-MALDI-MS/MS Fibrosarcoma 188 tissue. iTRAQ 113-117 refers to iTRAQ labelled control-72h post CA-4-P.

4.5.5 Protein relationship mapping of Fibrosarcoma 188 data using STRING

9.0

The proteomic networks to follow will feature the same format as the protein relationship analysis in section 4.4.5.



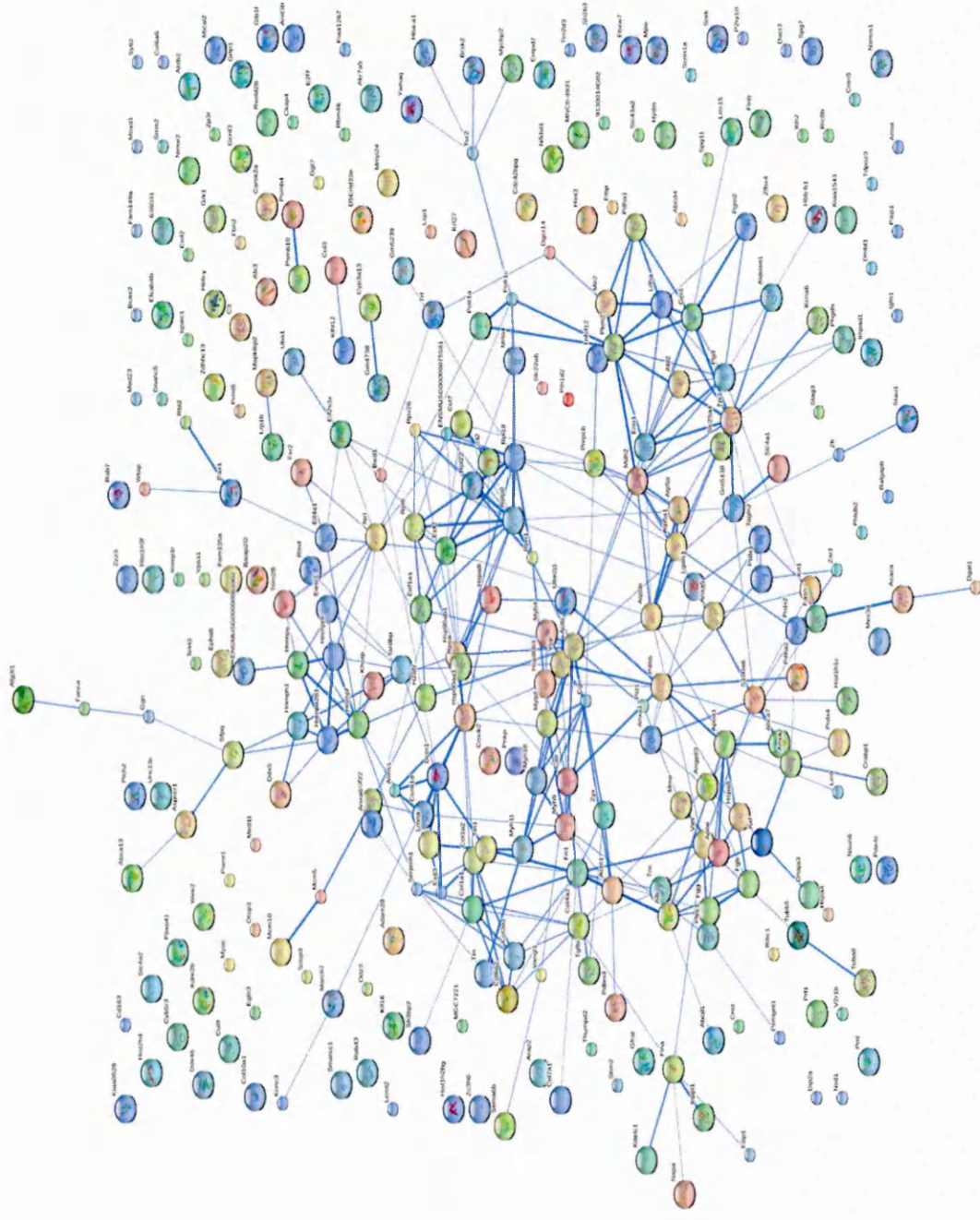


Figure 4. 31: iTRAQ Fixed modification search using Fibrosarcoma 188 tumours, visualised by STRING 9.0 (Confidence view).

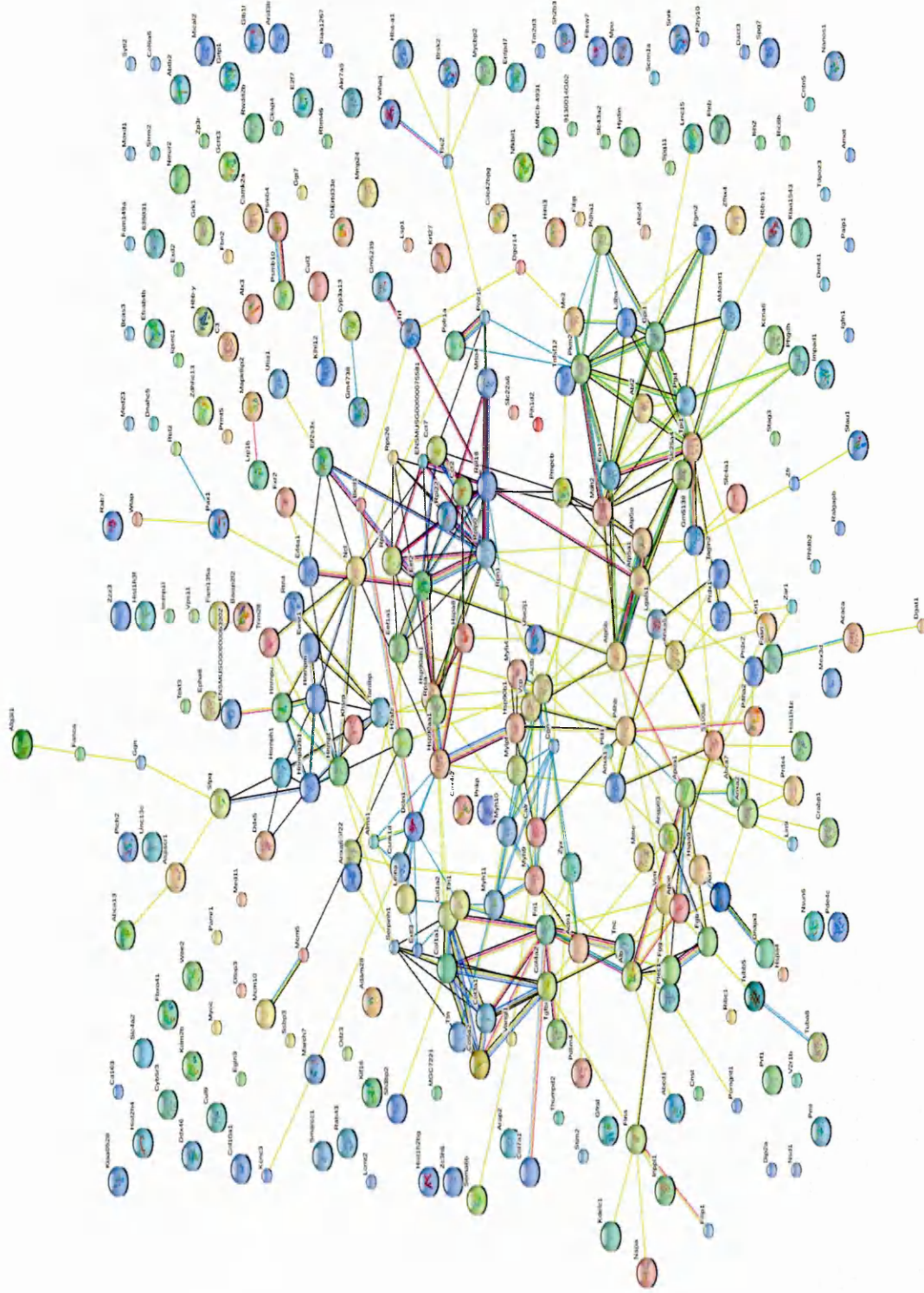


Figure 4. 32: ITRAQ Fixed modification search using Fibrosarcoma 188 tumours, visualised by STRING 9.0 (Evidence view).

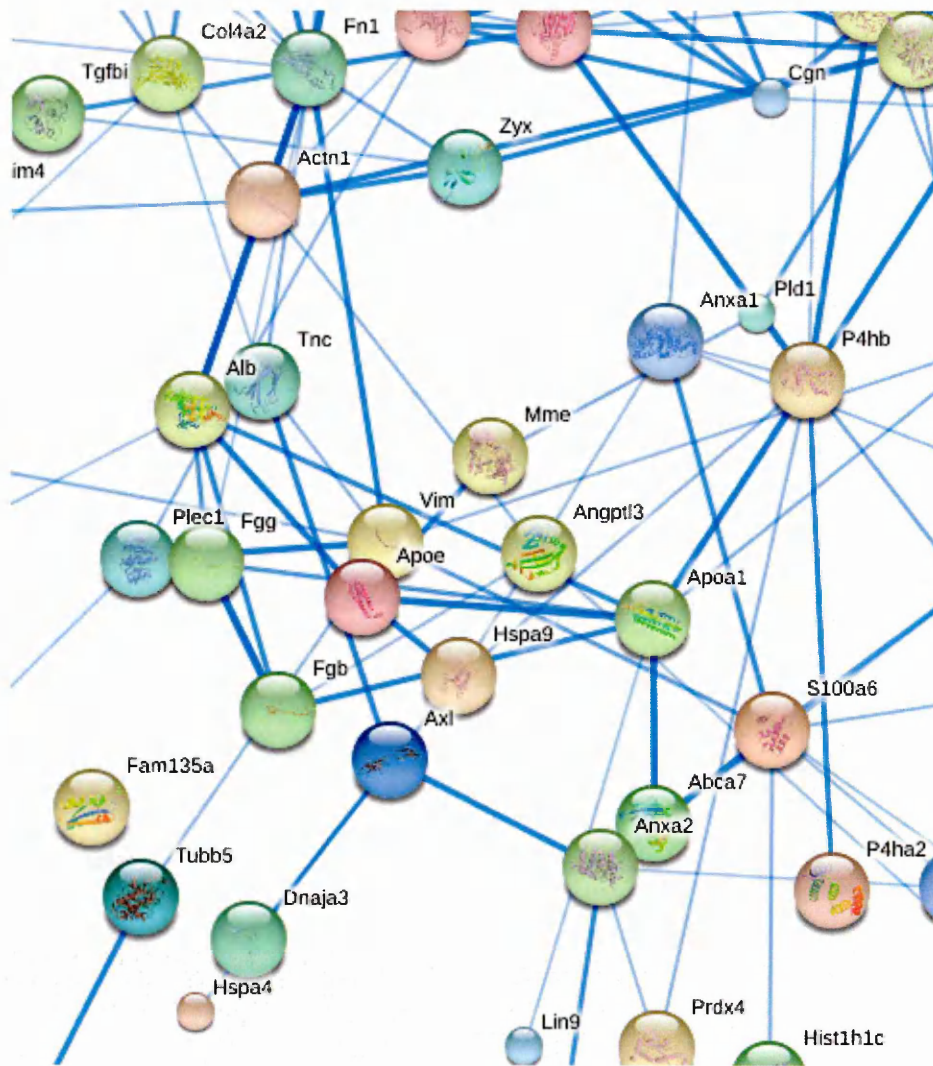


Figure 4. 33: Zoomed in region of a fixed modification search, iTRAQ fibrosarcoma 188 samples, visualised through STRING 9.0.

Vimentin, Tenascin and Plectin are all grouped together in this zoomed region from Figure 4.33. The roles of this trio all involve tumour progression through individual unique mechanisms as discussed earlier in this chapter. A clear link can be seen with Tenascin and Fibronectin (fn1) to support findings in the literature reported back in section 4.5.4.

Actin has associations either directly or indirectly with Vimentin, Tenascin and Plectin to ascertain their roles in actin dynamics and general integrity and structural reorganisation. Another strong association with Actin is the Zyxin Gene anadhesion plaque protein further linking the latter to a Heat shock 90 containing group (not shown) via the Cingulin gene (<http://string-db.org/>). Cingulin is thought to be involved with cell junction permeability.

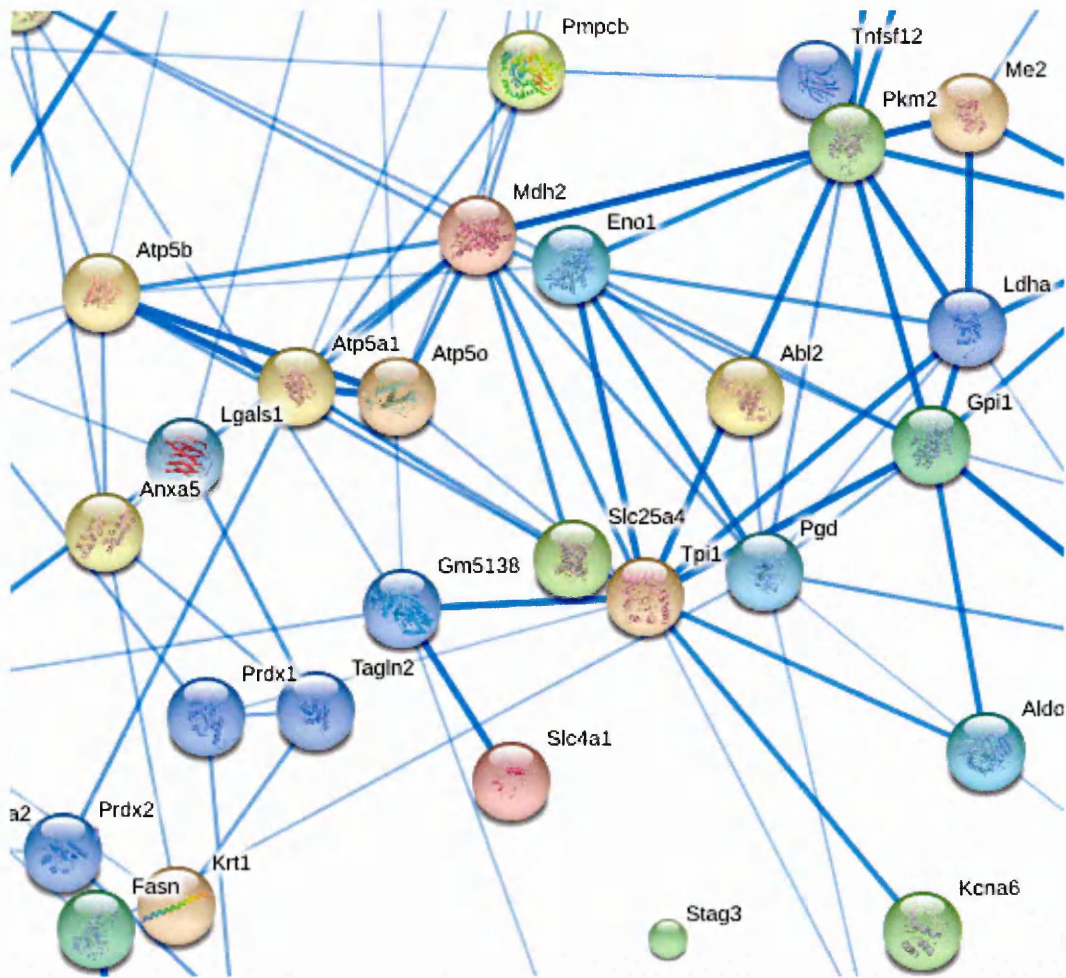


Figure 4. 34: iTRAQ fibrosarcoma 188 zoomed in region of a fixed modification search, visualised through STRING 9.0.

This section of the STRING fixed fibrosarcoma 188 search displays most of the proteins seen in the 120 STRING results; Galectin, Annexin A5, Peroxiredoxin, Enolase 1. A protein in Figure 4.34 however does not feature in the fixed fibrosarcoma 120 STRING results, this being Glucose-6-phosphate isomerase (Gpi1). It has strong associations with hypoxia tolerance regulator Enolase 1, interestingly Gpi1 is known to function as a ‘tumour-secreted cytokine’ and features in angiogenesis encouraging endothelial cell motility (Ahmad *et al* 2011).

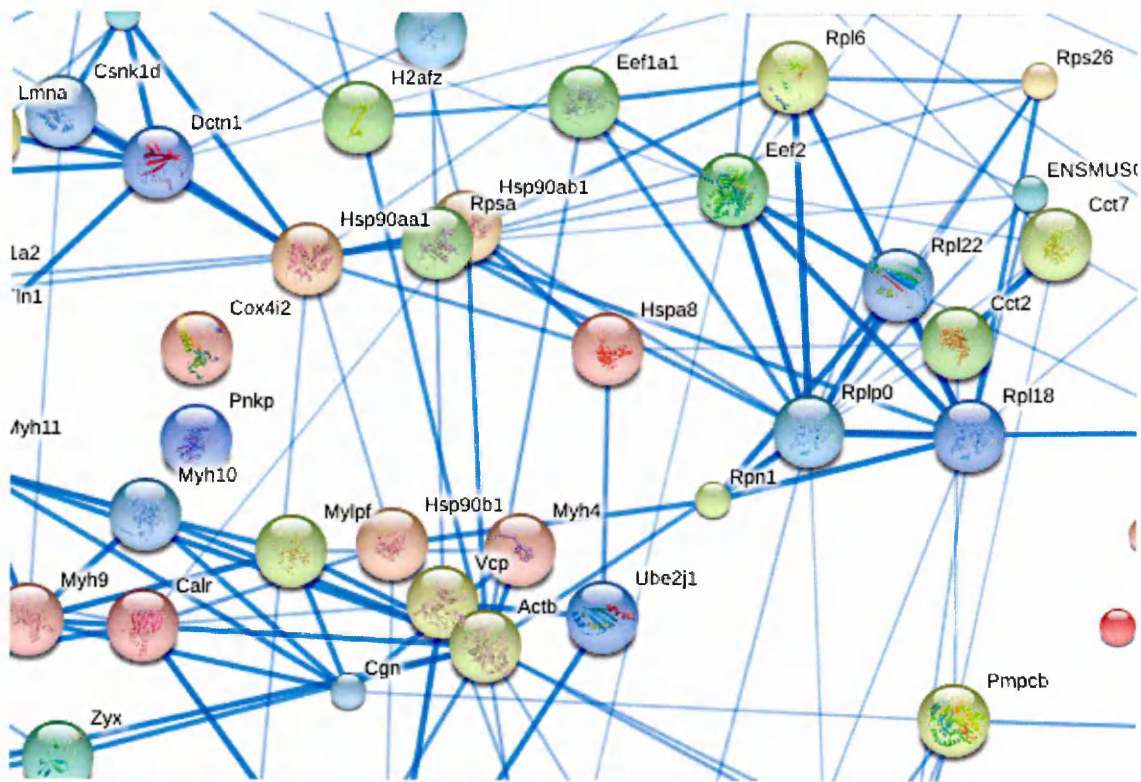


Figure 4. 35: iTRAQ fibrosarcoma 188 zoomed in region of a fixed modification search, visualised through STRING 9.0.

Many proteins that feature in Figure 4.35 are already familiar i.e. Heat shock proteins, Calreticulin, Elongation factor 1 alpha. Perhaps disregarded is the important connection between Histone 2A and Actin. Although widely acknowledged and easily detected in both MALDI profiling and imaging, this connection could be regarded as a marker of the re-organisational transition towards tissue necrosis during anti-cancer treatment. Numerous associations can be clearly seen branching from these links downstream from Hsp 90 and Elongation factor 1 alpha.

4.5.6 Protein dose response relationship analysis using String 9.0

The following data presented here analyses the protein dose response relationships and associated pathways using the iTRAQ results from fixed medication searches, employing a filter score of ≥ 28 . Fibrosarcoma 120 and 188 lists were prepared for import into proteomic pathway software String 9.0 to observe proteins that were flagged either to exhibit a marked increased expression or decreased expression. This proteomic information was taken from the original iTRAQ spreadsheets featured in Figures 4.4 and 4.21. The normalised values were highlighted in either green, yellow or red indicating response relative to the control either increased, no change or decreased respectively.

4.5.6.1 iTRAQ Fibrosarcoma 120 dose relationship results using String 9.0

The protein pathways featured in Figure 4.36 show the proteins that were found to demonstrate either increased or decreased responses in the particular treatment sample.

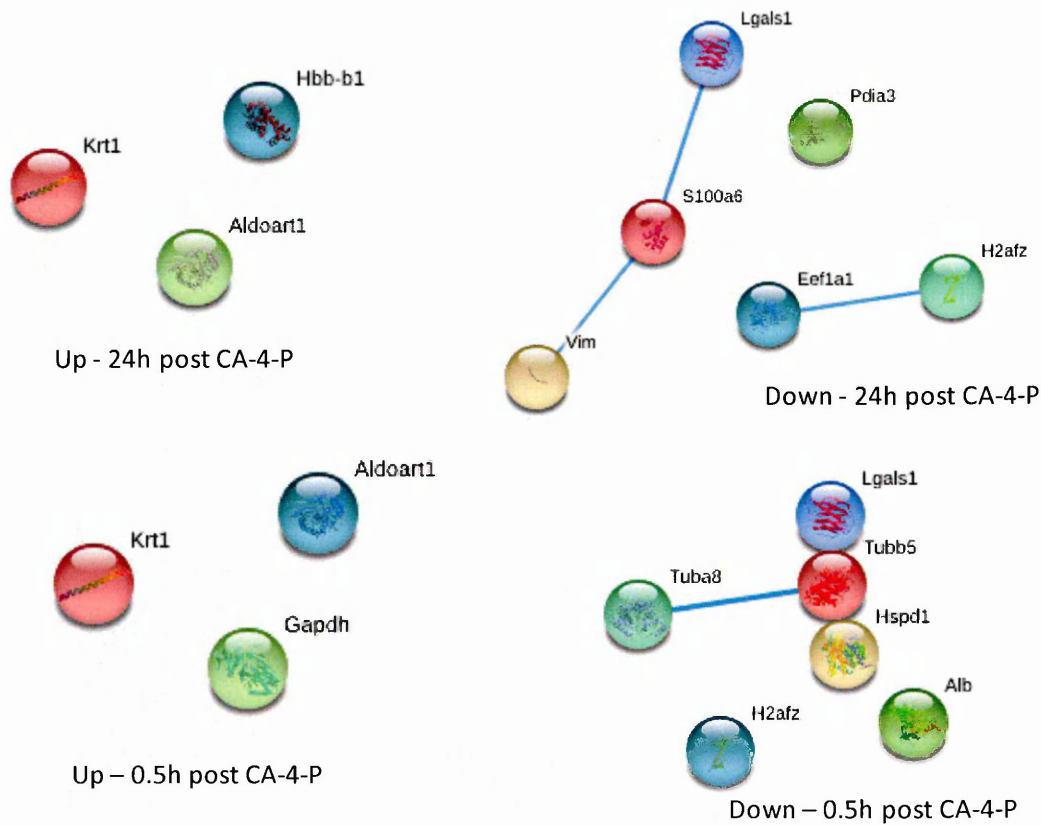


Figure 4. 36: iTRAQ proteomic response results using a Fibrosarcoma 120 treatment timecourse. Proteins are shown to either increase or decrease relative to the Control fibrosarcoma tissue, relationship links are shown between the proteins that have strong biological associations with each other.

In Figure 4.36 the increased proteins (Up – 24h post CA-4-P, Up – 0.5h post CA-4-P) displayed do not show any associations with each other. However both 0.5h and 24h share increased Keratin, type II cytoskeletal 1 (Krt1) and Fructose-bisphosphate aldolase A (Aldoart1). Mentioned earlier in this Chapter, Krt1 is thought key player in the mechanism of multidrug resistance in some cancers (Tang *et al* 2012). The unusual increase in GAPDH as previously discussed is seen here in the 0.5h.

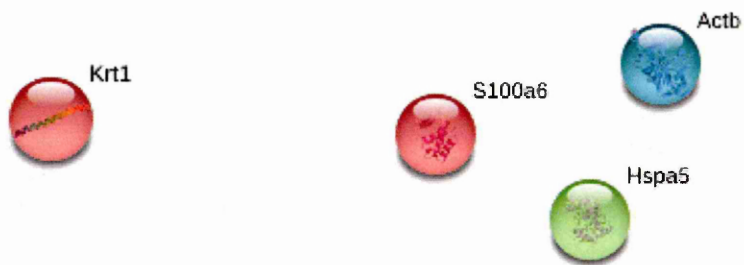
Aldoart1 is a component of the glycolytic pathway and increased expression of this enzyme is found in many cancers including cancer of the lung, kidney and cervix (Mhawech-Fauceglia *et al* 2011,. Takashi *et al* 1990,. Oijika *et al* 1991). Perhaps increased response of Aldoart1 here is an

indicator of a tumour survival strategy against CA-4-P treatment. Elevated levels of this enzyme could be indicative of a high glycolytic rate, a key factor in tumour survival and metabolism (Saw 2006, Beckner *et al* 1990).

The proteins that are decreased as a result in the 0.5h time point in Figure 4.36 include Tubulin alpha (Tuba8) and Tubulin beta-5 chain (Tubb5), linked by a strong association. This decrease could be as a result of disturbance due to the vascular disrupting agent. Although no direct link is seen between Tubb5 and adjacent proteins Galectin-1 (Lgals1) and Heat shock protein 60 (Hspd1), a close positioning is observed. The latter could echo the morphological transitions underway by Tubulin hence induction of Hspd1 and decrease in Lgals1 which mentioned previously to be involved in cell proliferation, apoptosis and differentiation (Banh 2011).

The 24h decreased proteins in Figure 4.36 show a greater degree of protein-protein interaction with triplet links between Lgals1, Calcyclin (S100a6) and Vimentin (Vim) and a further linkage between Elongation factor 1-alpha 1 (Eef1a1) and Histone H2A.V (H2Afz).

S100a6, involved in restructuring of the cytoskeleton along with Vimentin and Lgals1 are decreased in the 24h and appear to be retarded by the effects of CA-4-P. Low levels of Eef1a1 in this CA-4-P susceptible tumour model reflect that at 24h the tumour tissue is almost totally necrotic.



Up – 0h post CA-4-P

Down – 0h post CA-4-P

Figure 4. 37: Fibrosarcoma 120 proteomic response using String 9.0.iTRAQ increased and decrease protein response for tumour time point 0h post CA-4-P administration.

In the case of the fibrosarcoma 120 0h time point there was only one marked early increase, this being Keratin, type II cytoskeletal 1 (Krt1) (Figure 4.37). This remained elevated throughout the later time point as shown in Figure 4.36. No associations were seen in the corresponding decreased set of proteins in the 0h post CA-4-P. 78 kDa glucose-regulated protein (Hspa5, Grp78) remains low in this early time point and would be expected to be elevated here in the later time points. However the threshold levels determined in the spreadsheet featured in Figure 4.4 did not highlight the values to be included in the increased group of proteins. Upon close observation of the spreadsheet the values within the 'no change' (yellow) bracket for this protein did show a gradual increase throughout the time points.

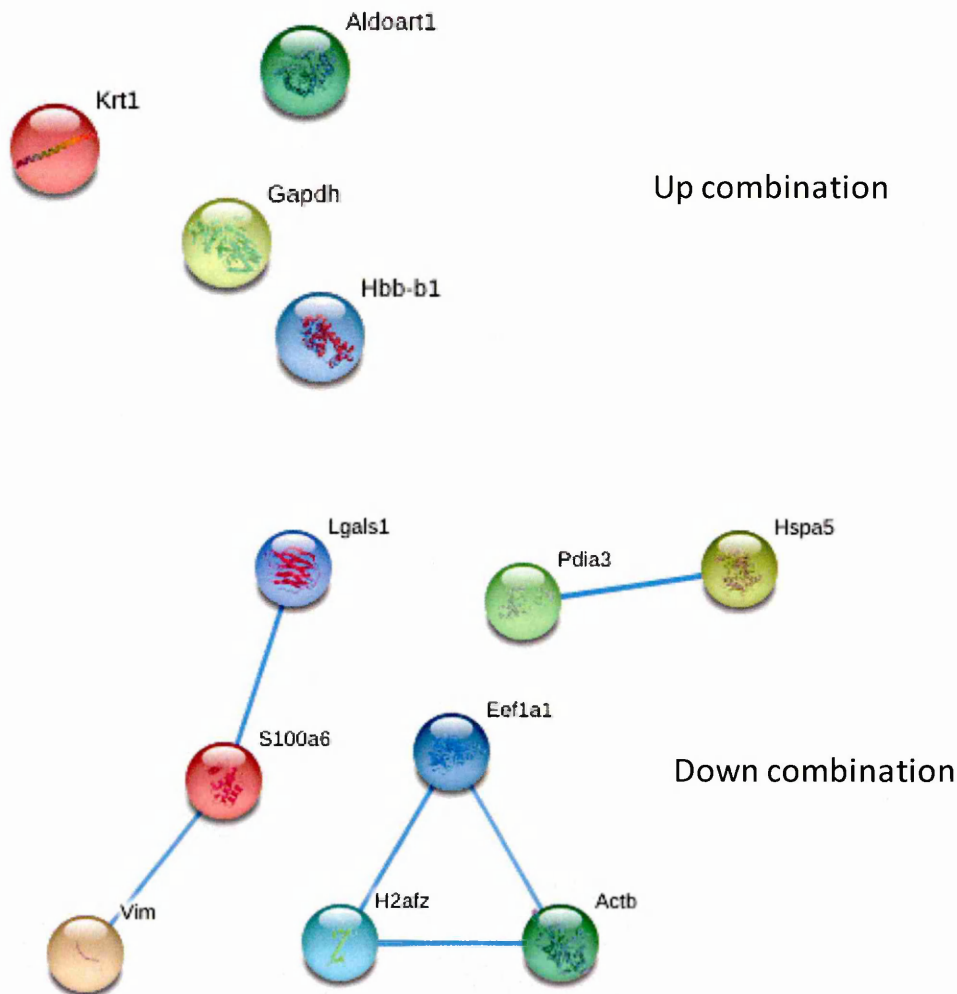


Figure 4. 38: iTRAQ combinations of fibrosarcoma 120 increased and decreased proteins. The protein relationships in Figure 4.38 are a representation of combined responses throughout the time points previously discussed.

In summary of the combined responses seen in Figure 4.38, the increased protein combination depicts the haemorrhagic pharmacological response, the potential multidrug strategy of Krt1, an uncharacteristic influence on GAPDH and evidence of a need for tumour cell survival due to the elevated levels of glycolytic enzyme Aldoart1. Amongst the proteins shown to decrease in Figure 4.38 is a triangular triplicate linkage between Actin, Histone 2A and Eef1a1. This appears to reflect the disrupting effects post CA-4-P treatment. The combination seen here encompassing the transitional changes in cellular integrity and attempts by the drug to retard growth and induce necrosis. The same effect is true for the other linear trio of proteins with the decrease of Lgals1, S100a6 and Vimentin. Links between Protein disulfide-isomerase A3 and Hspa5 imply evidence of the stress response and apoptotic processes respectively. Down

regulation of Protein disulfide-isomerase A3 was only seen in the 24h time point indicating that extensive tissue necrosis was already present.

4.5.6.2 *i*TRAQ Fibrosarcoma 188 dose relationship results using String 9.0

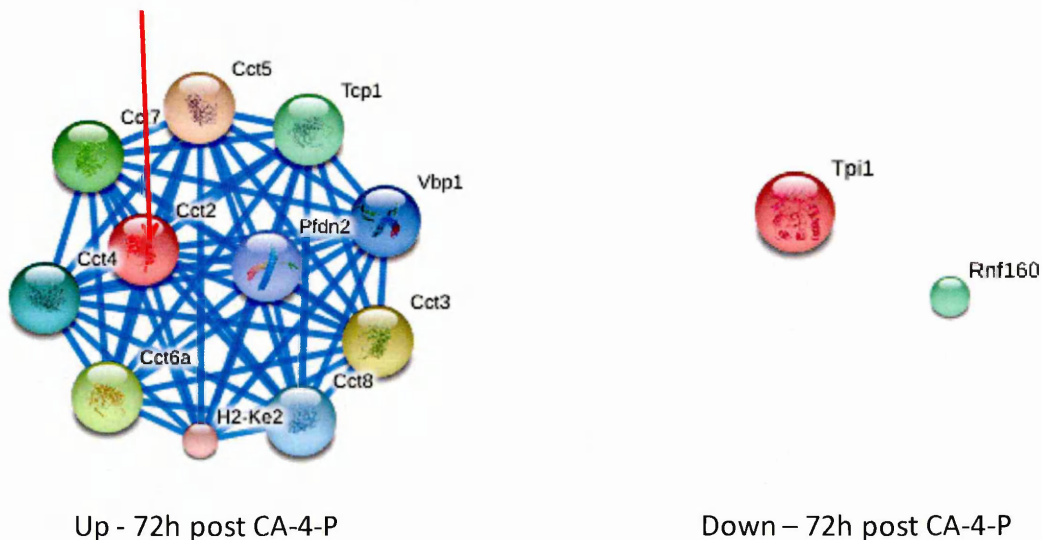


Figure 4. 39: *i*TRAQ proteomic response results using a Fibrosarcoma 188 treatment time course. Predicted functional partners are shown for increased Cct2 (indicated by the arrow) in the 72h time point and proteins that were decreased in the 72h post CA-4-P sample.

In Figure 4.39, the T-complex protein 1 subunit beta (Cct2) is shown with predicted functional partners which include fellow chaperone proteins. Cct2 is known to have actin/ tubulin re-organisational properties (<http://string-db.org/>). This increase could reflect a ‘switch back to viable tissue’ strategy with an army of chaperones which favour cell proliferation and tumour survival. RING finger protein 160 (Zinc finger protein 294, Rnf160) and Triosephosphate isomerase (Tpi1) are shown to decrease in the 72h time point. No known links are shown between the two proteins, Rnf160 can be implicated in cell death and Tpi1 involved in glycolysis (Orosz *et al* 2006, <http://www.uniprot.org/>).

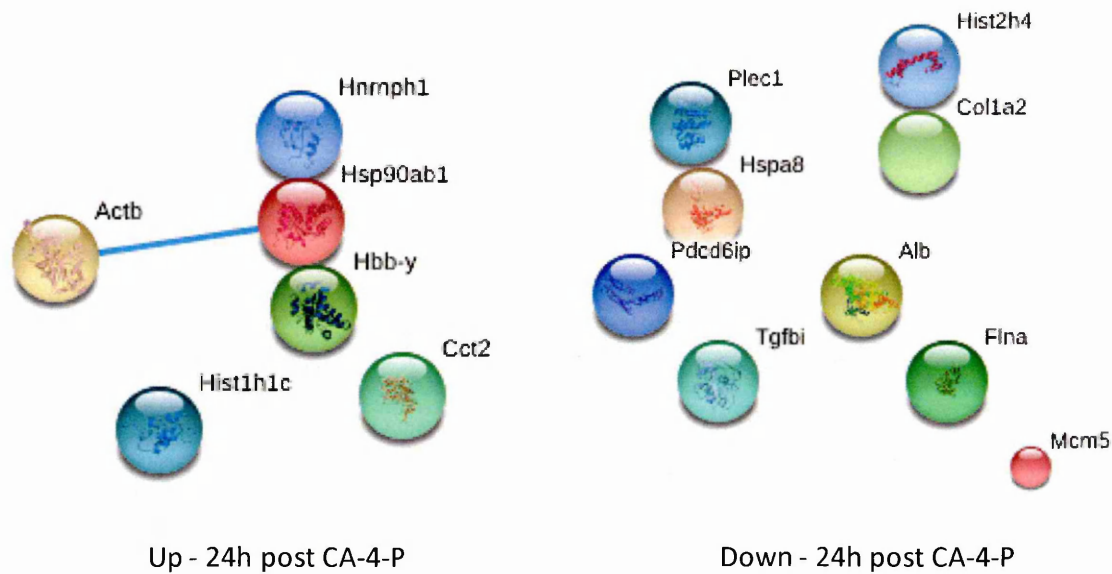


Figure 4. 40: iTRAQ proteomic response results using a 24h post CA-4-P Fibrosarcoma 188 treatment. The proteins shown here depict the responses seen that were either increased or decreased as a result of CA-4-P administration.

In Figure 4.40 there is a strong link evident connecting Actin and Hsp90 flanked by Hbb-y and Heterogeneous nuclear ribonucleoprotein H (Hnrnp1).

The notable increase in 24h Hsp90 is seen in the immunohistochemical/ MALSI-MSI in Chapter 3, where abundant appears to reach saturation point. Elevated levels of Hsp90 could be explained by the direct link here to Actin. The changes in Actin dynamics due to the drug could indeed have a positive effect on Hsp90 expression, due to the need for protection against the misfolding of Actin. Cct2 is also seen here to be increased as shown in the 72h (Figure 4.39) response, again involved in Actin re-organisation. The Histone H1 increased response could be another indication of architectural remodelling of the tumour cells. The Haemoglobin subunit epsilon-Y2 (Hbb-y) is again indicative of vascular disruption with Hnrnp1 having mRNA transcriptional influence on Hsp90.

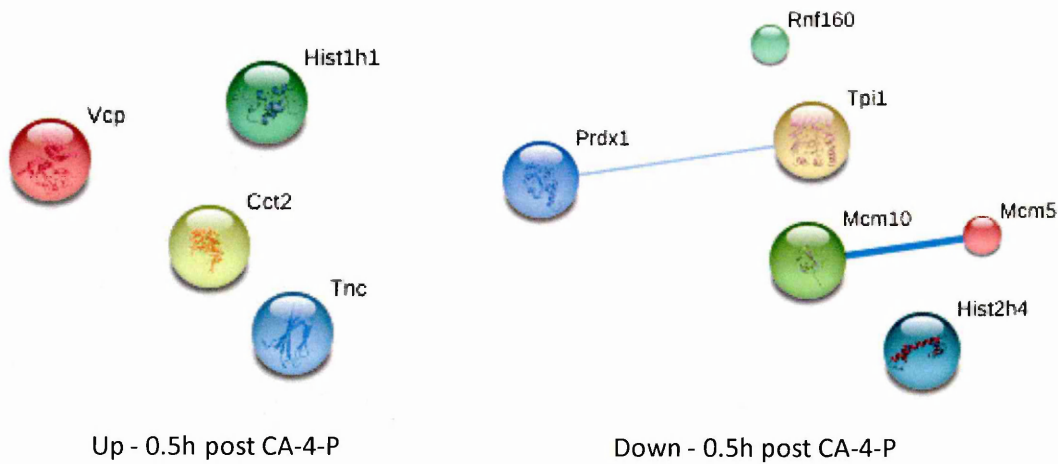


Figure 4. 41: iTRAQ proteomic response results using a 0.5h post CA-4-P Fibrosarcoma 188 treatment. The proteins in the 'Up' 0.5h time point do not have any associations here, in the 'Down' group a strong associative link is present between Mcm10 and Mcm5 with a weaker relationship clear between Prdx1 and Tpi1.

The protein corresponding to Tenascin (Tnc) in Figure 4.41 is shown to be increased in the 0.5h time point. This protein was discussed earlier in this Chapter, said to be involved in the aggressiveness of breast cancer cells and their ability to further produce lung metastases (Oskarsson *et al*2011). The other proteins in this group have no association here, but all seem to be a sign of an active proliferating tissue, characteristic of this CA-4-P resistant tumour model.

There are 2 linkages seen in Figure 4.41, a strong associative link is present between Mcm10 and Mcm5 and a weaker relationship clear between Prdx1 and Tpi1.

The precise function of Protein MCM10 homolog (Mcm10) is said to be unclear, it is thought to play a role in DNA replication and the prevention of DNA damage, but is reported to perform in different ways dependent on the particular organism (Ricke and Bielinsky 2004, <http://string-db.org/>). DNA replication licensing factor MCM5 (Mcm5) is known to have similar functions to Mcm10 (Schultz *et al* 2009).

There is a link between Peroxiredoxin-1 (Prdx1) and glycolytic enzyme Triosephosphate isomerase (Tpi1). As mentioned previously in this Chapter, elevated expression of the *PRDX1* gene is said to act as a protective mechanism against H₂O₂ induced apoptosis (Kalinina *et al* 2012). The level here is shown to be markedly decreased which could relate to the nature of the resistant tumour type, where at this early treatment time point there is no requirement as yet for protective mechanism against H₂O₂ induced apoptosis.

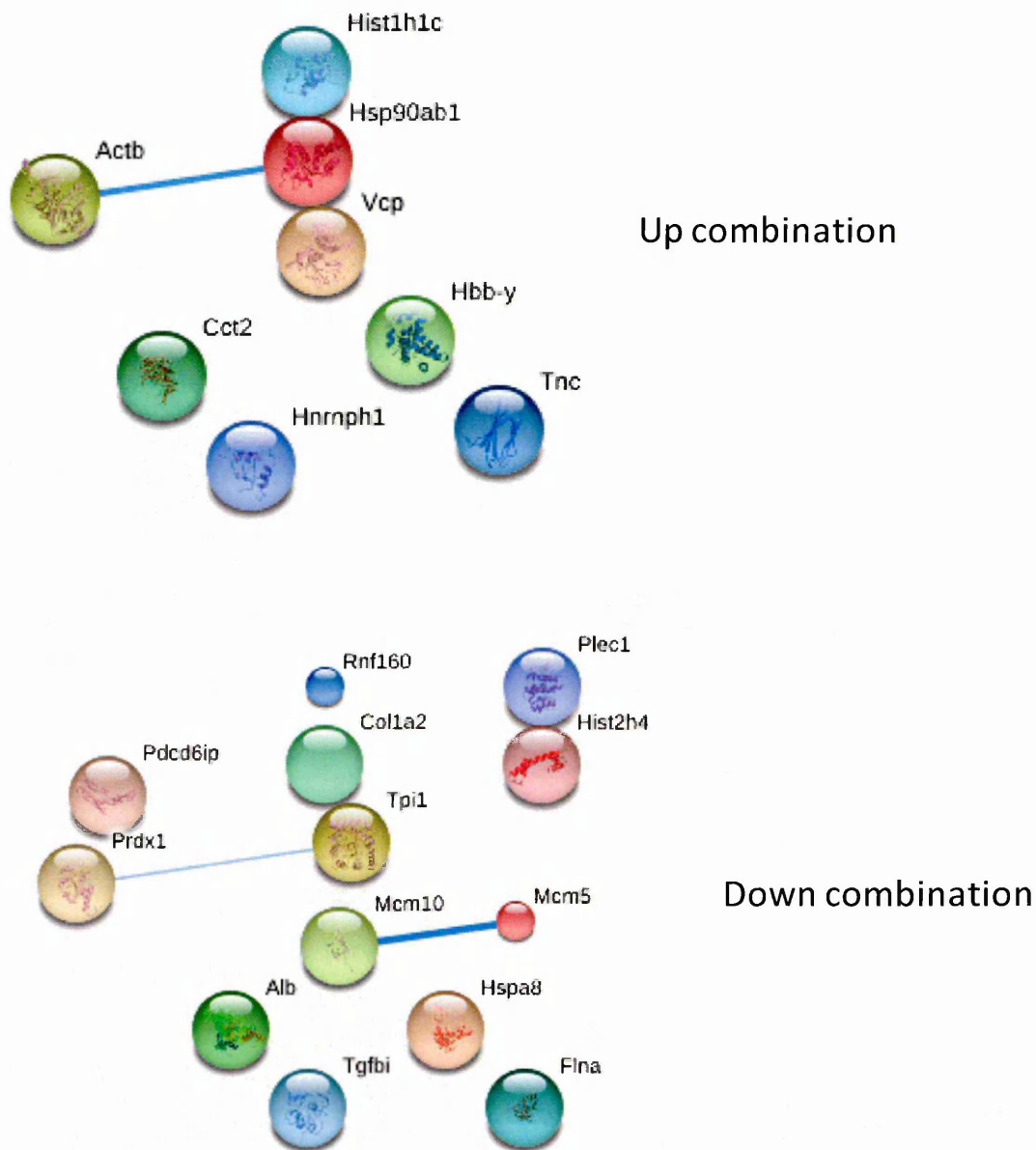


Figure 4. 42: iTRAQ combinations of fibrosarcoma 188 increased and decreased proteins. The protein response relationships in Figure 4.42 are a representation of combined responses throughout the time points previously discussed in the iTRAQ fibrosarcoma 188 treatment time points.

To summarise the combination of groups seen in Figure 4.42, the 'Up' combination of proteins similarly to those in the Fibrosarcoma 120 proteins includes increased Hb, however this is where the similarities cease. Tnc is now seen, a protein observed in aggressive cancers and along with Hsp90, Cct2 gives the notion of a more active, drug resistant class of tumour tissue.

4.5.7 Relation of MALDI-MSI to iTRAQ proteomic response

The relation of MALDI-MSI to other complementary proteomic results aims to authenticate the protein induction responses observed. Figure 4.40 demonstrates some of the proteins that have featured in the previous chapters in the format of an iTRAQ ratio response graph as seen in Figure 4.22a/b.

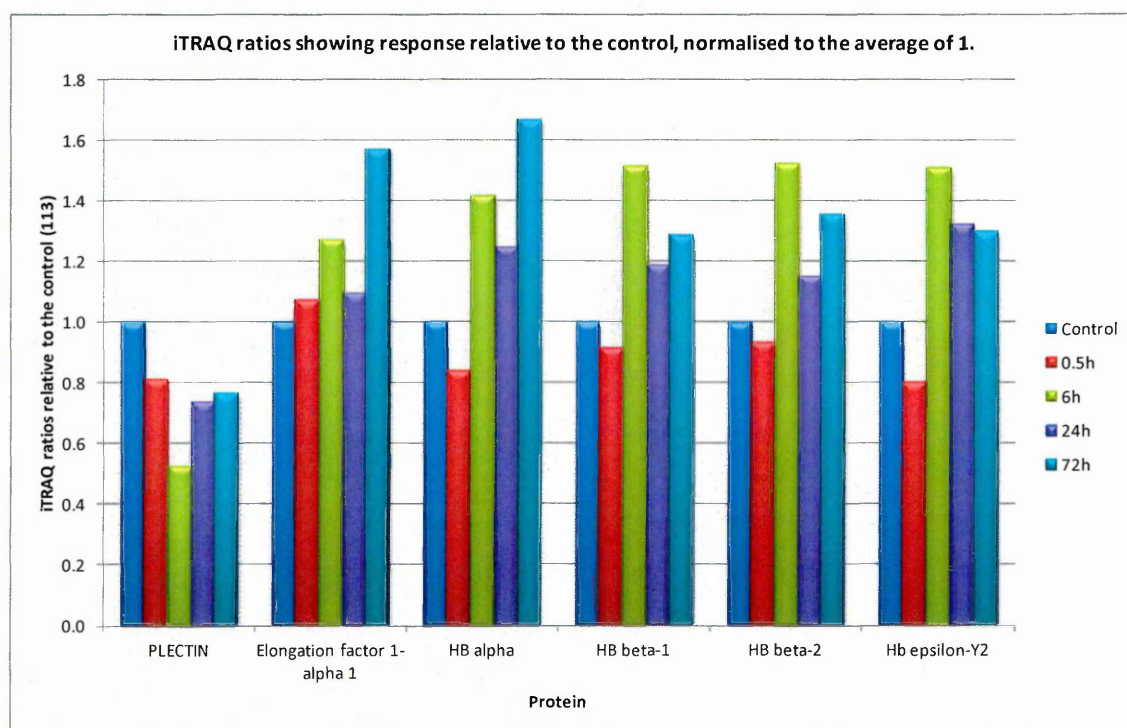


Figure 4. 43: Bar graph showing protein response relative to the control (113) normalised to an average of 1, using fibrosarcoma 188 tissue. The responses shown here depict a decreased expression if values are below 1 and increased expression if values are above 1 on the bar graph.

Figures 4.44 and 4.45 show MALDI-MSI images which are in agreement to the iTRAQ responses of Plectin and Hb subunit alpha seen in in Figure 4.34.

The time course images shown here in Figure 4.44 and Figure 4.45 match the response exhibited in the iTRAQ results graph (Figure 4.22a/ 4.22b) and label free quantitative LC-ESI-MS/MS results for plectin in Chapter 3.

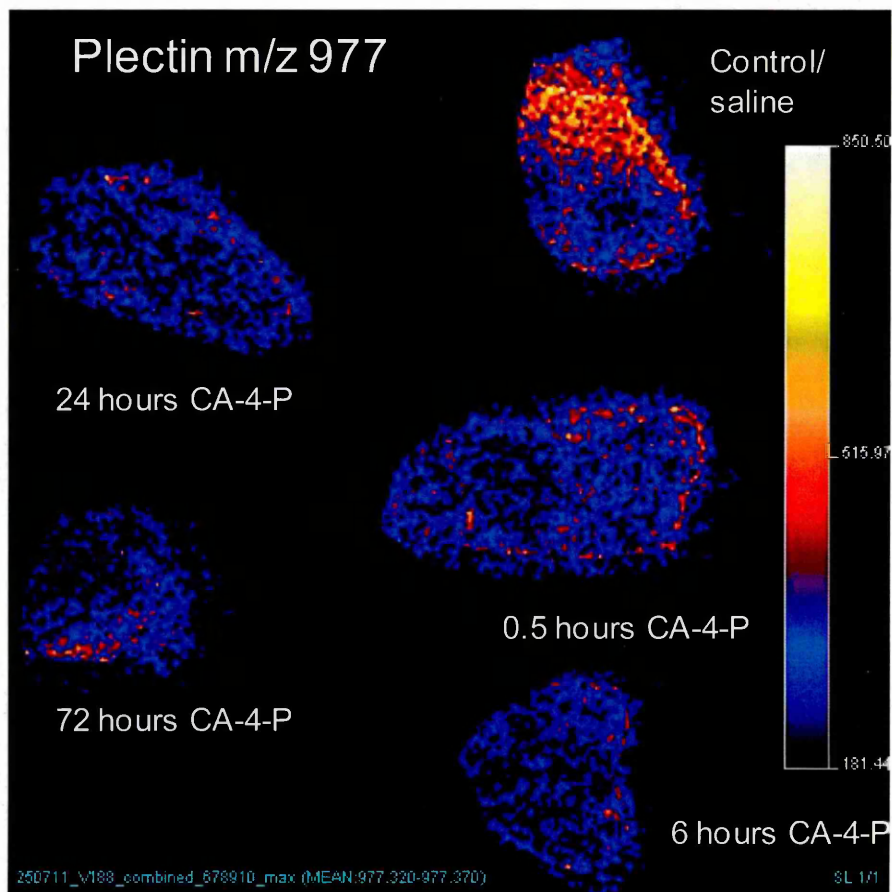


Figure 4. 44: MALDI-MSI multiple Fibrosarcoma 188 sample on tissue digest of Plectin at m/z 977.

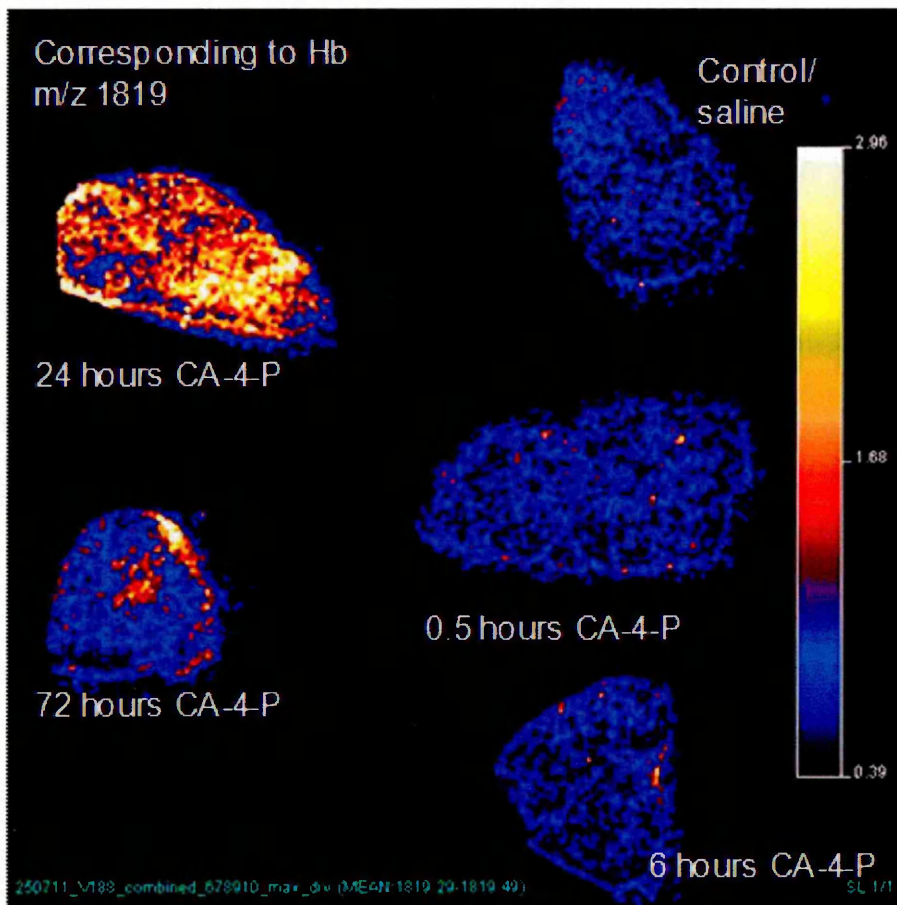


Figure 4. 45: MALDI-MSI multiple Fibrosarcoma 188 sample on tissue digest of Hb subunit alpha at m/z 1416.

4.5.8 Concluding Remarks

One of the basic challenges with iTRAQ is not only successful labelling but accurate interpretation and consistent peptide-protein identifications. Decisions regarding search thresholds greatly influence peptide/ protein yield and are important to reduce the *false positives* scenario. The alternative selection of search parameters to mine the iTRAQ data herein aimed to assess differences in peptide/ protein yield. The choice was made to use mainly fixed filtered search data to reduce data volume and ease interpretation/ validation for the purpose of this project. It would however be beneficial to perform further repeats of the iTRAQ experiments using the two tumour models to aid validation of proteins found using variable modification parameters. Over 1000 proteins were identified with the employment of variable database search parameters, validation of treatment response and elucidation of key effector molecules could be facilitated in conjunction with iTRAQ data processing packages.

The complimentary/confirmatory technique employed here in this chapter provided a powerful means of quantitatively assessing a treatment time course. A diverse approach to biomarker discovery could indeed aid validation of the temporal stability of a chosen experimental model. The more conventional gel based approaches i.e. difference gel electrophoresis could be employed in future work along with cleavable isotope-coded affinity tags involving the biotinylated labelling of cysteine residues (Wu *et al* 2006).

The experimental work described in the following chapter describes a novel method for MALDI-MSI image validation, employing an artificial construct as a standard which could be engineered to include any protein target of interest.

References

- Ahmad A, Aboukamee A, Kong D, Wang Z, Seth S, Chen W, Sarka FH, Raz A (2011) *1,2 Phosphoglucose Isomerase/Autocrine Motility Factor Mediates Epithelial-Mesenchymal Transition Regulated by miR-200 in Breast Cancer Cells*. *Cancer Research*. **71**. (9)
- Banh A, Zhang J, Cao H, Bouley DM, Kwok S, Kong C, Giaccia AJ, Koong AC, Le QT (2011) *Tumor Galectin-1 Mediates Tumor Growth and Metastasis through Regulation of T-Cell Apoptosis*. *American Association for Cancer Research*. **71**. (13) 4423-4431
- Barber RD, Harmer DW, Coleman RA, Clark BJ (2005) *GAPDH as a housekeeping gene: analysis of GAPDH mRNA expression in a panel of 72 human tissues*. *Physiological Genomics*. **21**.(3) 389-395
- Beckner ME, Stracke ML, Liotta LA, Schiffmann E (1990) *Glycolysis as primary energy source in tumor chemotaxis*. *Journal of the national cancer Institute*. **82**. 1836–1840.
- Bjorge L, Hakulinen J, Vintermyr OK, Jarva H, Jensen TS, Iversen OE, Meri S (2005). *Ascitic complement system in ovarian cancer*. *Br J Cancer* **92**.895–905.
- Capello M, Ferri-Borgogno S, Cappello P, Novellia (2011) *F-enolase: a promising therapeutic and diagnostic tumortarget*. *FEBS Journal*.1064–1074
- Chen Z, Wang Q, Lin L, Tang Q, Edwards JL, Li S, Liu S (2012) *Comparative evaluation of two isobaric labelling tags, DiART and iTRAQ*. *Analytical Chemistry*. **84**. 2908-2915
- Evans C, Noirel J, Yen S, Ow SY, Salim M, Pereira-Medrano AG, Couto N, Pandhal J, Smith D, Pham TK, Karunakaran E, Zou X, Biggs CA, Wright PC, (2012) *An insight into iTRAQ: where do we stand now?* *Analytical and Bioanalytical Chemistry*. **404**.1011–1027
- Handra-Luca A, Hong S-M, Walter K, Wolfgang C, Hruban R, Goggins M (2011) *Tumour epithelial vimentin expression and outcome of pancreatic ductal adenocarcinomas*. *British Journal of Cancer*. **104**. 1296 – 1302
- Karantza V (2011) *Keratins in health and cancer: more than mere epithelial cell marker*. *Oncogene*. **30**. (2) 127–138
- Kline KG, Wu CC (2009) *MudPIT Analysis: Application to human heart tissue*. *Methods In Molecular Biology*. **528**. 281–293.
- Knochenmuss and Zenobi (2003) *MALDI Ionization: The Role of In-Plume Processes*. *Chemical Reviews*. **103**. 441–452

Guy Lahat, Zhu QS, Huang K-L, Suizhao W, Bolshakov S, Liu J, Torres K, Langley RR, Lazar AJ, Hung MC, Lev D (2010) *Vimentin Is a Novel Anti-Cancer Therapeutic Target; Insights from In Vitro and In Vivo Mice Xenograft Studies*. PLoS ONE.5. (4) e10105

Kalinina EV, Berezov TT, Shtil' AA, N. N. Chernov, Glazunova VA, Novichkova MD, Nurmuradov NK (2012) *Expression of Peroxiredoxin 1, 2, 3, and 6 Genes in Cancer Cells during Drug Resistance Formation*. ONCOLOGY.153. (6)879-882

Katada K, Tomonagab T, Satoh M, Matsushita K, Tonoikea Y, Koderad Y, Hanazawa T, Nomura F, Okamotoa Y (2012) *Plectin promotes migration and invasion of cancer cells and is a novel prognostic marker for head and neck squamous cell carcinoma*. Journal of Proteomics.1803-1815

Liu R, Gong J, Chen J, Li Q, Song C, Zhang J, Li Y, Liu Z, Dong Y, Chen L, Jin B (2012) *Calreticulin as a potential diagnostic biomarker for lung cancer*. Cancer Immunology, Immunotherapy.61. 855–864

McMahon KM, Volpato M, Chi HY, Musiwaro P, Poterlowicz K, Peng Y, Scally AJ, Patterson LH, Phillips RM, Sutton CW (2012) *Characterization of Changes in the Proteome in Different Regions of 3D Multicell Tumor Spheroids*. Journal of Proteome Research.11. 2863–2875

Mhaweck-Fauceglia P, Wang D, Kesterson J, Beck A, de Mesy Bentley KL, Shroff S, Syriac S, r Frederick P, Liu S, (2011) *Kunle Odunsi Aldolase mRNA expression in endometrial cancer and the role of clotrimazole in endometrial cancer cell viability and morphology*. Histopathology.59 (5) 1015-1018

Minn AJ, Gupta GP, Siegel PM, Bos PD, Shu W, Giri DD, Viale A, Olshen AB, Gerald WL, Massague J (2005) *Genes that mediate breast cancer metastasis to lung*. NATURE Medicine.436. (28)518-524

Montgomery H, Rustogi N, Hadjisavvas A, Tanaka K, Kyriacou K, Sutton CW (2012) *Proteomic profiling of breast tissue collagens and sitespecific characterisation of hydroxyproline residues collagen alpha-1-(I)*. Journal of Proteome Research. ARTICLE IN PRESS

Ning X, Sun S, Zhang K, Liang J, Chuai Y, Yuan Li, Wang X (2012) *S100A6 Protein Negatively Regulates CacyBP/SIP Mediated Inhibition of Gastric Cancer Cell Proliferation and Tumorigenesis*. PLoS ONE.7. (1)

- Noirel J, Evans C, Salim M, Mukherjee J, Ow SY, Pandhal J, Pham TK, Biggs CA, Wright PC (2011) *Methods in quantitative proteomics: setting iTRAQ on the right track*. *Current Proteomics* **8**.(1):17–30
- Nunez-Cruz S, Gimotty PA, Guerra MW, Connolly DC, Wu Y-Q, DeAngelis RA, Lambris JD, Coukos G, Scholler N (2012) *Genetic and Pharmacologic Inhibition of Complement Impairs Endothelial Cell Function and Ablates Ovarian Cancer Neovascularization*. *Neoplasia*. **14**. (11) 994–1004
- Ojika T, Imaizumi M, Abe T, Kato K (1991) *Immunochemical and immunohistochemical studies on three aldolase isozymes in human lung cancer*. *Cancer* **67**. 2153–2158.
- Oskarsson T, Acharyya S, Zhang X H-F, Vanharanta S, Tavazoie S, Morris PG, Downey RJ, Manova-Todorova K, Brogi E, Massague J (2011) *Breast cancer cells produce Tenascin C as a metastatic niche component to colonize lungs*. *Nature Medicine*.**17**. (7) 867-874
- Orosz F, Oláh J, Ovádi J (2006) *Triosephosphate isomerase deficiency: facts and doubts*. *IUBMB Life*.**58**. (12) 703 – 715
- Park SY, Yu X, Ip C, Mohler JL, Bogner PN, Park YM (2007) *Peroxiredoxin 1 interacts with Androgen receptor and enhances its transactivation*. *Cancer Research*. **67**. (19) 9294-9303
- Rand JH, Wu XX, Lin EY, Griffel A, Gialanella P, McKittrick JC (2012) *Annexin A5 Binds to Lipopolysaccharide and Reduces Its Endotoxin Activity*. **3**. (2)1-6
- Reichelt J, Furstenberger G, Magin TM (2004) *Loss of Keratin 10 Leads to Mitogen-Activated Protein Kinase (MAPK) Activation, Increased Keratinocyte Turnover, and Decreased Tumor Formation in Mice*. *Journal of Investigative Dermatology*.**123**. (5) 973-81
- Remotti F, Fetsch JF, Miettinen M (2001) *Keratin 1 expression in endothelia and mesenchymal tumors: An immunohistochemical analysis of normal and neoplastic tissues*. *Human Pathology*.**32**. (8) 873–879
- Ricke RM, Bielinsky A-K (2004) *Mcm10 Regulates the Stability and Chromatin Association of DNA Polymerase- α* . *Molecular Cell*.**16**. 173–185
- Ross PL, Huang YN, Marchese JN, Williamson B, Parker K, Hattan S, Khainovski N, Pillai S, Dey S, Daniels S, Purkayastha S, Juhasz P, Martin S, Bartlet-Jones M, He F, Jacobson A, Pappin DJ (2004) *Multiplexed Protein Quantitation in *Saccharomyces cerevisiae* Using Amine-reactive Isobaric Tagging Reagents*. *Molecular & Cellular Proteomics*.**3**.(12) 1154 – 1169

Ruppen I, Grau L, Orenes-Piñero E, Ashman K, Gil M, Algaba F, Bellmunt J, Sánchez-Carbayo M (2010) *Differential Protein Expression Profiling by iTRAQ-Two-dimensional LC-MS/MS of Human Bladder Cancer EJ138 Cells Transfected with the Metastasis Suppressor KiSS-1 Gene*. *Molecular and cellular Proteomics*.**9**. (10) 2276–2291.

Said HM, Polat B, Hagemann C, Anacker J, Flentje M, Vordermark D (2009) *Absence of GAPDH regulation in tumor-cells of different origin under hypoxic conditions in – vitro*. *BMC Research Notes*.**2**. (8) 1-9

Saw RJ (2006) *Glucose metabolism and cancer*. *Current Opinion in cell Biology*.**18**. 598–08

Shiina N, Gotoh Y, Kubomura N, Iwamatsu A, Nishida E (1994) *Microtubule severing by elongation 1 α* . *Science*. **266**. 282-285

Shultz RW, Lee T-J, Allen GC, Thompson WF, Hanley-Bowdoin L (2009) *Dynamic Localization of the DNA Replication Proteins MCM5 and MCM7 in Plants*. *Plant Physiology*.**150**. 658–669

Sutton CW, Rustogi N, Gurkan C, Scally A, Loizidou MA, Hadjisavvas A, Kyriacou K (2010) *Comparative analysis among transfected, mock, and empty vector-exposed cell*. *Journal of Proteome Research*.**9**. 3891–3902

Takashi M, Haimoto H, Koshikawa T, Kato K (1990) *Expression of aldolaseC isozyme in renal cell carcinoma*. *American Journal of Clinical Pathology*.**93**. 631–636.

Tang S, Huang W, Zhong M, Yin L, Jiang H, Hou S, Gan P, Yuan Y (2012) *Identification Keratin 1 as a cDDP-resistant protein innasopharyngeal carcinoma cell lines*. *Journal of Proteomics*.**75**. 2352-2360

Veremieva M, Khoruzhenko A, Zaicev S, Negrutskii B, El'skaya A (2010) *Unbalanced expression of the translation complex eEF1 subunits in human cardioesophageal carcinoma*. *European Journal of Clinical Investigation*.**41**. (3) 269-276

Wu WW, Wang G, Baek SJ, Shen R:F (2006) *Comparative Study of Three Proteomic Quantitative Methods, DIGE, cICAT, and iTRAQ, Using 2D Gel- or LC-MALDI TOF/TOF*. *Journal of Proteome Research*. **5**. (3) 651-658

Ye H, Sun L, Xiaojun Huang X, Zhang P, Zhao X (2010) *A proteomic approach for plasma biomarker discoverywith 8-plex iTRAQ labeling and SCX-LC-MS/MS*. *Molecular and Cellular Biochemistry*.**343**. (1-2)91–99

Ye J, Mancuso A, Tong X, Ward PS, Fan J, Rabinowitz J, Thompson CB (2012) *Pyruvate kinase M2 promotes de novo serine synthesis to sustain mTORC1 activity and cell proliferation.* PNAS. **109.** (18) 6904-6909

Chapter 5

A novel multi-peptide recombinant
standard used in MALDI-IMS-MSI

5.1 Introduction

Many developments and innovations have been achieved in the field of mass spectrometry over the last decade. Technological advances to enhance both mass resolution and mass accuracy have been accomplished with various pioneering techniques.

Ion mobility has enabled observation of another dimension to mass spectrometry data with a further separation method of isobaric ions. Nano scale chromatographic instrumentation now provides a means to perform highly sensitive, high throughput proteomic analysis for both targeted and undirected investigations (Angel *et al* 2012).

It can now be said that electrospray ionization (ESI) and matrix assisted laserdesorption ionization (MALDI) are key techniques employable in all aspects of biomarker discovery and proteomic investigative analysis.

Work by Atkinson *et al* (2007) displayed overlaid MALDI images using BioMAp which showed the distribution of the bioreductive drug AQ4N and its active metabolite AQ4 in solid tumours. Here in this paper, standards were included in the MALDI-MSI using AQ4N, AQ4 and ATP. This enabled observation of the regional spatial distribution of the drug/ metabolite and whether any co-localisation was visible.

An article by Djidja *et al* (2009) studying GRP-78 within pancreatic adenocarcinoma ffpe tissue sections, reported the technique of using a digested recombinant standard for image validation. MALDI-MSI with the employment of ion mobility produced BioMap images which could be related to GRP-78 immunohistochemical staining.

Targeted proteomic MS methods aim to facilitate analyte identification and a novel method using a multi-peptide recombinant standard for the MALDI-MSI of *on tissue* tryptic digests is reported here.

5.2 Materials and Methods

5.2.1 Peptide sequences chosen for a recombinant protein standard based on MALDI-MSI and conventional proteomic analysis of fibrosarcoma 120 and 188 tissue.

The pET vector detailed here was supplied by MWG-biotech (Germany). Unless otherwise, stated the chemicals were purchased from Sigma Aldrich (UK).

The peptides listed in Table 9 were chosen based on the Mass spectrometric identifications reported in Chapters 2-4 (with the exception of EGFR and Epiregulin).

The design of the 12 peptide construct was undertaken by Dr David Smith of Sheffield Hallam University (UK). Organisation of the sequence was arranged to ensure that the charges were evenly spaced across the synthetic protein in order to prevent intra cellular aggregation during expression. The final protein had an expected mass of 16,667.26 Da. The DNA construct was then sub cloned into the expression vector pET23a(+) and *E-coli* BL21 DE3 was chosen for transformation.

Plasmid preparation, transformation and purification was performed by Dr David Smith of Sheffield Hallam University (UK).

Peptide	m/z	Peptide Sequence
GRP-78	1887.9	VTHAVVTVPAYFNDAQR
EGFR	1564.7	MHLPSPTDSNFYR
HSP- 90 beta	1513.7	GVVDSLELNISR
Plectin	1385.7	AQAELEAQELQR
	1350.5	DSQDAGGFGPEDR
Haemoglobin beta chain	1302.6	VNSDEVGGEALGR
Tenascin	1219.6	ETFITGLD
Actin	1198.7	AVFPSIVGRPR
HSP-90 alpha	1168.5	LGIHEDSQNR
Vimentin	1093.5	FADLSEAANR
Epiregulin	983.4	CEVGYTGVR
Rho GTPase activating protein 2	844.5	RLTSLVR
Tag reporter	A WLE HHH HHH	

Table 9: Twelve peptides from target proteins chosen for positive identification.

MHL PSP TDS NFY RVN SDE VGG EAL GRA VFP SIV GRP RRL
 TSL VRE TFI TGL DAP RGV VDS EDL ELN ISR LGI HED SQN
 RFA DLS EAA NRA QAE LEA QEL QRD SQD AGG FGP EDR CEV
 GYT GVR VTH AVV TVP AYF NDA QRA WLE HHH HHH

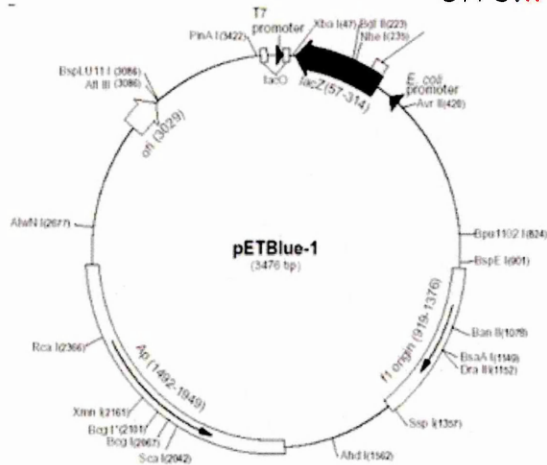


Figure 5. 1: pETBlue-1 vector and sequence used for the synthesis of the recombinant protein standard.

**MHLPSPTDSNFYRVNSDEVGGEALGRAVFP SIVGRPRRLTSLVR
 ETFITGLDAPRGVVDS EDLELNISRLGIHEDSQNRFADLSEAANR
 AQAELEAQELQRDSQDAGGFGPEDRCEVGYTGVRVTHAVVTVP
 AYFNDAQRA **W**LE **HHHHHH****

Tryptophan His Tag

Figure 5. 2: The final sequence of the recombinant standard.

5.2.2 Bacterial culture

Bacterium - BL21(DE3) HsdS gal (llts 857 ind1 Sam7 nin5 lacUV5-T7gene1)

Growth Media - Luria-Bertani (LB) media, Bacto-tryptone (10g/L), Yeast extract (5g/L), NaCl (10g/L).

The above materials were dissolved in 900 ml deionised water and made up to 1 L. LB media was sterilised by autoclaving for 20 min at 15 lb/sq inch. After cooling filter-sterilised carbenicillin (final concentration of 250 mg/ml) was added as appropriate.

1.5 g of bacto-agar was added to 100 ml of LB media before autoclaving. Antibiotics were added (carbenicillin, final concentration of 250 mg/ml), to the cooling agar and mixed

thoroughly. 15-20 ml of molten agar mixture was added per 100 mm diameter Petri dish and allowed to set, before storage at 4 °C.

Cultures were inoculated from freshly transformed bacteria (Section 2.2.7) grown on agar plates (Section 2.2.3) or directly from existing glycerol stocks (15 % v/v glycerol). Liquid cultures of less than 100 ml were inoculated directly, whereas for larger scale cultures (1 L), overnight starter cultures of 5 ml were used for inoculation. Cultures were incubated at 37 °C in an orbital incubator with shaking at 200 rpm.

5.2.3 Plasmid preparation

Plasmid DNA was isolated from fresh overnight liquid cultures of *E. coli* BL21(DE3) with carbenicillin selection using a Qiagen plasmid midi kit as described in the manufacturer's instructions. Isolated DNA was deemed of suitable purity if the observed ratio of the absorbance at 260 nm (A260) to that at 280 nm (A280) was ³ 1.8. An A260 of 1.0 was assumed equivalent to 35 mg/ml of single stranded (ss) and 50 mg/ml of double stranded (ds) DNA.

5.2.4 E. coli- transformation

Tubes containing 200 µl aliquots of competent cells were thawed at 4 °C and 20 ng or 200 ng of plasmid DNA were added to separate 14 ml round bottom Falcon tubes.

A negative control lacking DNA was also included. Cells / DNA mixtures were incubated on ice for 30 min and then heat shocked at 42 °C for 90 sec with mixing every 10 min. Cells were then put on ice for 2 min and 800 µl of liquid LB media was added to each tube. These cultures were incubated at 37 °C for 45 min to allow the cells to express antibiotic resistance. Transformed cells were spread onto LB / agar plates containing carbenicillin (250mg/ml) and incubated at 37 °C for 12 h.

A 20 ml starter culture was grown overnight at 37 °C in liquid LB media (Section 2.2.2) with antibiotic selection (carbenicillin, 250 mg/ml). This culture was used to inoculate 10 x 2 L flasks each containing 1 L of LB liquid media and carbenicillin (100 mg/ml). Cultures were grown at 37 °C with shaking until the OD600 reached 0.6, protein expression was induced with 1 mM (IPTG). The cells were then incubated at 37 °C overnight and harvested by continuous-flow centrifugation at 15,000 rpm at 4 °C (Heraus Contifuge 17RS). The cell paste was frozen and stored at -80 °C until required.

5.2.5 Protein Purification

The required DNA sequence was synthesised by MWG-biotech (Germany), and sub cloned into the bacterial expression vector pET23a(+) (Novagen). The plasmid was then transformed into

the E-coli strain BL21 DE3 (Promega Corporation). All bacterial cultures were grown in Luria Broth(LB) media with 100 µg/ml ampicillin for selection. 10 ml of a 100 ml overnight starter culture was used to inoculate a 1 L of LB media. Cultures were grown at 37 °C with shaking until the OD₆₀₀ reached 0.5, protein expression was induced with 1 mM isopropyl-β-D-thiogalactoside (IPTG). The culture was incubated for a further 2.5 h before the bacterial cells were harvested by centrifugation at 10,000g for 20 min using a Sorvall RC G+.

Bacterial pellets were resuspended in binding buffer (20mM Sodium Phosphate + 20mM imidazole pH 7.4) 3ml per 1g of cells before being lysed by sonication (10x 20sec pulses at a 35% duty cycle) using a Vibra Cell VCX 750 (750 Watts). Phenylmethylsulphonyl fluoride (PMSF) (50 µg/ml), DNase (20 µg/ml), RNase (20 µg/ml) were added to the lysate which was then cleared of insoluble material by centrifugation at 8,000 g for 1h using an Eppendorf 5804R centrifuge. The clear lysate was filtered through a 0.2 µm syringe filter and loaded onto a 1 ml HisTrap FF column (GE) at a flow rate of 1 ml/min. The protein was eluted over 20 column volumes using a 0 to 100% gradient into elution buffer (20mM Sodium Phosphate + 500mM imidazole pH 7.4). Fractions containing the recombinant protein were then desalted into 50mM ammonium bicarbonate using a PD10 column (GE). Trypsin digestion was performed on a 50 µl sample of desalted protein using 1 µl of trypsin (1mg/ml) added for 1h plus a further 1 µl of trypsin overnight.

Samples were stored at -80°C until further use.

5.4.6 Digestion

Trypsin was added (1µl) (20µg/ml) for 1h plus a further 1µl of trypsin for overnight incubation at 37°C and 5% CO₂.

5.4.7 MALDI-MSI - Chemicals and Materials

a-Cyano-4-hydroxycinnamic acid (CHCA), aniline (ANI), ethanol (EtOH), chloroform (CHCl₃), acetonitrile (ACN), octyl-a/b-glucoside (OcGlc), tri-fluoroacetic acid (TFA), ammonium bicarbonate, were from Sigma– Aldrich (Dorset, UK). Modified sequence grade trypsin (20 µg lyophilised) was obtained from Promega (Southampton, UK).

Tissue samples

Mice were injected sub-cutaneously in the flank with a 50 µl tumour cell suspension containing 1×10^6 cells in serum-free medium. The cells employed in this study were from the mouse fibrosarcoma cell line, VEGF188. This has been engineered to express only the VEGF188 isoform. Tumours were allowed to grow to approximately 500 mm³, before CA-4-P treatment (a single dose of 100 mg/kg i.p). The dosage for CA-4-P are consistent with animal studies performed at clinically relevant doses (Galbraith 2003., Prise 2002). Mice were killed and tumours excised at various times after treatment. All animal work carried out documented herein was performed by Dr. J. E. Bluff, Tumour Microcirculation Group, University of Sheffield, UK. Samples were provided as frozen excised tumours and stored at -80°C.

Experimental sections for on tissue tryptic digestion and MALDI-MSI

6_2 Control (no treatment, saline i.p), 8_1 (6 h after treatment with CA-4-P) and 10_1 (72 h after treatment with CA-4-P).

Tissue preparation

Frozen tissue sections were cut to give approximately 10µm sections, using a Leica CM3050 cryostat (Leica Microsystems, Milton Keynes, UK) (Djidja *et al* 2009). The sections were then freeze thaw mounted on poly-lysine glass slides. Mounted slides were either used immediately or stored in an airtight tube at -80 °C for subsequent use.

In situ tissue digestion and trypsin deposition

The tissue samples were washed initially with 70% and then 90% ethanol for 1 min then left to dry, subsequently slides were immersed in chloroform for 10 s. Prior to matrix application, in situ tissue digestion was performed with trypsin solution prepared (from lyophilised trypsin) at 20 µg/ml by addition of 50 mM ammonium bicarbonate (NH₄HCO₃) pH 8, containing 0.5% octyl-a/b-glucoside (OcGlc) based on a protocol by Djidja *et al* (2009).

The “Suncollect” (SunChrom, Friedrichsdorf, Germany) automatic pneumatic sprayer was used to spray trypsin in a series of layers. The sections for MALDI-MS and MALDI- MSI were incubated overnight in a humidity chamber containing H₂O 50%: methanol 50% overnight at 37°C and 5% CO₂.

5.4.8 Methods and instrumentation

Matrix deposition

The matrix, α -cyano-4-hydroxycinnamic acid (CHCA) and aniline in acetonitrile:water:TFA (1:1:0.1 by volume), was applied using either the Suncollect (at 5 mg/ml). Identical coordinate settings were used as with the trypsin deposition, to ensure sample uniformity. Equimolar amounts of aniline were added to the CHCA solution, i.e. 1 ml of 5 mg/ml CHCA solution contained 2.4 μ l of aniline. These matrix deposition parameters were based on methods from Djidja *et al* (2009).

Instrumentation

MALDI- IMS/MS and MALDI- IMS/MSI were performed using a HDMS SYNAPT™ G2 system (Waters Corporation, Manchester, UK) and Mass Lynx software (Waters Corporation, UK). Image acquisition was performed using raster imaging mode at 100 μ m spatial resolution, Biomap 3.7.5.5 software (<http://www.maldi-msi.org/>) and HDI 1.1 software was used for image generation. Instrument calibration was performed using standards consisting of a mixture of 217 polyethylene glycol (Sigma-Aldrich, Gillingham, UK) ranging between m/z 100 to 218 3000 Da prior to MALDI-IMS-MSI analysis. HDI 1.1 parameters were set to the following; specificity type – IMS MS, MS, Number of most intense peaks – 1000, resolution – 10,000, Low energy intensity threshold – 50. The low intensity threshold was to allow low abundant species to be potentially included. HDI images were chosen for analysis based on the highlighted recombinant standard and m/z ratio listed in the software displaying the peak intensity and corresponding drift time. HDI correlation filter tool was set to R1 minimum 0.5 and R maximum 1.0 for peaks analysed at m/z 1350 and m/z 1032.

To enable simple visual comparison between images, BioMap data were normalised to m/z 877/ m/z 1066 (peaks arising from the α CHCA matrix).

5.3 Results and Discussion

5.3.1 MALDI-IMS-MS Peptide mass fingerprint of the digested recombinant DNA construct

The following MALDI-IMS peptide mass fingerprint is from a tryptic digest of the recombinant synthetic DNA construct, used as a protein standard for MALDI-IMS image peptide validation.

The PMF in Figure 5.3 displayed a clean tryptic digest spectra with chosen peptides easily observable showing excellent spectrum intensity.

5.3.2 MALDI-IMS-MSI of fibrosarcoma 188 tumour tissue, Control and post CA-4-P treatment

The following MALDI-MSI was acquired at 100 μ m resolution using various fibrosarcoma 188 treatment time points to investigate this novel multi-peptide recombinant standard.

The images featured in Figures 5.4- 5.7, display an assortment of peptides from the digested construct visualised by BioMap imaging software, therefore there is no ion mobility component to ion selection here. Such images feature further on within this Chapter.

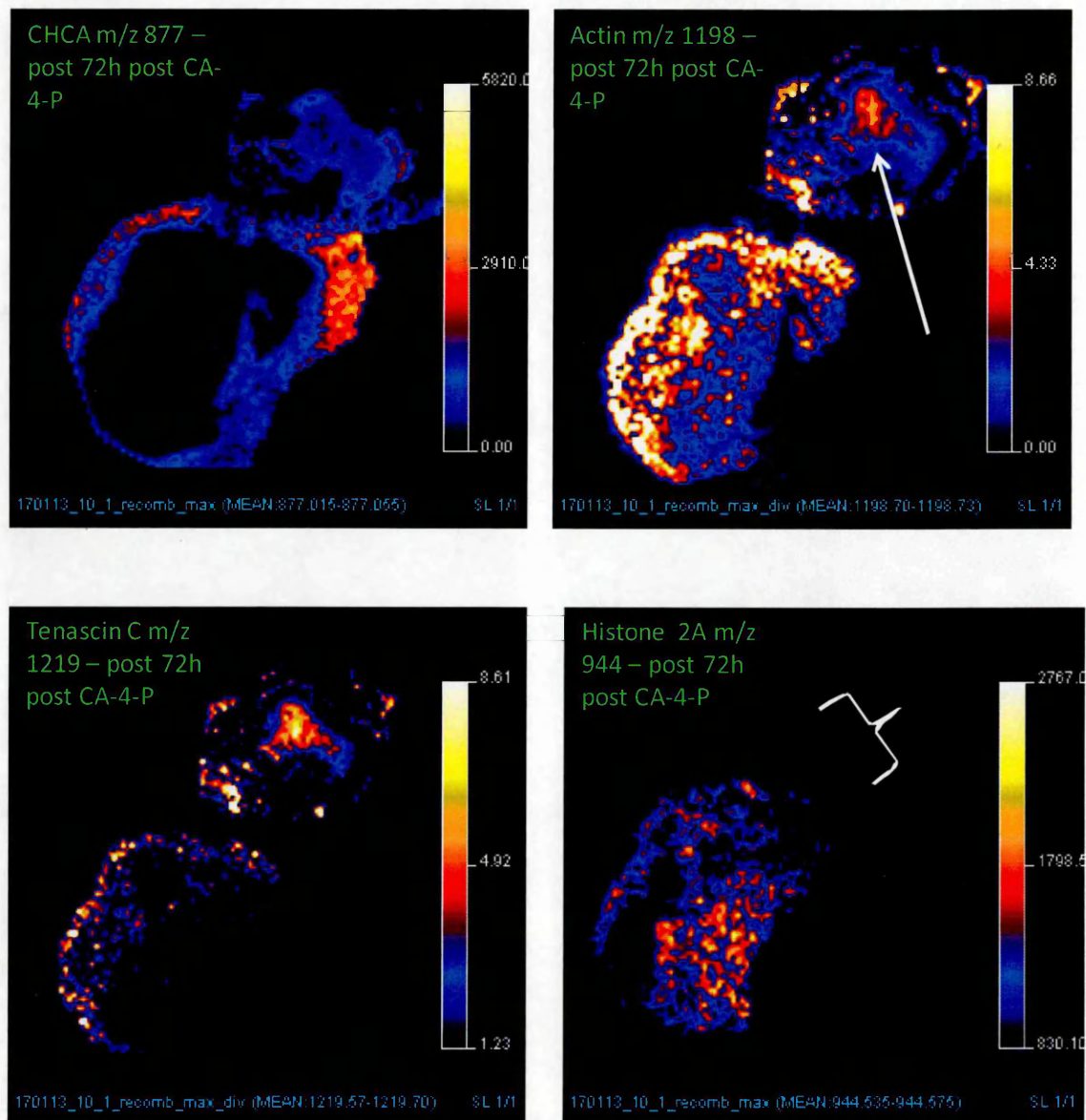


Figure 5. 4: MALDI-MSI of on tissue tryptic digests and digested recombinant standard in 72h treated tissue. *The spatial distribution of peptides; Actin (m/z 1198) with arrow indicating position of the spotted recombinant standard, Tenascin (m/z 1219), Histon 2A (m/z 944) with bracket showing the absence of the standard and CHCA peak at 877 to show inverse image correlation.*

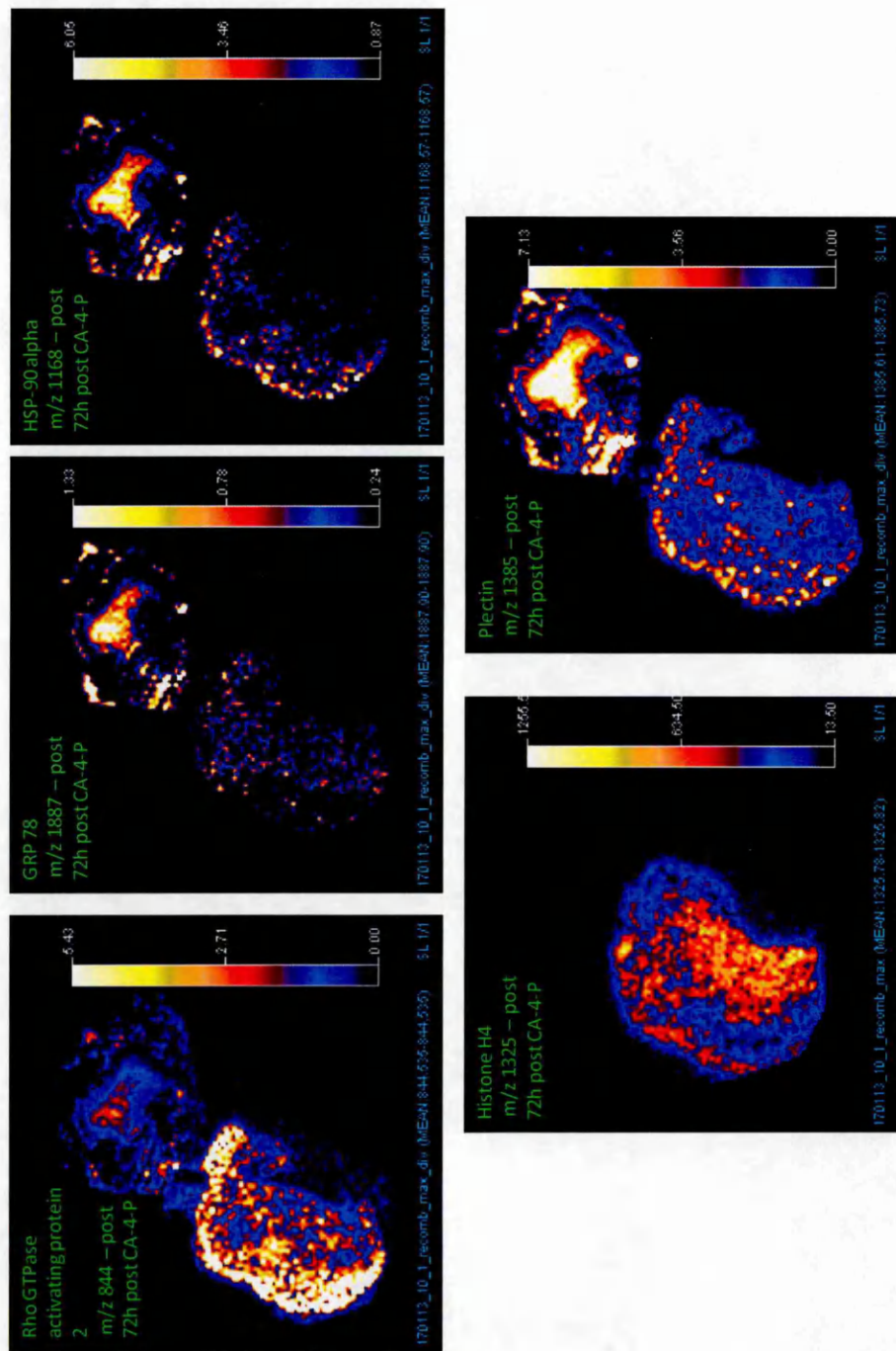


Figure 5: MALDI-MS images for the distribution peptides in fibrosarcoma 188 72h tissue, employing a DNA artificial construct for image validation.

Figure 5.5 - The spatial distribution of peptides; Rho GTPase activating protein 2 (N-chimaerin m/z 844), GRP-78 (m/z 1887), HSP-90 α (m/z 1168), Histone H4 (m/z 1325) displaying absence of the standard to validate recombinant signal and Plectin (m/z 1385).

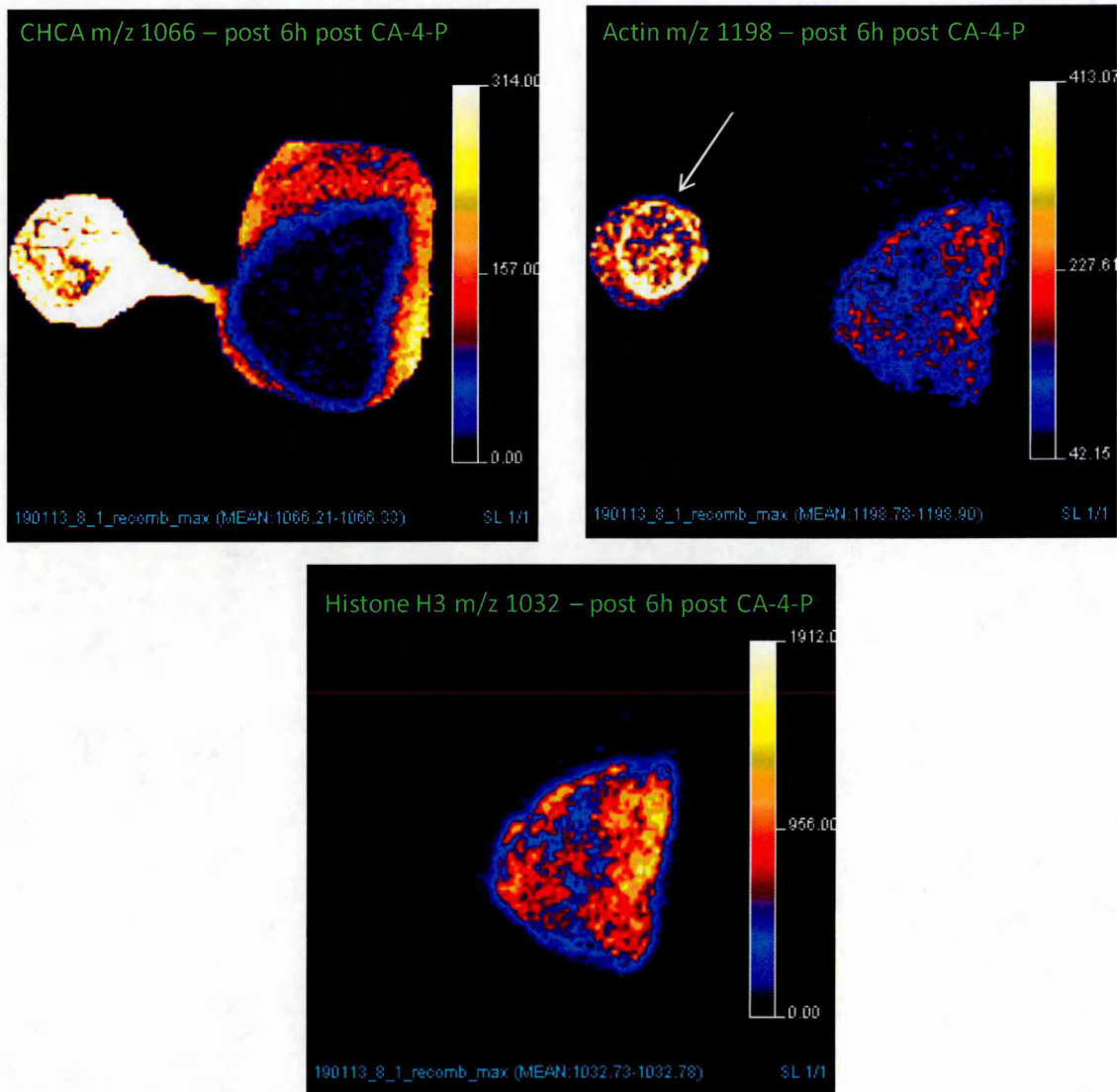


Figure 5.6: MALDI-MS images displaying peptides distribution in fibrosarcoma 188 6h treated tissue, employing a DNA artificial construct for image validation. The spatial distribution of peptides; Actin (m/z 1198) with arrow indicating position of the spotted recombinant standard, Histone H3 (m/z 1032) showing the absence of the standard and CHCA peak at 1066 to show inverse image correlation.

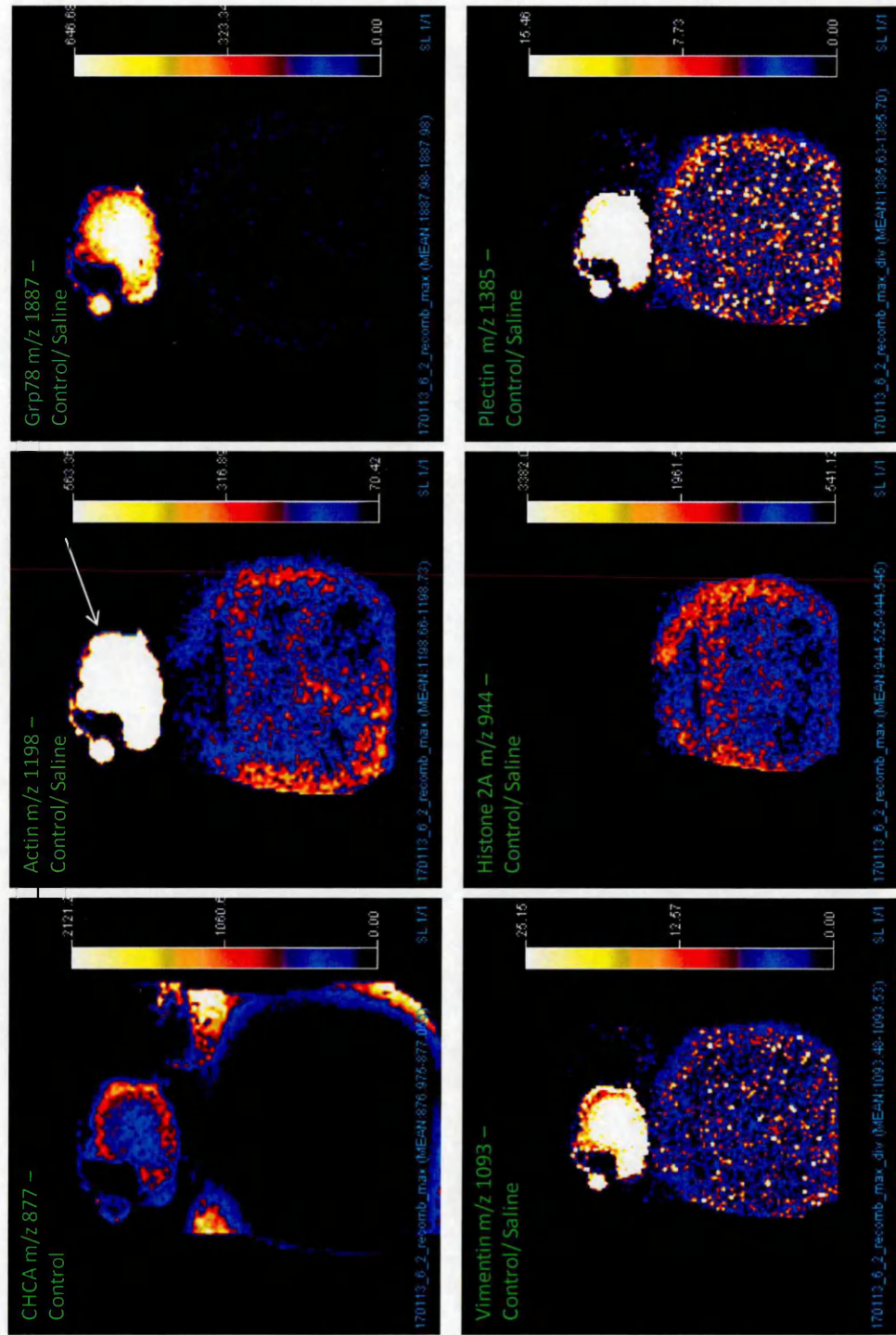


Figure 5. 7: MALDI-MS images for the distribution peptides in fibrosarcoma 188 Control tissue, employing a DNA artificial construct for image validation.

Figure 5.7 - The spatial distribution of peptides; Actin (m/z 1198) with arrow indicating position of the spotted recombinant standard, GRP-78 (m/z 1887) displaying apparent low intensity as seen in Chapter 3 Figure 3.31 also using Fibrosarcoma 188 time course results post CA-4-P treatment except via LC-ESI-MS/MS., Vimentin (m/z 1093), Histone 2A (m/z 944) showing the absence of the standard and CHCA peak at 877 to show inverse image correlation.

The MALDI-MSI in Figures 5.4 - 5.7 all display good validation of the multi-peptide standard due to the absence in signal intensity of peptides; Histone 2A, Histone H3 and Histone H4 which are typically high abundant within *on tissue* tryptic digests. These peptides were not chosen for the construct and therefore co-validate the MALDI images in conjunction with the recombinant standard.

Interestingly, there is a signal for Rho GTPase activating protein 2 in the fibrosarcoma 188 tissue here (Figure 5.5), albeit low intensity. Some of the proteins identified by ESI-LC-MS/MS and iTRAQ LC-MALDI are highlighted in the tumour tissue images which again are of low intensity. This reiterates the apparent ion suppression discussed in previous Chapters, a factor typical of high abundant species in MALDI digest spectra. It has to be considered what ions of interest are present within the so called '*spectral grass*' and in future experiments how this data can be amplified for analysis.

5.3.3 Recombinant MALDI-IMS-MSI visualised through HDI 1.1 software

HDI 1.1 imaging software is a useful tool for the processing and visualisation of MALDI-IMS-MSI.

Interactive spectra and drift time plots enable further confirmation of species of interest.

The HDI analysis that follows has the capacity for the user to preset threshold and peak picking parameters to facilitate the analysis of low abundant species.

The peptides Actin, HSP-90 and Histone H3 are featured in the following HDI analysis using the identical recombinant standard MALDI-MSI results in Figures 5.4 - 5.7.

The HDI images here are shown as superimposed images on top of the original histological section used for *on tissue* tryptic digestion and CHCA deposition.

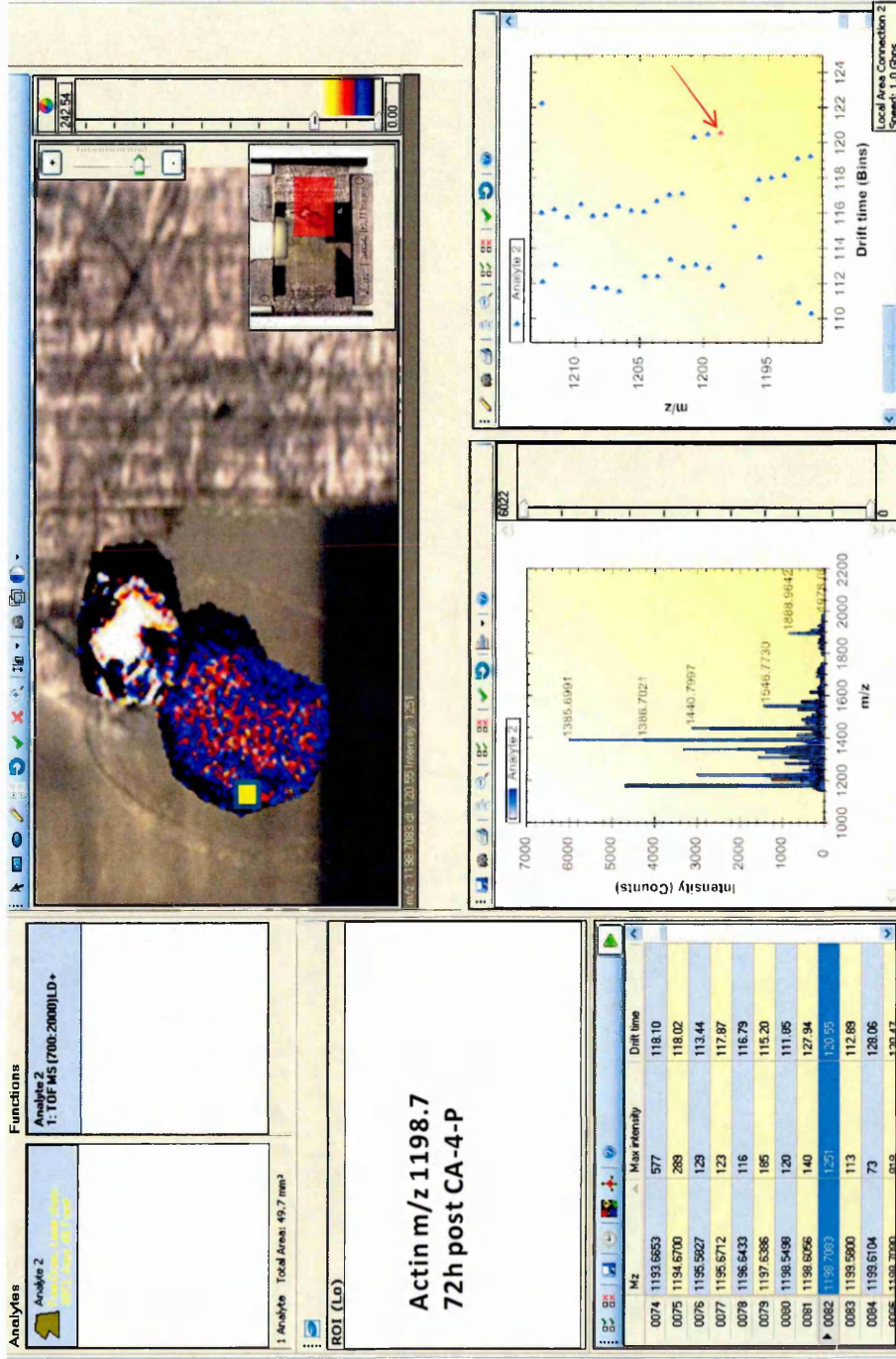


Figure 5. 8: HDI visualisation of Actin at m/z 1198.7. Arrow indicates the ion of interest separated by drift time and yellow square denotes the ROI for exportation.

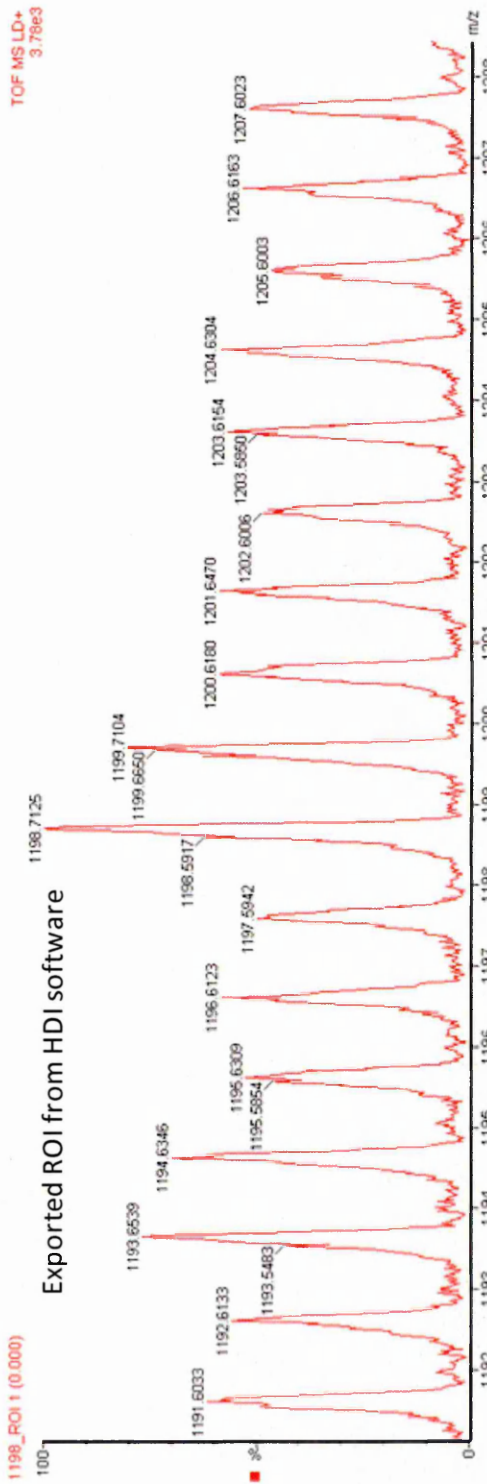
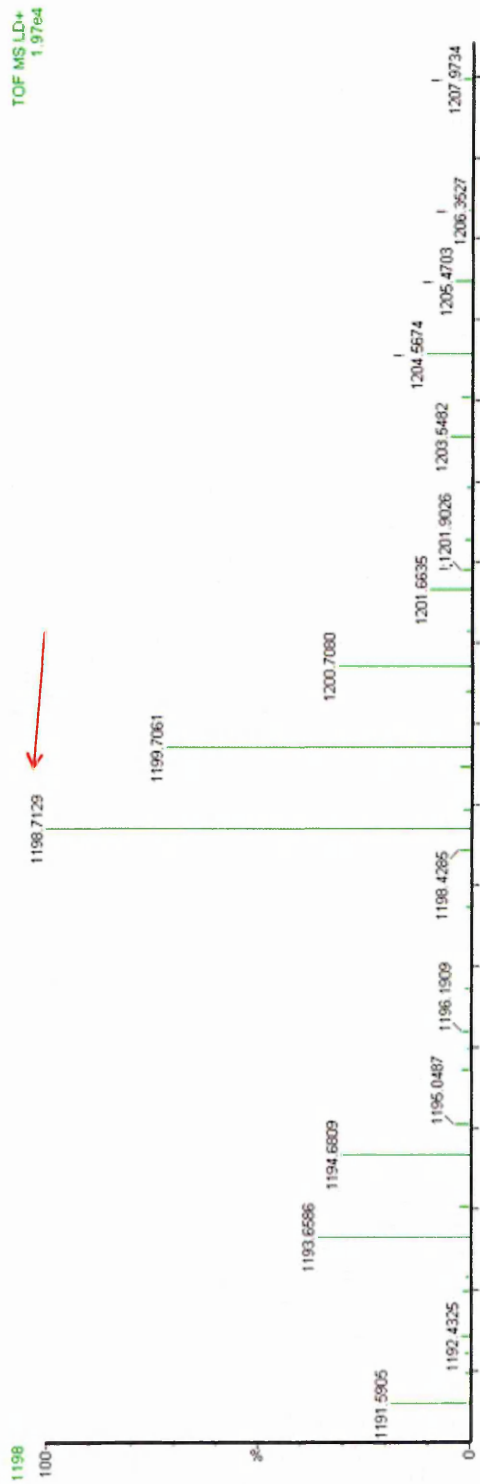


Figure 5.8. b: Actin at m/z 1198.7 after exportation to Mass Lynx software from the selected ROI in HDI 1.1. The raw data and centroided spectra after employment of the automatic peak detection function are shown.

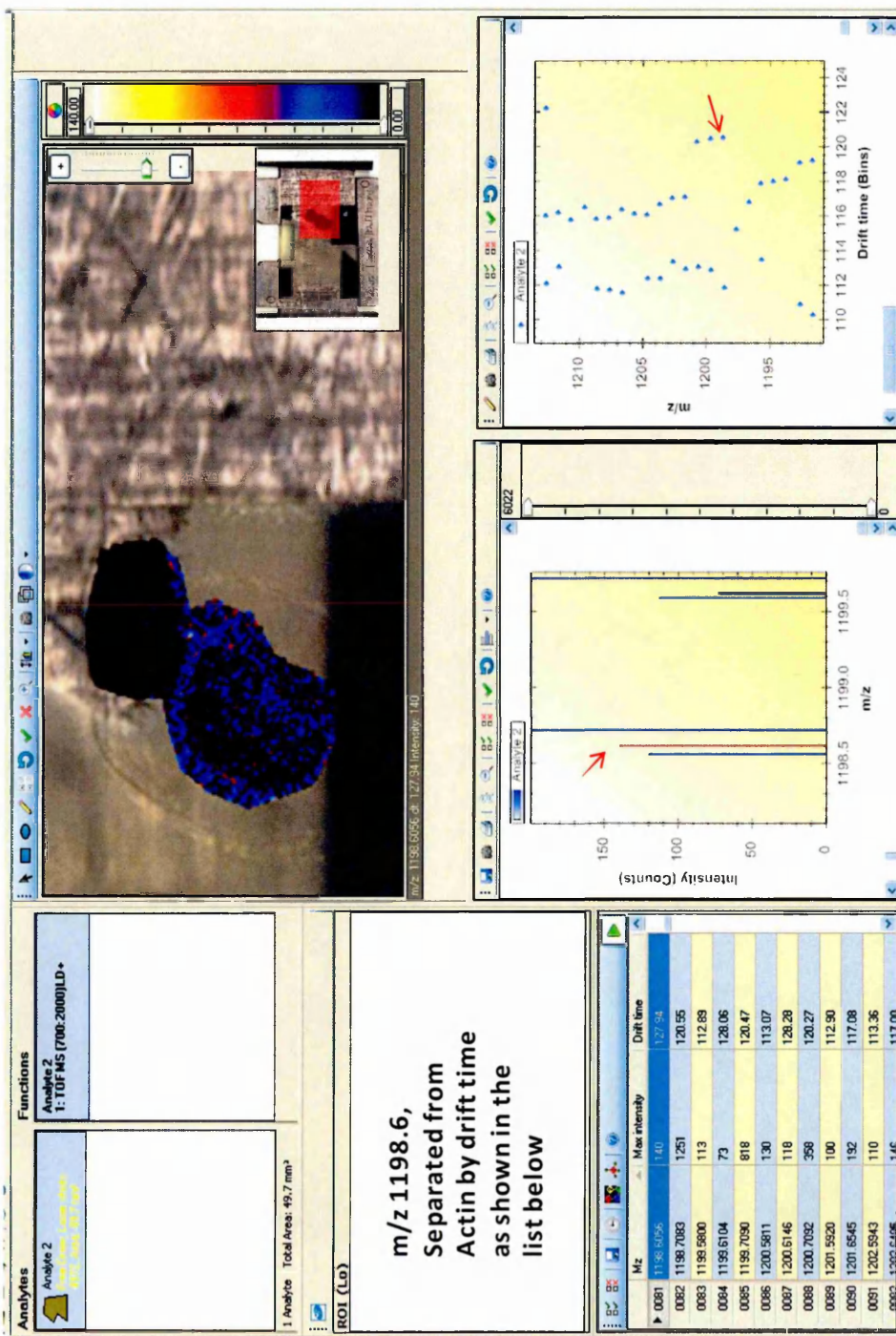


Figure 5. 9: HDI visualisation of m/z 1198.6 to display the differentiation in tissue and standard image due to separation in drift time compared to m/z 1198.7.

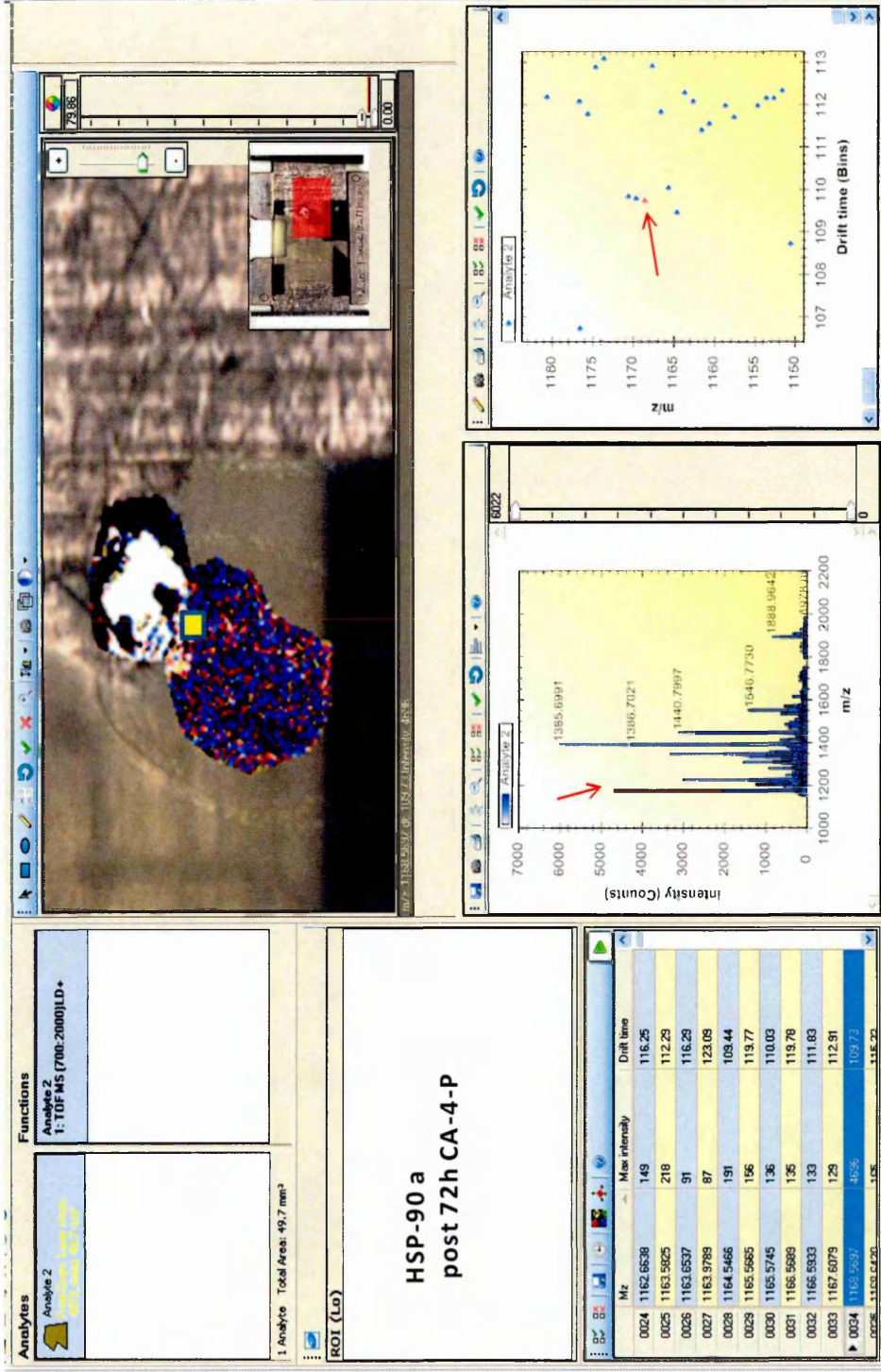


Figure 5. 10: HDI visualisation of HSP-90 α at m/z 1168.5. Arrows indicates the ion of interest separated by drift time, and yellow ROI square is shown.

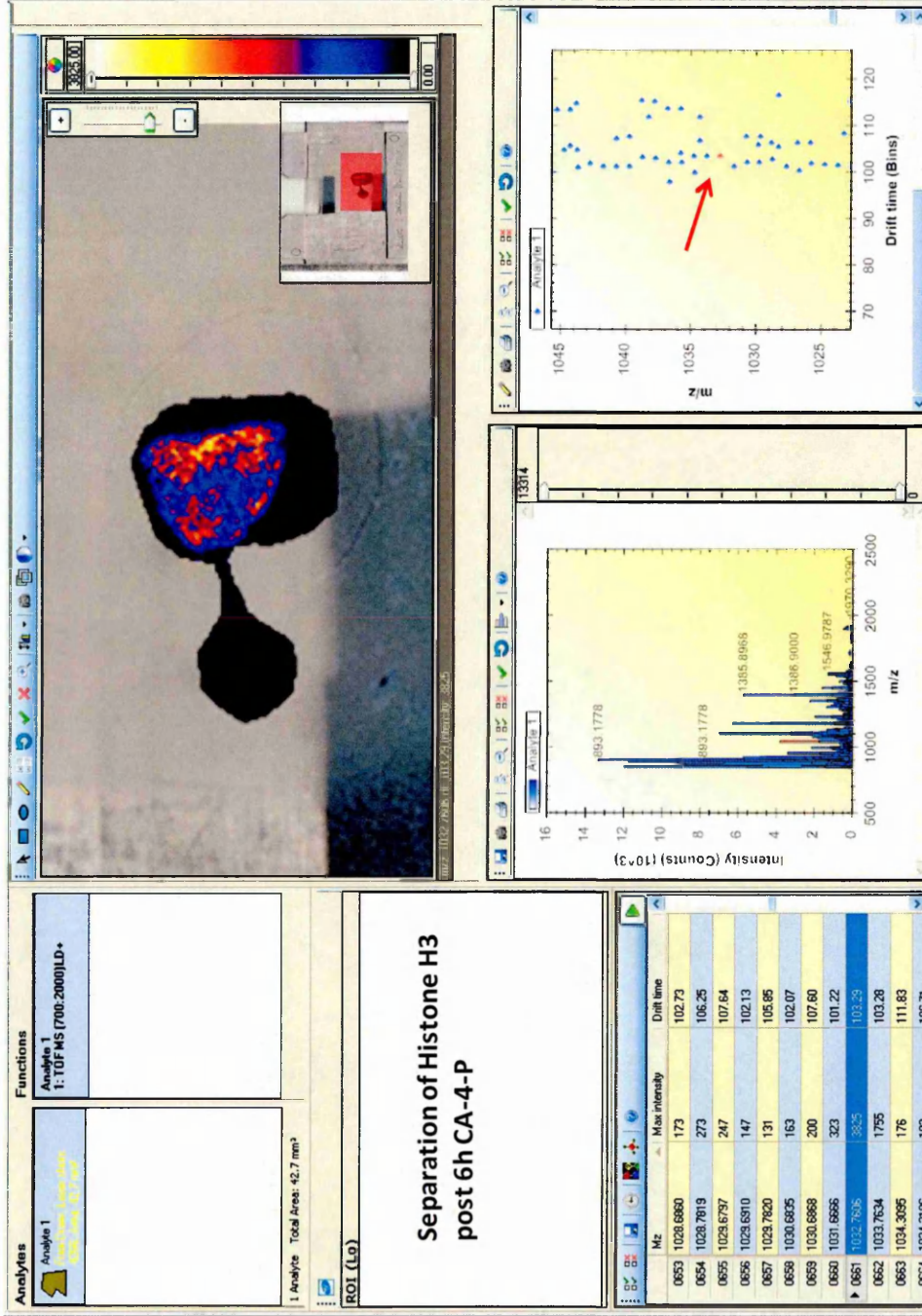


Figure 5. 12: HDI visualisation of Histone H3 at m/z 1032.7. The arrow indicates the ion of interest separated by drift time and no signal apparent in the standard.

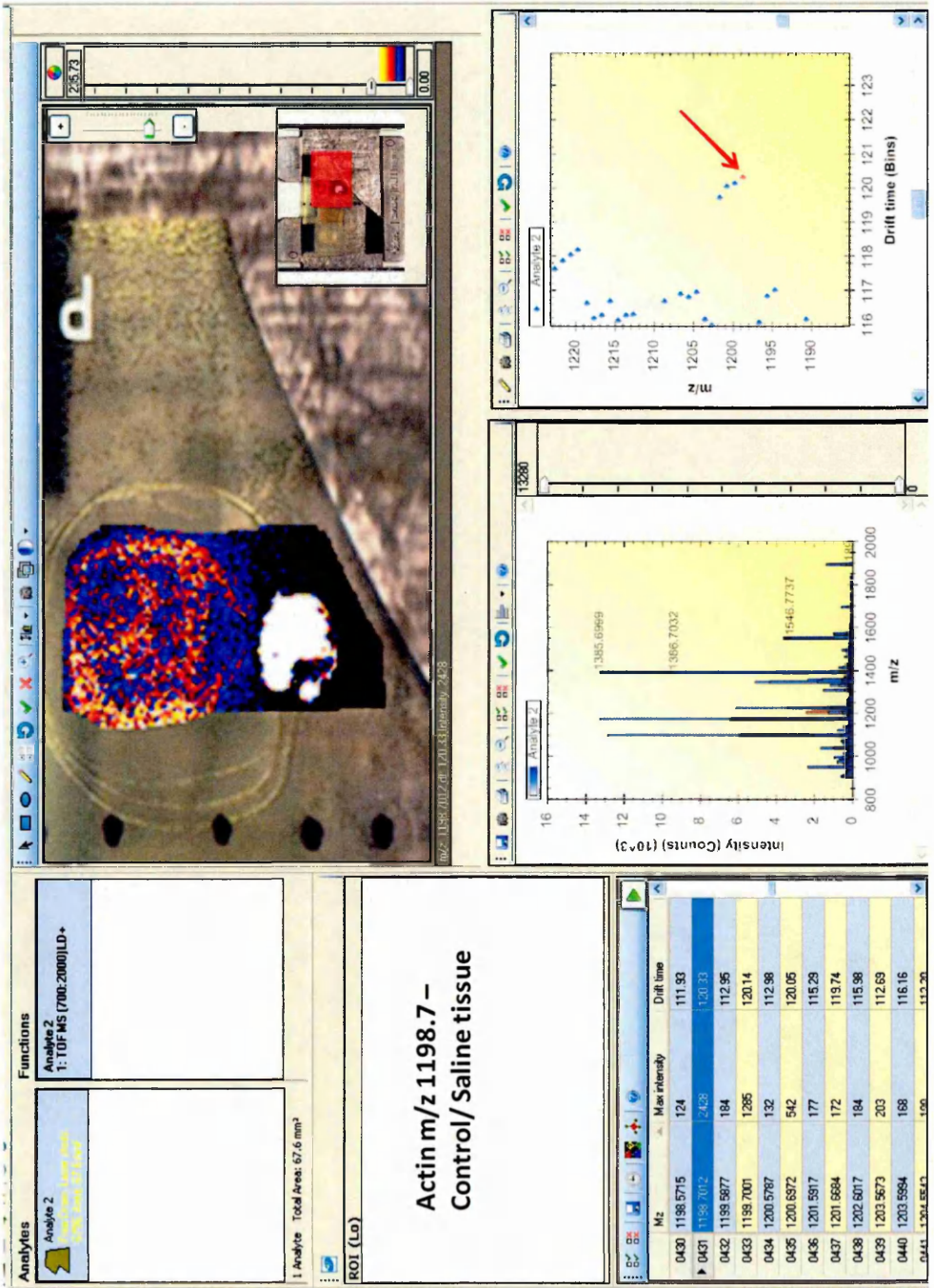


Figure 5. 13: HDI visualisation of Actin at m/z 1198.7. The arrow indicates the ion of interest separated by drift time.

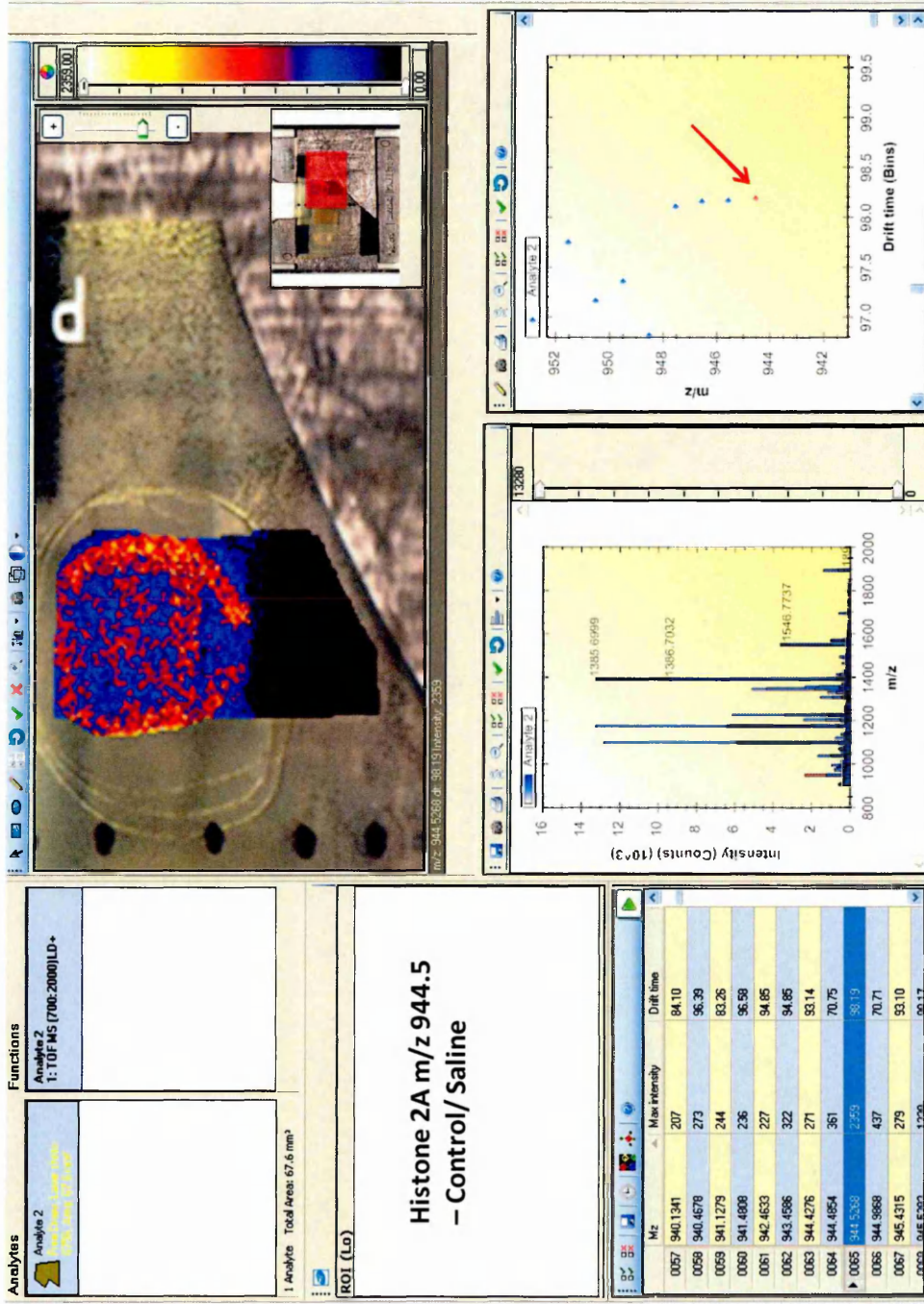


Figure 5. 14: HDI visualisation of Histone 2A at m/z 944.5. The arrow indicates the ion of interest separated by drift time.

The MALDI-IMS-MSI visualised by HDI 1.1 software in Figures 5.7 and 5.9 gives a good conceptual illustration of separation by drift time. Furthermore how this unique technology can benefit MALDI image analysis and validation due to the vast dissimilarity in the corresponding images for m/z 1198.7 and m/z 1198.6.

Another useful tool of the HDI software is the image correlation filter as shown in Figures 5.15 and 5.16. After selection of a particular ion of interest, running the image correlation filter option displays the peaks within the spectrum that have the same spatial distribution pattern as the peak picked. Therefore peaks that co-exist are observable. The following HDI screen images are by using this option and show examples of Plectin m/z 1350 and Histone H3 m/z 1032. The correlation peak lists generated by selecting m/z 1032 mostly contained other histones i.e. Histone 2A m/z 944.5, which confirms the correlation between the spatial distribution of other Histones. However this was unsuccessful for Plectin m/z 1350 as fellow Plectin peaks were not selected. This was thought to be due to the strong peptide signals from the spotted recombinant standard which were all listed in the peak list correlation results. In order to discriminate between each peak when using a recombinant standard in future work, the standard could be sprayed directly to the tissue when using the HDI correlation filter tool.

Teamed with the recombinant digested construct, the MALDI-IMS images reported here therefore propose a novel methodology for inclusion into the MALDI-MSI workflow.

The potential for this dynamic recombinant standard is very promising and could be engineered to include any prospective biomarkers for both research and diagnostic screening applications in the clinical workplace. This concept alone is in accordance with the forward momentum of MS applications.

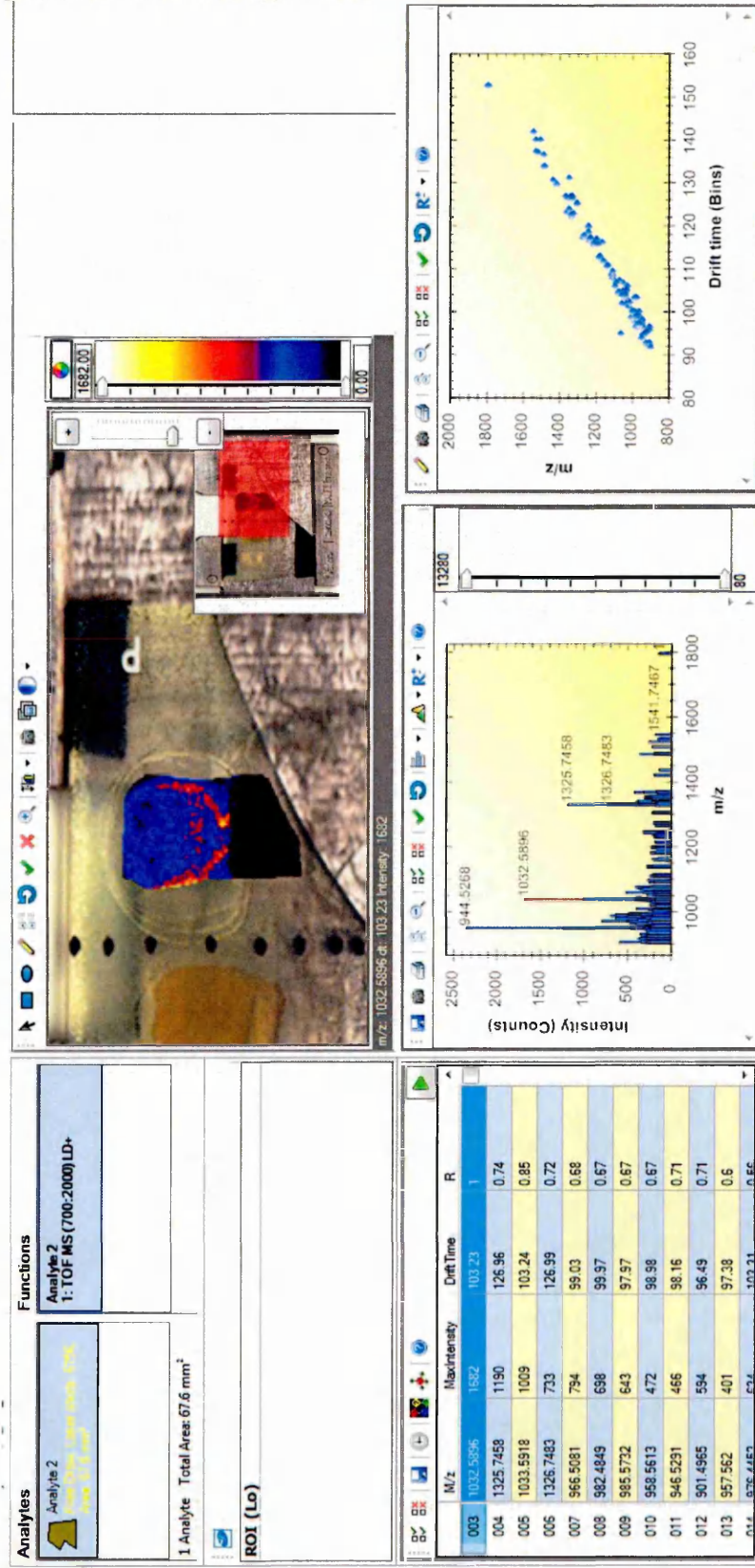


Figure 5. 15: HDI software with image correlation filter for Histone H3 m/z 1032 displaying fellow Histones.

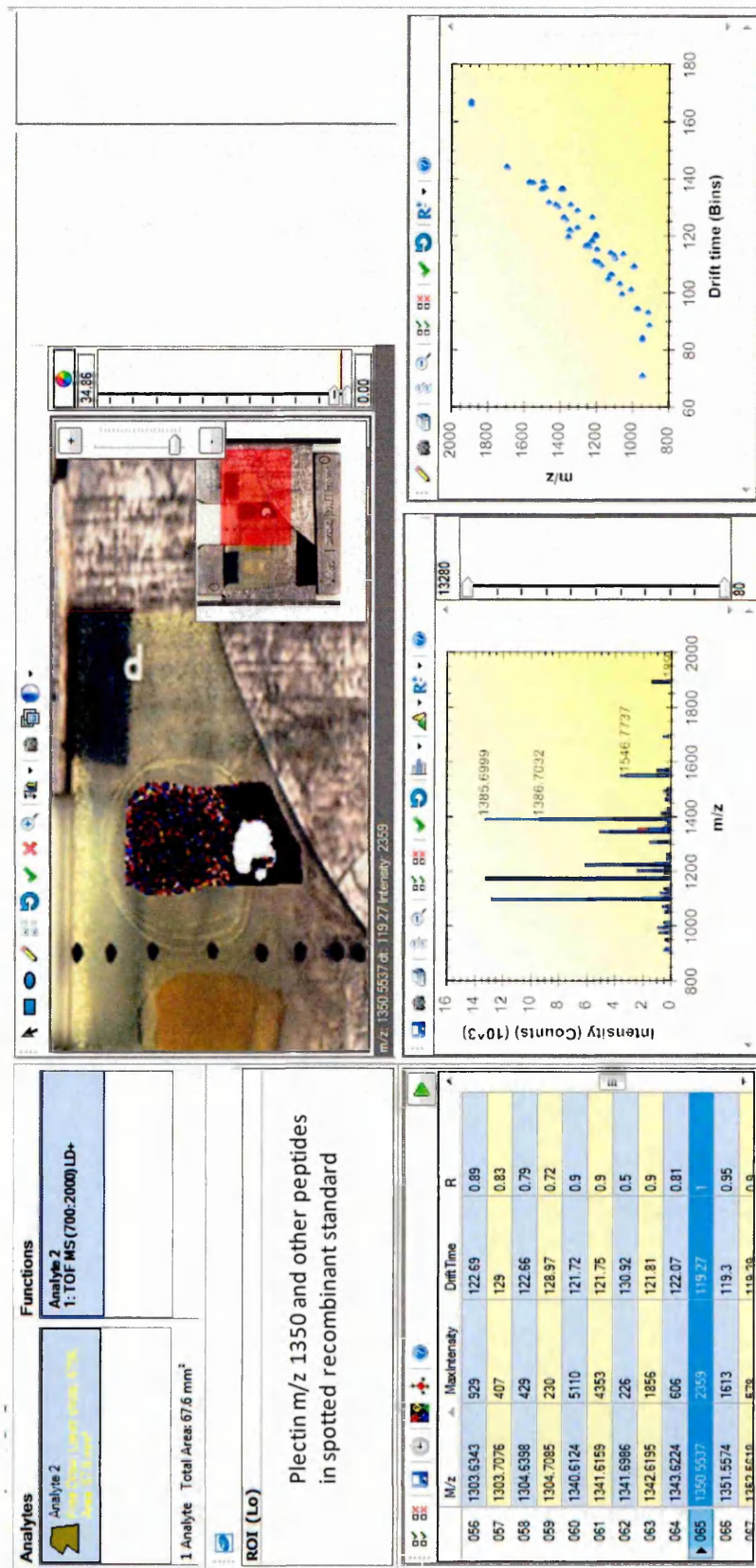


Figure 5. 16: HDI software with image correlation filter for Plectin m/z 1350 showing no discrimination between other peaks.

5.3.4 Cross validation of Plectin and HSP-90 response in fibrosarcoma 188 tissue employing a multimodal proteomic strategy.

The confirmation and validation of any scientific hypothesis is regarded a challenge, a range of complementary techniques could indeed affirm marked responses seen in data generated.

The changes in the levels of Plectin throughout the treatment time course displayed a high percentage of co-variance in the LC-ESI-MS/MS, with the same trend visible in the iTRAQ and immunohistochemical results of the fibrosarcoma 188 data set.

The MALDI-IMS-MSI of plectin that follow include images from the Control fibrosarcoma 188 tissue and the 72h post CA-4-P time point with recombinant digested standard.

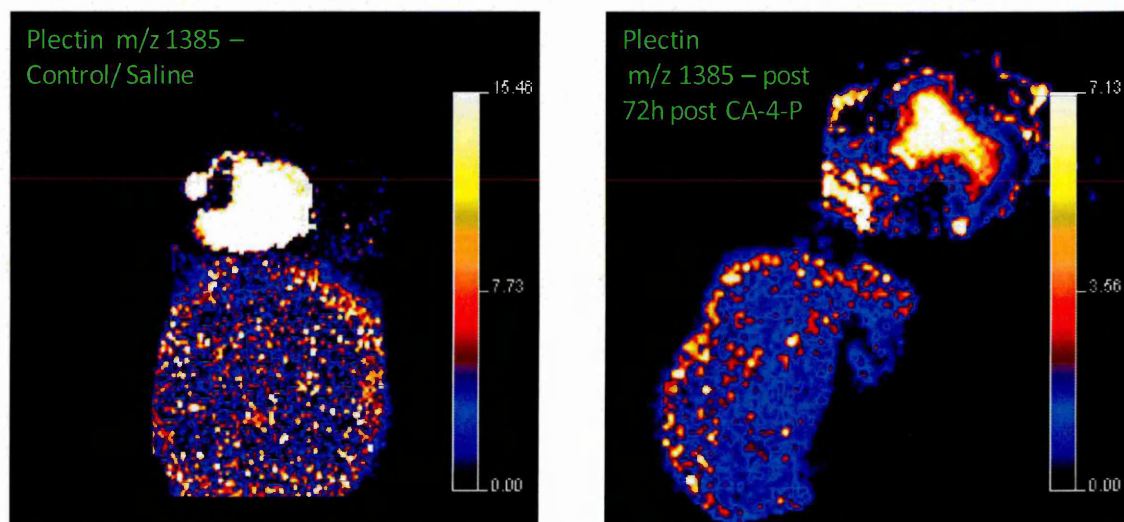


Figure 5. 17: MALDI-MSI of fibrosarcoma 188 on tissue tryptic digests for the spatial distribution of Plectin at m/z 1385.

The spatial distribution of Plectin in Figure 5.17 is in good agreement with the anti-Plectin immunohistochemical staining featured previously in Chapter 3.

Figures 5.18 and 5.19 use Plectin and HSP-90 to show some of the cross validation that the techniques in this project aimed to achieve. The samples used for ESI-LC-MS/MS and iTRAQ were performed on different biological sample time course sets but are still in good agreement.

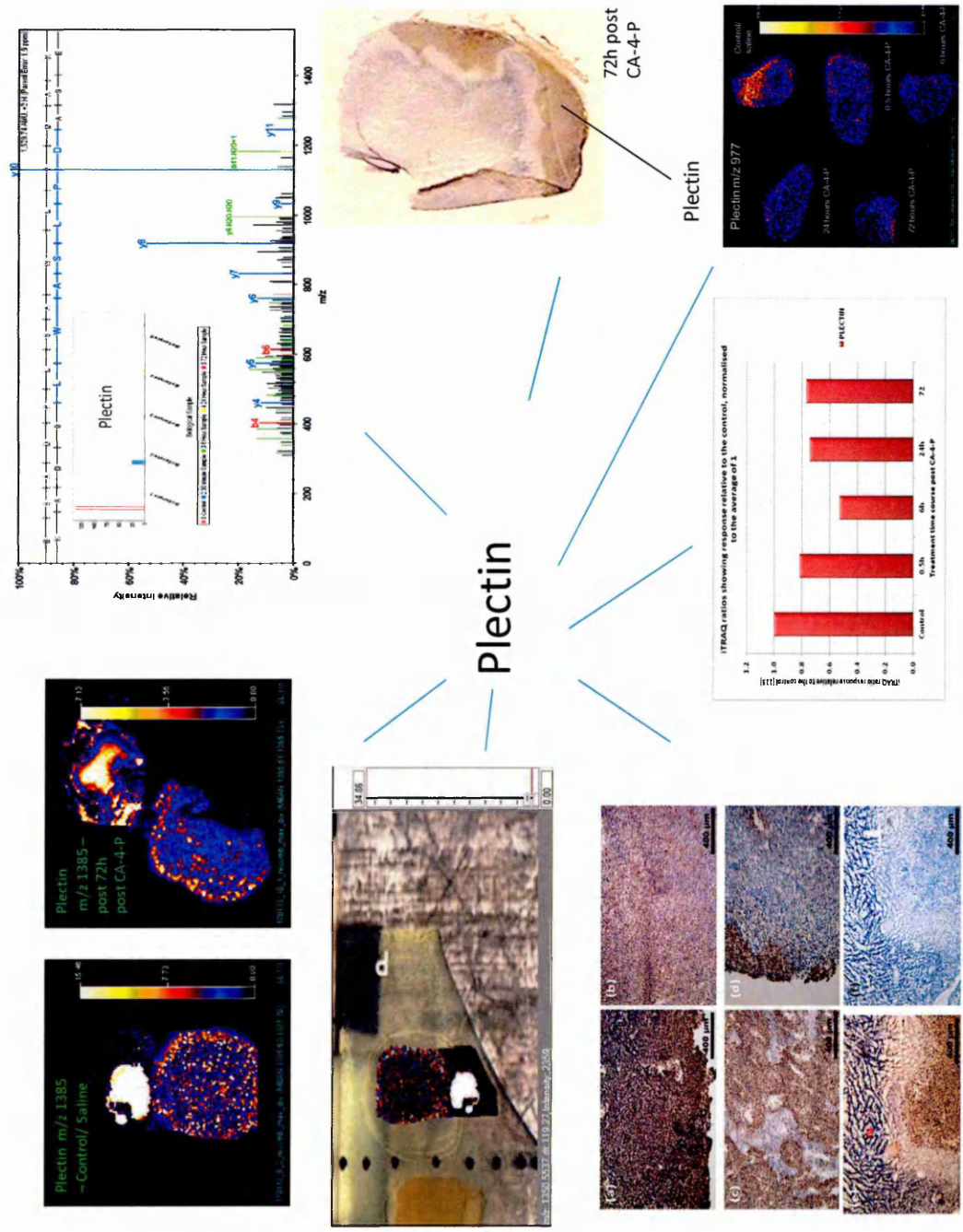


Figure 5. 18: MALDI-MSI and conventional proteomic techniques to assess a dose relationship in Plectin.

5.4 Concluding Remarks

Prediction of the future requirements to progress MS experimental analysis could focus on further technological advancement of ion mobility for proteins. In scientific publications, much of the subject matter has focused on pharmaceutical and metabolomic analysis (Thelen and Miernyk 2012).

Future progression in the separating capacity of ion mobility could improve peptide resolution thus peptide identification in MALDI-MS, during the acquisition of complex tryptic digest samples. This could potentially result in a peptide yield comparable to high throughput shotgun LC chromatographic systems.

If such advancements in ion mobility separation come into fruition, this technology along with many other additional components could reveal numerous concealed biological molecules.

Optimisation in sample preparation, solution chemistry and enzymology could also result in prevention of lost proteins to minimise the suppression and spectral dominance by haemoglobin, structural proteins and such like (Laphorn *et al* 2013).

The chart in Figure 5.20 contains points to consider when performing *on tissue* enzymatic digestion for MALDI-MSI. The issues and factors included are mainly based on personal experience throughout the project reported herein. Insights were also gained from an oral presentation by Hamzah Neil Freeman during a workshop entitled 'On-Tissue Enzymatic Digestion for MALDI MS Imaging' (H Freeman 2012).

The recombinant protein reported here could hold great potential for quantification techniques; N15 labelling is one such method for relative quantification. Labelled and unlabelled samples can be combined and analysed using LC-MS/MS. The only difference between the two samples being their mass, this then will be used to quantify the peptides within the sample. The latter is a novel method that could also be applied to MALDI-MSI where the N15 labelled recombinant could be applied as an internal standard directly to tissue section and used for peptide quantification analysis.



Figure 5. 20: Issues and factors to consider when performing on tissue digestion for MALDI imaging experiments.

References

Angel TE, Aryal UK, Hengel SM, Baker ES, Kelly RT, Robinson EW, Smith RD (2012) *Mass spectrometry-based proteomics: existing capabilities and future directions*. The Royal Society of Chemistry.**41**. 3912–3928

Atkinson SJ, Loadman PM, Sutton C, Patterson LH, Clench MR (2007) *Examination of the distribution of the bioreductive drug AQ4N and its active metabolite AQ4 in solid tumours by imaging matrix-assisted laser desorption/ionisation mass spectrometry*. Rapid Communications in Mass Spectrometry. **21**. 1271–1276

Djidja M-C, Claude E, Snel MF, Scriven P, Francese S, Carolan V, Clench MR (2009) *Maldi-ion mobility separation-mass spectrometry imaging of glucose-regulated protein 78 kDa (Grp78) in human formalin fixed paraffin-embedded pancreatic adenocarcinoma tissue sections*. Journal of Proteome Research. **8**. (10) 4876-4884

Freeman HN (2012) *Optimisation of a low-volume on-slide protocol for imaging collagen-specific peptide fragments*. Workshop – On-tissue enzymatic digestion for MALDI MS Imaging. Stevenage BioScience Catalyst, GlaxoSmithKline.

Laphorn C, Pullen F, Chowdhrylon BZ (2013) *Mobility Spectrometry-Mass Spectrometry (IMS-MS) of Small Molecules: separating and assigning structures to ions*. Mass Spectrometry Reviews.**32**. 43– 71

Thelen JJ and Miernyk JA (2012) *The proteomic future: where mass spectrometry should be taking us*. Biochemical Journal.**444**. 169–18

Chapter 6

Conclusion and Future Work

The aims of the study reported in this thesis were to develop and utilise mass spectrometry imaging techniques (MALDI-MSI), in combination with conventional proteomic methodologies, to investigate protein induction in vascular-targeted strategies.

Proteins thought to be involved in tumourigenesis and drug treatment resistance and were observed along with the responses from proteins identified via the techniques used, in this global analysis study.

The collaboration between the techniques used; MALDI-MSI, ESI-LC-MS/MS, LC-MALDI-MS/MS with iTRAQ labelling was intended to provide cross validation of the effects post administration of vascular disrupting agent CA-4-P.

During the initial experimental work reported in Chapter 2 using MALDI-MSI, one of the major challenges was the management and analysis of the large amounts of data generated. The latter especially applicable to ion mobility MALDI-MSI.

The gross haemorrhagic pharmacological response elicited by CA-4-P was visible by MALDI-MSI throughout the fibrosarcoma 120 time course. The latter encouraged the prospect that other proteins could potentially be observed induced via a dose response relationship.

It was hoped that the use of PCA-DA, PCA and PLSDA would reveal more subtle changes taking place in the tumour samples however at present these are masked by the dominance of the changes in the haemoglobin signals and other proteins of high abundance. MALDI-MS of the fibrosarcoma 120 tissue in Chapter 2 was one such example, most likely to be due to the CA-4-P susceptible nature of this tumour model.

The manually performed MALDI-IMS-MS/MS in Chapter 2 contained numerous signals which may have been post translationally modified in ways other than what was pre-selected for searching, thus hampering peptide identifications. Many of the MS/MS spectra studied clearly contained overlapping MS/MS fragmentation patterns.

The Fibrosarcoma 188, a CA-4-P resistant experimental was introduced in Chapter 3. The use of immunohistochemistry and label free LC-ESI-MS/MS shotgun proteomics aimed to complement and aid interpretation of the MALDI-MSI data.

The experimental work carried out using LC-ESI-MS/MS and label free quantitation revealed many proteins connected with necrosis, cell structural reorganisation, polymerisation, tumour survival and stress induced molecular chaperones. The inverse correlation of structural proteins, haemoglobin and heat shock molecular chaperones gave the required validation and identification to relate these responses to those seen in MALDI-MSI.

In addition to this the striking differences between HSp-90 and Plectin showed the distinct regional differences in the MALDI-MSI, immunohistochemistry and LC-ESI-MS/MS results.

The haemoglobin time course using the resistant 188 tumour model gave quite different results to those previously seen in the MALDI-MSI of the fibrosarcoma 120 data set. The first indication of the 'switch back to viability' concept was revealed. This regenerative attempt by the tumour could also be correlated to the HSp-90 and Plectin responses recently discussed.

The relationship pathways generated by using STRING 9.0 proteomic network software gave an invaluable insight into the activity of the active tumour milieu and provided a means of linking the identified proteins to their functional partners. Protein-protein interactions could be observed to help interpretation of the MALDI-MSI and LC-ESI-MS/MS response graphs.

One such pathway revealed a link incorporating Ras GTPase-activating-like protein (IQGAP1), a protein thought to be involved with tumour progression and metastasis. The decreased response from IQGAP1 over the time course suggests an inhibitory effect by CA-4P. Similar responses to treatment were exhibited by Plectin and Transforming growth factor-beta-induced protein ig-h3 (Tgfbi). Future anti-IQGAP1/ anti-Tgfbi immunohistochemistry of the fibrosarcoma 188 tissue could determine whether the staining of these two proteins reveals co-localisation with Plectin, potential implicated in the 'viable tissue switch'.

Another protein that would be expected to show an inverse correlation to Plectin/IQGAP1/Tgfbi, is the protein Alpha-enolase. Increased expression of Alpha-enolase is said to be indicative of aggressive tumour progression as claimed of Plectin. However in these data Alpha-enolase showed an increase in abundance overtime whereas Plectin quite markedly decreases.

Over a thousand proteins were present in the LC-ESI-MS/MS results but only a fraction were selected by Scaffold 3 proteomic software for analysis. Conclusions were made that further optimisation not only during sample preparation but throughout data-dependent acquisition mode could prove invaluable to advance proteome analysis and coverage. This would result in a greater number of unique peptides per protein.

An opportunity to analyse the fibrosarcoma 120 samples with LC-ESI-MS/MS could serve to complete the comparison between the susceptible and resistant tumour models

iTRAQ quantitation of both fibrosarcoma 120 and 188 samples was performed in Chapter 5. Similarly to the LC-ESI-MS/MS results, numerous proteins were identified and various PTM parameters were employed in order to reduce and affirm the relative responses observed.

Different biological tumour samples were used compared to those of the ESI study with an aim to validate overall responses previously seen.

The main differences in the responses observed between the two tumour models employed (120 and 188) here were that of Elongation factor 1-alpha 1 and Vimentin.

In the fibrosarcoma 188 samples Elongation factor 1-alpha 1 levels are elevated throughout the time points relative to the control. In contrast to this, levels in the fibrosarcoma 120 iTRAQ results are all decreased relative to the control. It was thought that elevated levels seen in the fibrosarcoma 188 samples maybe due to some form of pharmacological conflict elicited by this CA-4-P resistant tumour model.

Vimentin levels decrease overtime in the fibrosarcoma 120 iTRAQ response results with a more erratic response leading to an increase seen by the 188 results.

Overall the dose relationships observed in the iTRAQ data by the proteins involved in haemorrhaging, structural remodelling, tumour survival and the stress response were in good agreement with the other techniques employed here. Further optimisation and/or more experimental repeats could both ascertain the relative responses seen and achieve optimum percentage of iTRAQ labelling.

Although a widely practised technique, it was concluded that MALDI *on tissue* digestion imaging still has many potential courses for optimisation. The chart in Chapter 5 aimed to summarise points and issues for consideration. The requirement for the best buffer, enzyme, solvent and matrix could indeed reveal numerous concealed biological molecules, essential in the understanding of cancer. Additionally, another consideration in the assesment of proteomic dose response relationships using MALDI-MSI is the effect of post translational modifications. The apparent disappearance of a protein within an image time course could be due to such alteration i.e. phosphorylation of peptides due to having a serine/threonine/tyrosine present in the sequence or having undergone methylation/acetylation.

MALDI-MSI has the potential to forge a place in the workflow of clinical diagnostics. Targeted approaches for the observation of disease biomarkers could be visualised using MALDI-MSI and serve as a complimentary technique to standard clinical imaging.

The novel method reported here using a multi-peptide recombinant standard could prove an important diagnostic tool for the analysis of patient biopsies and tissue micro-arrays. The exciting prospect is the diversity of a multi-peptide recombinant standard. As mentioned

earlier in Chapter 5, the artificial construct can be engineered to include any prospective biomarkers for both research and diagnostic screening applications.

This initiative could indeed further the impetus of MS applications in cancer research.

Appendices

Appendix 1: Publications

Cole LM, Mahmoud K, El Enazi M, Mohamed S, , Tozer GM, Smith DP, Clench MR (2013) *Recombinant "IMS TAG" Proteins – A new method for validating bottom up matrix assisted laser desorption – ion mobility separation – mass spectrometry imaging 9MALDI-IMS-MSI*. *Rapid Communications in Mass Spectrometry. In Press*

Cole LM, Djidja M-C, Bluff J, Claude E, Carolan VA, Paley M , Tozer GM, Clench MR (2011)*Investigation of protein induction in tumour vascular targeted strategies by MALDI MSI*. *Methods*.**54**. 442–453

Trim PJ, Djidja M-C, Muharib T, Cole LM, Bryn Flinders, Carolan VA, Francese S. Clench MR (2012)*Instrumentation and software for mass spectrometry imaging—Making the most of what you've got*. *Journal of Proteomics*.**75**. (16) 4931–4940

Trim PJ, Djidja MC, Atkinson SJ, Oakes K, Cole LM, Anderson DM, Hart PJ, Francese S, Clench MR(2010)*Introduction of a 20 kHz Nd:YVO4 laser into a hybrid quadrupole time-of-flight mass spectrometer for MALDI-MS imaging*.**397**. (8) 3409-19

Appendix 2: Oral presentations

- Cole LM, Bluff J, Claude E, Carolan VA, Paley M, Tozer GM and Clench MR. *MALDI-MSI and Conventional Proteomic Techniques to Compare Protein Induction in Combretastatin Resistant and Susceptible Tumours*. Ourense Imaging Conference, Spain, September 2012
- Cole LM, Bluff JE, Claude E, Wulfert F, Carolan VA, Paley M, Tozer GM, Clench MR, *Investigating Treatment Response of Combretastatin Resistant and Susceptible Tumours using MALDI-MSI and Conventional Proteomic Techniques*, ASMS Conference, Vancouver, May 2012
- Cole LM, Bluff JE, Claude E, Carolan VA, Paley M, Tozer GM and Clench MR. *Proteomics of Combretastatin Treated Fibrosarcomas Using Ion-Mobility MALDI Mass Spectrometry Imaging*. East Midlands Proteomics Workshop, Loughborough University, November 2011.

Appendix 3: Poster presentations

- Cole LM, Bluff J, Claude E, Carolan VA, Paley M, Tozer GM and Clench MR. *Potential Markers of Tumour Viability and Necrosis in CA-4-P Treated Fibrosarcomas Employing a Multimodal Proteomic Approach*. ASMS Minneapolis, June 2013.
- Cole LM, Bluff J, Claude E, Carolan VA, Paley M, Tozer GM and Clench MR. *MALDI-MSI and Conventional Proteomic Techniques to Compare Protein Induction in Combretastatin Resistant and Susceptible Tumours*. NCRI Liverpool, November 2012
- Cole LM, Bluff JE, Claude E, Carolan VA, Paley M, Tozer GM and Clench MR. *Investigations into Treatment Response in Tumour Vascular Targeted Strategies Using MALDI-MS*. British Mass Spectrometry Society, Cardiff, Wales, September 2011.
- Cole LM, Djidja M-C, Bluff JE, Claude E, Carolan VA, Paley M, Tozer GM and Clench MR. *MALDI-MSI to Investigate Treatment Response in Tumour Vascular Targeted Therapy*. American Society for Mass Spectrometry, Denver, USA, June 2011.
- Cole LM, Djidja M-C, Bluff JE, Claude E, Carolan VA, Paley M, Tozer GM and Clench MR. *MALDI-Mass Spectrometry Imaging to Investigate Treatment Response in Tumour Vascular Targeted Therapy*. Cancer Imaging Conference, City University, London, April 2011.
- Cole LM, Djidja M-C, Bluff JE, Claude E, Carolan VA, Paley M, Tozer GM and Clench MR. *Peptide Analysis with In-situ Tissue Tryptic Digestion using MALDI-MS Techniques to Investigate Protein Induction in Tumour Vascular Targeted Strategies*. East Midlands Proteomics Workshop, Nottingham November 2010.
- Cole LM, Djidja M-C, Bluff J, Claude E, Carolan VA, Paley M, Tozer GM and Clench MR. *In-situ Tissue Tryptic Digestion to Facilitate Peptide Analysis using MALDI-MS Techniques to Investigate Protein induction in Tumour Vascular Targeted Strategies*. BMSS Cardiff 2010
- Cole LM, Djidja M-C, Bluff J, Claude E, Carolan VA, Paley M, Tozer GM and Clench MR. *MALDI-MS Techniques to Investigate Protein induction in Tumour Vascular-Targeted Strategies*. British Association for Cancer Research, Hallmarks of Cancer Conference, Edinburgh, June 2010.
- Cole LM, Djidja M-C, Bluff J, Claude E, Carolan VA, Paley M, Tozer GM and Clench MR. *In-situ Tissue Tryptic Digestion to Facilitate Peptide Analysis using MALDI-MS*

Techniques to Investigate Protein induction in Tumour Vascular Targeted Strategies.
American Society for Mass Spectrometry, Salt Lake City, USA, May 2010.

- Cole LM, Djidja M-C, Bluff J, Claude E, Carolan VA, Paley M, Tozer GM and Clench MR.
MALDI-MS Techniques to Investigate Protein induction in Tumour Vascular-Targeted Strategies. Cancer Imaging Conference, Oxford University, April 2010.
- Cole LM, Djidja M-C, Bluff J, Claude E, Carolan VA, Paley M, Tozer GM and Clench MR.
Comparative Study of Detergent Addition for In-situ Tissue Tryptic Digestion to Facilitate Peptide Analysis Using MALDI-MS Techniques. East Midlands Proteomic Workshop 2009
- Cole LM, Djidja M-C, Bluff J, Claude E, Carolan VA, Paley M, Tozer GM and Clench MR.
A Comparative Study of Detergent Addition for In-situ Tissue Tryptic Digestion to Facilitate Peptide Analysis Using MALDI-MS Techniques. Bremen IMSC 2009